JETS IN A CROSSFLOW INCLUDING THE EFFECTS OF DUAL ARRANGEMENTS, ANGLE, SHAPE, SWIRL AND HIGH TURBULENCE

by

Mehmet Serif Kavsaoglu

Dissertation submitted to the Faculty of the
Virginia Polytechnic Institute and State University
in partial fulfillment of the requirements for the degree of
DOCTOR OF PHILOSOPHY
in
Aerospace Engineering

APPROVED:

J. A. Schetz, Chairman

A. K. Jakubowski

W. L. Neu

W. F. O'Brien

B. Grossman

December, 1986

Blacksburg, Virginia

JETS IN A CROSSFLOW INCLUDING THE EFFECTS OF DUAL ARRANGEMENTS, ANGLE, SHAPE, SWIRL AND HIGH TURBULENCE

by

Mehmet Serif Kavsaoglu

J. A. Schetz, Chairman

Aerospace Engineering

(ABSTRACT)

In this experimental research, jets injected from a flat plate into a crossflow at large angles have been studied. Results were obtained as surface pressure distributions and mean velocity vector plots and turbulence intensities and Reynolds stresses in the jet plume. Rectangular jets (length/width = 4) and circular jets were tested. The rectangular jets were aligned streamwise as single and side-by-side dual jets. For the rectangular jets, the jet injection angles were 90° and 60°. The circular jet results were obtained for a single circular jet injected at a 90° angle. Different types of the circular jets were studied with low exit turbulence, high exit turbulence, 40 % swirl and 58 % swirl. The surface pressure distribution results were obtained for jet to freestream velocity ratios of 2.2, 4 and 8 for most of the cases mentioned. Mean velocity vector plots were obtained for the 90° and 60° side-by-side dual rectangular jets and all the circular jet types, mainly for the jet to freestream velocity ratio of 4. Turbulence results were obtained for a jet to freestream velocity ratio of 4 for the 90° and 60° side-by-side dual rectangular jets and for the circular jet with low exit turbulence cases. The results

showed that the higher exit turbulence reduced the penetration height, and it also reduced the surface area influenced by the negative pressures. The swirl caused asymmetric pressure distributions, and the swirl effects were more pronounced for lower velocity ratios. The rectangular jets featured strong negative pressure peaks near the front nozzle corners. The 60° rectangular jets produced lower magnitude negative pressures which are distributed over a lesser area when compared to the 90° rectangular jets.

Acknowledgements

I would like to express my gratitude to my advisor Dr. J. A. Schetz for his advice, support, encouragement and understanding. He spent his valuable time with me and gave me a chance to benefit from his knowledge and experience.

I thank Dr. A. K. Jakubowski, for his close interest and discussions. Thanks also go to Drs. W. L. Neu, W. F. O'Brien, and B. Grossman for serving on my committee and for reviewing and commenting on this dissertation.

I would like to thank to the technical staff of the Aerospace and Ocean Engineering Department: F. Shelor, R. Frazier and K. Morris, for their expert work on the manufacturing and servicing of the test models and equipment and G. Bandy and G. Stafford for their quality work on electrical/electronical matters and help in the wind tunnel.

I thank R. Hyde and S. Holland for helping me in the wind tunnel. I thank R. Hyde also for writing a convenient plotting program. Thanks also go to D. Less, M. Kotb, B. Sung, S. Olcmen and some other past and present stu-

dents of the Aerospace and Ocean Engineering Department for sharing their experience on instrumentation and other technical matters.

I would like to acknowledge the financial support provided for this resarch by NASA Ames Research Center, Dr. K. Aoyagi being the technical monitor.

I also acknowledge a scholarship provided by the Scientific and Technical Research Council of Turkey (TUBITAK). This scholarship paid my full expenses at the begining of my studies at Virginia Tech. Later on it continued to pay my tuition.

For my education, the contributions of my parents and all my teachers are beyond description.

Table of Contents

List of Illustrations

List of Tables

Nomenclature

A .....area

A, B .....linearized D.C. outputs of the X-wire sensors

a, b .....linearized R.M.S. outputs of the X-wire sensors

C_p .....pressure coefficient

ΔC_p ..... $C_{p_{jet\ on}} - C_{p_{jet\ off}}$

D .....diameter

D_{ref} .....diameter of a same area circle

E .....D.C. output of a hot wire sensor

e .....R.M.S. output of a hot wire sensor

L .....length

p .....static pressure, pressure

q .....dynamic pressure

R .....jet to freestream velocity ratio

S .....center to center spacing

U,V,W .....velocity components

u' , v' , w' .....fluctuating velocity components

W .....width

X,Y,Z .....cartesian coordinates

γ .....pitch angle of the X-wire probe

φ .....roll angle of the X-wire probe

subscripts

j .....jet

∞ .....freestream

T .....total

S .....static

p .....probe

Chapter 1

INTRODUCTION

1.1 MOTIVATION

Fluid injection into another fluid, basically the subject matter of jet flows, is one of the major subdivisions of fluid mechanics. The mixing of two or more streams with different velocities and sometimes with different direction, concentration, temperature, density, phase and other properties produces a complicated turbulent (often 3D) flow field, and this introduces difficulties for theoretical and computational workers. The subject is important, because there are numerous practical applications involving such flows. Experimental determination of these flowfields is also not routine, particularly when it comes to obtaining turbulence information. Throughout the years there has been a lot of research work done in the field, the majority of it being experimental. A recent monograph on the sub-

ject (Ref.1) cites close to 250 selected references. It is not difficult to imagine that the actual number of research works in the literature is much higher. Research is still going on, because the number of parameters involved is large, and new applications are appearing continuously.

Looking at previous works, one sees that the majority deal with coaxial jet injection. There are also quite a number of works on transverse jet injection at large angles into a crossflow. Sewage outfalls and industrial chimneys are some of the applications of that case related to the pollution problem. Fuel injection into combustion chambers, film cooling and transition flight of VTOL aircraft are among the aerospace applications of this type of jet injection. There are also numerous industrial applications.

The present work is a fundamental research study aimed primarily towards the application to VTOL aircraft, although the results have broader utility. This flow problem can be idealized as crossflow jet injection from a slender body of revolution or from a flat plate. Usually, both jet (or jets) and crossflow are subsonic flows. During take-off, the jet to freestream velocity ratio changes from infinity (when there is no forward motion of the aircraft) to zero (when the aircraft is in horizontal flight, and the jets are off). During landing, just the opposite happens. Crossflow jet injection from a surface produces negative pressures on the surface, particularly towards the downstream and to the sides of the jet exit. There will also be a positive pressure region in front of the jet due to crossflow deceleration. Negative pressures on the bottom surface of a wing means loss of lift for an aircraft. When these negative pressures combine with the positive pressure

region in front of the jet, the resultant effect is to produce a nose-up pitching moment. This pressure distribution on the surface is strongly dependent on the jet to freestream velocity ratio, which is continuously changing during the transition flight. Of course, the aircraft designer wants the maximum possible lift with minimum losses. He also wants maximum stability. This alone is enough reason that crossflow jet injection should be studied extensively.

The number of parameters involved in the general jet in a crossflow problem is large - jet to freestream velocity ratio, jet exit geometry (circular, rectangular, etc.), jet injection angle, single jet or side-by-side or tandem multiple jets, jet exit velocity profile (uniform, nonuniform, swirling etc.), jet exit turbulence level, temperature difference between jet and freestream, concentration profiles, possibility of two phase flows, and buoyancy effects, to name some of these parameters. If one or both of the streams is supersonic, additional parameters would be involved. Here, because of the main application of the present research, subsonic jet injection into a subsonic crossflow has been considered. Indeed, the flow has been idealized to the point where the jet and freestream flows are essentially incompressible.

Even though the literature in this field is already rich, the present research has some unique characteristics. First of all, single and side-by-side dual rectangular jets aligned streamwise have been studied. Streamwise aligned rectangular jets might have some practical advantages over the circular ones for VTOL aircraft. For example, they can be placed to the sides of an aircraft more easily, and they make less blockage against the crossflow for the same jet exit area. The rec-

tangular jets studied had sharp corners, and the effects of two different injection angles and three different velocity ratios have been studied. Next, the effects of jet exit turbulence level and swirling exit velocity profile for a 90° circular jet have been investigated. These effects are present in the jets formed by fans or jet engines used for VTOL airplanes. In aircraft propulsion systems, swirl may be permitted for noise reduction purposes. On the other hand, swirl is often eliminated by using flow straighteners to increase thrust. The swirl ratios used for the present research (40 % and 58 %) were strong enough to produce visible changes in the pressure distribution and flowfield. These swirl ratios may be high for aircraft applications, but the results have fundamental importance and may also be useful for some other type of applications. To the best of the author's knowledge, these areas have received little or no previous attention.

Results are presented as surface pressure distributions and mean velocity vectors. For the jet centerplane, turbulence intensities and Reynolds stresses obtained for 90° and 60° rectangular dual jets and a 90° single circular jet for a jet to freestream velocity ratio of 4 are presented. For the VTOL application, the pressure distributions have the most direct use. The mean flowfield results are helpful to interpret surface pressure distribution measurements and for other engineering applications. The mean flowfield and turbulence data obtained can also be useful for the turbulence modeller and computational fluid dynamicist.

This work was an experimental study. Even though they are expensive and troublesome, experimental studies on flowfields of this complexity are still necessary. Approximate prediction methods may not always be suitable to provide the

information needed, and numerical solutions of the Navier-Stokes equations are not yet routine even for the single circular jet. Such solutions will be much more difficult for rectangular jets, multiple jets, high turbulence jets, and jets with swirl.

1.2 GENERAL INFORMATION AND LITERATURE SURVEY

A jet injected at a right angle into a crossflow bends towards downstream under the effect of crossflow. The core of the jet takes a kidney-like shape. During this process, two counterrotating bound vortices form in the jet. Going downstream, the two streams mix rapidly. There are similarities between a crossflow passing a solid object and a crossflow passing a transverse jet. Let us assume that the solid object is a circular cylinder, and the jet is a round jet. The crossflow passing a circular cylinder will first decelerate in front of the cylinder, then accelerate around and separate from the rear forming the wake region. The same general type of flow will occur about a round jet, but entrainment between the two streams further complicates the situation. If the solid object is sharp-cornered such as a rectangular body, the crossflow will separate right from the front corners, and there will be a base flow region at the rear. Replacing the rectangular body with a rectangular jet will again introduce further complications due to viscous entrainment of the two streams.

In Fig.1.a (from Ref.2),the deformation of a round jet into a kidney shape under the effect of the crossflow can be seen. In Fig.1.b, the form of the constant total and static pressure contours and the diminishing of the potential core along the arc length of the jet can be seen. In that figure, s is the arc length along the centerline trajectory, and D is the jet exit diameter. Fig.2, taken from Ref.3, is also helpful for an understanding of this complex flowfield. One must also consider the possibility of periodic unsteadiness. Motion picture flow visualisation studies using a tuft screen behind the jet (Ref.29) showed formation of periodic eddies in the wake region for a blunt jet. The blunt jet used was a rectangular jet with rounded corners, whose long axis was perpendicular to the crossflow direction. According to the same reference, the same phenomena were observed for a circular jet, but the magnitude of the disturbances was less.

A list of selected publications and research papers related to crossflow jet injection is given here as References 1 through 79. Due to the nature of the present work, papers related to subsonic jet injection into a subsonic crossflow were chosen. However, crossflow jet injection into supersonic flow is also a large area of research because it has applications like fuel injection into ramjet combustors. The interested reader on this subject should refer to Ref.1. General information on crossflow jet injection can also be obtained from Ref.1. This is a recent book, and it is quite extensive in coverage. Crossflow jet injection is treated as a separate chapter, and information on single phase flows, particle laden jets, injection into supersonic flow as well as information on prediction

methods are given. Reference 2 is a classic and comprehensive older book on the subject that also covers the earlier work of Russian scientists.

Reviews of the previous works on jets in a crossflow can be found in Refs. 4, 5 and 6 and also in 16 and 19. Reference 6 which was prepared in 1981, extensively evaluates 27 of the previous works; it also tabulates the surface pressure distribution information obtained from these works. References 23, 24 and 50 through 67 cited in the present work were also among the subjects of Ref.6. Reference 7 is particularly concentrated on prediction methods, and it contains 15 articles on experimental information together with empirical and potential flow prediction methods.

The general features of the jet in a crossflow problem was described in Ref.49 as follows:

a) A pair of diffuse, counter-rotating vortices is formed by the interaction of the jet and the crossflow that lie on the concave side of the jet centerline. They are the primary feature in the jet flowfield and are the dominant contributors to the surface pressure distribution.

b) Air from the freestream is accelerated in the direction of the jet by the viscous entrainment of surrounding fluid. A low-pressure region is created on the plate surface. This effect becomes more pronounced as the jet velocity ratio increases.

c) The boundary of the jet acts like a solid cylindrical body placed in the crossflow. This blockage effect causes the flow to separate as it travels around the jet, and a low-pressure wake region forms near the surface. Blockage also causes high pressures in front of the jet.

According to Ref.24, variation of the surface boundary layer thickness may cause differences on the surface pressure distribution. The largest effects can be seen for the region closest to and to the side and behind the jet. According to Ref.6, jet to freestream density ratios lower than 1.5 do not effect penetration significantly. Jets with swirl or high turbulence will have lower penetration due to the weaker or no potential core. Swirl and high turbulence will also effect the entrainment of the freestream into the jet, which is a major cause for the negative pressures on the surface.

In Table 1 on page 11 some of the previous works can be seen comparatively. The first part of this table was taken from Ref.15, and some additions were made here. A prediction method based on solution of the integral conservation equations is presented in Refs. 8 and 9. This method can predict jet flow properties and the jet path and effects of turbulence, entrainment, buoyancy and heat transfer are taken into account. The method utilizes a fast iterative solution procedure. This method was also applied to multiple jets in Ref.18. An example of an exact numerical Navier-Stokes solution can be found in Ref.77. Calculations of this type even with a coarse grid are expensive and still rare.

The majority of the previous works deal with a single round jet injected at a 90° angle into a crossflow. There are also limited studies involving some of the other parameters mentioned above, e.g. multiple jets, jet injection angle, heated jets, etc. Previous researchers have usually presented their results as surface pressure distributions, jet trajectories and/or mean velocity vector plots. Sparse temperature field and turbulence information are also available.

The present work is most closely related to Refs. 10, 11, 12, 13 and 68, because this work is actually a continuation of those. In Ref.10, single and tandem dual circular jets injected into crossflow from a body of revolution were investigated. Surface pressure distributions and meanflow information were given for jet to freestream velocity ratios ranging from 3.2 to 8.0. For tandem jets, the ratios of center-to-center spacing to jet diameter (S/D) were 2, 4 and 6. Jet injection angles were chosen as 90° and 60°. In Ref.11, side-by-side dual and tandem dual jets injected into crossflow from a flat plate were considered. Results were presented as surface pressure distribution plots. Both for tandem and side by-side-jets, the S/D ratios were chosen as 2 and 4. The jet to freestream velocity ratios (R) were 4, 6 and 8, and the jet injection angles were 105°, 90° and 75°. In Ref.12, the effects of nonuniform velocity profiles on crossflow jet injection from a flat plate have been studied. Side-by-side and tandem dual circular jets injected at a 90° angle into crossflow were used. For both cases, S/D was 2 and jet to freestream velocity ratios were 2.2 and 4. Information was given as surface pressure distributions and mean velocity plots. The nonuniform profile had the same mass flow as the uniform one, but it had lower velocities at the center and higher velocities at the periphery. It was found that this type of nonuniformity caused a behavior as if the jet to freestream velocity ratio was higher than what it was. In Ref.13, single and side-by-side dual rectangular jets injected at a 90° angle were studied. Those tests were repeated during the course of the present work. The difference between the jets of Ref.13 and the present work is that the jets of Ref.13 were found to have had some rotation in their center, but the jets

of the present work had quite uniform exit profiles. Reference 14 is an example of earlier experimental studies related to rectangular jets. In this reference, an aspect ratio 4.0 (same as the present work) single rectangular jet was studied. The jet was aligned across and streamwise, and the injection angle was varied from 15° to 90°. The injection was from a flat plate or from a faired body. Surface pressure distribution and vortex data were obtained for velocity ratios of 4.0, 8.0 and 10.

References 15, 17 (or 16 with more details), 75 and 76 are examples of the limited available turbulence measurements in the plume of circular jets injected at 90° angle into a crossflow. In Ref.15, LDV was used for the upstream and a hot wire was used for the downstream region. Measurements were done for a single jet at jet to freestream velocity ratios of 1.15 and 2.3. In Ref.17, data was obtained for the downstream region ($X/D \geq 3$) by using hot wire at a velocity ratio of 2. Single, side-by-side dual and tandem dual jets were tested. For both of the dual jet arrangements, the jet spacing was 4 jet diameters. For Refs. 75 and 76, the subject was a single jet, and hot wire techniques were used to obtain data. For Ref. 75, the velocity ratios were 0.5, 1.0 and 2.0, and for Ref.76 the velocity ratio was 0.5. Spectral analysis and conditional sampling of various turbulence quantities were obtained.

Table 1. Some of the Previous Experimental Investigations

Part 1 (From Ref.15)

Ref.	jet diameter (mm)	incident angle	jet velocity profile	cross-flow velocity (m/s)	velocity ratio	measured
20	6.35, 9.5 12.7, 15.9	90	orifice	-	-	penetration parameters
21	6.35, 9.5 12.7, 15.9	30, 45 60, 90	orifice	72 122	2-8	correlation between parameters
22	12.7 25.4	90	orifice	-	4,6,8	total pressures, flow directions
23	9.5	90	pipe	1.5	4,6,8	velocity, turbulence intensity, entrainment
24	25.4	90	pipe	18.3, 36.6	2,4,8 11.3	static pressure distributions
25	6.35	± 15, ± 30, ± 45, ± 90	pipe	1.6	4,6,8	jet, trajectory, entrainment
26	25.4	-180,30, 60, 90, 120,150,180	nozzle	-	1.18-10	trajectory by photographs
27	50.8	90	pipe	7.6,15.2	4.12	wall static pressures
28	8.4	90	nozzle	MACH 0.1, 0.2 0.4, 0.6	1.4	wall static pressures
29	50.8	90	nozzle	15.2	8,12	turbulence in wake region
30	23.5	35, 90	pipe	30.5 61	0.1-2	temperature, velocity, turbulence intensity contours
31	25.4	90	nozzle	12.2	2,4,8 12,16,20	wall static pressures turbulence intensity vorticity
32	23.5 11.8	35,90	pipe	30.5 61	0.1-2.18	adiabatic wall temperature, film cooling effectivenes
33	6.35	90	pipe	6-9	2.8-8.5	velocity and temperature distributions
34	23.5	35,90	pipe	30.5 61	0.1-2.0	adiabatic wall temperatures,pitot and static pressures
35	38.1 76.2	90	orifice	-	2,4,6,8 12	wall static pressure distribution
36	8.4	90	nozzle	MACH 0.1,0.2 0.4,0.6	dynamic pressure ratio 0-1000	floor static pressures
37	40	90	pipe	3.4	2.37,3.95 6.35	velocity distributions
38	101.6	90	orifice	30.4	53.3	velocity and vorticity
39	101.6	45,60,75 90,105	nozzle	30.5 55.3	8	velocity
40	19.05	90	pipe	26	0.046-0.1	static pressure, velocity, film cooling effectiveness
3	23.6	90	pipe	8.5	3.48	velocity,vorticity
41				pipe flow	2-5-12.3	
42	varied	90	orifice	15	2.45-7.75	temperature profiles

Table 1.(continued)
Part 2 (Recent additions)

Ref.	jet diameter (mm)	incident angle	jet velocity profile	cross-flow velocity (m/s)	velocity ratio	measured	remarks
10	49.2	90,75,60	nozzle	14.5-38.5	3-8	surface pressures, velocity vectors	single and tandem dual (S/D = 2,4,6) from a body of rev. $D_j/D_{body} \cong 1/2$
11	49.2	105,90,75	nozzle	14.5-38.5	4,6,8	surface pressures	side by side dual, tandem dual from a flat plate,S/D = 2,4 for both type
12	49.2	90	uniform, high perip. low center nonuniform	8.6-15.7	2.2,4	surface pressures, velocity vectors	side by side dual, tandem dual from a flat plate,S/D = 2
13	L = 86 W = 21.5	90	nozzle	8.5-31	2.2,4,8	surface pressures velocity vectors	single, side by side dual rectangular,streamwise, L/W = 4,for side by side S/D_{ref} = 0.95 D_{ref}: *D of eq. area circ.*
14		15,30,45 60,75,90	nozzle		4,8,10	surface pressures vortex strength trajectory	single rectangular jet, L/W = 4 blunt,streamwise
15	25.4	90	pipe	12	1.15,2.3	velocity,turbulence Reynolds stress, vel. probability	LDV upstream, hot-w. downstr.
16 or 17	50.8	90	nozzle	15.2	2.0	turbulence int., Reynolds str.	single,side by side dual, tandem dual, for dual dual types S/D = 4
19	50.8	90	nozzle	3	1,2	trajectory,velocity, flow vis., temp.	cold jet(amb.) and heated jet (177°C)
50	25.4	90	nozzle	37-124	1-5	surface pressures	
69	$\frac{A_c}{A_j}$ = 100 D_c = 146.1	90	nozzle		4	mean velocity components	swirling crossflow swirler wane ang. = 45,70 six orientation single normal hot-wire
71		135	67		q_j/q_∞ = 5,20,40	trajectory, reverse flow zone dimensiones	paired jets from a plane slot T_j = 288°K, T_∞ = 343°K
72		90			1,4,7	mean and RMS temp. profiles, temp. contours	heated jet temp. diff. = 28-42 °C fluids: water
73		90			1.4-2.5	trajectory dispersion, density	solid-gas jet ρ_j/ρ_∞ = 12 − 23
74	50.8	90	nozzle	10.65	8	mean vel. vectors, streamlines	3-D LDV
75	50	90	pipe	13.9	0.5,1,2	terms in TKE eq., turbulence, meanflow	triple hot-wire
76	50	90	pipe	13.9	0.5	spectral anal., flow vis.,conditional avgs. of turb. quantitites	
78	101.6	45,60,75 90,105	nozzle		4,8	velocity vector, pressures in the jet plume	
79		90			2-9	flow vis.	nonsymmetric jet, yaw ang.

1.3 SCOPE OF THE PRESENT RESEARCH

The test matrix for the present research can be seen in Table-2. During the course of the present study, 90° and 60° single and side-by-side dual rectangular jets were studied. The rectangular jets were aligned streamwise and had sharp corners. For 90°, the rectangular jet length to width ratio (L/W) was 4.0. For side-by-side 90° rectangular jets, the ratio of jet spacing to reference diameter (S/D_{ref}) was 0.95, where D_{ref} is defined as the diameter of a circle with the same area. The 60° rectangular jets had the same shape and dimensions as the 90° ones when cut with a plane perpendicular to the jet axis. These quantities were selected as representative of the VTOL cases. The rectangular jets had uniform velocity profiles and low exit turbulence ($\cong$ 3%).

For a 90° single circular jet, the effects of different jet exit velocity profiles were studied. These profiles were: 1) low turbulence, uniform; 2) high turbulence, uniform and 3) swirling. The low and high turbulence, circular jets had uniform exit mean velocity profiles. The exit turbulence intensity was around 3 % and uniformly distributed for the low case. For the high turbulence case, the intensity was around 10 % in the center and higher at the periphery. For the swirling jets, swirl ratios of 40 % and 58 % were tested, where swirl ratio was defined as the swirl component of the velocity at the periphery divided by the average total velocity. All the jets were injected from a flat plate that was large compared to the jet/crossflow interaction area.

Results were obtained as surface pressure distributions, mean velocity vector plots and turbulence intensities and Reynolds stresses. Surface pressure distribution tests were done for jet to freestream velocity ratios (R) of 2.2, 4.0 and 8.0. These tests were for 90° and 60° single and side-by-side dual rectangular jets, single circular jet, circular jet with high turbulence and circular jet with 40 % and 58 % swirl. For the circular jet with high turbulence case, R = 8.0 was omitted due to the very low freestream velocity needed. For meanflow measurements, a five-hole, yawhead probe was used. Turbulence quantities were obtained by using an X hot wire probe which was supported by a probe rotator mechanism. Pitch and roll angles of the probe could be set as desired, and the probe axis was always aligned with the flow direction. Mean velocity vector plots were obtained for R = 4.0, for 90° and 60° side-by-side dual rectangular jets, single circular jet, circular jet with high turbulence, and circular jet with 40 % and 58 % swirl. For the 90° rectangular jet case, data for R = 2.2 was also obtained. Turbulence intensities and Reynolds stresses in the plume of the jet were obtained for R = 4.0 and 90° and 60° dual rectangular jets and a single circular jet. These data were obtained for the jet centerplane only.

Table 2. Scope of the Present Research

jet type	jet velocity profile	jet velocity (m/sec)	U_j/U_∞ pressure data	U_j/U_∞ meanflow data	U_j/U_∞ turbulence data
90° single rectangular	uniform nozzle	66	2.2,4,8	-	-
90° side-by-side dual rectangular	"	"	2.2,4,8	2.2,4	4
60° single rectangular	"	"	2.2,4,8	-	-
60° side-by-side dual rectangular	"	"	2.2,4,8	4	4
90° single circular	"	62	2.2,4,8	4	4
90° single circular,high turbulence	"	35	2.2,4	4	-
90° single circular, 40 % swirl	swirling nozzle	62	2.2,4,8	4	-
90° single circular, 58 % swirl	"	"	2.2,4,8	4	-

Remarks
For rectangular jets, L = 86mm, W = 21.5mm, L/W = 4, jet aligned streamwise.
For side-by-side dual rectangular jets, S/D_{ref} = 0.95 (D_{ref}: D of same area circle).
For circular jet, D = 49.2mm.

Chapter 2

APPARATUS

2.1 WIND TUNNEL AND DATA ACQUISITION

The experiments were carried out in the 6ft. by 6ft. (1.83m by 1.83m) Stability Tunnel of Virginia Tech. This is a closed circuit tunnel with 24ft. (7.32m) long interchangable test section. The tunnel has a very low turbulence flow (less then 3/100 of a percent at low speeds). A 600 H.P. D.C. motor drives a 14 foot (4.27m) propeller and provides up to 220 ft/sec (67 m/sec) continuous velocity in the test section. During these experiments, tunnel speeds in the range of 24 ft/sec (8.52 m/sec) to 102 ft/sec (31.04 m/sec) were used according to need. The facility is equipped with appropriate sensors and transducers for measurement of atmospheric pressure , tunnel temperature and dynamic pressure. This

tunnel can be seen in Fig.3, and more detailed information about the tunnel can be found in Ref.80.

The tunnel is equipped with a two component probe traverse system. It is also equipped with an HP 9836 microcomputer, HP 2763A printer , HP 9872A plotter and a 200 channel HP 3052A Automatic Data Acquisition System. This data acquisition system included an HP 3495A Channel Selector (Scanner) , an HP 3455A Digital Voltmeter and an HP 59306A Relay Actuator. The voltmeter has about a 20 sample per second sampling rate. This data acquisition system can obtain readings from various transducers and can command up to six relays. By using these facilities, many of the experiments can be run fully or partly automated. Collected data can be stored on floppy discs and also transfered to the mainframe computers of the university.

2.2 TEST MODEL AND JET NOZZLES

Photographs of the model in the wind tunnel can be seen in Fig.4. This is actually a flat plate mounted 18in (45.52cm) below the top of the test section. Jets are injected downwards from the surface. The model has a rounded leading edge, and a tapered trailing edge. At 4.5in (11.43cm) downstream of the leading edge there is a 2in (5.08cm) wide 100 grit sandpaper glued to the surface of the model to create a turbulent boundary layer on the model surface at the injection station. The model was a little bit wider then the width of the wind tunnel. For that rea-

son, neccesary adjustments have been made to the wind tunnel to allow part of the model to be out of the test section. Before starting an experiment, all the openings on the wind tunnel walls were sealed by tape.

A special section at the center of the model was instrumented with pressure taps, and this section had an L-shaped cut where jet nozzles could be mounted with different spacings (see Figs.4b and 5). The dimensions of the flat plate model can be seen in Fig.5, and in Fig.6 the experimental set up is shown.

Two D.C. blowers (Filtron Type FA 1734B) mounted at the top of the test section were used to provide jet air as shown in Fig.6. These blowers were rated at 1400 CFM, and the maximum permissible voltage was 28 volts. An arc-welder power supply was used to generate D.C. power for the blowers. Air from the blowers passed through a flexible tubing and a nozzle assembly before being injected. Some heating of the jet air by the blowers was observed, and some precautions were taken to reduce it such as replacing the blower bearings and minimizing the friction generating parts (screens, etc) inside the nozzle assembly. Finally, the jet exit temperature could be reduced down to about 100°*F*. The dimensions of the flat plate model can be seen in Fig.5, and in Fig.6 the experimental set up is shown.

For this research, three different types of jet nozzles were used: 90° rectangular, 60° rectangular and 90° circular. The 90° jets were injected perpendicular to the freestream, and the 60° jets were inclined downstream. Rectangular jets (90° and 60°) were tested as single jets and side-by-side dual jets. Circular jet measurements were only done for single jets. For single jet experiments, one

of the nozzle exits was closed with a plexiglas piece flush with the surface of the model. A 4in × 4in (10.16*cm* × 10.16*cm*) area in the immediate vicinity of each jet was instrumented more densely then the rest of the instrumented section. In these areas, there was a pressure tap at every 0.25in (0.64cm) for rectangular jets and at every 0.33in (0.85cm) for circular jets. The rest of the instrumented section was covered with pressure taps at every 0.67in (1.69cm). The diameter of each pressure tap was about 0.5 mm. Each pressure tap was connected to an approximately 0.5 mm inner and 1.0 mm outer diameter steel tubing 0.375in (0.95cm) long. Then, flexible plastic tubing was used to connect these ports to the Scanivalves. In Fig.7, the locations of the pressure taps for the 90° rectangular jets can be seen. For this configuration, a total of 926 ports distributed over a 16in by 16in (40.16cm by 40.16cm) area were used for data reading, and 425 of these ports were in the 8in by 8in (20.32cm by 10.16cm) region covering the immediate vicinity of the jets. The locations of pressure taps were almost the same for the 60° jets, and in Fig.8 pressure tap locations for the circular jet experiments can be seen. For circular jet experiments, an area of 12in × 12in (30.48*cm* × 40.64*cm*) was covered with pressure tabs.

In Figure 9, the dimensions of the 90° rectangular jet exits are given. There was a 4in (10.16cm) spacing between the two jets. In this figure, we also see the flow direction and the coordinate system chosen. The Z coordinate (not shown) completes the right hand system. The dotted lines show the measurement planes for the mean flowfield experiments. The 60° jets had the same center-to-center spacing and jet width, but the exit lengths of the 60° jets was longer. However,

when cut with a plane perpendicular to the jet axis, the 60° and 90° jets had the same crossectional area. The exit diameter of the circular jet was 1.95in (4.95cm).

In Fig.10, the nozzle assembly for rectangular jets is shown. This is same for the 90° and 60° jets except for the nozzle section. A plastic honeycomb was used with about 0.188in (0.476cm) spacings. In Fig.11, the nozzle assembly for the circular jet can be seen. In this case, a honeycomb was made of 0.25in (0.64cm) diameter soda straws cut 2in (5.08cm) long. Also in this figure, two 0.625in (1.59cm) pieces of copper tubing are shown. These were used to produce swirl by tangential air injection for swirling jet experiments. For other cases, the exit areas of these tubes were closed. These tubes were connected to a larger tubing and that was connected to the 120 PSI air tanks of the VPI&SU Aerospace and Ocean Engineering Department, which are normally used to run the supersonic tunnel. Air pressure was adjusted by using valves. Also seen in Fig.11, is an insert section after the nozzle chamber. This insert is actually a thin-walled, open-ended cylinder. However, for the high turbulence jet experiments, there was a screen at the nozzle chamber side of this insert. This screen was made of about 0.313in (0.079cm) wires with 0.125in (0.32cm) spacing. In Fig.12, the contraction section for the rectangular jets is shown. This was made of aluminum, and the curved part was of thin copper sheet of 0.313in (0.079cm) thickness. Details of the nozzle geometries for the 90° and 60° rectangular jets and 90° circular jet can be seen in Figs. 13, 14 and 15. The rectangular jet nozzles were mainly made of brass to prevent corrosion, and their thin walls were from copper sheet. The cir-

cular jet nozzle was from steel. Further information about that nozzle can be found in Refs.10,11,12.

2.3 INSTRUMENTATION FOR PRESSURE DISTRIBUTION MEASUREMENTS

Two groups of six (total of 12) Scanivalve-transducer systems were used as the main instrumentation. Each transducer was manufactured by Druck Ltd. England, model: PDCR 22, range: 1 PSI and required 12 volts of D.C. power. The Scanivalves were manufactured by Scanivalve Corporation, San Diego, California model: 48SGM. These Scanivalve-transducer systems are shown in Fig.16. Each scanivalve had 48 ports, and the 48th port was connected to a 1 PSI constant pressure source and 47th port was open to ambient. This made it possible to calibrate the transducers continuously during the experiments. The rest of the ports were connected to the pressure taps on the model surface. The 1 PSI constant pressure reference was obtained by using a nitrogen bottle and a dead weight tester. The dead weight tester was also employed to check the integrity of every pressure lead connecting the flat plate model with the Scanivalves. A known pressure was applied to every pressure tap on the model surface and compared with the corresponding output from the transducers. This made it possible to ignore damaged ports during data reduction. During the experiments, after the test conditions are obtained and stabilized, the rotation of the

Scanivalves, data reading and storage were done by computer through the data acquisition system as a fully automated process. In Fig.17, instrumentation for these tests is shown schematically. The computer program which was used to scan transducers, rotate Scanivalves, and gather data can be found in Appendix A. This program (SCANNER1) required about a 24 minute run time when all 12 transducers were used.

2.4 INSTRUMENTATION FOR MEAN FLOW MEASUREMENTS

A three dimensional yawhead probe (United Sensor DC 125) was used for the mean flowfield measurements. The probe had a blunt conical head with five pressure ports. The central hole was surrounded by the remaining four ports located at 90° intervals around the head of the probe. Pitch and yaw angles and the magnitude of the velocity vector were determined by processing the data coming from all five ports. Geometrical details and coordinate directions of this probe can be seen in Fig.18. More information about this probe can be found in Ref.86. During the experiments, referring to the previously defined coordinate system, Y and Z locations of the probe were changed by a two dimensional traverse mechanism, and X location of the probe was changed by hand adjustment of the position of the strut which supported the probe. The X-Z plane of the probe was always parallel to our X-Z plane. However, the probe made a 45° angle with the

model surface in order to cover the maximum possible range of flow angularities. During the data reduction process, necessary corrections have been applied due to the differences between coordinate systems. If the calibration given in Ref.81 was used, this probe was capable of determining velocity vectors staying in a 42° cone from probe axis. When the calibration given in Ref.82 was used, this cone angle was 60°. The five pressure ports of this probe were connected to a Scanivalve (Model J Scanivalve Corporation) and read by a transducer. A computer and data acquisition system, which was explained above, were also used for these experiments. Schematical description of this instrumentation is given in Fig.19.

2.5 INSTRUMENTATION FOR TURBULENCE MEASUREMENTS

A normal single wire probe (TSI 1210) was used for measuring the jet exit turbulence levels when there is no crossflow. These measurements were done without using a linearizer.

The main part of the turbulence measurements was turbulence intensities and Reynolds stresses in the plumes of the jets in a crossflow. For these measurements, an X-wire probe (TSI 1241-T2)was used. The sensors were 0.00058 cm in diameter and 0.127 cm in length and made of Tungsten. Two TSI 1050 constant temperature anemometers, and two TSI 1052 linearizers were used. Data

coming from the linearizers passed through a TSI 1015C turbulence correlator and were read by a DISA 55D35 RMS voltmeter and a TSI 1076 integrated D.C. voltmeter.

It is known that for good accuracy with X-wire probes, probe should be aligned with the flow direction at least within 10° . Since for the jet in a crossflow situation the flow angle varies considerably, a probe rotator mechanism was necessary. Also, in order to measure all six of the turbulence intensities and Reynolds stresses, an X-wire probe must be rotated around its axis at three different angles, basically 0° , 90° and 45° . For these reasons, a probe rotator mechanism was designed and built. Mechanical and electrical manufacturing of this device was done by the VPI&SU Department of Aerospace and Ocean Engineering shops. This device changed the pitch and roll angles of the hot wire probe. A motor changed the pitch angle, and a potentiometer read this angle. Another motor and potentiometer did the same for the roll angle. The potentiometers were calibrated before putting the device into service. The Z coordinate of the probe was changed by a one dimensional traverse mechanism, which supported the probe rotator mechanism rigidly. The X location of the probe was changed manually. To save weight, most parts of the probe rotator mechanism were made of aluminum. A 6in (15.24cm) long TSI 1155 probe support for X-wires was removed from its end box and mounted to the shaft of the roll motor of this mechanism. Individual parts and most corners were streamlined, and the probe was not subject to vibrations at least for the wind tunnel speeds of our interest. The maximum tunnel speed for turbulence measurements was about 50 ft/sec (15.24 m/sec). The testing

of this device above 100 ft/sec wind tunnel speed did not show vibrations. The same was true for jet in a crossflow situations for our velocity ranges. The hot wire probe and the probe rotator mechanism can be seen in Fig.20. More details about this mechanism are given in Appendix C. The computer and data acquisition system, which was mentioned before, were also used for these experiments. The computer read the R.M.S. and D.C. outputs coming from hot wire sensors and set pitch, roll angles and Z locations by reading potentiometer outputs, receiving manual information and commanding the pitch, roll and Z motors. Data reduction was also done by the same computer, and the data was stored on floppy discs. A schematic diagram of the instrumentation for the turbulence measurements can be seen in Fig.21. The computer program which was used for this experiments is given in Appendix B. In Fig.22, the coordinate system of the X-wire probe and sensor numbering with this coordinate system can be seen. Linearized output of the sensor#1 is proportional to (U + V) and of sensor#2 to (U-V). A sample linearized calibration curve is given in Fig.23, and the effect of temperature on the linearized output can be seen in Figure 24 taken from Ref.16. Note that temperature change affects the gain of the curves, but it has less effect on the zero shift.

2.6 TEST CONDITIONS

Throughout the experiments, different jet to freestream velocity ratios were obtained by keeping the jet velocity constant and adjusting the freestream velocity. This is done because accurate adjustment of the freestream velocity was much easier than the jet velocity. During the experiments the freestream velocity was changed from 28 ft/sec (8.52 m/sec) to 102 ft/sec (31.04 m/sec), depending on jet exit velocity and the jet to freestream velocity ratio chosen. The freestream turbulence intensity was about 0.04 %. The Reynolds number based on the jet exit diameter (or D_{ref} for the rectangular jets) and the freestream velocity was 2.56×10^4 for 28 ft/sec freestream velocity and 9.36×10^4 for 102 ft/sec freestream velocity. The Reynolds number at the nozzle, based on flat plate length up to this point was 2.5×10^5 for the 28 ft/sec freestream velocity and 9.1×10^5 for the 102 ft/sec freestream velocity. However, the boundary layer profile at the jet exits was always turbulent due to the early transition caused by the sandpaper strip glued to the flat plate. Moore (Ref.96) obtained boundary layer profiles at the nozzle location for the same model and found that the boundary layer thickness was 0.75 in (1.91cm) for 28.31 ft/sec (8.63 m/sec) freestream velocity and 0.56 in (1.42 cm) for 51.47 ft/sec (15.69 m/sec). His results are shown in Fig.25. Freestream temperature varied according to seasonal atmospheric conditions, ($40°F$ - $90°F$). Since the jet temperature was around $100°F$, hot wire measurements were done during the summer and warm fall days,

when the temperatures changed from 65 to 90° F to minimize temperature variations in the flow.

In Figs. 26 through 31, jet exit velocity profiles which were obtained when there is no crossflow are presented. These are the jet exit profiles for 90° rectangular jets, 60° rectangular jets, circular jet with low exit turbulence and no swirl, circular jet with 40% swirl, circular jet with 58% swirl and circular jet with high exit turbulence. These profiles were obtained by using the five hole yawhead probe except for the circular jet with high exit turbulence case, which was obtained by using a Pitot tube. All the circular jets were injected with a 90° angle to the freestream. In order to obtain 40% swirl, air pressure at the larger tube, which fed two tangential tubes connected to the circular jet nozzle was kept at 5 PSI. This pressure was 30 PSI for 58% swirl. For jets with swirl, the swirl ratio was defined as the ratio of the swirl component of the velocity at $X/D \cong 0.41$ to average total velocity. As can be seen from the figures, uniformity of the profiles were quite satisfactory. For most cases, jet exit velocities were in the 200-220 ft/sec (61-67 m/sec) range. Jet exit velocity for the circular jet with the high exit turbulence was about 115 ft/sec (35 m/sec) due to the additional drag caused by the turbulence generating screen.

Pressure distribution and mean flowfield measurements were done while running the blowers at maximum speed. For these cases, jet exit temperature reached up to 110°F. (43°C). Turbulence measurements were done at a little lower blower speed. This helped to reduce the jet exit temperature to 100°F (

38°C) as mentioned before. This also caused about 5 % reduction in the jet exit velocity. The tunnel speed was adjusted accordingly.

In Fig.32, the jet exit turbulence profile for the 90° rectangular jet is given. As can be seen from this figure, exit turbulence intensity was about 3%. Since they had quite similar nozzle geometries, the turbulence profile for the 60° rectangular nozzle was about the same.

In Fig.33, circular jet exit turbulence profiles are given compared with the cases of Refs.10,11 and 12. The no swirl, low turbulence case had about 3% exit turbulence, which was close to the case of Ref.12. For the case of that reference, turbulence was a little higher at the center due to an additional inner pipe used inside the nozzle. The exit turbulence of Refs.10 & 11, which was measured about 1 cm from the exit, was about 8 to 9 % and had a uniform profile. For the high exit turbulence case of the present research, the turbulence level was about 10 to 12 % for the inner region, but it was considerably higher at the edges due to the way the turbulence generating screen was manufactured.

Chapter 3

EXPERIMENTAL TECHNIQUES AND DATA REDUCTION

For each run, first the jet blowers were turned on, and then the tunnel speed was adjusted for the required jet to freestream velocity ratio.

3.1 PRESSURE DISTRIBUTION MEASUREMENTS

The part of the model surface which was instrumented with the pressure taps was divided into a number of subdivisions, and each of these subdivisions contained 46 or less pressure taps. Every pressure tap in the same subdivision was connected to a certain connector, which could be connected to one of the Scanivalves. There were 23 subdivisions for the 90° and 60° rectangular jets, and

the number of subdivisions was 16 for circular jets. Since there were 12 Scanivalves available, not all of the pressure ports could be scanned in one run. First, the connectors belonging to the first 12 subdivisions were connected to the Scanivalves, and the rest of the connectors were sealed to prevent air leakage into the test section. The remaining subdivisions were scanned later.

At each run after reaching the required velocity ratio, the computer program, which was written for scanning the pressure ports, reading and storing data, was started on its run. This program first connects the first transducer to the digital voltmeter through the channel selector. After opening each port, the program waits 1 second and then takes a sample from the digital voltmeter. This first sample will be thrown away. Then, the program takes 25 more samples, takes their average and keeps this in the memory. After this process, the program opens another port. After completion of the first Scanivalve, the program connects the second transducer to the digital voltmeter, and this goes on until all the Scanivalves have been scanned. Storage of the data onto a floppy disc completes the run. As mentioned before, each Scanivalve had 48 ports. The 47th port was open to the atmosphere (reference pressure), and the 48th port was connected to a 1 PSI constant pressure source. These two ports were needed for the calibration of the transducer which was connected to that particular Scanivalve. For each velocity ratio, tare readings were also obtained by running the tunnel at the same speed but with the jets off and the jet exit areas closed flush with the model surface.

Nondimensionalized pressure coefficients have been obtained for jet(s) on and off cases by the following formula;

$$C_p = \frac{p - p_\infty}{q_\infty} \tag{3.1}$$

and the data is plotted as

$$\Delta C_p = (C_{p,jet\ on} - C_{p,jet\ off}) \tag{3.2}$$

Before plotting, ΔC_p values were transferred to the mainframe computer of the university and matched with their corresponding coordinate locations. The results are plotted as isobars by a computer program by California Computer Productions, Inc.. Information about this program is given in Ref.83. The computer programs used for data gathering and reduction and an example input file for the plottting program can be seen in Appendix A.

An aspect about these experiments is in the measurement of tare ($C_{p,jet\ off}$) and calculation of ΔC_p . Sometimes jet(s) on and jet off cases might have same freestream velocity but different q_∞ due to slight changes in ambient conditions. However, q_∞ seems more fundamental then the freestream velocity. In such cases, q_∞ should match rather than U_∞, or the jet off case should be normalized with the q_∞ of the jet on case. This may particularly be important for low freestream velocities, like for R=8 cases where the pressures generated on the surface were low. Care was taken about this issue.

3.2 MEANFLOW MEASUREMENTS

Mean flow measurements have been carried out by using the yawhead probe described in Chapter 2. A computer program scanned the five ports of the yawhead probe for each location. After opening a port, the program waited 6 seconds, then sampled 25 readings from the digital voltmeter and took their average. The program also recorded the freestream dynamic pressure and temperature. Three components of the velocity vector are first obtained in probe coordinates, and then the necessary coordinate corrections were made for plotting. Probe coordinates and flow angles with respect to probe are defined in Fig.18. In this figure, the locations of the five holes can also be seen. The dimensionless pressure coefficients for data reduction are given as;

$$
\begin{aligned}
C_{p_{pitch}} &= (P_4 - P_5)/A = f_1(\alpha, \beta) \\
C_{p_{yaw}} &= (P_2 - P_3)/A = f_2(\alpha, \beta) \\
C_{p_{total}} &= (P_1 - P_T)/A = f_3(\alpha, \beta) \\
C_{p_{static}} &= (P_{S,avg} - P_S)/A = f_4(\alpha, \beta)
\end{aligned}
\tag{3.3}
$$

where,

$A = P_1 - P_{S,avg}$

$P_{S,avg} = (P_2 + P_3 + P_4 + P_5)/4$

P_T = *Total pressure*

P_S = *Static pressure*

α = *Pitch angle*

β = *Yaw angle*

Since P_1 through P_5 are measured, $C_{P_{pitch}}$, $C_{P_{yaw}}$, $P_{S,avg}$ and A can be calculated immediately. Then, α and β can be found from the available calibration curves f_1 and f_2. Next, $C_{P_{total}}$ and $C_{P_{static}}$ can be found from the calibration curves f_3 and f_4. After this, the total and static pressures can be calculated by

$$\begin{aligned} P_T &= P_1 - A \times C_{P_{total}} \\ P_S &= P_{S,avg} - A \times C_{P_{static}} \end{aligned} \tag{3.4}$$

The total velocity can be found from the Bernoulli's equation for incompressible flows.

$$P_T - P_S = \frac{1}{2}\rho_\infty V^2 + \frac{1}{2}\rho_\infty \overline{v'^2} \tag{3.5}$$

The turbulence term can be neglected; the error caused by this assumption is around 1 % for up to 14 % turbulence intensity. Thus

$$V = \sqrt{\frac{2(P_T - P_S)}{\rho_\infty}} \tag{3.6}$$

gives the total velocity. Finally, the components of this velocity in the probe coordinates can be found as

$$\begin{aligned} V_x &= |V| \cos\alpha \cos\beta \\ V_y &= |V| \sin\beta \\ V_z &= |V| \sin\alpha \cos\beta \end{aligned} \tag{3.7}$$

There were two different set of calibration curves and corresponding data reduction programs available for data reduction. The first calibration was made by Lee (Ref.81), and his approach was influenced by the method of Treaster and Yocum (Ref.84). Lee defined the probe angle of attack and bank angle for easy calibration. His calibration was valid up to ± 42° flow angles with respect to the probe axis. His data reduction program used a two dimensional interpolation subroutine called IBCIEU of the International Mathematical and Statistical Libraries (IMSL) for obtaining flow angles and $C_{p_{total}}$, $C_{p_{static}}$ from the calibration curves. This provided good accuracy at the cost of CPU time. The second calibration was made by Sung (Ref.82). Sung calibrated the yawhead probe up to 60° flow angles and developed a method based on that of Gerner *et al* (Ref.85) for determining flow properties. Sung divided his calibration curves into five different regions based on flow angularity with respect to the probe and obtained different data reduction equations for each region. For example, if for a particular data, P_1 is the maximum pressure, this data should be reduced by the data reduction equations of zone#1. If P_2 was the maximum pressure, equations of zone#2 should be used, etc. In his program, fourth order polynomial equations are used in the following form;

$$\begin{aligned} \theta(\alpha \textit{ for zone\#1}) &= f_1(B_1, B_2) \\ \varphi(\beta \textit{ for zone\#1}) &= f_2(B_1, B_2) \\ C_{p_{total}} &= f_3(B_1, B_2) \\ C_{p_{static}} &= f_4(B_1, B_2) \end{aligned} \tag{3.8}$$

θ = *cone angle*

φ = *roll angle* (*see Fig.*18)

For the first zone (lowest flow angularity zone), B_1 was equal to $C_{p_{pitch}}$, and B_2 was equal to $C_{p_{yaw}}$. For other zones, B_1 was the cone angle coefficient, and B_2 was the roll angle coefficient defined as (for ith zone);

$$C_{p_{cone}} = \frac{P_i - P_1}{q'}$$

$$C_{p_{roll}} = \frac{P_{icc} - P_{ic}}{q'} \tag{3.9}$$

$$q' = p_t - \frac{P_{ic} + P_{icc}}{2}$$

where

P_i : highest pressure from P_2 to P_5

P_{ic} : pressure from the port next to P_i in clockwise

P_{icc} : pressure from the port next to P_i in counterclockwise.

Sung's program was much faster in CPU time when compared to Lee's program. Also, because of its advantage of handling flow angles up to 60°, this second program was preferred for reducing the majority of the data of the present research. However, some of the earlier data was reduced with the first program. Both of the programs were tested for a group of data, and no practically important differences were observed.

Using a five hole probe is a good way of obtaining mean flow information. It provides magnitude and direction of the velocity vector accurately in a cheap,

easy and fast way. It also measures total and static pressures which can not be measured by hot wire or LDV. Sistla (Ref.19) investigated the temperature sensitivity of the yawhead probe by conducting measurements in cold air and at $200°F$ ($93° C$) for low velocities (10-20 ft/sec) and couldn't see any sensible effect. Uncertainities of the five hole probe, which was used for our experiments, were reported by Sung (Ref.82) as follows:

1. The RMS (root mean square) error of the pitch angle 3.93°
2. The RMS error of the yaw angle 2.36°
3. The RMS error of the total pressure was 4.82 % of the actual total pressure
4. The RMS error of the dynamic pressure was 5.33 % of the actual dynamic pressure.

According to Ref.87, the error in $C_{p_{pitch}}$ due to turbulence is 0.67 % for 10 % turbulence intensity and 2.68 % for 20 % turbulence intensity. From the same reference, the error in total velocity is 0.33 % for 10 % turbulence intensity. Again, according to same reference, there were no Reynolds number effects. As far as wall effects are concerned, a yawhead probe should be kept at least two probe diameters away from a solid wall (Ref.87). This condition was always satisfied for the present research. More information about these type of probes and error sources can be found in Refs.87 and 88.

3.3 TURBULENCE MEASUREMENTS

The jet exit turbulence levels presented in Chapter 2 were measured with a single normal hot wire probe without using a linearizer. Data reduction formula for these measurements can be obtained from the following hot wire response equation.

$$E^2 = E_0^2 + BU^n \tag{3.10}$$

U : velocity

E : voltage corresponding to U

E_0 : voltage corresponding to $U = 0$

n : constant, its value is approximately 0.45 for most applications.

Differentiating eq. 3.10

$$2EdE = BnU^{n-1}dU$$

and writing eq. 3.10 in the form

$$E^2 - E_0^2 = BU^n$$

gives

$$\frac{2EdE}{E^2 - E_0^2} = n\frac{dU}{U}$$

Finally this can be written as

$$\frac{\sqrt{\overline{u'^2}}}{U} = \frac{2}{n}\frac{E}{E^2 - E_0^2}e_{RMS} \tag{3.11}$$

When using this formula, one should be carefull about measuring E and E_0 at the same fluid temperature. Otherwise, for small temperature differences, a correction given in Ref.89 can be applied by multiplying E by

$$\left(\frac{t_s - t_{E_0}}{t_s - t_E}\right)^{\frac{1}{2}} \tag{3.12}$$

t_s : sensor temperature

t_{E_0} : fluid temperature when E_0 was measured

t_E : fluid temperature when E was measured.

Turbulence in the plumes of the jets was measured with an X-wire probe which was supported by the probe rotator mechanism mentioned in Chapter 2. An overheat ratio of 1.8 was used. Before and after each run, the probe was placed in the freestream with zero pitch and zero roll angle, and a calibration check was made. At zero pitch and zero roll angle, the probe coordinates were parallel to the coordinate system chosen for this research, and the probe axis was aligned with the freestream direction. At zero pitch but 90° roll angle, the probe X coordinate was parallel to the main X coordinate, but the probe Y coordinate was parallel to the main Z coordinate. What is meant by checking the calibration is checking if the linearized outputs of sensor#1 and sensor#2 were linear functions of U, both passing through zero and both having the same gain for the same

U. In other words, it was checked if the calibration curves in the form given in Fig.23 could be obtained. The matter of what voltage corresponds to what velocity was actually not important, because turbulence intensities were obtained as ratios of R.M.S. voltages to D.C. voltages, and it was not our intention to measure the magnitude of the mean velocity by hot wire. If at the end of a run there was an important change in the calibration such as the gain of sensor#1 was different than the gain of sensor#2, which happened once, that data was thrown away.

All the measurements were done for the Y=0 plane. After calibration check, the X location of the probe was set by hand. Then, the smallest Z location was set by using the Z traverse. The next step was turning the jet(s) and wind tunnel on and obtaining the desired velocity ratio. Then, the computer program named XWIRE was started (see Appendix B for details of this program). This program actually sets the Z location and the pitch angle of the probe and reads data for three different roll angles. Then, it reduces this data and stores the results onto a floppy disc. At each measurement point, the pitch angle of the velocity vector was known from the previously made yawhead measurements. This helped to align the hot wire probe with the probe direction in the X-Z plane. This was necessary because it is known that serious errors can happen if the flow makes more than about a 10° angle with the probe axis. Data readings were made at 0° , 90° and 45° roll angles. Before each reading, the stability of D.C. and R.M.S. voltmeters were checked by eye. After the READ command, the computer waits an additional three seconds and takes the average of 20 samples for

each voltage being read. Before each reading, the range of the R.M.S. voltmeter was checked and adjusted, if necessary, for the maximum possible accuracy.

Defining D.C. output of sensor#1 as A and of sensor#2 as B and R.M.S. output of sensor#1 as "a" and of sensor#2 as "b", the following formulas were used for obtaining turbulence quantities. These formulas were written for **probe coordinates** and normalization was made with the local total mean velocity.

$$
\begin{aligned}
U_p &= [(A + B)_0 + (A + B)_{90} + (A + B)_{45}]/3. \\
V_p &= (A - B)_0 \\
W_p &= (A - B)_{90} \\
U_T &= \sqrt{U_p^2 + V_p^2 + W_p^2}
\end{aligned}
\tag{3.13}
$$

0,90,45: roll angles

p : probe

U_T : total mean velocity

$$
\begin{aligned}
\sqrt{\overline{u_p'^2}} &= [\overline{(a + b)_0} + \overline{(a + b)_{90}} + \overline{(a + b)_{45}}]/3. \\
\sqrt{\overline{v_p'^2}} &= \overline{(a - b)_0} \\
\sqrt{\overline{w_p'^2}} &= \overline{(a - b)_{90}} \\
\overline{u_p'v_p'} &= \overline{a_0^2} - \overline{b_0^2} \\
\overline{u_p'w_p'} &= \overline{a_{90}^2} - \overline{b_{90}^2} \\
\overline{v_p'w_p'} &= -\overline{v_p'^2} - \overline{w_p'^2} + \overline{(a - b)_{45}^2}
\end{aligned}
\tag{3.14}
$$

Now, these quantities can be written in the coordinate system of this research, γ being the pitch angle of the probe:

$$
\begin{aligned}
\sqrt{\overline{u'^2}} &= \sqrt{\overline{u_p'^2}\cos^2\gamma + \overline{w_p'^2}\sin^2\gamma - 2\,\overline{u_p'w_p'}\cos\gamma\sin\gamma} \\
\sqrt{\overline{v'^2}} &= \sqrt{\overline{v_p'^2}} \\
\sqrt{\overline{w'^2}} &= \sqrt{\overline{u_p'^2}\sin^2\gamma + \overline{w_p'^2}\cos^2\gamma - 2\,\overline{u_p'w_p'}\cos\gamma\sin\gamma} \\
\overline{u'v'} &= \overline{u_p'v_p'}\cos\gamma - \overline{v_p'w_p'}\sin\gamma \\
\overline{u'w'} &= \overline{u_p'^2}\cos\gamma\sin\gamma + \overline{u_p'w_p'}\left(\cos^2\gamma - \sin^2\gamma\right) - \overline{w_p'^2}\cos\gamma\sin\gamma \\
\overline{v'w'} &= \overline{u_p'v_p'}\sin\gamma + \overline{v_p'w_p'}\cos\gamma
\end{aligned}
\tag{3.15}
$$

Equations 3.15 can be nondimensionalized by dividing the first three equations by U_T and the last three by U_T^2. After this these equations can also be obtained in the form normalized with the freestream velocity (U_∞). For this, the first three equations should be multiplied by

$$\frac{U_T}{U_\infty}$$

and the last three equations should be multiplied by

$$\left(\frac{U_T}{U_\infty}\right)^2 \quad .$$

The value of U_T/U_∞ was known from the previously made yawhead measurements. U_T/U_∞ could also be measured with hot wire, but this was not done in order to eliminate effect of any temperature differences at the measurement locations of U_T and U_∞ .

For hot wire measurements, changes in the mean temperature field may cause important errors on the magnitude of the mean velocity, but such errors are not important for turbulence intensities (see Ref.92). For example, the effect of temperature on the calibration curves of Fig.23 can be shifting the zeros and

drifting of the gains. Zero shift effect was checked and found to be negligible. If the temperature drift of the gains are the same for both wires (normally it should be), then there will be no error due to temperature for the turbulence intensities normalized with the local total velocity. This fact allowed us to permit some temperature difference between jet(s) and freestream, jet(s) being hotter. However, the temperature in the plumes of the jet(s) was continuously monitored by a thermocouple which was placed about 2.5in behind the hot wire probe. It was observed that there was not much temperature difference between the jet plume and freestream due to rapid mixing of two streams. Particularly, for the rear stations this difference was less then a few $^{\circ}F$. On the other hand, temperature fluctuations might be an important source of error, especially for the regions very close to the jet exit where the correlation between temperature and velocity fluctuations may be significant (see Ref.95). Since the probe was always aligned with the flow direction with the aid of the pitch mechanism, the errors which could occur due to flow angularity were also minimized. For reference, according to Ref.91 for a 10° angle, the error is less then 1.5 %. However, one should be cautioned for the locations with more then 30 % turbulence. The hot wire is not a very suitable technique for this type of situation due to the possibility of reverse flow. However, in our case, the flow direction was known. There is a considerable literature available on hot wire measurements and errors. Some of the earlier ones (up to 1969) are listed in Ref.93, and a review article published in 1979 (Ref.94) is also useful.

Chapter 4

RESULTS

In this chapter, experimental results obtained from surface pressure distribution, mean flow field and turbulence measurements will be presented.

4.1 PRESSURE DISTRIBUTION MEASUREMENTS

As also mentioned in Chapter 3, the pressure distribution results will be presented here as;

$$\Delta C_p = (C_{p_{jet\ on}} - C_{p_{jet\ off}}) \tag{4.1}$$

and C_p is defined as;

$$C_p = \frac{p - p_\infty}{q_\infty} \tag{4.2}$$

Here $C_{p_{jet\ on}}$ is the pressure coefficient obtained when the jet(s) and freesream were on. $C_{p_{jet\ off}}$ is the pressure coefficient when the jet(s) off and their exit area closed flush with the model surface, but freestream was on at the same velocity with the jet(s) on case. This method of presentation eliminates the small effects which might be due to model details and irregularities, etc. The surface pressure distribution tests were carried out for rectangular jets which are aligned at 90° or 60° angle with respect to the freestream as a single jet or side-by-side dual jets. Tests were also carried out for a single circular jet at a 90° angle with respect to the freestream. Circular jets with low exit turbulence, with high exit turbulence, and with two different swirl ratios were the different configurations tested. For most of these configurations pressure distributions were obtained for jet to freestream velocity ratios of 2.2, 4.0, and 8.0. The only exception is the circular jet with high exit turbulence. For this case, tests were carried out for R = 2.2 and 4.0.

For most of the pressure distribution results presented in this chapter thin isobar lines are drawn with ΔC_p = 0.2 intervals, and thick isobar lines are drawn with ΔC_p = 1.0 intervals. Thin lines are omitted when the lines are very close to each other, but thick lines are not. An exception to this rule is Fig.40. For this figure thin lines are drawn with ΔC_p = 0.4 intervals, and thick lines are drawn with ΔC_p = 2.0 intervals. All the results are plotted with the same scale (except Fig.40), so the dimensiones and areas are comparable.

4.1.1 90° Rectangular Jets

Pressure distribution results for 90° rectangular jets are presented in Figs. 34 through 40. In Fig.34, one can see the results for a single jet with R=2.2. Observe the large area influenced with negative pressures which extends towards the sides and downstream from the jet leading edge. In front of the jet, there is a positive pressure region due to deceleration of the freestream. There are very high negative pressures at both sides of the front corners, which should be due to sharp and sudden changes in the magnitude and direction of the velocity vector and flow separation. Although lower in magnitude, there is another high negative pressure region around the rear corners. This should also be due to flow separation and other effects. The pressure distribution is quite symmetrtic, and the high negative pressures in the close vicinity of the jet decays rather fast. By increasing jet to freestream velocity ratio to 4.0, the downstream extent of the negative pressures reduces, but their upstream extent increases. This can be seen by observing the shift of the pressure line labeled "0.0" from Fig.34 to Fig.35. Negative peak pressures at the front corners are also larger. The effect of the rear corners reduces. The decay of negative pressures is slower, and this is why the $\Delta C_p = -0.2$ line covers a larger area. There is again a positive region in front of the jet, however this region has a smaller area when compared to R=2.2. Increasing the velocity ratio to 8.0 as shown in Fig.36, further reduces the downstream extent of the negative pressures and increases their extent towards the sides and upstream. Again, there is a positive region in front of the jet, which is

surrounded by the negative pressure region from all sides. Decay of the negative pressures is even slower (see the larger area covered by $\Delta C_p = -0.2$ line). However, the sharp peaks at the front corners seem to be less in magnitude when compared to the R=4.0 case.

For 90° rectangular jets, the flow structure in the close vicinity of the front corners is quite complicated. In particular, the magnitude and location of the peak negative pressures are interesting to observe. For these reasons, these areas are enlarged in Fig.40. At the right hand side of Fig.40, compare the front corner regions of the single jets for R=2.2, 4.0 and 8.0. Unfortunately, there were only one or two pressure taps available to measure the location and magnitude of these peak negative pressures in these small areas. The asymmetry seen for R=4.0 and 8.0 can be due to imperfections of the jet exit velocity or they can also be due to uncertainity caused by an insufficient number of pressure taps. However, the general trend is observable. The locations of the negative peaks are a little closer to the front edge for R=4.0 and R=8.0 when compared to R=2.2. The magnitude of the peaks increases when the velocity ratio increases from 2.2 to 4.0. They decrease again when the velocity ratio is increased to R=8.0.

The experimental results for 90° rectangular jets given in Appendix D and also in Ref.13 are actually the earlier versions of these tests, and they also show the same trend for the region around front corners. The only difference between those earlier results and these new ones is, the jet exit velocity profile had some nonuniformity for the earlier tests. However, this difference wouldn't effect the flow structure near the front corners. One argument is quite helpful to under-

stand what is happening by changing the velocity ratio. The R=2.2 case is closer to the case of R=0, and for R=0, the jet is off, and the freestream is the only stream. Assuming the jet exit area is closed flush with the surface, there would be no negative or positive pressure regions on the flat plate surface. The case R=8.0 is closer to R= ∞, and for R= ∞, the jet is the only stream and freestream is off. For R= ∞, there will be negative pressure areas around the jet exit which are distributed symmetrically towards upstream, downstream and sides. However, there will not be sharp negative corner peaks based on interaction of two streams. The case R=2.2 has the highest freestream dominancy when compared to R=4.0 and R=8.0. That is why for this case, one doesn't observe upstream extension of negative pressure areas. Increasing the velocity ratio to 4.0 reduces the dominancy of the freestream and increases the dominancy of the jet. Thus, negative pressure areas start moving upstream. It seems like this also increases the degree of interaction between the two streams, which causes higher negative pressure peaks around the front corners. For R=8.0, dominancy of the jet is quite observable on the pressure distribution. Also, the degree of interaction between two streams starts reducing again, and this causes front corner peaks with lower magnitudes.

Results for 90° side-by-side, dual rectangular jets are presented in Figs. 37, 38 and 39, for R=2.2, 4.0 and 8.0. Most of the arguments made for the single jet are also valid for this configuration. Dual jets produce a larger negative pressure area particularly towards the downstream. This is quite clear when one observes how the "0.0" line in the downstream area moves by changing the

configuration from single jet to dual jets. Again, the decay of negative pressures slows down by increasing velocity ratio. This is clear when one observes, for example, how the area covered by $\Delta C_p = -0.2$ line enlarges with increasing velocity ratio. Also, the upstream extent of negative pressures increases with increasing velocity ratio.

The flow between two jets and the influence of each jet on the other causes additional complication on the flow structure for dual jets. These effects increase with increasing velocity ratio. Looking at Fig.37 for R=2.2, one can still say that there is some symmetry on the inner and outer sides of each jet. This is no longer true for R=4.0 and 8.0. For these cases, symmetry is valid with respect to a line passing from the middle of the two jets and parallel to the freestream. However, the inner and outer sides of each jet are not symmetric. For example, if one compares the inner corner peaks to the outer corner peaks for R=8.0 in Fig.40, the inner peaks have magnitudes like -25.3 and -30.2 and the outer peaks -10.5 and -14.7. The outer side of each jet behaves more like one side of a single jet, which is not true for the inner sides. Also, negative pressures with higher magnitude and larger area effect the surface. Comparing the areas covered by the -1.0 line for a single jet (R=4.0) and for dual jets (R=4.0), one can see that for dual jets, the -1.0 line covers an area larger than twice the area covered for single jets. One thing that should be remembered is that by further increasing the velocity ratio (even more than 8.0) the effects of channel flow between the jets will start reducing, but the effect of one jet on the other area will continue to increase due to weaker crossflow and stronger jets.

4.1.2 60° Rectangular Jets

Pressure distribution results for 60° injection are presented in Figs. 41 through 46. These results are qualitatively similar to the 90° rectangular jet results. The same things can be said about the effects of velocity ratio or the differences of single and dual jets. However, the interaction of 60° jet(s) with the freestream is smoother, and this produces lower magnitude negative pressure areas in the near vicinity of jet exits. Comparing single jet results for R = 4.0 for 90° and 60° (Figs. 35 and 42), one can see that the areas covered by 0.0 line haven't been influenced much. However, the area covered by -0.2 line is lesser, and the area covered by -1.0 line is even less for 60° jets.

For the 60° jets, one no longer sees dramatically high negative pressure peaks around the front corners. Instead of negative pressure peaks to -16.0 as for 90° jets, the maximum peak for 60° jets is abaut -4.0. The importance of the rear corners seems to increase for the 60° jets. One observes higher magnitude negative pressures around these corners. One can compare dual rectangular jets for R = 4.0 from Figs. 38 and 45. Again, the area covered with lower magnitude negative pressures doesn't seem to be influenced too greatly. However, the area covered by the -1.0 line is clearly lesser for 60° jets, and the area covered by the -2.0 line is much less. Instead of peak negative pressures of -16.0 for 90° jets, the peak pressure for 60° jets is about -4.0 around the front corners. On the other hand, the inside rear corners of the 60° dual jets produce negative pressures of roughly -5.0 in magnitude, which is not found for 90° jets at R = 4.0. It seems that there

is a strong flow interaction around the rear corners for 60° jets. These same things can be said for the other velocity ratios too. However, for R = 2.2, even the low magnitude ΔC_p lines, like 0.0 and -0.2, cover a smaller area (compare Fig. 34 to 41 and Fig. 37 to 44). This might be due to stronger crossflow effects. Like the 90° jets, the 60° jets also produced symmetric pressure distributions.

4.1.3 90° Circular Jet

Pressure distribution results for the 90° single circular jet in the baseline configuration are presented in Figs. 47 through 49. As explained in Chapter 2, this jet had a uniform exit velocity profile with low turbulence ($\cong$ 3 %). The jet exit area was the same as the exit area of the single rectangular jet. The circular jet causes more blockage of the freestream, and the negative pressures extend to a larger area towards the sides and downstream (compare Figs. 34-37 to 47-49). However, the circular jet has a smoother interaction area with the freestream. Since it doesn't have sharp front corners, one doesn't observe the sharp negative peak pressures of rectangular jet front corners. The negative pressures are distributed more evenly around a circular jet, but they cover larger areas (compare the -1.0 line for 90° circular and rectangular single jets). There are similarities with rectangular jets on the development of the pressure field with increasing velocity ratio. There is always a positive pressure region in front of the jet due to flow deceleration. For R = 8.0 these positive pressures are surrounded with negative pressures from all sides. The downstream extent of negative pressures de-

creases with increasing velocity ratio, and their upstream extent increases. Higher magnitude negative pressures are produced around the jet for R=4.0 and 8.0 when compared to R=2.2. The decay of negative pressures becomes faster towards the downstream but it gets slower towards sides when increasing velocity ratio (compare the distances between -0.2 and -1.0 lines). Maximum magnitude negative pressures are produced either on or a little rear of the largest width of the circle. To understand this phenomena, one should consider the effects of crossflow acceleration towards these locations and flow separation.

The pressure distribution can be judged as symmetric, particularly when looking at the areas a little away from the jet exits. For R=2.2, the -1.0 line shows some asymmetry. The reason for this might need further investigation, but there are also some clues. Some geometries are not always suitable for producing symmetric loads. A cylindrical missile body may produce asymmetric loads due to asymmetric vortex shedding under a crossflow, while a sharp edged delta wing wouldn't do the same thing under the same conditions. Perhaps there is an analogous situation for jets in a crossflow with low R.

4.1.4 90° Circular Jet With High Exit Turbulence

The results presented in Figs. 50 and 51 for R=2.2 and 4.0 belong to a circular jet with a uniform velocity profile but high exit turbulence. Information about this jet was given in Chapter 2. Exit velocity and turbulence profiles were given in Figs. 31 and 33. At the central part of the jet, turbulence was around 10

%, but at the edges it was considerably higher. By increasing the jet exit turbulence, the size of the negative pressure area was reduced (compare 0.0, -0.2 and -1.0 lines for the same velocity ratios from Figs. 47 and 48 vs. Figs. 50 and 51). It seems increasing exit turbulence also helped to produce more symmetric pressure distributions (compare the -1.0 lines for R = 2.2). The maximum magnitudes of negative pressures didn't seem to change for R = 2.2 which are between -3.0 and -4.0 for low and high exit turbulence cases. The same is true for R = 4.0. For this velocity ratio, the maximum magnitudes are between -5.0 and -6.0 for both cases. Since the maximum values did not change, but the area around them reduced, the decay of negative pressures is, obviously, faster for the high turbulence case.

4.1.5 90° Circular Jet With Swirl

Results for the circular jet with swirl are presented in Figs. 52 through 57. These tests were carried out for two different swirl ratios (40 % and 58 %) and for three different velocity ratios (R = 2.2, 4.0 and 8.0) for each swirl ratio. Jet exit profiles and the definition of the swirl ratio were given in Chapter 2. In Figs. 52 through 57, the swirl direction is shown. Swirl is more influential on the areas close to the jet exit. It is also more influential for the low velocity ratios. The R = 2.2 case shows the highest swirl effect. Naturally, 58 % swirl produces more swirl effect than the 40 % swirl.

Now, for R = 2.2 look at the results for low turbulence, high turbulence, 40 % swirl, 58 % swirl together (Figs. 47, 50, 52 and 55). At the left rear side of the jet, the swirl flow and crossflow run together. They accelerate each other to a higher velocity, thus producing higher magnitude negative pressures around this location. It is logical to think that swirl even delays the separation of the crossflow. For the right rear side of the jet, the swirl flow runs against the crossflow. They decelerate each other and cause a reduction in the magnitude of negative pressures. For 40 % swirl, the maximum negative pressure around the left rear side is between -5.0 and -6.0. This value is about -3.0 for the right rear side. For 58 % swirl, the maximum negative pressure at the left rear side is between -8.0 and -9.0, and this value is between -2.0 and -3.0 for right rear side. For 40 % swirl, the area covered by -0.2 line seems to be close to the area for the low turbulence, no swirl case. However, an asymmetric pressure distribution is visible even for the far field. For 58 % swirl, the asymmetric pressure distribution in the far field is even more pronounced (see the shape of -0.2 line or 0.0 line). Now, if one looks at the circular jet results for R = 4.0 (Figs. 48, 51, 53, 56) there is little difference between the low turbulence, no swirl data and the 40 % swirl data. Swirl effects are still visible for 58 % swirl at a reduced rate when compared to R = 2.2. For R = 8.0, the pressure distribution around the jet is nearly symmetric, indicating a lessened direct influence of the swirl.

4.2 MEAN FLOWFIELD MEASUREMENTS

Mean flowfield measurement results are presented in Figs. 58 through 85. These measurements were done for 90° and 60° side-by-side dual rectangular jets, single circular jet, single circular jet with high turbulence, single circular jet with 40 % swirl and single circular jet with 58 % swirl. Most of the data was obtained for a jet to freestream velocity ratio of 4.0 chosen as representative. For 90° rectangular jets, data for R=2.2 is also available. The results are presented in X=constant, Y=constant, and Z=constant crossections. A velocity vector presented in X=constant crossection represents the Y and Z components of the total velocity vector. All the figures representing the X=constant and Y=constant planes are plotted with the same scale, so geometric dimensions are comparable. All the figures representing the Z=constant planes also have same scale. However, their scale is about 64 % of the scale of X=constant and Y=constant figures. As mentioned before, meanflow data presented here was taken with the yawhead probe described in Chapter 2.

4.2.1 90° Side By Side Dual Rectangular Jets

Results for 90° side by side dual rectangular jets are presented in Figs. 58-61 for R=2.2 and in Figs. 62-65 for R=4.0. During the tests, both jets were on, but measurements were made only for the jet at the Y=0.0 in. location.

From Fig.58, one can see that penetration height of the center of the jet plume for R=2.2 is about 6 inches. Little actual flow reversal is seen at these measurement stations. From the X=0.0 in. and X=2.0 in. crossections, vortical flow formation at both sides of the jet is quite clear. When looking at these figures one should imagine that the same type of flow structure also exists for the jet at Y=4.0 in. location. At low Z locations, the jet sucks in the outside air, and for the high Z locations, the jet spreads out. The same type of flow can be observed for R=4.0. For that case, the penetration height is about 12 inches, and somewhat more flow reversal is evident right behind the jet column.

4.2.2 60° Side By Side Dual Rectangular Jets

These results are given in Figs. 66-70 for R=4.0. Data were taken for the jet at Y=4.0 in. location, when both jets were on. Of course, interaction of two streams is smoother, and the jet penetrates to a lower Z distance compared to 90° injection. From Fig.66, one can say that the penetration height is about 9 inches. There is no flow reversal. A plot of velocity vectors in the Y=2.0 in. plane given in Fig.67, which is the plane at the middle of the two jets, shows how crossflow is drawn down for low Z locations and bent up for high Z locations under the effects of the vortical flow. The vortices in the plume are much smaller than for the 90° case.

4.2.3 90° Circular Jet

Results for a single circular jet with low turbulence and no swirl injected into a crosstream with a 90° angle are given in Figs. 71-74. From Fig.71, the penetration height seems around 10.5 in. (Z/D = 5.38). Lower penetration when compared to 90° rectangular jets is logical, because a circular jet has a larger area against the freestream, which increases the bending power of the freestream. It should be remembered that the rectangular jet results presented earlier in this section were obtained for side-by-side, dual jets. Here, there are larger regions of stronger reverse flow observable. The flowfield might be judged as symmetric by the cross-plane results. Again, flow separation and vortex formation in the jet is clear. In Fig.74, for Z/D locations lower than 2.0, one observes small right-left asymmetry at X/D $\cong$ 1.0. However, this small difference might well be a true feature of the flowfield rather than a result of some small defect.

4.2.4 90° Circular Jet With High Exit Turbulence

These results are presented in Figs. 75-77. Jet exit velocity and turbulence were given in Chapter 2. It seems increasing the turbulence reduced the penetration height. Penetration height can be said to be about 9.5 in. (Z/D = 4.87) for R = 4.0. It seems increasing the turbulence reduced the penetration height. Also, it is interesting to note that comparison of Fig.71 with Fig.75 shows that the

highly turbulent jet entrains more air in from the rear. This can be seen by comparing velocity vectors around X/D=0.5.

4.2.5 90° Circular Jet With Swirl

These results are presented in Figs. 78-81 for 40 % swirl and in Figs. 82-85 for 58 % swirl. The direction of the swirl is clear in the Z/D=constant figures. For the X/D=constant figures, the swirl velocity is in the same direction as the freestream for negative Y/D's, and in the opposite direction for positive Y/D's. For 40 % swirl, the penetration height is about 10 in. (Z/D=5.13), and for 58 % swirl, the penetration height is around 7 in. (Z/D=3.59). It is clear that the swirl effect is very strong for 58 % swirl. For this swirl ratio, there is more than a 30 % reduction in penetration height when compared to the no swirl case. In Fig.84, asymmetric vortex formation can be observed. The vortex on the left hand side of this figure has higher velocities, and its core is closer to the flat plate surface when compared to the other one. The left hand side of this figure is the side where the swirl velocity and crossflow velocity accelerate each other, and the right hand side of this figure is the side where they decelerate each other. From the Z/D=constant plots in Fig.85 these accelerated and decelerated velocity vectors can be seen clearly.

4.3 TURBULENCE MEASUREMENTS

Results of turbulence measurements are presented in Figs. 86-103. These measurements were done for 90° and 60° side-by-side dual rectangular jets and for a 90° single circular jet. For all the cases, data was taken for only one plane, i.e. Y = 0.0 in.. Jet exit velocity and turbulence profiles were presented earlier. The circular jet measurements were done for the jet with low exit turbulence and no swirl. All the data were obtained for jet to freestream velocity ratio of 4.0.

Meanflow results which were obtained by hot wire are also presented with the turbulence data. The magnitudes of the mean velocity vectors, which are presented in Figs. 86, 92 and 98 were taken from previously made yawhead measurements and their direction came from hot wire measurements. Here, the main reason for presenting meanflow data obtained by hot wire, is to help reader to better understand turbulence information. Because for every data point presented in turbulence figures there is a corresponding mean flow vector. For example if one wants to know mean velocity vector of a data point presented in Fig.87, he can just look for it in Fig.86 at the same X and Z location. There is not much difference between this meanflow data and the mean flow data presented in the previous section and obtained using yawhead probe.

There are several ways to normalize turbulence data. Here, the data is presented in two different ways - normalized by local total velocity, and normalized by freestream velocity. Normalizing turbulence intensity in one direction with the component of the local mean velocity vector in that direction is not very

suitable for the jet in a crossflow problem, because, for some locations, this will give infinite values. Data normalized by the local total velocity should be judged as having better meaning than the data normalized by freestream velocity. Because, as explained in Chapter 3, data normalized with local total velocity is actually the ratio of the R.M.S. and D.C. outputs of the hot wire, it is not subject to effects of calibration changes due to temperature, etc. In order to obtain data normalized by the freestream, one needed to know the ratio of freestream velocity to local total velocity, and this information came from previously made yawhead measurements. However, presentation of the data normalized by the freestream velocity is also useful, because this gives a chance to compare results with some of the other researchers data. Also, this helps to compare the magnitudes of the turbulence intensities for regions with different total mean velocities.

4.3.1 90° Side By Side Dual Rectangular Jets

These results are presented in Figs. 86-91. In Fig.87, turbulence intensities in the X, Y and Z directions normalized with the local total velocity are presented ($\sqrt{\overline{u'^2}}/U_{TOT}, \sqrt{\overline{v'^2}}/U_{TOT}, \sqrt{\overline{w'^2}}/U_{TOT}$). One can see that $\sqrt{\overline{u'^2}}/U_{TOT}$ and $\sqrt{\overline{w'^2}}/U_{TOT}$ have a similar behaviour, while $\sqrt{\overline{v'^2}}/U_{TOT}$ behaves differently. It seems in jet dominated regions, $\sqrt{\overline{u'^2}}/U_{TOT}$ and $\sqrt{\overline{w'^2}}/U_{TOT}$ are higher, and in wake dominated regions, $\sqrt{\overline{v'^2}}/U_{TOT}$ is higher. Both the jet and the freestream are actually low turbulence flows. Therefore, the jet core and freestream dominated regions have low turbulence intensities. Turbulence increases with in-

creased mixing and interaction of each stream. For X=0.0 in., all three turbulence intensities increase with increasing Z, and they have peak values around Z=5.5 inch. Then, they start decreasing to their freestream values. Peak values are around 40 % for $\sqrt{\overline{u'^2}}/U_{TOT}$, 30 % for $\sqrt{\overline{w'^2}}/U_{TOT}$ and 15 % for $\sqrt{\overline{v'^2}}/U_{TOT}$. $\sqrt{\overline{v'^2}}/U_{TOT}$ has considerably lower values than the other two. For low Z locations, turbulence intensities are below 5 %. These areas actually correspond to the core of the jet. The same type of argument is true for X=1.0 inch; More data points fell into the core of the jet. Peak turbulence intensities shift to around the Z=7.5 in. location. Peak values are about 45 % for $\sqrt{\overline{u'^2}}/U_{TOT}$, 40 % for $\sqrt{\overline{w'^2}}/U_{TOT}$ and 15 % for $\sqrt{\overline{v'^2}}/U_{TOT}$. These peak values occur at the outer edge of the jet in the mixing layer between jet and freestream. At X=2.0 in., one can't observe the effect of jet core any more. Instead, low Z locations are now under the influence of the wake flow behind the jet and also under the influence of the vortex flows separated from both sides of the jet. In this wake-dominated region, all three turbulence intensities have values around 20 to 30 %. By coming closer to the jet-dominated region, $\sqrt{\overline{u'^2}}/U_{TOT}$ and $\sqrt{\overline{w'^2}}/U_{TOT}$ start increasing, and $\sqrt{\overline{v'^2}}/U_{TOT}$ starts decreasing. All the turbulence intensities again have their peak values in the outer mixing region of the jet and freestream. The peak for $\sqrt{\overline{v'^2}}/U_{TOT}$ is less pronounced. Peak values for $\sqrt{\overline{u'^2}}/U_{TOT}$ and $\sqrt{\overline{w'^2}}/U_{TOT}$ are about 45 % and for $\sqrt{\overline{v'^2}}/U_{TOT}$ about 20 %, which is lower than the value of $\sqrt{\overline{v'^2}}/U_{TOT}$ in the wake region. For X=4.0 in., $\sqrt{\overline{v'^2}}/U_{TOT}$ is considerably larger then $\sqrt{\overline{u'^2}}/U_{TOT}$ and $\sqrt{\overline{w'^2}}/U_{TOT}$ in the wake region, and it decreases smoothly when coming to the jet region. For $\sqrt{\overline{u'^2}}/U_{TOT}$ and

$\sqrt{\overline{w'^2}}/U_{TOT}$, two peaks are pronounced - one at the lower edge of the jet and other at the outer edge of the jet. The peaks at the lower edge are about 40 %, and the ones at outer edge are about 35 %. By going further downstream, the differences between jet and wake regions diminish. These two actually start becoming the same region. Turbulence intensities decay further, and they start becoming isotropic. Peak values become less pronounced.

Reynolds stresses normalized by the square of the local total velocity are presented in Fig.88. In Fig.89, $-\overline{u'w'}/U_{TOT}^2$ is presented again after being enlarged, since $-\overline{u'w'}/U_{TOT}^2$ is usually smaller in magnitude compared to $-\overline{u'v'}/U_{TOT}^2$ and $-\overline{v'w'}/U_{TOT}^2$. It is seen that $-\overline{u'v'}/U_{TOT}^2$ usually takes negative values, and $-\overline{v'w'}/U_{TOT}^2$ usually takes positive values. If one looks at the plots for X=0.0 in., 1.0 in. and 2.0 in. from Fig.88, one can see that $-\overline{u'v'}/U_{TOT}^2$ makes a negative peak and $-\overline{v'w'}/U_{TOT}^2$ makes a positive peak. For X=4.0 in., the situation is a little more complicated because of the increased effect of the wake. By going further downstream, the curves get smoother. From Fig.89, one can see that $-\overline{u'w'}/U_{TOT}^2$ makes a negative peak for X=0.0 in. and X=1.0 in. For X=6.0 in., 8.0 in. and 10 in. there is one negative peak which corresponds to the lower edge of the jet and one positive peak which corresponds to the outer edge of the jet. The situation is a little more complicated for X=2.0 in. and 4.0 in. probably due to more pronounced wake effects.

Data normalized by the freestream velocity can be seen in Figs. 90 and 91.

4.3.2 60° Side By Side Dual Rectangular Jets

Hot wire results for the 60° rectangular jets can be seen in Figs. 92-97. In Fig.92, meanflow data, in Fig.93 turbulence intensities normalized by local total velocity, and in Fig.94 Reynolds stresses normalized by the square of local total velocity can be seen. In Fig.95, $-\overline{u'w'}/U_{TOT}^2$ is presented again with a finer scale. Turbulence data normalized by freestream velocity is presented in Figs. 96 and 97.

From Fig.97, one can see that the functional behaviour of turbulence intensities are quite similar to that for the 90° rectangular jets. The profiles are a little compressed in the Z direction, because the 60° jets have lower penetration height. The jet has higher velocities than the freestream even for the downstream locations like X=8.0 in. and X=10.0 in.. For that reason, the shear layer between jet and freestream produces observable peak values for $\sqrt{\overline{u'^2}}/U_{TOT}$ and $\sqrt{\overline{w'^2}}/U_{TOT}$ at these stations. Again, $\sqrt{\overline{v'^2}}/U_{TOT}$ takes higher values in the wake dominated region and lower values in the jet dominated region. This can be judged as logical, because for the wake dominated region, the measurement plane is presumed to be the symmetry plane for two counter rotating vortices. Two flows with opposite direction Y component velocities meet each other in this plane, therefore velocity fluctuations in Y direction are high. For the jet dominated region, two flows with almost no Y component velocities hit each other (jet and freestream). The directions and magnitudes of these two flows in the X-Z plane are different. This causes higher fluctuating velocities in the X and Z di-

rections. From Fig.94, one can see that the functional behaviour of $-\overline{u'v'}/U_{TOT}^2$ and $-\overline{v'w'}/U_{TOT}^2$ Reynolds stresses are again quite similar to that for 90° jets. From Fig.95, one can note some differences for $-\overline{u'w'}/U_{TOT}^2$, e.g. for X = 1.0 in. and 2.0 in., the profile makes one positive and one negative peak. This behaviour is not very clear for 90° jets. Data normalized by freestream velocity amplifies the apparent turbulence intensities and Reynolds stresses for locations where the local total mean velocity is higher than the freestream velocity and reduces them where the total mean velocity is lower than the freestream. It is interesting to observe the Reynolds stress results normalized by the square of the freestream velocity. Looking at the results from Fig.97, one can observe that for X locations like 6.0 in., 8.0 in. and 10.0 in., $-\overline{u'v'}/U_\infty^2$ makes two negative peaks and $-\overline{v'w'}/U_\infty^2$ makes two positive peaks. These peak values occur in the mixing and shear layers at the lower and upper edges of the jet.

4.3.3 90° Circular Jet

Results for the 90° jet can be seen in Figs. 98-103. In Fig.98, mean flow information, in Figs. 99-101 turbulence data normalized by the local total velocity and in Figs. 102 and 103 turbulence data normalized with freestream can be seen. Looking to the turbulence intensity results from Fig.99, one can see similarities with the rectangular jet results. However, the turbulence intensity profiles for the circular jet are closer to isotropy, at least, the Y component of the turbulence intensity does not differ so much from the X and Z components. For X stations like

X = 1.0 in. and 2.0 in. (X/D = 0.53 and 1.05) $\sqrt{\overline{w'^2}}/U_{TOT}$ makes higher peaks than $\sqrt{\overline{u'^2}}/U_{TOT}$ and $\sqrt{\overline{v'^2}}/U_{TOT}$. There are also similarities and differences for Reynolds stresses when compared to rectangular jet results. Again $-\overline{u'v'}/U_{TOT}^2$ usually takes negative values and $-\overline{v'w'}/U_{TOT}^2$ takes positive values.

Chapter 5

DISCUSSION

5.1 COMPARISONS

In Table-3 all single jet pressure distribution results of the present work are compared. In this table, the ratios of the areas covered by the $\Delta C_p = -1$ line and the $\Delta C_p = -0.2$ line to jet exit area are presented. For the 60° rectangular jet, instead of the jet exit area, the projection of this area on a plane perpendicular to the jet axis is taken. These comparisons were made for R = 4.0. As can be seen, the negative pressure areas were smallest for the 60° rectangular jet and largest for the circular jet with low exit turbulence.

Table 3. Comparison of surface pressures, single jets, R = 4.0.

jet type	A_{-1}/A_{exit}	$A_{-0.2}/A_{exit}$
90° rectangular	1.90	14.33
60° rectangular	0.68	10.86
90° circular	4.31	22.66
90° circular (high turbulence)	2.45	13.30
90° circular (40 % swirl)	3.94	18.72
90° circular (58 % swirl)	3.94	15.52

In Figures 104 through 110, the pressure distribution results of the present work are compared with some of the earlier results, and in Table-4, some information is given about the works compared. In Figures 104 and 105, the low turbulence and high turbulence circular jet results of the present work are compared with the single jet results obtained during the course of Ref.11. These comparisons were made for R = 2.2 and 4.0 and for the $\Delta C_p = -0.5$ and -1 lines. The high turbulence case of the present work compared very well with the case of Ref.11. This is expected, because both cases had high exit turbulence levels. Also, the jets of the present work and Ref.11 were injected from the same flat plate model, but the tests were conducted in different wind tunnels. In figure 106, the present results (low turbulence, circular, R = 4) are compared with the results of Ref.24. The good agreement between the two cases can be seen clearly. Comparison with the results of Ref.55 can be seen in Fig.107. Agreement is good for the upstream locations, however the negative pressures extended to a larger downstream area for the case of Ref.55. In Figure 108, comparison is made with the results of Ref.57. Agreement is good except for the downstream locations. In figure 109, a comparison is made with the results of Ref.52 as it appeared in

Ref.14. The negative pressures of Ref.52 extended upstream as if the velocity ratio was higher than 4. In Fig.110, the 90° rectangular jet result for R=4 of the present work is compared with that of Ref.14. The results of Ref.14 behaves like the circular jet results of Ref.52, i.e. as if the velocity ratio is higher and the negative pressures extend upstream. Results agreed better for the downstream locations. Note that there is a jet exit Mach number difference between the cases of the present work and Ref.14. Mach numbers are 0.1 and 0.5 respectively for this two cases. Differences among the the results of the various studies can be attributed to the effects of differences in jet exit velocity profile, jet exit turbulence level, Mach number, surface boundary layer, wind tunnel, pressure tap density etc. Some of these items are not documented in other studies. Also, the present work had the highest density of pressure taps, so the results are presumably the most reliable.

Table 4. Description of tests for data comparison

Ref	surface b.l.	jet exit velocity profile	jet exit turbulence (%)	C_p or ΔC_p	M_{jet}	# of ports	port density, nearfield	port density, farfield
11 (1984)	turb.	uniform nozzle	10	ΔC_p	0.3		high	med.
24 (1965)	turb.	uniform nozzle		C_p	0.24			
55 (1970)								
57 (1978)	turb.	uniform nozzle		ΔC_p	0.4	226	high	med.
52 (1975)		nozzle		ΔC_p				
14 (1979) rectangular				ΔC_p	0.5	217		
present low turb.	turb.	uniform nozzle	3	ΔC_p	0.2	> 450	high	med.
present high turb.	turb.	uniform nozzle	> 10	ΔC_p	0.1	> 450	high	med.
present rectangular	turb.	uniform nozzle	3	ΔC_p	0.2	930	very high	med.

In Fig.111, the jet centerline trajectories are compared for the various circular jets. The low turbulence, high turbulence, 40 % swirl and 58 % swirl cases of the present research are compared with each other and with the experimental results of the Refs. 22 and 23, as well as with the prediction of Ref.9. The low turbulence data of the present work agreed well with the results of Refs. 22 and 23. Lower penetration heights for the high turbulence and 58 % swirl cases are visible. Ref.9 predicted higher penetration. In Fig.112, the low turbulence single circular jet mean flowfield result of the present work is compared with the Navier-Stokes solution of Ref.77. Ref.77 predicted faster bending of the jet. There is only qualitative agreement; the largest differences are mainly at the transition regions between the jet and wake.

In Figures 113 through 119, the turbulence data of the present research is compared with that of Ref.16. In these figures, the distance from the flat plate surface (Z) is normalized with the distance to the jet center from the flat plate. Qualitatively, the shape of the profiles agrees. Quantitative agreement shouldn't be expected because, the results of Ref.16 are for $R=2$, and the results of the present work are for $R=4$. Also the results of Ref.16 were normalized with the X component of the local total velocity, and the results of the present work were normalized with the local total velocity.

5.2 CONCLUSIONS

A jet in a crossflow induces negative pressure regions, which extend towards downstream and sides. The downstream extent of these negative pressures decreases by increasing velocity ratio while their upstream extent increases. A single rectangular jet aligned streamwise, and injected at 90° angle caused less blockage to the freestream when compared to a same exit area circular jet. This caused an important reduction in the downstream extent of the negative pressures. The rectangular jets tested here had sharp front and rear corners. Particularly around the front corners, sharp increases in the magnitude of the negative pressures were observed. The rear corners also produced high negative pressure regions in their immediate vicinity with lesser magnitudes. For a circular jet, the distribution of the negative presssures around the jet is smoother, and the highest magnitudes appear on or rear of the maximum width of the circle. The sharp peak pressures around the corners of a rectangular jet may be reduced by rounding the front and rear corners. A rectangular jet injected at 60° angle into the crossflow produced lesser magnitude negative pressures, distributed more smoothly over a lesser area. For this case, the magnitude of the negative pressures around the front corners reduced, but the magnitude of the negative pressures around the rear corners increased. The side-by-side dual rectangular jets caused more blockage to the freestream, and the negative pressures extended to a larger downstream area. These effects were less for 60° side-by-side dual rectangular jets. On the other hand, a major advantage of the streamwise rectangular jets over the circular jets

could be for the side-by-side arrangements. For the side-by-side dual rectangular jets tested here S/D_{ref} was 0.95. Two circular jets cannot be brought that close to each other.

Testing of circular jets with two different exit turbulence levels showed that, for the high turbulence jet, the area covered by the negative pressures was lesser. The maximum magnitudes of the negative pressures didn't change much. The high turbulence jet produced more symmetric pressure distribution.

The circular jet with swirl produced an asymmetric pressure distribution. The magnitudes of the negative pressures increased at the rear side of the jet where the swirl velocity and the crossflow velocity were in the same direction. The magnitudes of the negative pressures decreased for the other rear side. Swirl effects were more pronounced for lower velocity ratios. The effect of swirl is an important function of the swirl ratio. The 58 % swirl produced considerably more swirl effects than the 40 % swirl. As far as the VTOL application is concerned, the jets with swirl can best be used in side-by-side dual arrangements, where the two jets have opposite swirl directions.

Meanflow results showed that for the 90° jets, the streamwise aligned rectangular jet had a higher penetration ratio than the circular one for the same velocity ratio and same jet exit area. Among the circular jets, the circular jet with low turbulence and no swirl had the highest penetration. Increasing the turbulence level reduced the penetration. The effect of swirl was also to reduce the penetration height. In particular, the 58 % swirl case caused more than a 30 %

reduction in penetration height when compared to the low turbulence, no swirl case.

Turbulence intensities and Reynolds stresses in the jet centerplane were obtained for R=4.0, for the 90° and 60° side-by-side dual rectangular jets, and for the 90° circular jet with low turbulence, no swirl. Most of the other turbulence data in the literature belongs to cases with $R \leq 2$, where flow angularities in the jet plume are less. Since at some locations turbulence intensities above 40 % were observed, it will be interesting to compare these results with a possible future 3-D LDV investigation.

For the rectangular jets turbulence intensities, $\sqrt{\overline{u'^2}}/U_{TOT}$ and $\sqrt{\overline{w'^2}}/U_{TOT}$ behaved similarly, and $\sqrt{\overline{v'^2}}/U_{TOT}$ differed in behavior. For the upstream stations, two regions are observable- jet core and jet/freestream mixing region. For the downstream stations, there are also two regions- wake region and jet/freestream mixing region. In the jet core, all the turbulence intensities are very low. In the wake region, $\sqrt{\overline{v'^2}}/U_{TOT}$ is higher than $\sqrt{\overline{u'^2}}/U_{TOT}$ and $\sqrt{\overline{w'^2}}/U_{TOT}$, because in this region, two bound vortices meet each other with opposite direction v velocities. In the jet-freestream mixing region, $\sqrt{\overline{u'^2}}/U_{TOT}$ and $\sqrt{\overline{w'^2}}/U_{TOT}$ are higher than $\sqrt{\overline{v'^2}}/U_{TOT}$, because in this region, two flows (jet and freestream) with different magnitude and direction velocities in the X-Z plane hit each other. Going downstream, the turbulence intensities decay, and isotropy increases. Peak values, particularly for $\sqrt{\overline{u'^2}}/U_{TOT}$ and $\sqrt{\overline{w'^2}}/U_{TOT}$ occur at the outer and sometimes at the inner edges of the jet. Similar things can

be said for the 90° circular jet. For this case, the differences in $\sqrt{\overline{v'^2}}/U_{TOT}$ from $\sqrt{\overline{u'^2}}/U_{TOT}$ and $\sqrt{\overline{w'^2}}/U_{TOT}$ are less.

Based on these results some suggestions for future studies can be made. First, it will be useful to study dual rectangular jets with other length to width ratios and spacings. Second, more turbulence results of the type obtained here are clearly needed to aid basic physical understanding and turbulence modeling. Third, higher jet Mach numbers should be studied for VTOL application and others. Last, a more detailed understanding of the effects of high turbulence and swirl in the jet on the surface pressure distribution should be pursued.

REFERENCES

1. Schetz, J.A.: *Injection and Mixing in Turbulent Flow,* Progress in Astronautics and Aeronautics Volume 68, AIAA, New York, 1980.

2. Abramovich, G.N.: *The Theory of Turbulent Jets,* MIT Press, Cambridge, MA, 1960 (English Edition).

3. Moussa, Z.M., Trischka, J.W., and Eskinazi, S.: "The Near Field in the Mixing of a Round Jet with a Cross-Stream", Journal of Fluid Mechanics, Vol.80, 1977, p. 49.

4. Lee, C.C.: "A Review of Research on the Interaction of a jet With an External Crosstream", Tech. Note R-184, (Contract No. DA-01-021-AMC-11528(z)), Res. Lab., Brown Engineering Co., Inc., Mar. 1966. (Available from DDC as AD 630 294).

5. Garner, Jack E.: "A Review of Jet Efflux Studies Application to V/STOL Aircraft." AEDC-TR-67-163, U.S. Air Force, Sept. 1967. (Available from DDC as AD 658 432).

6. Perkins, S.C. Jr. and Mendenhall, M.R.: "A Study of Real Jet Effects on the Surface Pressure Distribution Induced by a Jet in a Crossflow", NASA CR-166150 (N81-23029), Mar. 1981.

7. "Analysis of A Jet in a Subsonic Crosswind", NASA-SP-218, 1969.

8. Campbell, J.F. and Schetz, J.A.: "Analysis of the Injection of a Heated Turbulent Jet into a Cross Flow", NASA TR R-413, Dec. 1973.

9. Campbell, J.F. and Schetz, J.A.: "Flow Properties of Submerged Heated Effluents in a Waterway", AIAA Journal, Vol.11, Feb. 1973, pp. 223-230.

10. Schetz, J.A., Jakubowski, A.K., and Aoyagi, K.: "Jet Trajectories and Surface Pressures Induced on a Body of Revolution with Various Dual Jet Configurations", AIAA Journal of Aircraft v. 20, n. 11 Nov. 1983, p. 975-982.

11. Schetz, J.A., Jakubowski, A.K., and Aoyagi, K.: "Surface Pressures Induced on a Flat Plate with In-Line and Side-by-Side Dual Jet Configurations", AIAA Journal of Aircraft v. 21, n. 7 Jul. 1984, p. 484-490.

12. Moore, C.L. and Schetz, J.A.: "Effects of Nonuniform Velocity Profiles on Dual Jets in a Crossflow", AIAA-85-1674, July 1985.

13. Kavsaoglu, M., Schetz, J.A., Jakubowski, A.K.: "Dual Rectangular Jets From a Flat Plate in a Crossflow", AIAA-86-0477, January 1986.

14. Weston, R.P., Thames, F.C.: "Properties of Aspect Ratio 4.0 Rectangular Jets in a Subsonic Crossflow", Journal of Aircraft vol.16 no.10, October 1979 pp 701-707.

15. Crabb, D., Durao, D.F.G., Whitelaw J.H.: "A Round Jet Normal to a Crossflow", Journal of Fluids Engineering, Transactions of the ASME vol. 103, March 1981 p.142-152.

16. Isaac, K.M.: "Experimental and Analytical Investigation of Multiple Jets in a Cross-Flow", Ph.D. Dissertation, Virginia Polytechnic Institute and State University, Blacksburg, VA, 1982.

17. Isaac, K.M. and Jakubowski, A.K.: "Experimental Study of the Interaction of Multiple Jets with a Crossflow", AIAA Journal, vol. 23, no. 11, pp. 1679-1683, 1984.

18. Isaac, K.M. and Schetz, J.A.: " Analysis of Multiple Jets in a Cross-Flow", ASME Journal of Fluids Engineering, vol. 104, Dec. 1982 pp. 489-492.

19. Sistla, R.: "Heated Jet in a Cross-Flow" Master of Science Thesis, Virginia Polytechnic Institute and State University, Blacksburg, VA 1984.

20. Callaghan, E.E., and Ruggeri, R.S.: "Investigation of the Penetration of an Air Jet Directed Perpendicularly to an Air Stream", NACA TN 1615, 1948.

21. Ruggeri, R.S.: "Genaral Correlation of Temperature Profiles Downstream of a Heated Air Jet Directed at Various Angles to an Air Stream", NACA TN 2855, 1952.

22. Jordinson, R.: "Flow in a Jet Directed Normal to the Wind", A.R.C. R. and M. 3074, 1956.

23. Keffer, J.F. and Baines, W.D.: "The Round Turbulent Jet in a Cross Wind", Journal of Fluid Mechanics, Vol. 15, 1963, p.481.

24. Bradbury, L.J.S., and Wood, M.N.: "The Static Pressure Distribution around a Circular Jet Exhausting Normally from a Plane Wall into an Airstream", A.R.C.CP822, 1965.

25. Platten, J.L., and Keffer, J.F.: "Entrainment in Deflected Axisymmetric Jets at Various Angles to the Stream", Univ. of Toronto UTME TP 6808, 1968.

26. Margason, R.J., and Fearn, R.: "Jet Wake Characteristics and their Induced Aerodynamic Effects on V/STOL Aircraft in Transition Flight", NASA SP 218, 1969.

27. McMahon, H.M., and Mosher, D.K.: "Experimental Investigation of Pressures Induced on a Flat Plate by a Jet Issuing into a Subsonic Cross Wind", NASA SP 218, 1969.

28. Street, T.A., and Spring, D.J.: "Experimental Reaction Jets at Subsonic Speeds", NASA SP 218, 1969.

29. McMahon, H.M., Hester, D.D., and Palfery, J.G.: "Vortex Shedding From a Turbulent Jet in a Cross Wind", Journal of Fluid Mechanics, vol. 48, 1971, p.73.

30. Ramsey, J.W., and Goldstein, R.J.: "Interaction of a Heated Jet with a Deflecting Stream", NASA CR 72613, 1972.

31. Thompson, A.M.: "The Flow Induced by Jets Exhausting Normally from a Plane Wall into an Air Stream", Ph.D. Thesis, Univ. of London, 1971.

32. Eriksen, V.L.: "Film Cooling Effectiveness and Heat Transfer with injection through Holes", NASA CR 72981, 1972.

33. Kamotani, Y., and Greber, I.: "Experiments on a Turbulent Jet in Cross-Flow", AIAA Journal, Vol. 10, 1972, p. 1425.

34. Goldstein, R.J., Eckert, E.R.G., and Ramsey, J.W.: "Film Cooling with Injection through a Circular Hole", NASA CR 54604, 1973.

35. Mikolowsky, W., and McMahon, H.M.: "An Experimental Investigation of a Jet issuing from a Wing in a Cross-Flow", Journal of Aircraft, vol. 10, no 9, 1973, p. 546.

36. Shaw, C.S., and Margason, R.J.: "An experimental Investigation of a Highly Underexpanded Sonic Jet Ejecting From a Flat Plate into a Subsonic Cross-Flow" NASA TN D 7314, 1973.

37. Chassaing, P., George, J., Claria, A. and Sananes, F.: "Physical Characteristics of Subsonic Jets in a Cross-Stream", Journal of Fluid Mechanics, Vol. 62, 1974, p.41.

38. Fearn, R., and Weston, R.P.: "Vorticity Associated with a Jet in a Cross-Flow", AIAA Journal, Vol. 12, 1974, p.1666.

39. Weston, R.P.: "A Description of the Vortex Pair Associated with a Jet in a Cross-Flow", Workshop Proc. "Prediction Methods for Jet/V STOL Propulsion Aerodynamics". Inst. for Defence Analyses, Arlington VA, 1975.

40. Bergeles, G.: "Three Dimensional Discrete Hole Cooling Processes", Ph.D. thesis, Univ. of London, 1976.

41. Rathgeber, D.E., and Becker, H.A.: "Mixing Between a Round Jet and a Transverse Pipe Flow", Proceedings of 1st Symposium on Turbulent Flows, Penn. State University, 1977.

42. Holdeman, J.D., and Walker, R.E.: "Mixing of a Row of Jets with a Confined Cross-Flow" AIAA Journal, Vol. 15 1977, p. 243.

43. Patankar, S.V., Basu, D.K., and Alpay, S.A.: "Prediction of the Three Dimensional Velocity Field of a Deflected Turbulent Jet", ASME Journal Of Fluids Engineering, Vol. 99, 1977, p.758.

44. Pratte, B.D. and Baines, W.D.: "Profiles of the Round Turbulent Jet in a Cross Flow", Proceedings of ASCE, Journal of the Hydraulics Division, Nov. 1967, pp. 56-63.

45. McMahon, H.M. and Antani, D.L.: "An Experimental Study of a Jet Issuing from a Lifting Wing", Journal of Aircraft, Vol. 16, April 1979, pp. 275-281.

46. Krausche, D., Fearn, R.L., and Weston, R.P.: "Round Jet in a Cross Flow: Influence of Injection Angle on Vortex Properties", AIAA Journal, Vol. 16, June 1978, pp. 636-637.

47. Salzman, R.N., and Schwartz, S.H.: "Experimental Study of a Solid-Gas Jet Issuing into a Transverse Stream", Journal of Fluids Engineering, Vol. 100, Sept. 1978, pp. 333-339.

48. Rudinger, G.: "Some Aspects of Gas-Particle Jets in a Cross Flow", American Society of Mechanical Engineers, Paper 75-WA/HT-5, 1975.

49. Fearn, R., Kalota, C., and Dietz, W.E., Jr.: "A Jet/Aerodynamic Surface Interference Model", in Proceedings of V/STOL Aircraft Aerodynamics Workshop at NADC, Monterey, Calif., May 1979.

50. Vogler, R.D.: "Surface Pressure Distributions Induced on a Flat Plate by a Cold Air Jet Issuing Perpendicularly from the Plate and Normal to a Low-Speed Free-Stream Flow. NASA TN D-1629, Mar. 1963.

51. Ousterhout, D.S.: "An Experimental Investigation of a Cold Jet Emitting from a Body of Revolution Into a Subsonic Free Stream", NASA CR-2089, Aug. 1972.

52. Fearn, R.L., and Weston, R.P.: "Induced Pressure Distribution of a Jet in a Crossflow", NASA TN D-7916, June 1975.

53. Soullier, A.: "Testing at S1.MA for Basic Investigations on Jet Interactions: Distributions of Pressure Around the Jet Orifice", NASA TT F-14066, Jan. 1972.

54. Fricke, L.B., Wooler, P.T., and Ziegler, H.: "A Wind Tunnel Investigation of Jets Exhausting Into a Crossflow", AFFDL-TR-70-154, Vol. I - Test Description and Data Analysis, Vol. II - Additional Data for the One-Jet Configuration", Dec. 1970.

55. Mosher, D.K.: "An Experimental Investigation of a Turbulent Jet in a Cross Flow." Georgia Inst. of Tech. Rept. GIT-AER-70-715, Dec. 1970, (Ph.D Thesis)

56. Taylor, P.: "An Investigation of an Inclined Jet in a Crosswind." Aeronaut. Quart., Vol. XXVIII, Part 1, Feb. 1977.

57. Kuhlman, J.M., Ousterhout, D.S., and Warcup, R.W.: "Experimental Investigation of Effect of Jet Decay Rate on Jet-Induced Pressures on a Flat Plate.", NASA CR-2979, Apr. 1978.

58. Schwendemann, M.F.: "A Wind Tunnel Investigation of Stratified Jets and Closely Spaced Jets Exhausting into a Crossflow", Northrop Aircraft Division, Rept. NOR 73-98, May 1973.

59. Kuhlman, J.M., Ousterhout, D.S., and Warcup, R.W.: "Experimental Investigation of Effects of Jet Decay Rate on Jet-Induced Pressures on a Flat Plate: Tabulated Data" NASA CR-158990, Nov. 1978.

60. Ziegler, H. and Wooler, P.T.: "Analysis of Stratified and Closely Spaced Jets Exhausting into a Crossflow", NASA CR-132297, Nov. 1978.

61. Perkins, S.C., Jr. and Mendenhall, M.R.: "A Correlation Method to Predict the Surface Pressure distribution on an Infinite Plate from which a Jet is Issuing", NASA CR-152,160, May 1978.

62. Perkins, S.C., Jr. and Mendenhall, M.R.: "A Correlation Method to Predict the Surface Pressure distribution on an Infinite Plate or a Body of Revolution from which a Jet is Issuing", NASA CR-152,345, May 1980.

63. Margason, R.J.: "The Path of a Jet Directed at Large Angles to a Subsonic Free Stream", NASA TN D-4919, Nov. 1968.

64. Camelier, I. and Karamchetti, K.: "An Experimental Study of the Structure and Acoustic Field of a Jet in a Cross Stream", Joint Institute for Aeronautics and Acoustics Rept. TR-2, Stanford University, Jan. 1976.

65. Golubev, V.A., Klimkin, V.F. and Makarov, I.S.: "Trajectories of Single Jets of Different Densities Propagating in a Deflecting Airstream (translation)", Journal of Engineering Physics, Vol. 34, No. 4, Oct. 1978, pp. 395-398.

66. Harms, L.: "Experimental Investigation of the Flowfield of a Hot Turbulent Jet with Lateral Flow", Part 2. NASA TT F-15706, Sept. 1973.

67. Kamotani, Y. and Greber, I.: Experiments on a Turbulent Jet in a Crossflow. NASA CR-72893, June 1971.

68. Jakubowski, A.K., Schetz, J.A., Moore, C.L. and Joag, R.: "Effects of Velocity Profile and Inclination on Dual-Jet-Induced Pressures on a Flat Plate in a Crosswind", NASA CR-177361, October 1985.

69. Ong, L.H., McMurry, C.B., and Lilley, D.G.: "Hot-Wire Measurements of a Single Lateral Jet Injected Into Swirling Crossflow", AIAA Paper 86-0055, January 1986.

70. Chiang, H.C. and Sill, B.L.: "Entrainment Models and Their Application to Jets in a Turbulent Cross Flow", Atmospheric Environment Vol.19, No.9 pp.1425-1438, Pergamon Press, Great Britain.

71. Kosterin, V.A., Maschenko, G.I., and Shalev, G.M.: "Paired Jets in Crossflow", Izvestiya VUZ. Aviatsionnaya Tekhnika, Vol.28, No.1, pp. 37-42, 1985, UDC 629.7.036.3.533.6.011.3 Allerton Press Inc. 1985.

72. Sherif, S.A., Pletcher, R.H.: "Measurement of Thermal Characteristics of Heated Turbulent Jets in Cross Flow", AIAA/ASME Heat Transfer and Thermophysics Conference Session on Heat Transfer in Three-Dimensional Flows, Boston, Massachussets, June 2-4, 1986.

73. Salzman, R.N.: "Injection of a Solid-Gas Jet Into a Transverse Stream", Ph.D. Dissertation, West Virginia University, 1973, Morgantown, West Virginia.

74. Snyder, P. and Orloff, K.L.: "Three-Dimensional Laser Doppler Anemometer Measurements of a Jet in a Crossflow", NASA TM-85997, September 1984.

75. Andreopoulos, J., and Rodi, W.: "Experimental Investigation of Jets in a Crossflow", J. Fluid Mech. (1984) vol. 138, pp. 93-127.

76. Andreopoulos, J.: "On the Structure of Jets in a Crossflow", J. Fluid Mech. (1985) vol. 157, pp. 163-197.

77. Chien, C.J. and Schetz, J.A.: "Numerical Solution of Three-Dimensional Navier-Stokes Equations with Application to Channel Flows and a Buoyant Jet in a Cross-Flow", Journal of Applied Mechanics, Vol. 42, September 1975, pp.575-579.

78. Fearn, R.L., Weston, R.P.: "Velocity Field of a Round Jet in a Crossflow for Various Jet Injection Angles and Velocity Ratios", NASA Tech. Pap. n. 1506, Oct. 1979.

79. Wu, J.M., Vakili, A.D. and Yu F.M.: "Investigation of the Interacting Flow of Non-Symmetric Jets in Crossflow" AIAA Paper 86-0280, January 1986.

80. Marchman III, J.F.: "Wind Tunnel Lab Manual", VPI&SU, Aerospace & Ocean Engineering, Blacksburg, VA, 1983.

81. Lee, H.W.: "Computational and Experimental Study of Trailing Vortices", Ph.D. Dissertation, Virginia Polytechnic Institute and State University, Blacksburg, Va, 1983.

82. Sung, B.: "Analysis of the Vortical Flows Around a 60 Degree Delta Wing with Vortex Flaps", Ph.D. Dissertation, Virginia Polytechnic Institute and State University, Blacksburg, VA, 1985.

83. "General Purpose Contouring Program User's Manual", California Computer Products, Inc., Anaheim, CA, April 1971.

84. Treaster, A. and Yocum, A.: "The Calibration and Application of Five-Hole Probes", ISBN 87664-403-5, Proc. ISA, Vol. 18, 1978, pp. 255-266.

85. Gerner, A.A., Maurer, C.L., and Gallington, R.W.: "Non-Nulling Seven-Hole Probes for High Angle Flow Measurements", Experiments in Fluids, Vol.2, 1984, pp. 95-103.

86. "United Sensor Probes Catalog" S-7 Rev-B.

87. Sitaram, N., Lakshminarayana, B., and Ravindranath, A.: "Conventional Probes for the Relative Flow Measurement in Turbomachinery Rotor Blade Passage", Transactions of the ASME, Journal of Engineering for Power Vol. 103, April 1981.

88. Chue, S.H.: "Pressure Probes for Fluid Measurements", Progress in Aerospace Science, vol. 16, no. 2, 1975.

89. "Model 1050/1050AA Constant Temperature Anemometer Instruction Manual" TSI Incorporated, 1984 Revision B, TSI P/N 1990215.

90. Champagne, F.H., and Sleicher, C.A.: "Measurements with Inclined Hot-Wires, Hot Wire Response Equation", Journal of Fluid Mechanics, vol. 28, Part I, pp. 177-182, 1967.

91. Kotb, Mohamed A.: "Experimental Investigation of 3-D Turbulent Free Shear Flow Past Propellers and Windmills", Ph.D. Dissertation, Virginia Polytechnic Institute and State University, 1984.

92. Bearman P.W.: "Corrections for the Effect of Ambient Temperature Drift on Hot-Wire Measurements in Incompressible Flow", DISA Information No.11 May 1971.

93. Humphrey, R.L.: "Bibliography of Hot Wire/Film Anemometry in Liquids", Sept. 1969. Dept of Chemical Engineering, U. of Missouri-Rolla.

94. Bruun, H.H.: "Interpretation of Hot-Wire Probe Signals in Subsonic Airflows", Journal of Physics E: Scientific Instruments v. 12 n. 12 Dec. 1979, p. 1116-1128.

95. Smits, A.J., and Perry, A. E.: "A note on hot-wire anemometer measurements of turbulence in the presence of temperature fluctuations.", Journal of Physics E: Scientific Instruments, Vol. 14, p. 311-312, 1981.

96. Moore, C.L.: "The Effect of Nonuniform Velocity Profiles on the Surface Pressures", Master of Science Thesis, Virginia Polytechnic Institute and State University, Blacksburg, VA 1985.

FIGURES

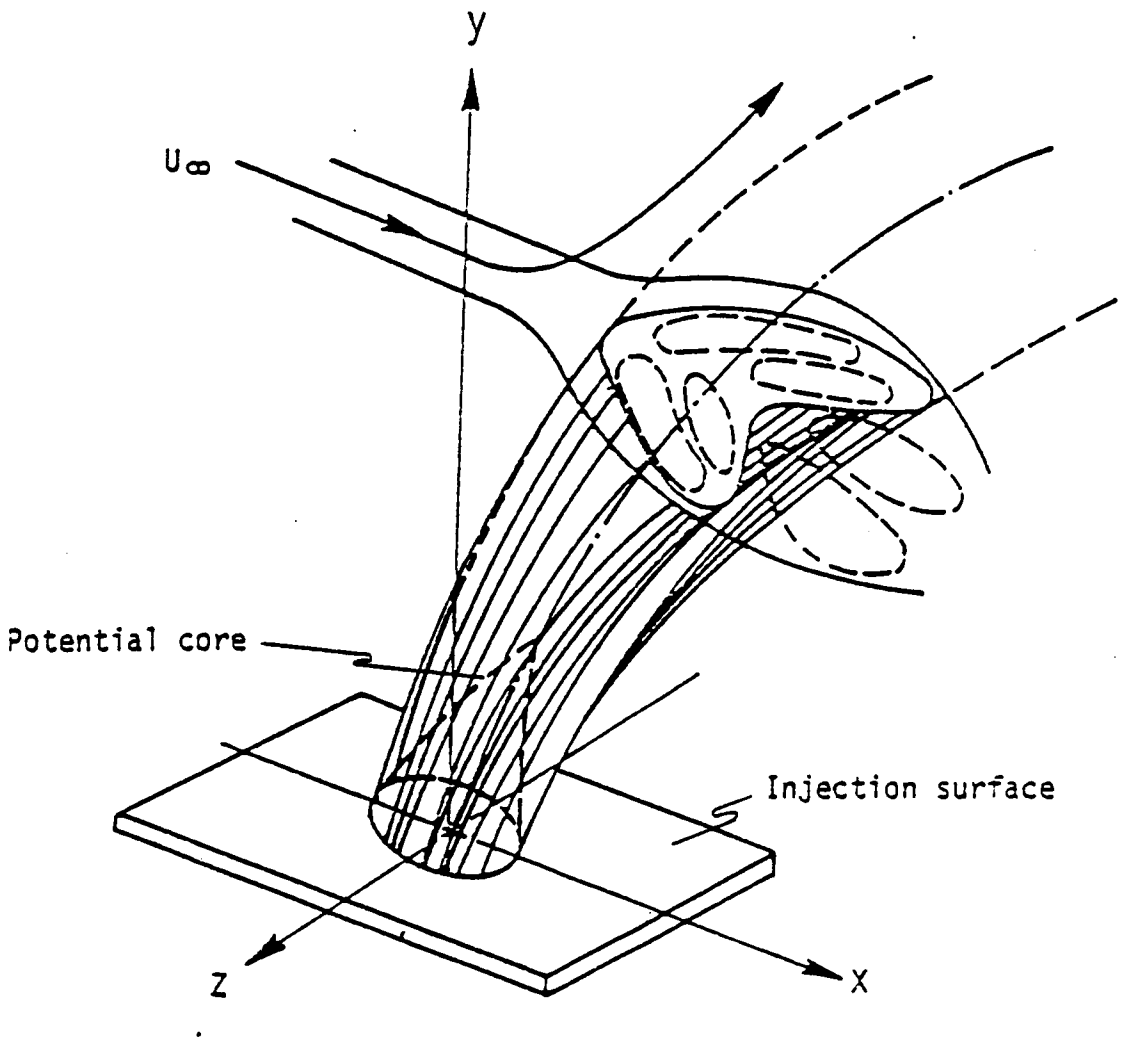

Figure 1. Description of the flowfield.: a) Diminishing of the potential core and formation of the kidney shape (from Ref.2).

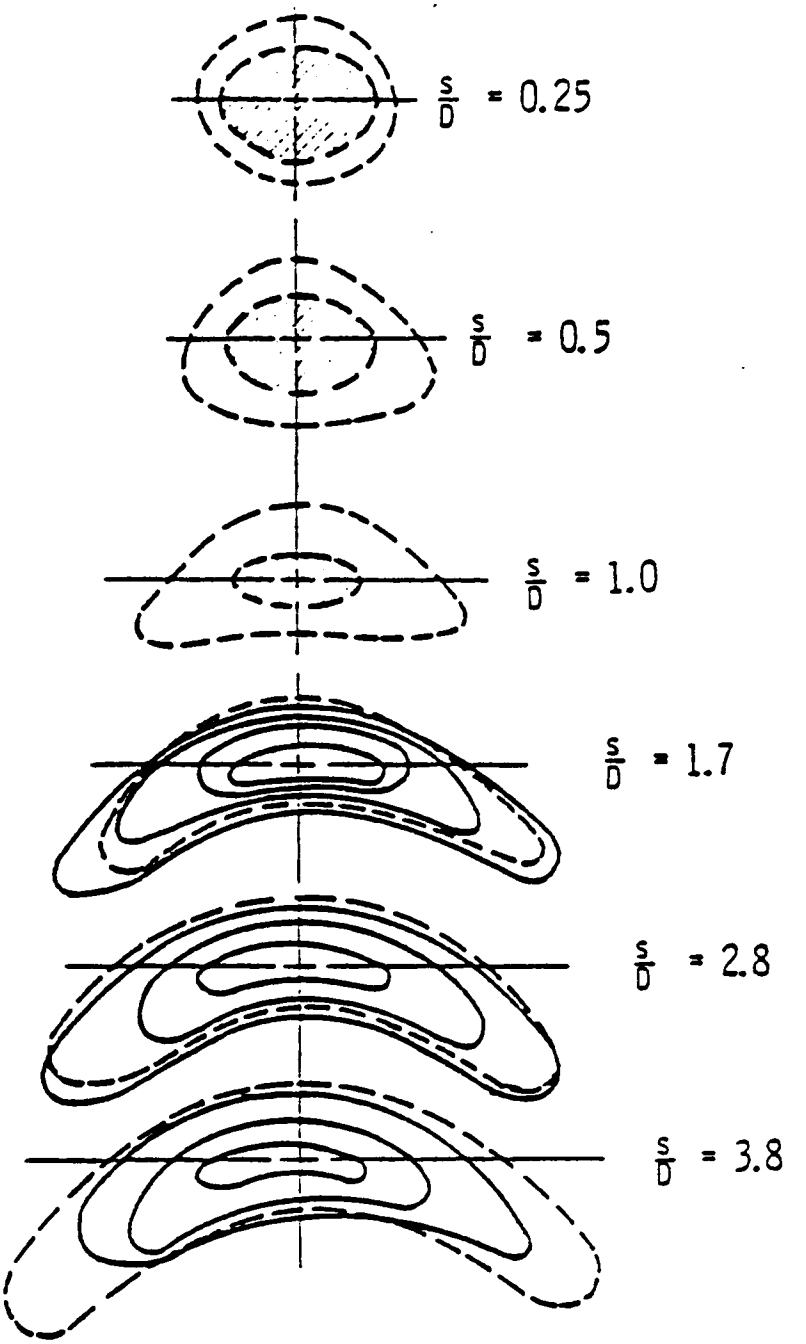

Figure 1. b) Cross-sectional pressure contours in a transverse jet with U_j/U_∞ = 2.2 (from Ref.2); solid and dashed lines correspond to constant total and static pressure, and the shaded areas denote the potential core.

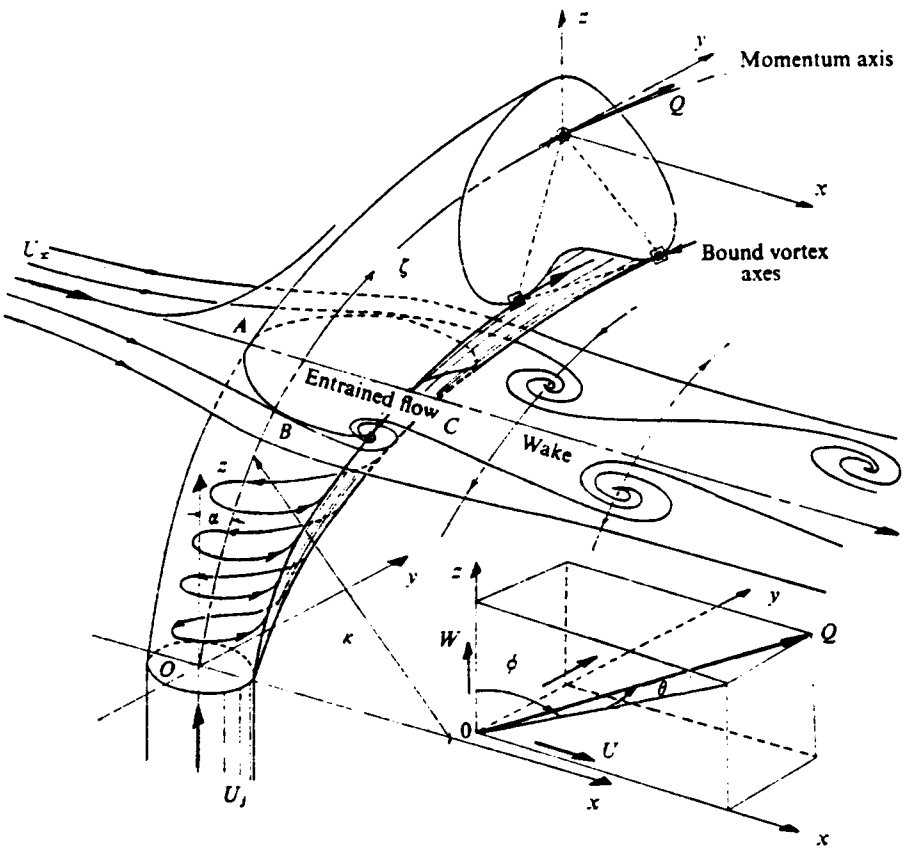

Figure 2. Flow description and co-ordinates (from Ref.3)

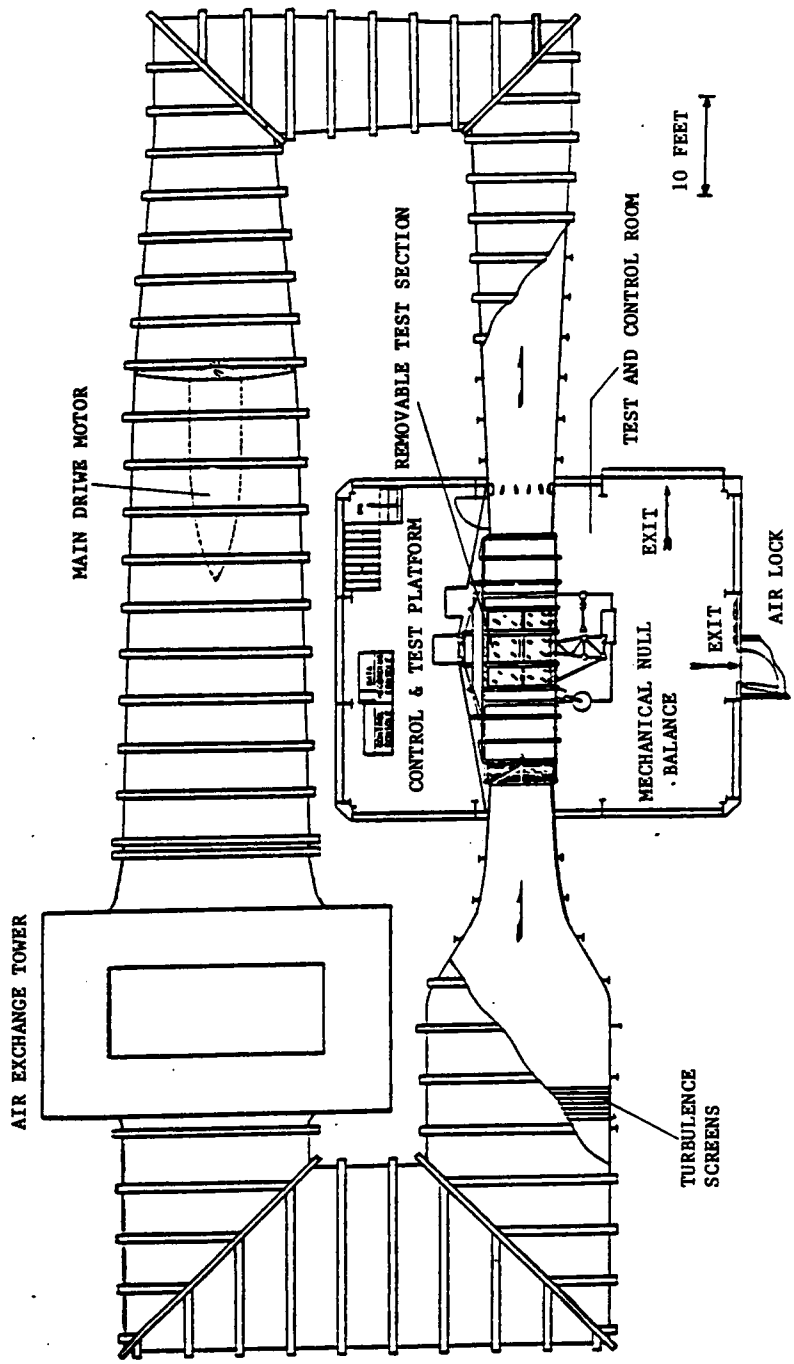

Figure 3. Wind Tunnel.

a) Model in the Test Section. View looking downstream.

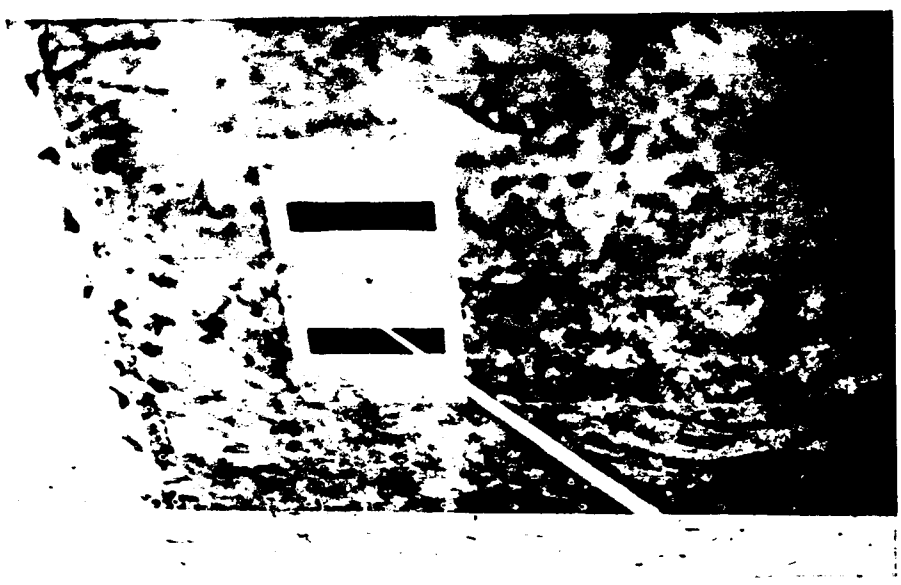

b) Instrumented Nozzle Section.

Figure 4. Photographs of the Model.

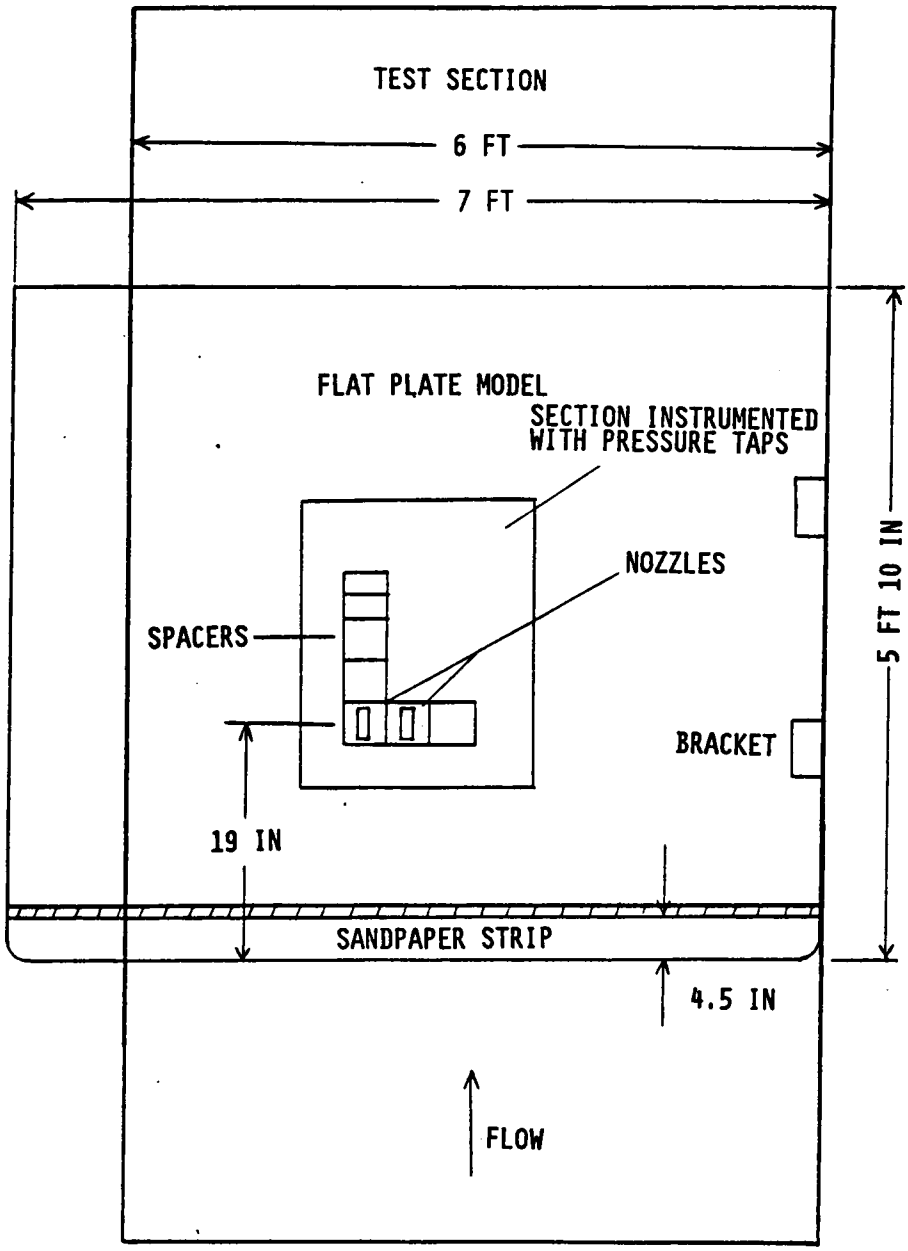

Figure 5. Model in the Tunnel (topview).

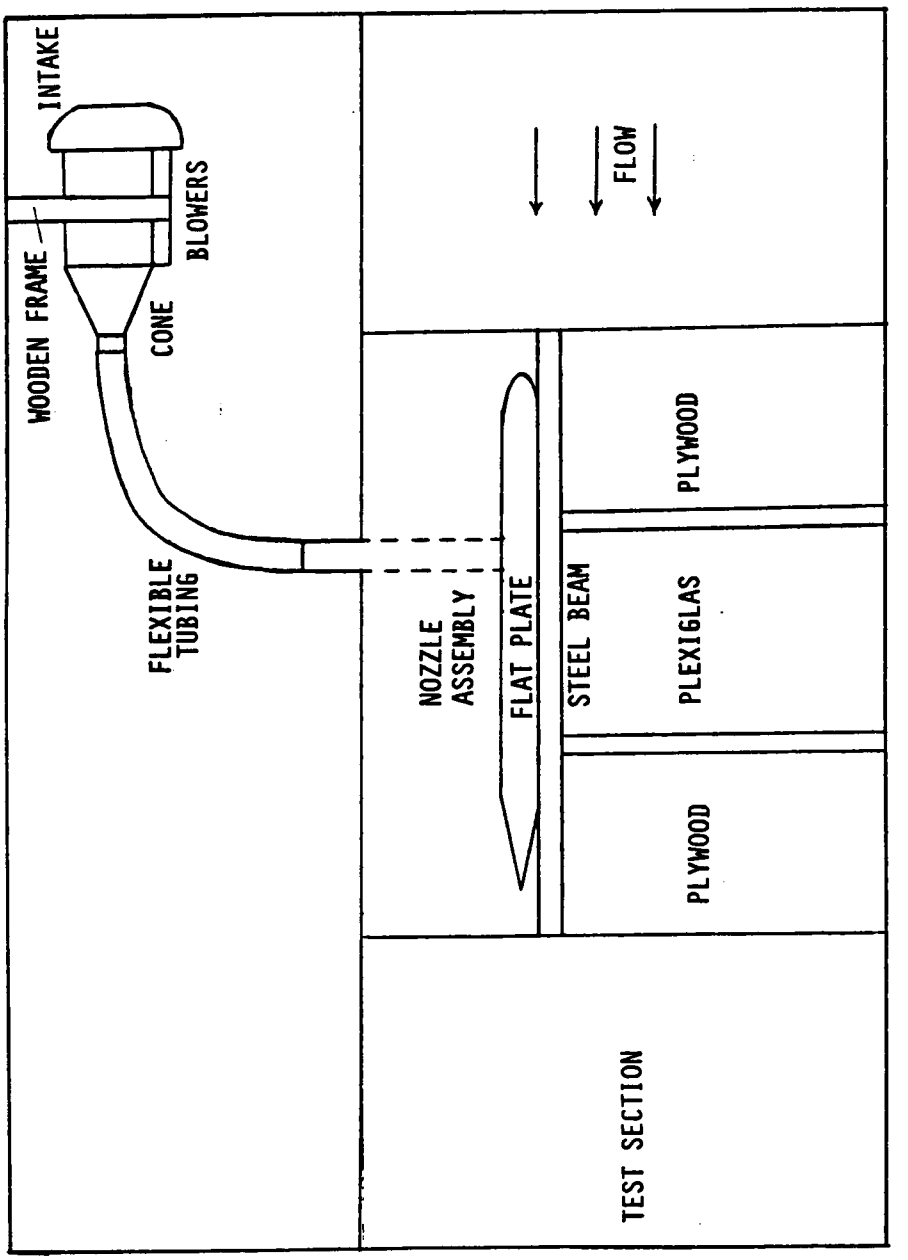

Figure 6. Model in the Tunnel (sideview).

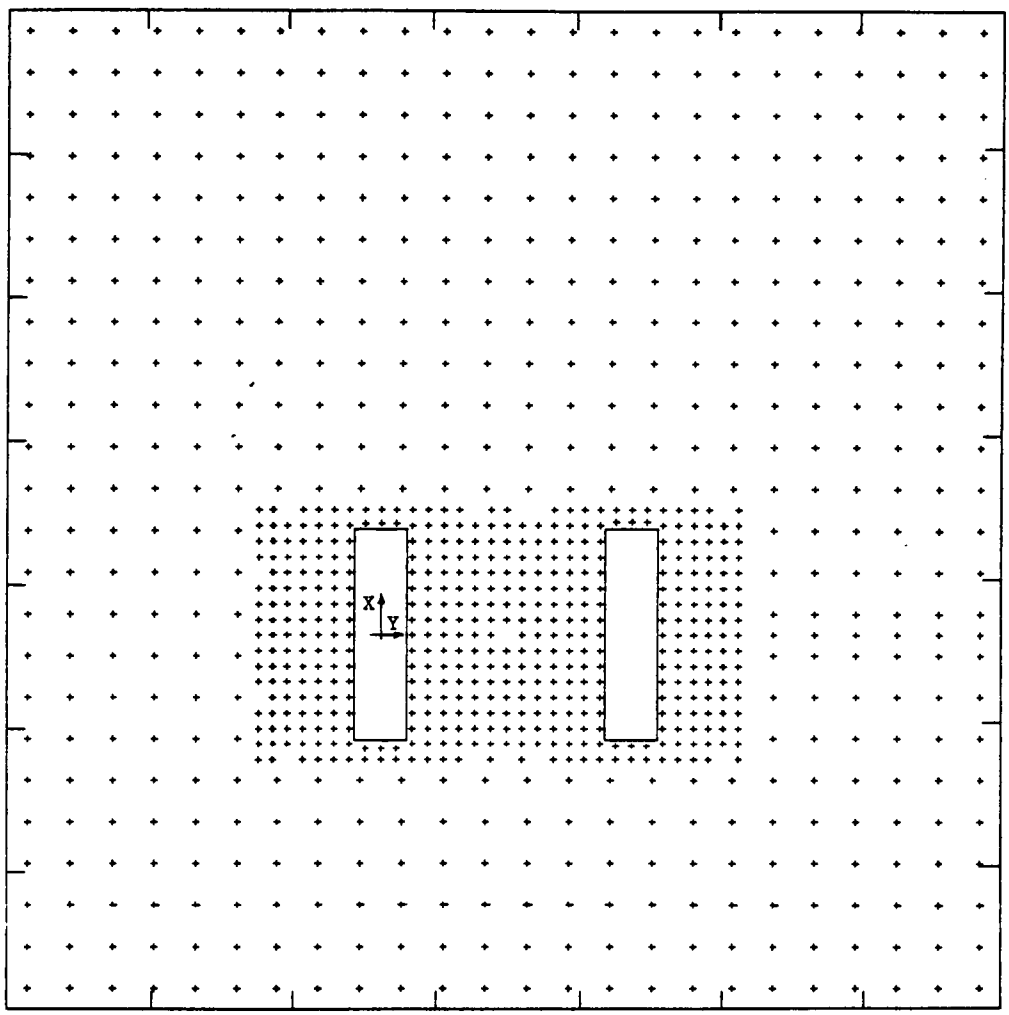

Figure 7. Pressure tap locations for 90° rectangular jets.

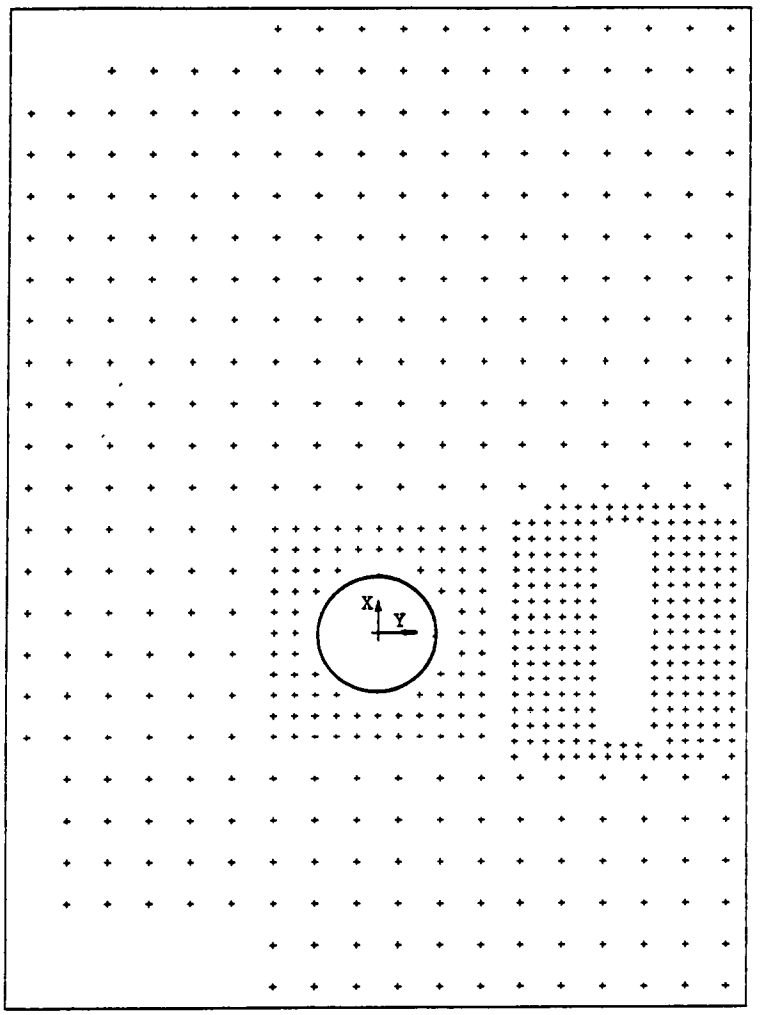

Figure 8. Pressure tap locations for 90° circular jet.

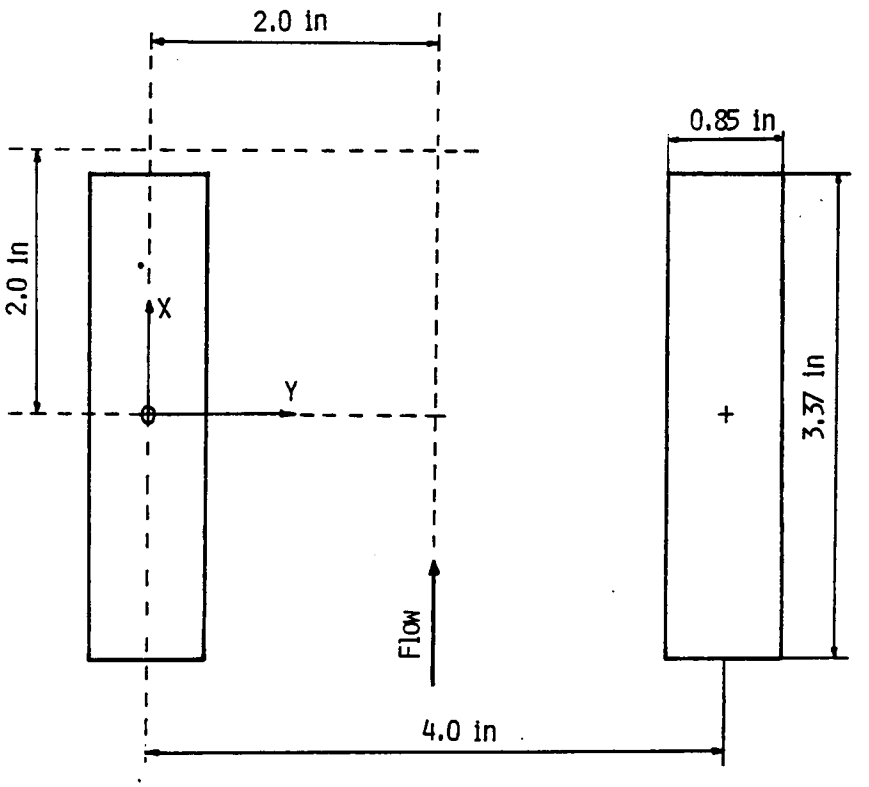

Figure 9. 90° rectangular jets; dimensions and coordinates.

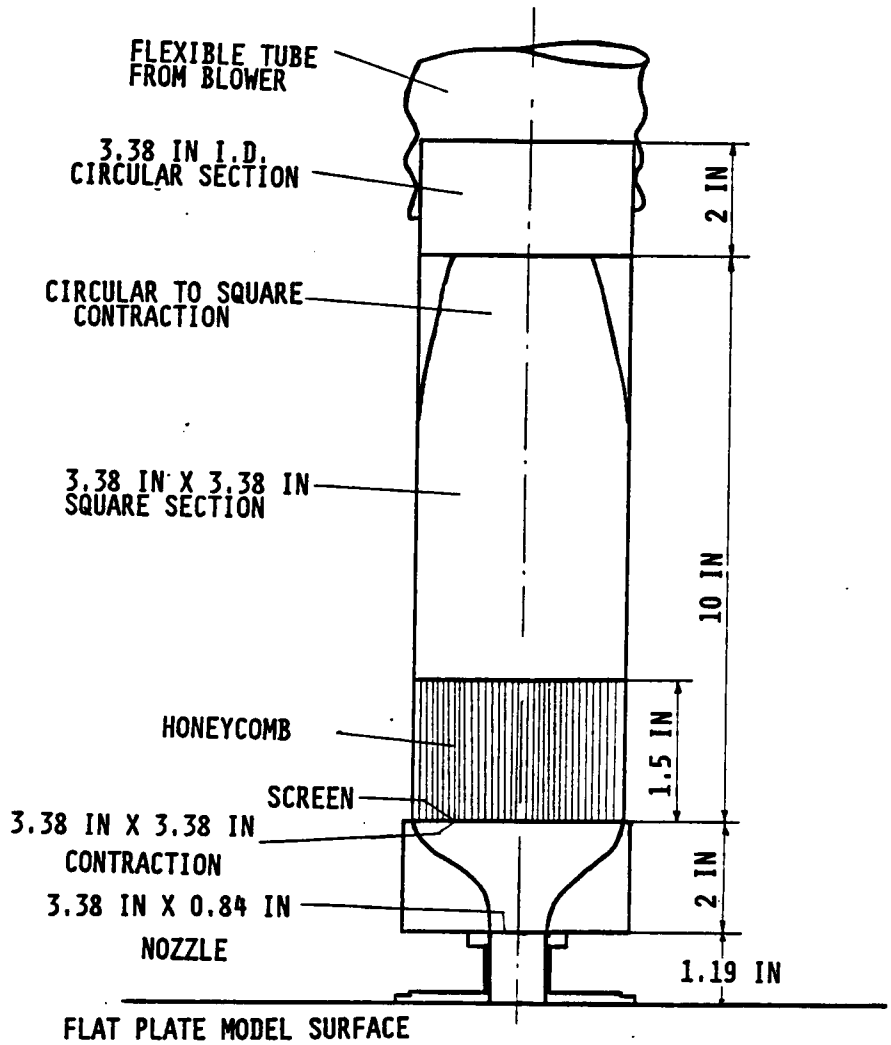

Figure 10. Rectangular jet nozzle assembly.

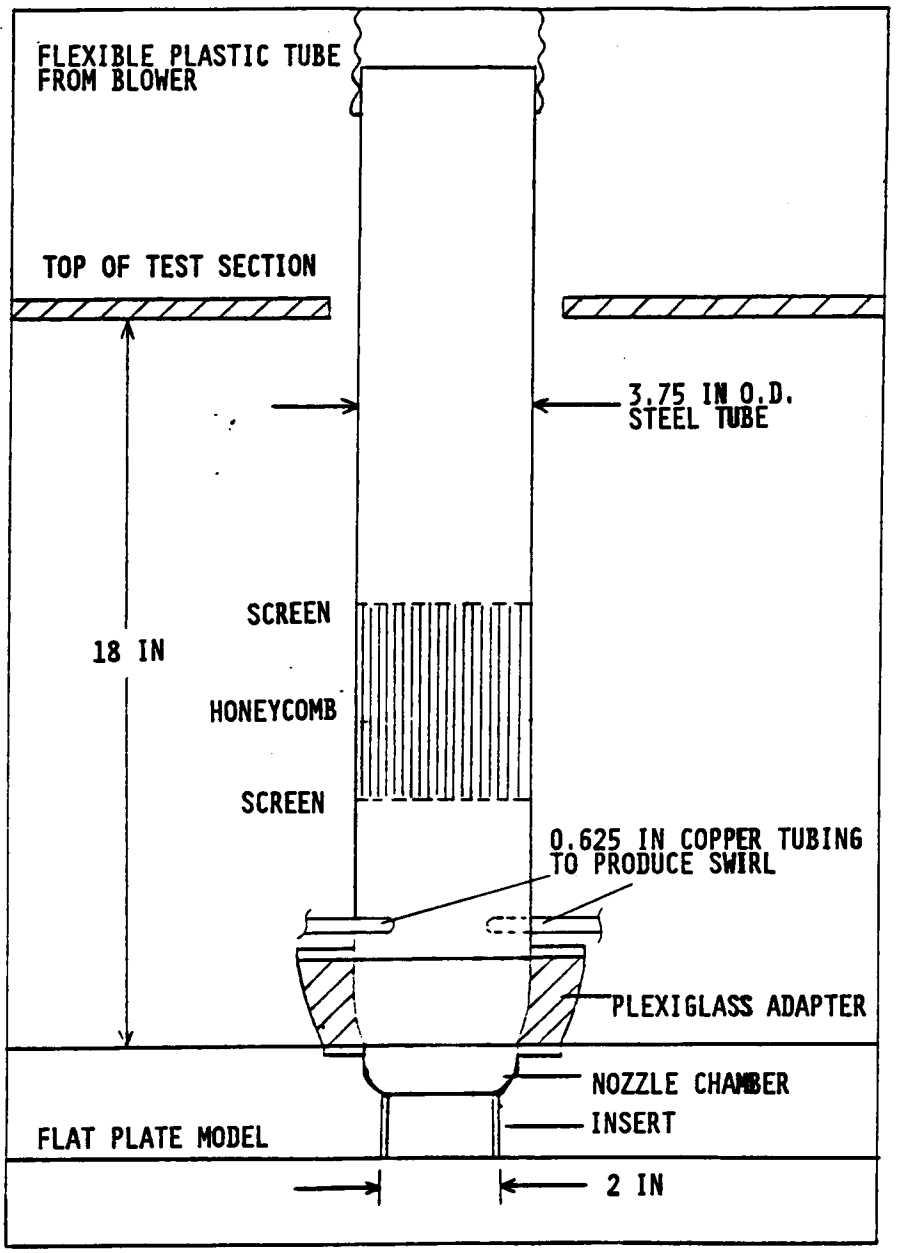

Figure 11. Circular jet nozzle assembly.

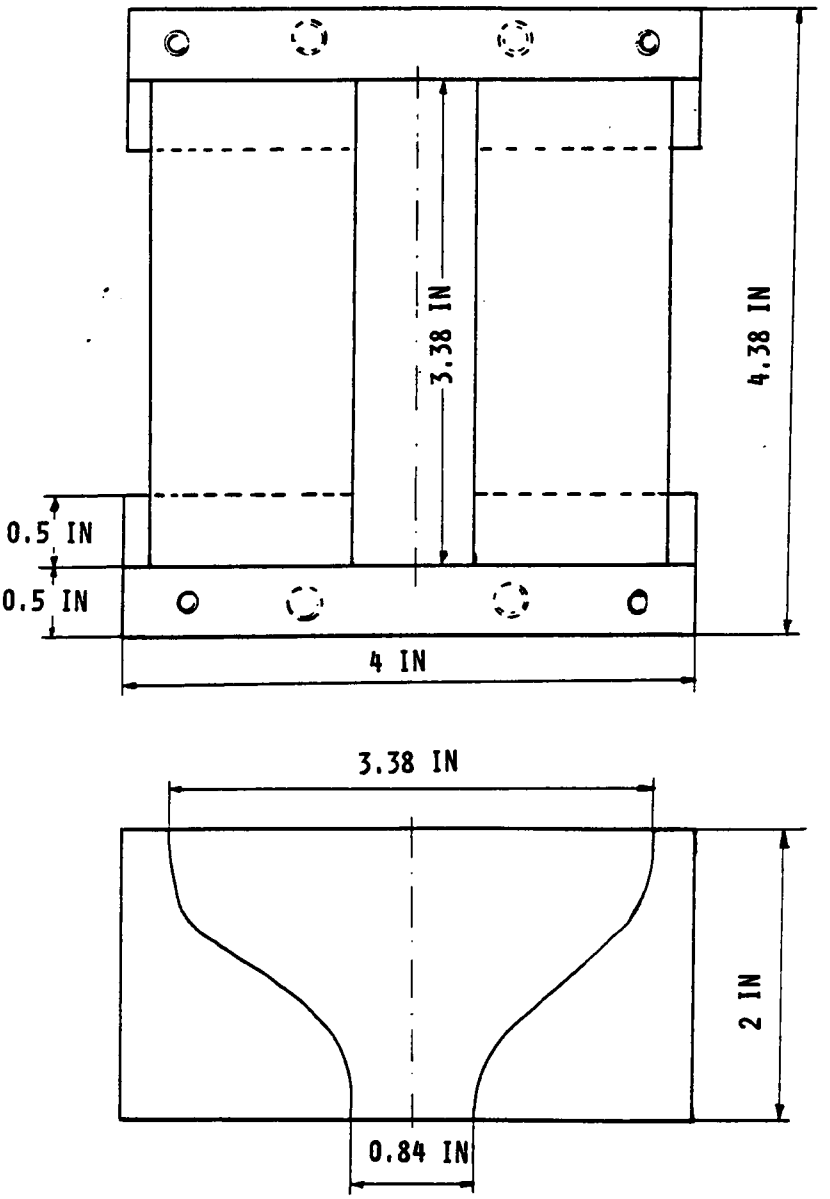

Figure 12. Rectangular jet contraction.

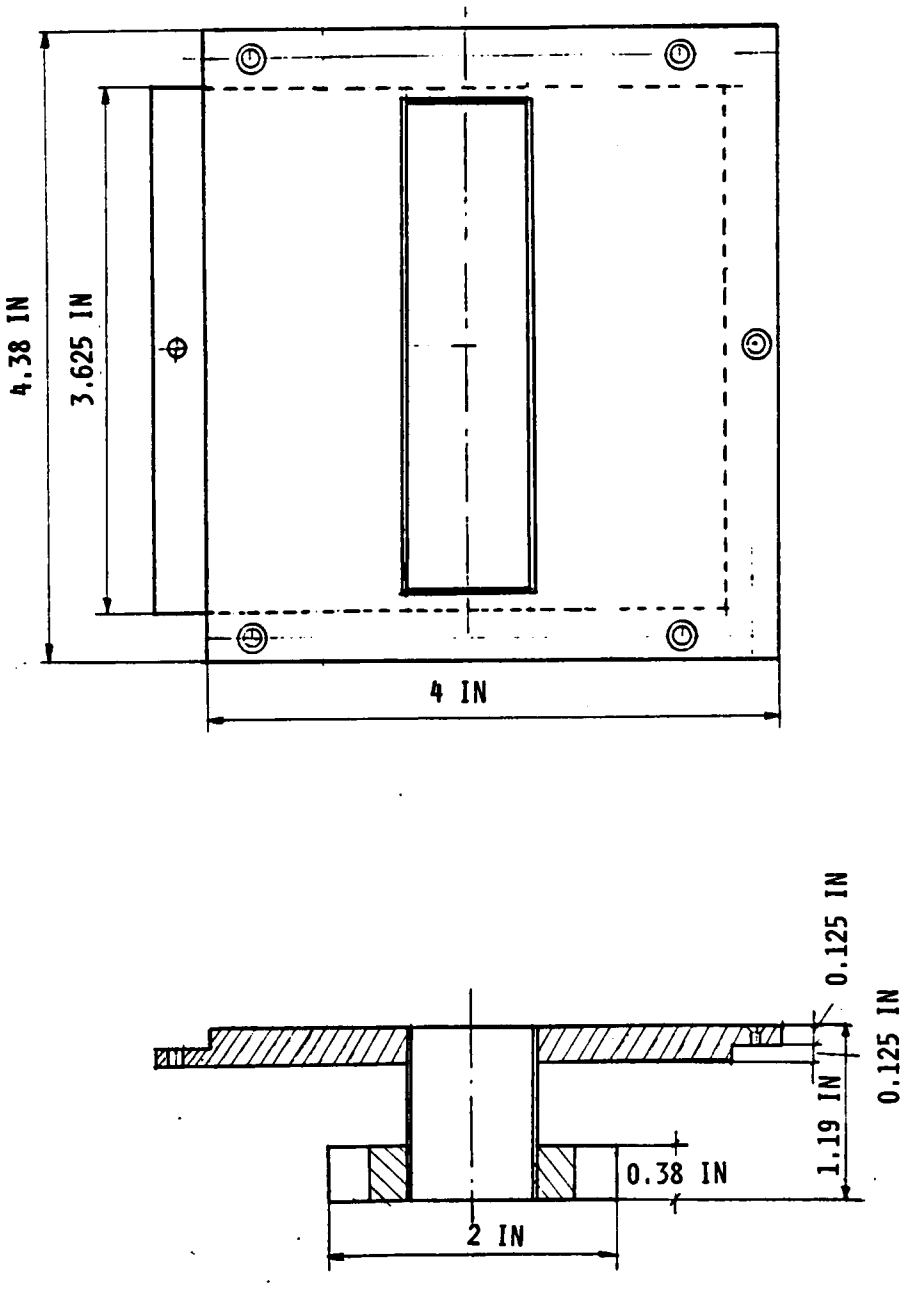

Figure 13. 90° rectangular jet nozzle.

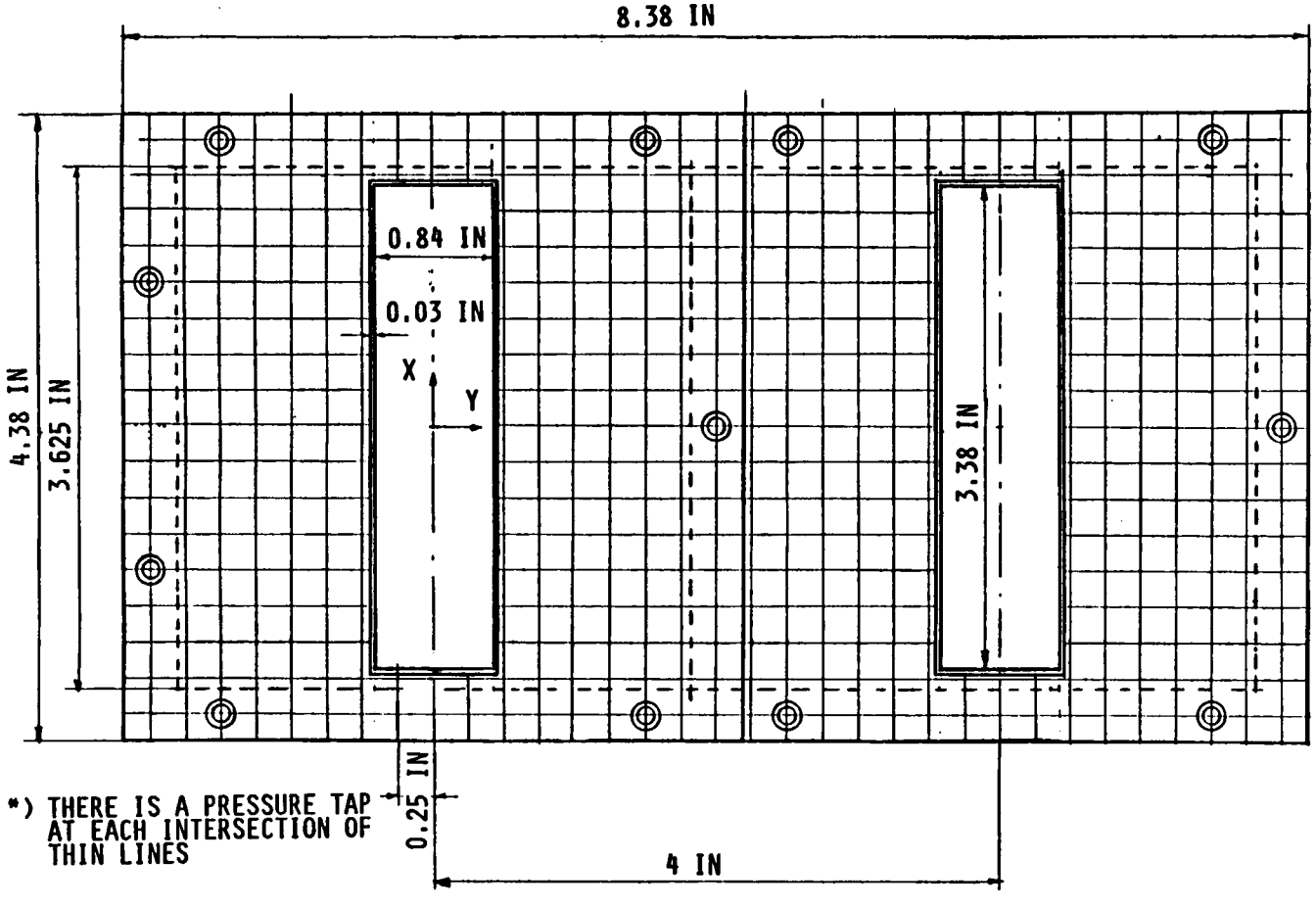

Figure 13. (continued)

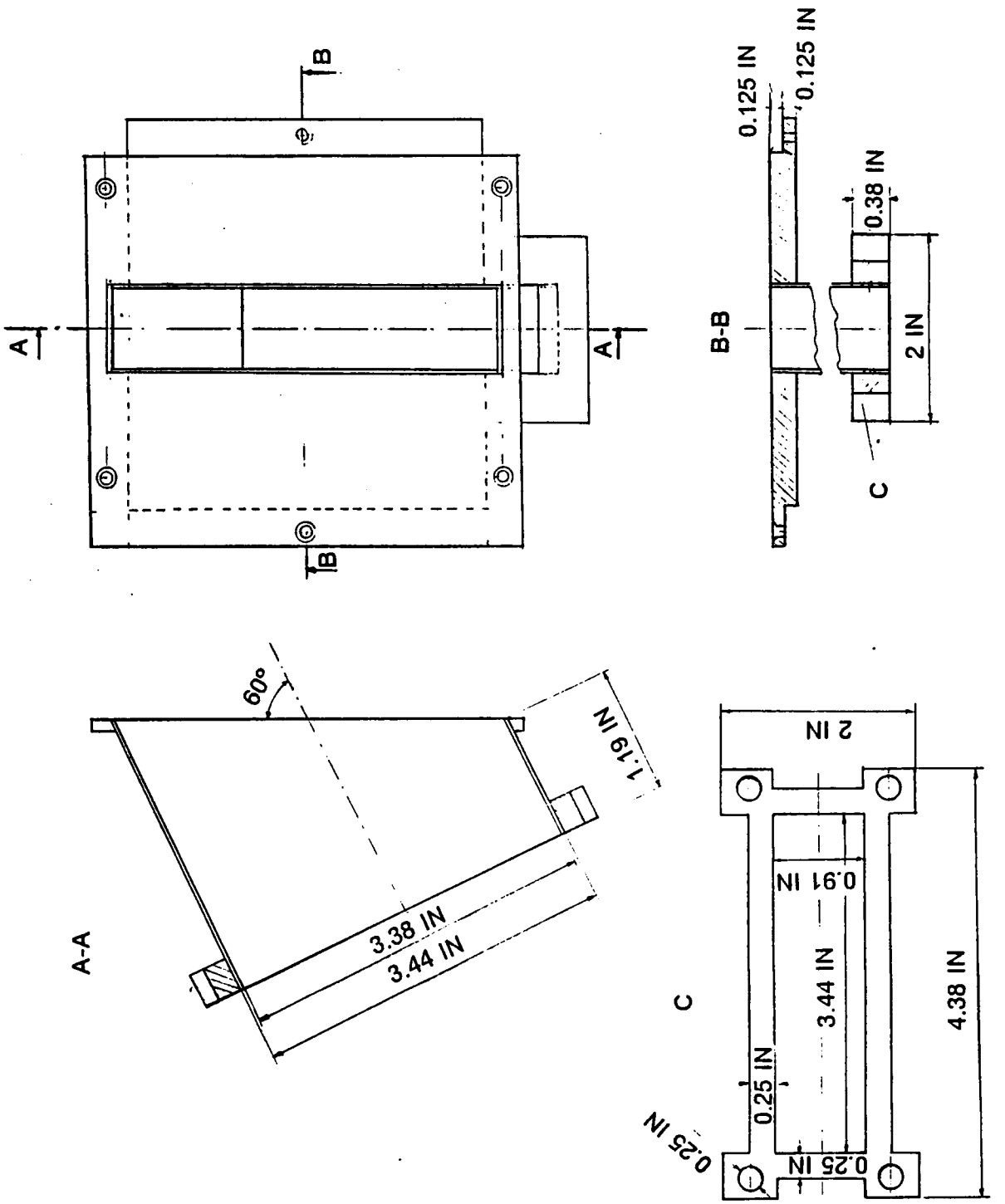

Figure 14. 60° rectangular jet nozzle.

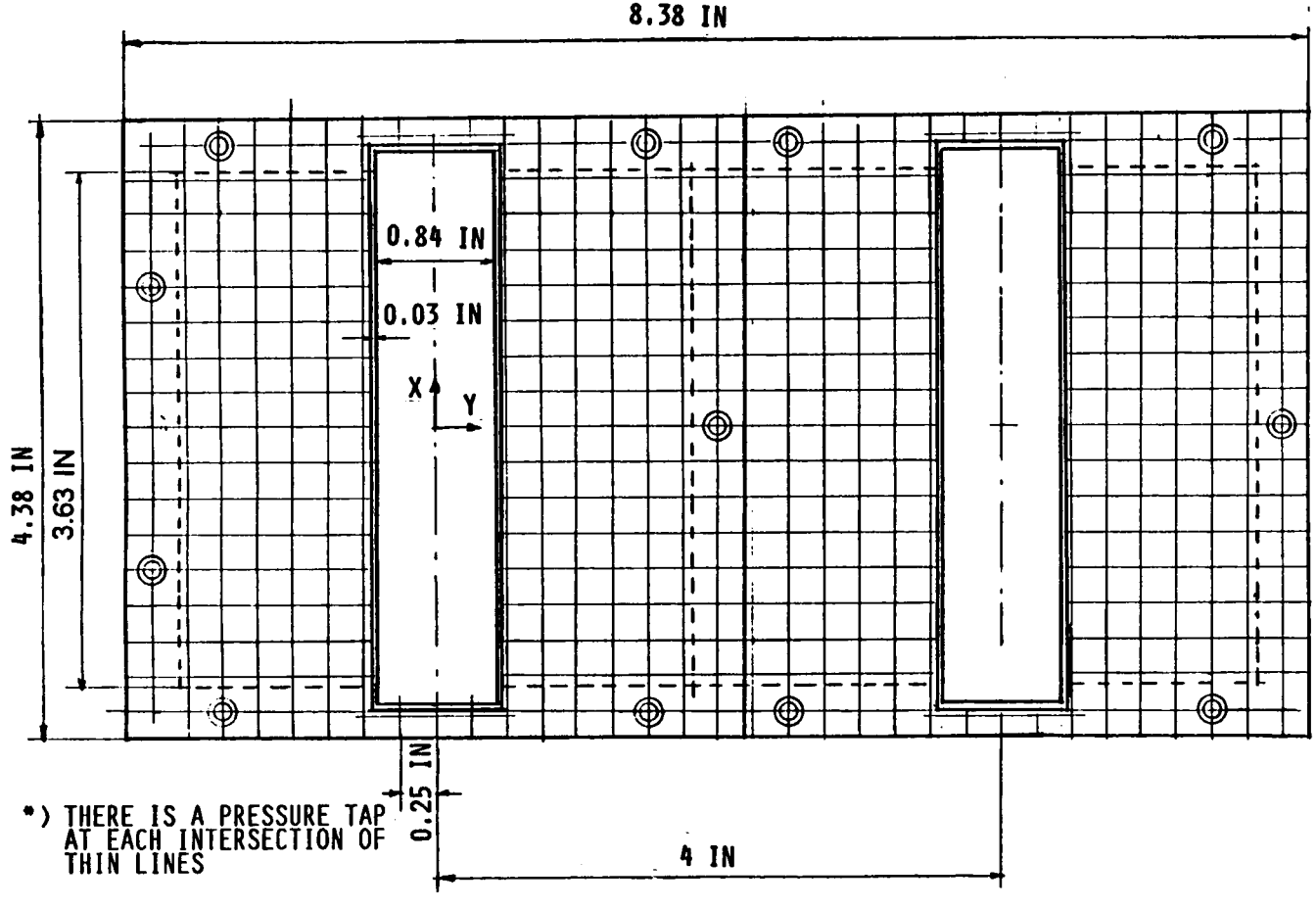

Figure 14. (continued)

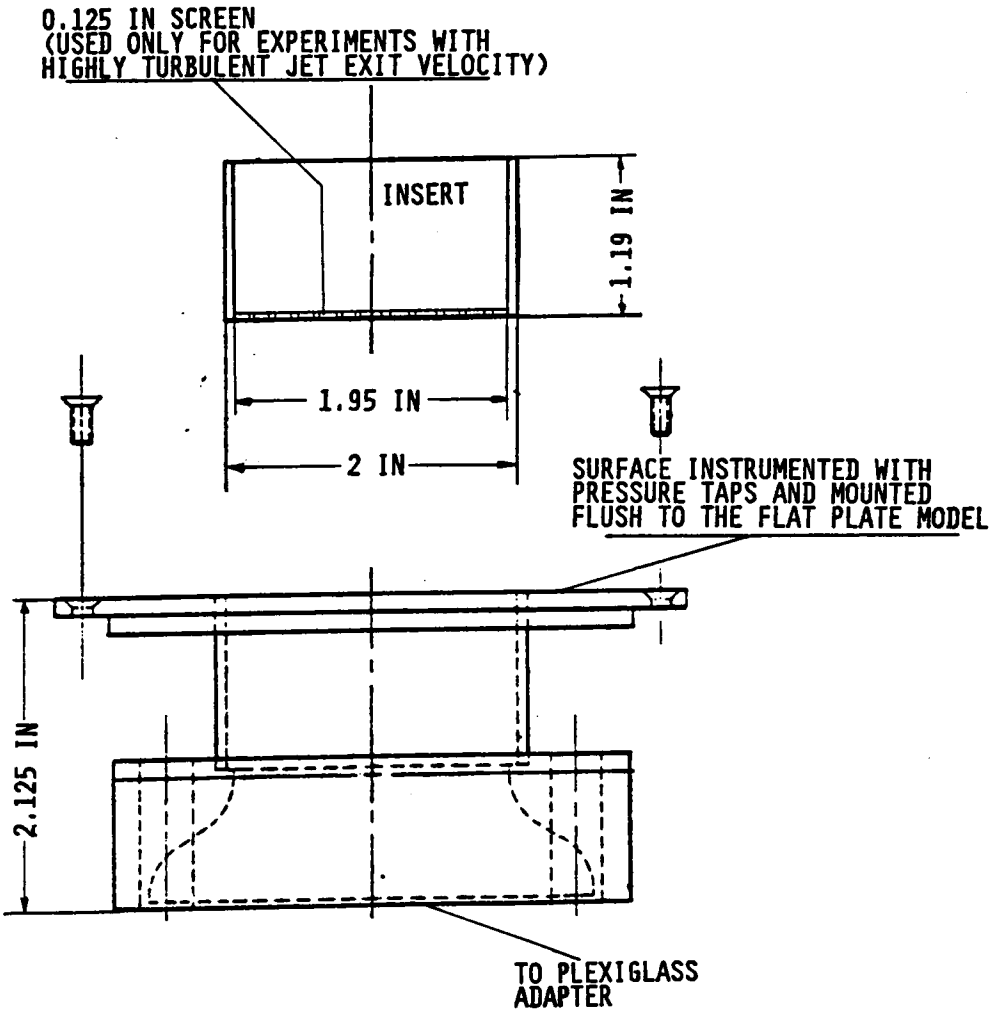

Figure 15. 90° circular jet nozzle.

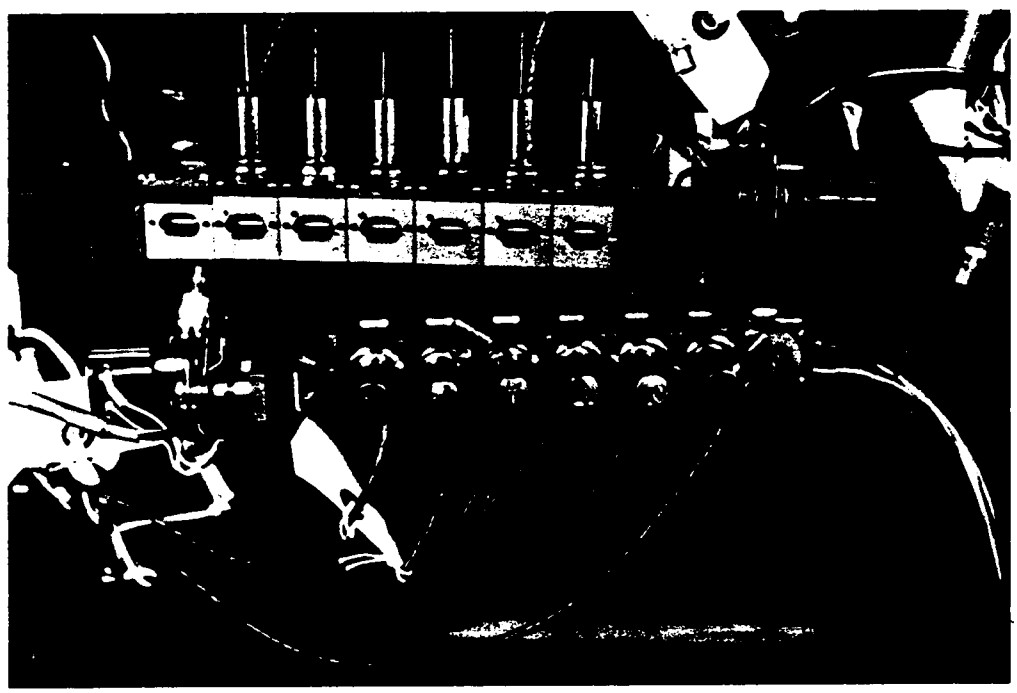

Figure 16. Scanivalves and Transducers.

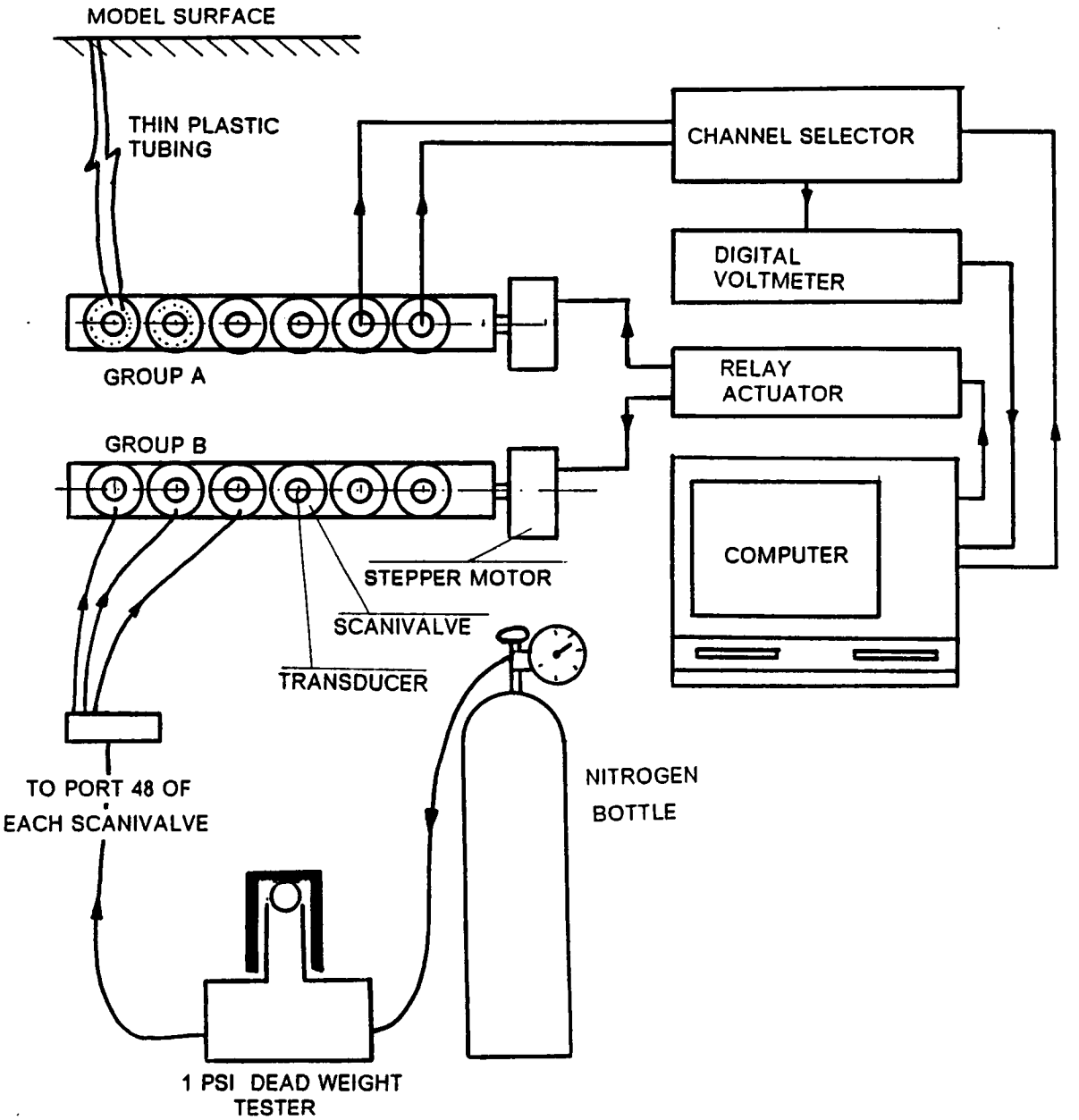

Figure 17. Instrumentation for pressure measurements.

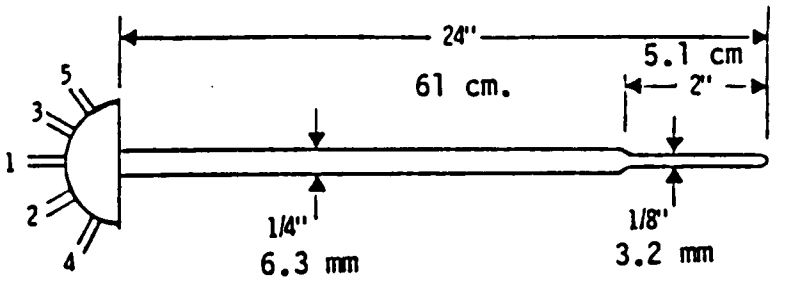

a) Dimensions (in mm).

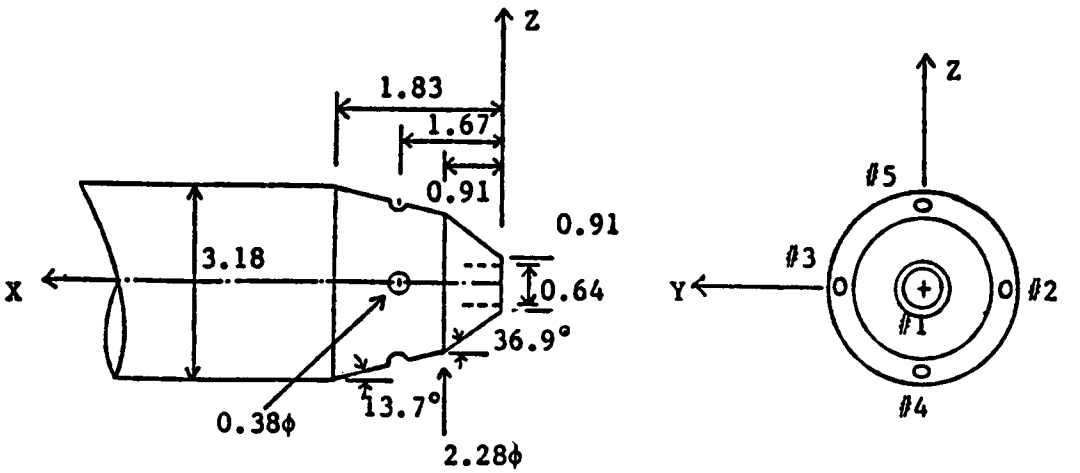

b) Details of the nose section

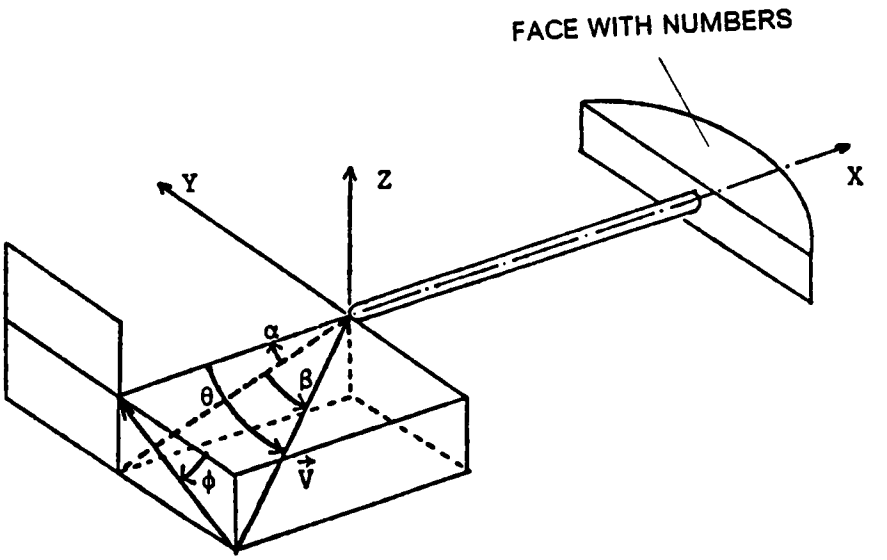

c) Probe coordinates and angles

Figure 18. Yawhead Probe.

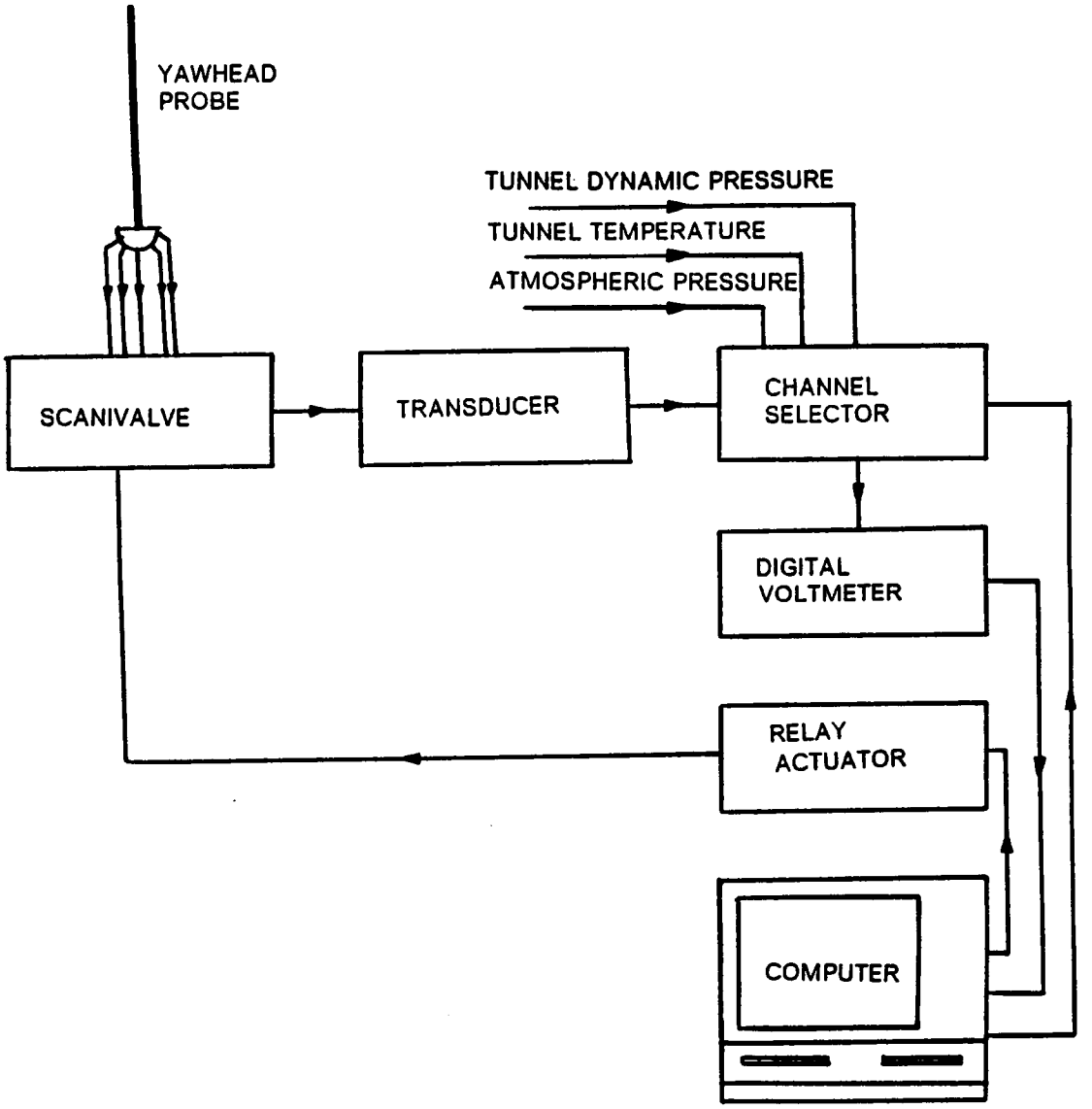

Figure 19. Instrumentation for mean flowfield measurements.

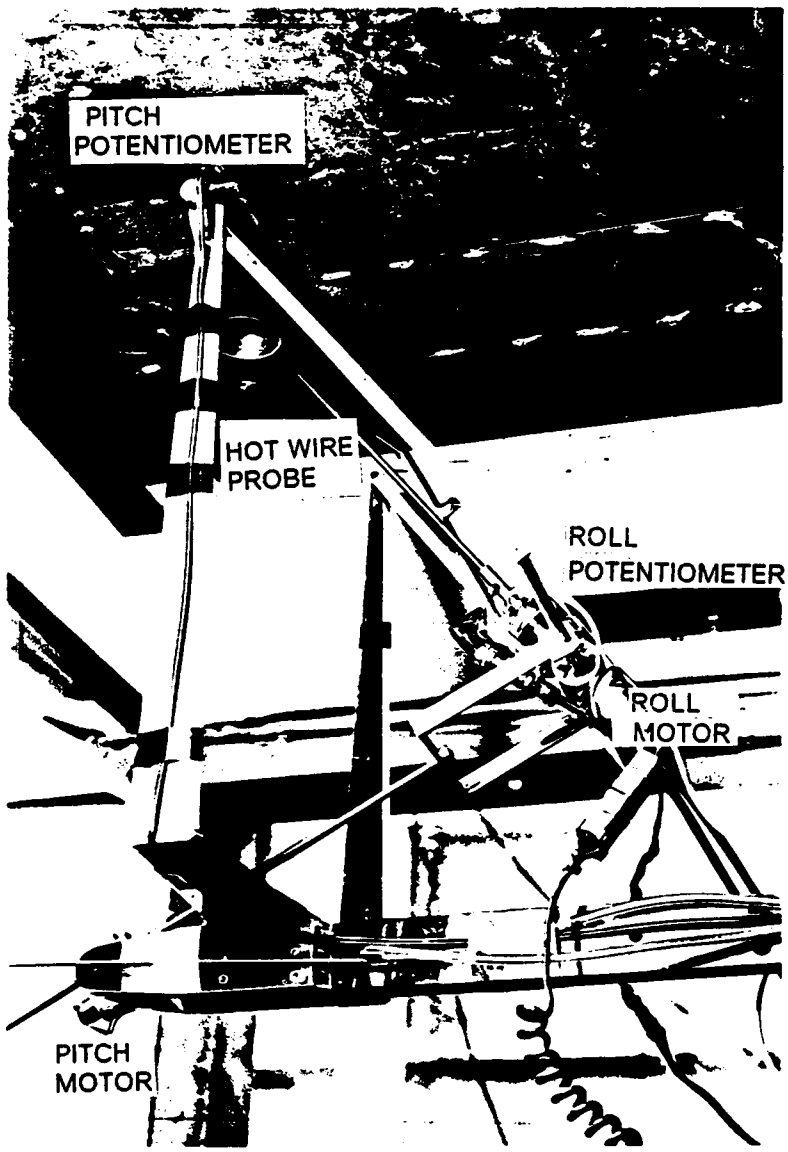

Figure 20. Hot-wire probe and probe rotator.

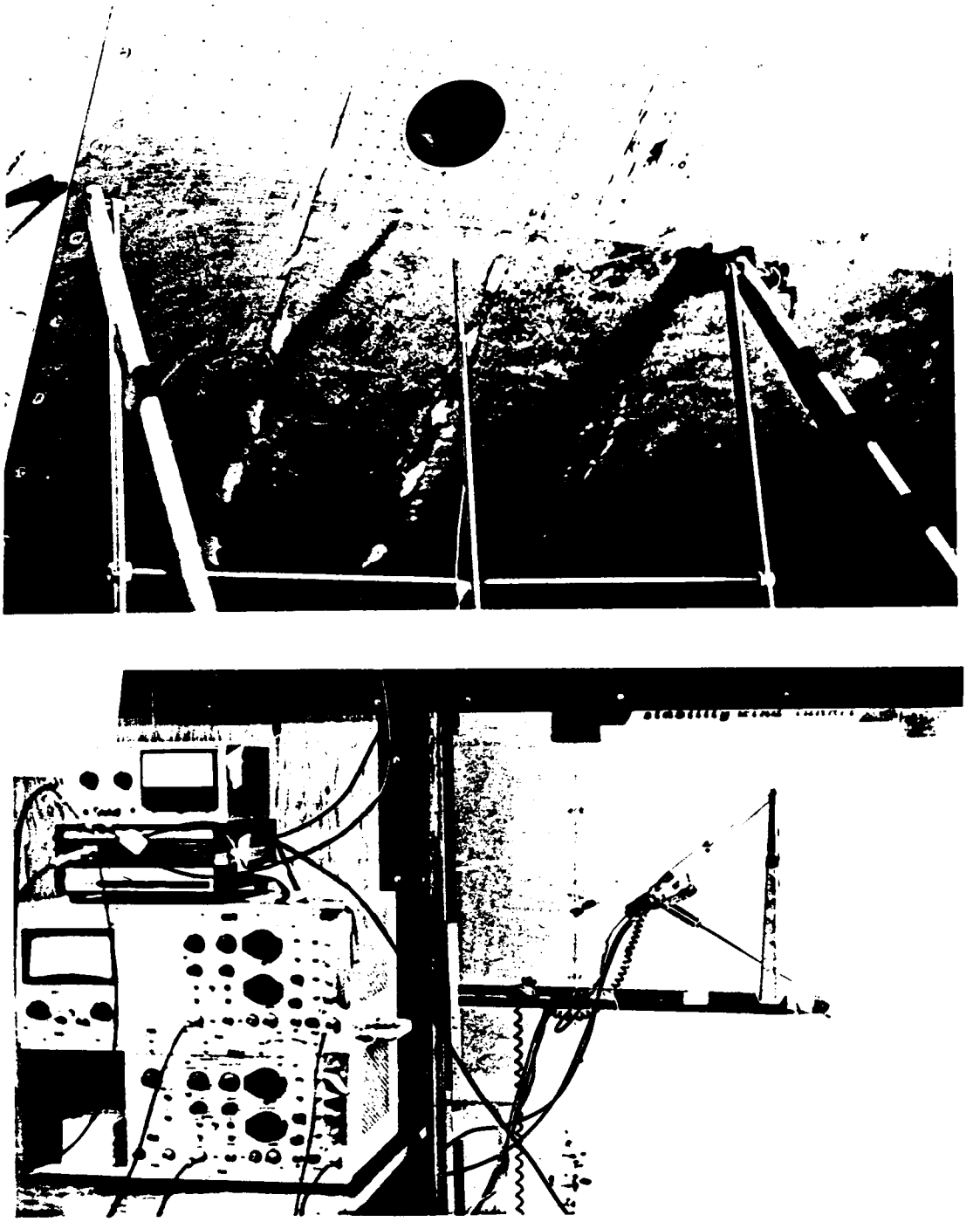

Figure 20. (continued)

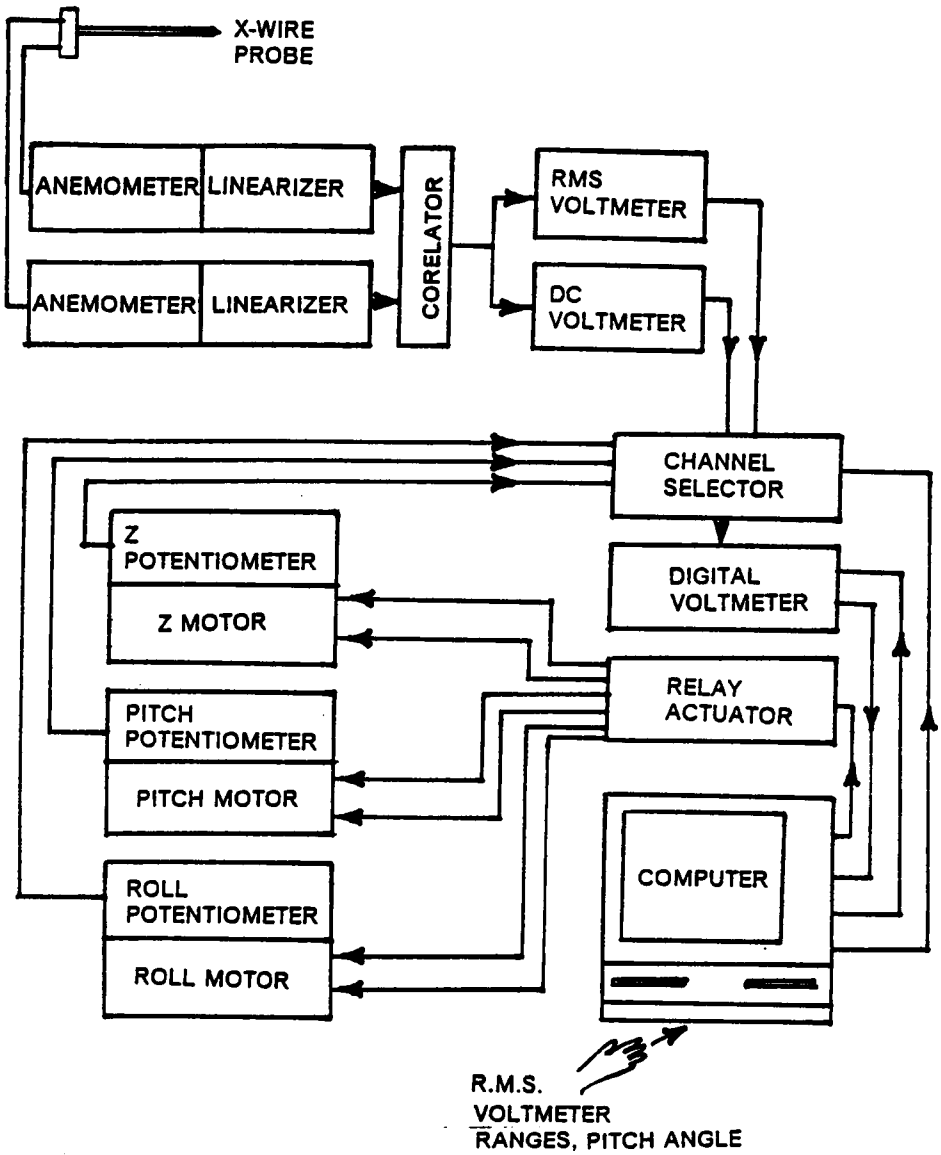

Figure 21. Instrumentation for turbulence measurements.

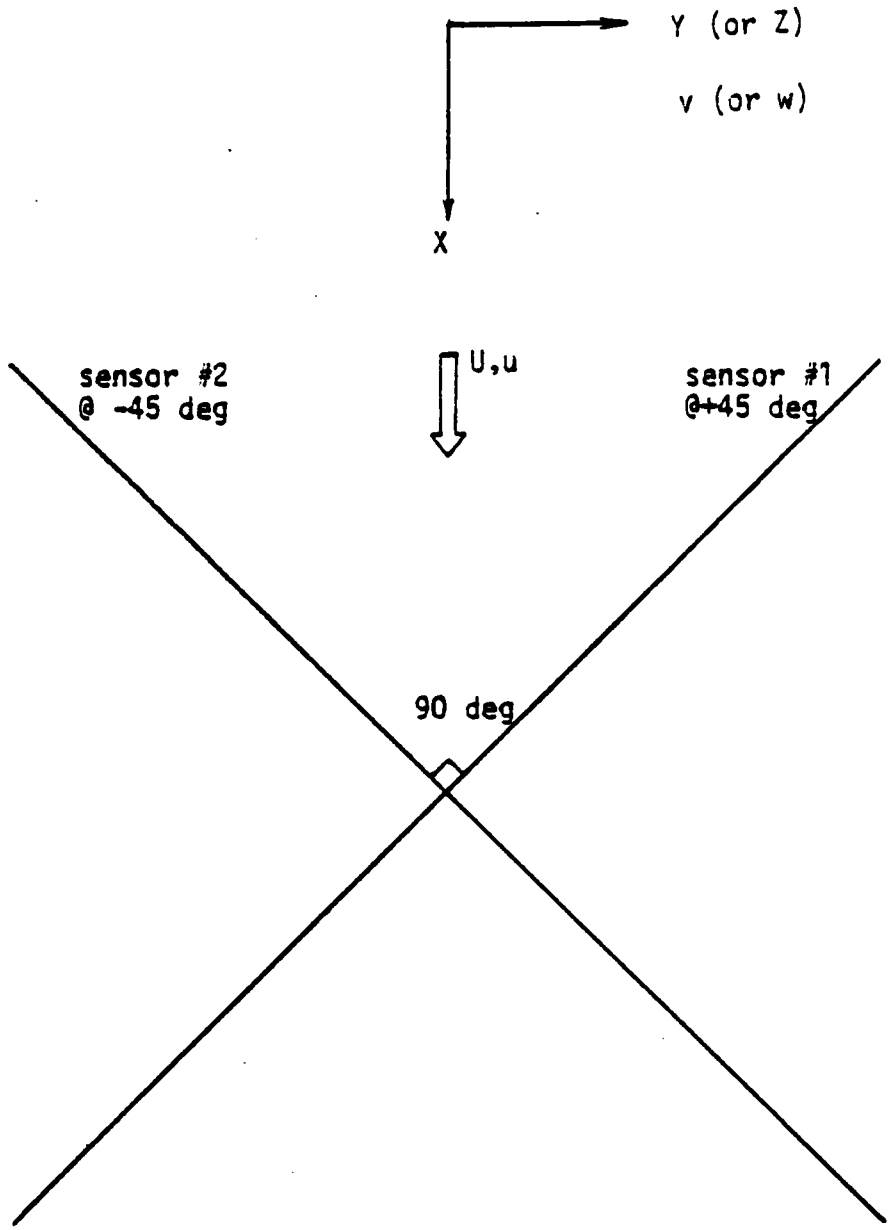

Figure 22. X-wire probe and probe coordinates.

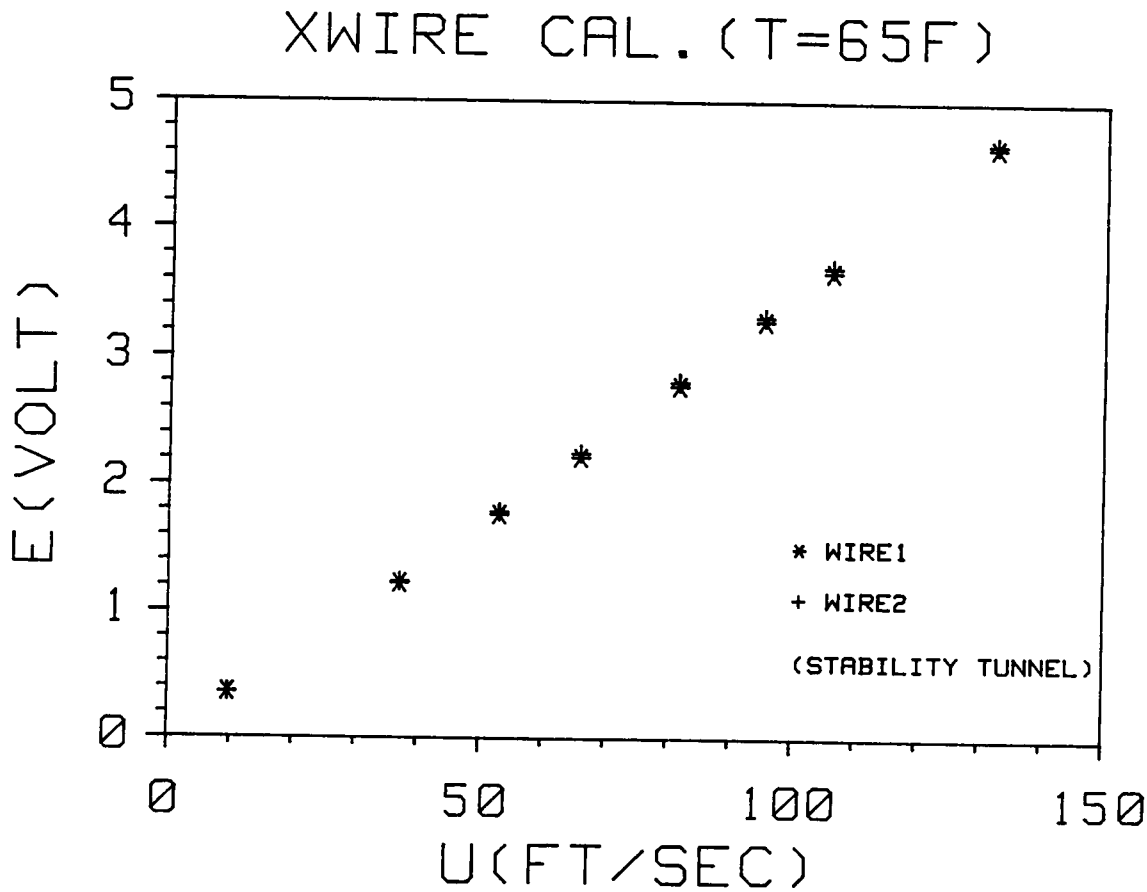

Figure 23. A sample linearized X-wire calibration.

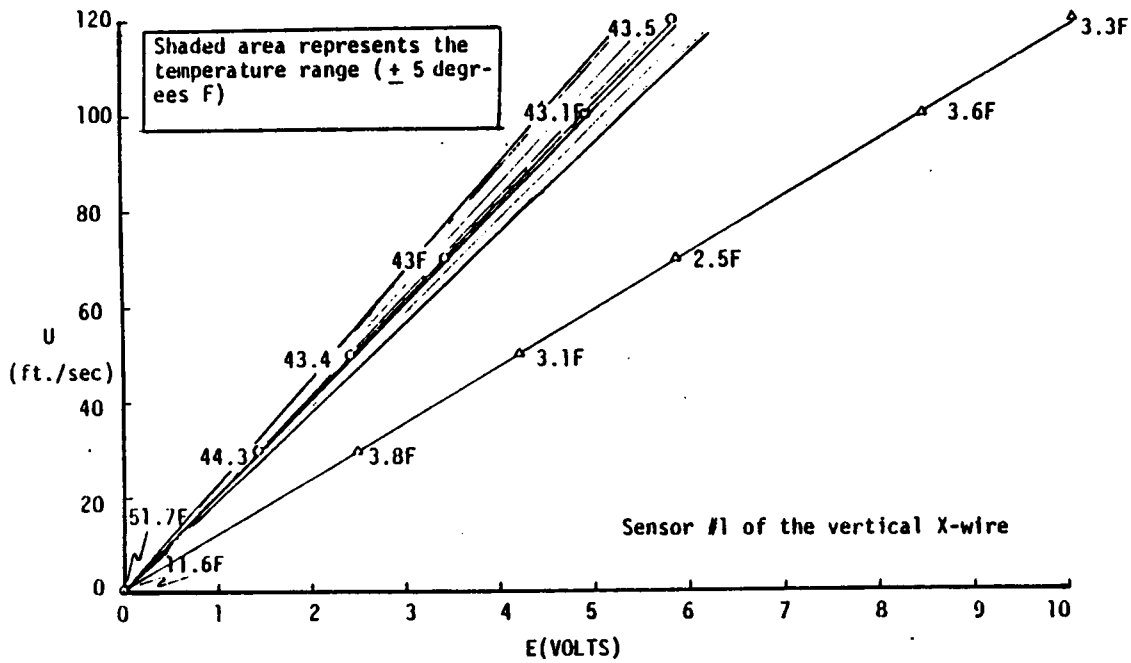

Figure 24. Effect of temperature on the linearized hot wire output: (from Ref.16)

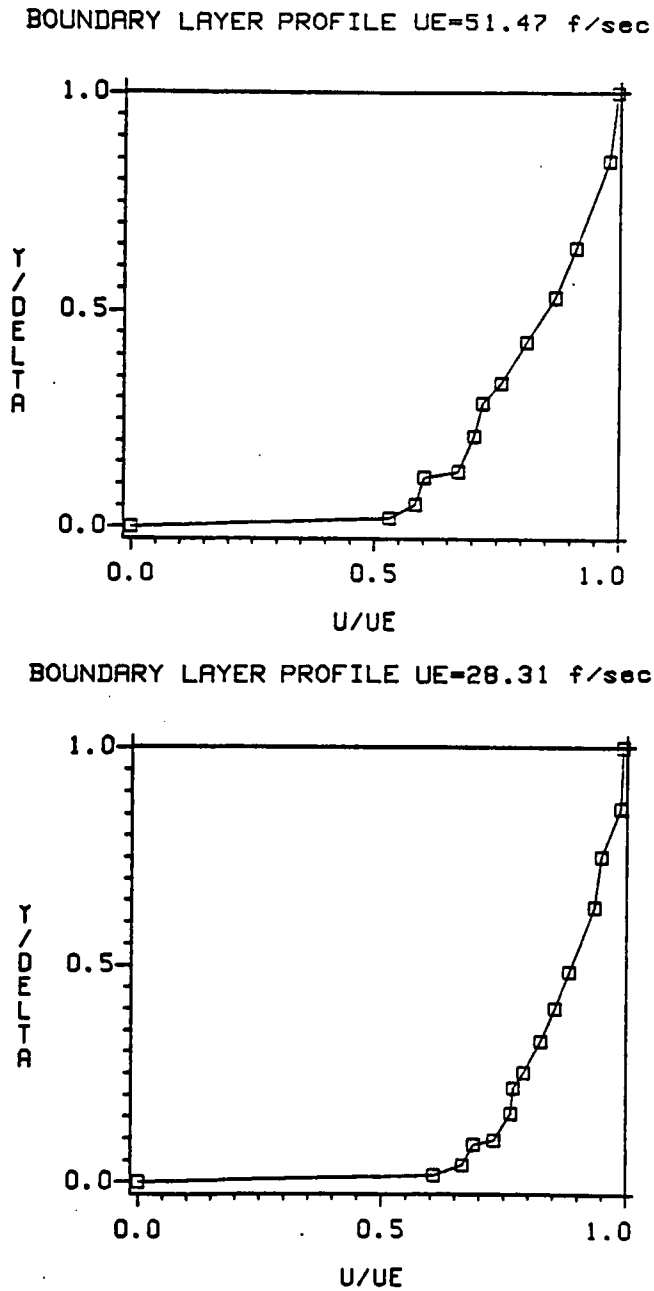

Figure 25. Boundary layer profiles at the nozzle location.: (from Ref.96)

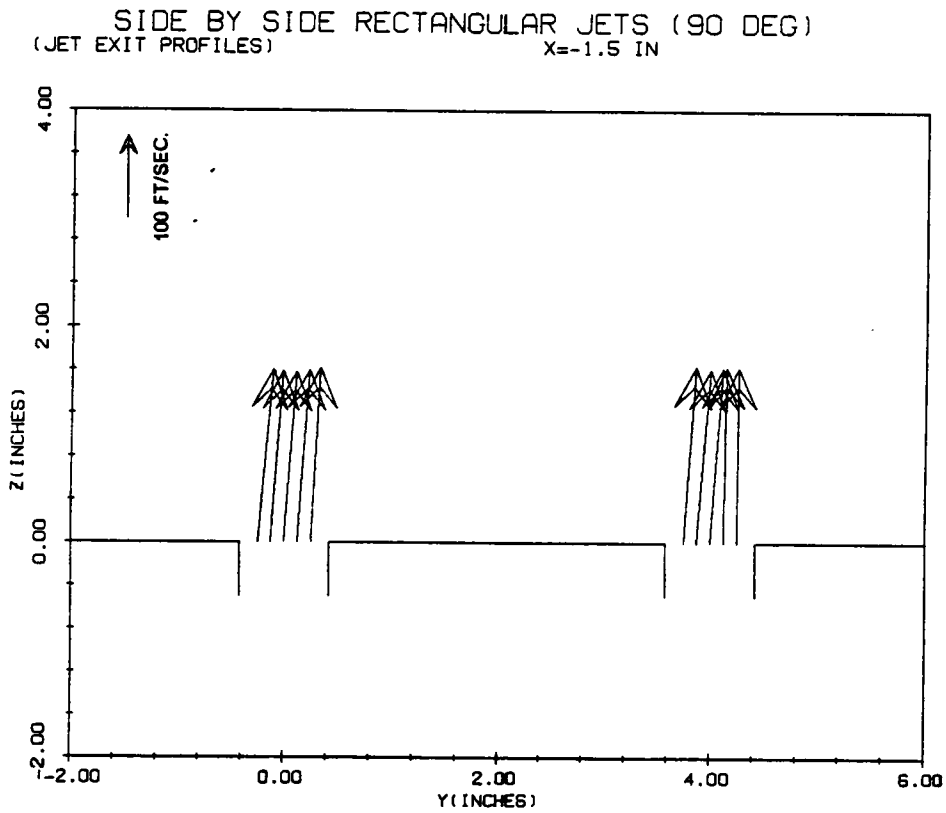

Figure 26. 90° rectangular jet exit profiles.: a) X = -1.5 in.

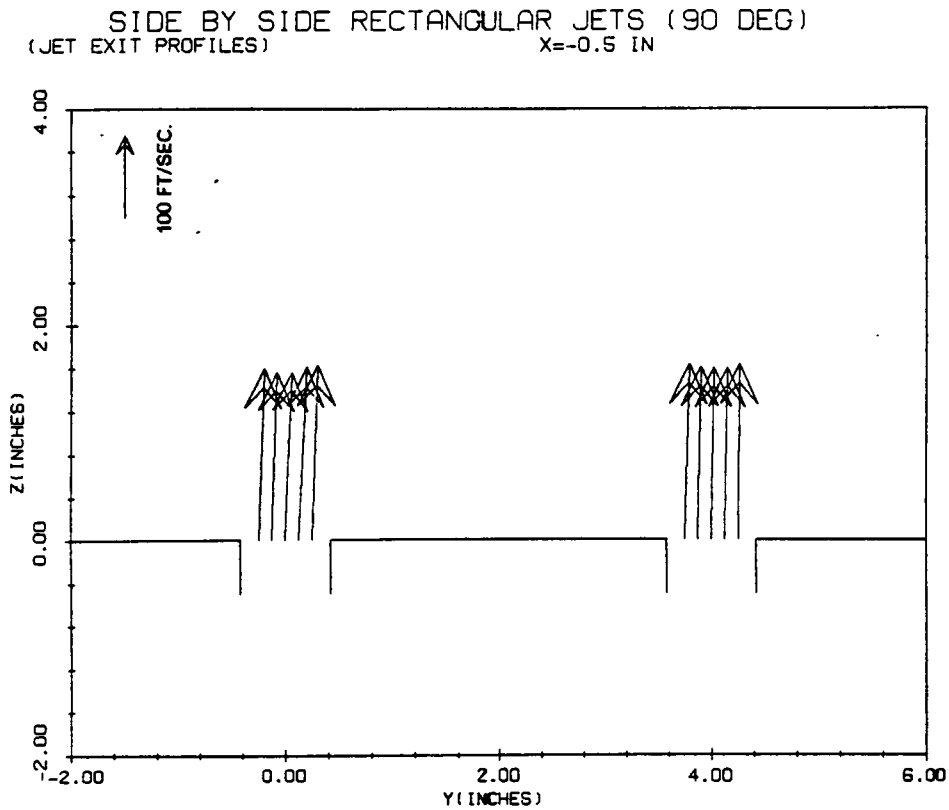

Figure 26. b) X = -0.5 in.

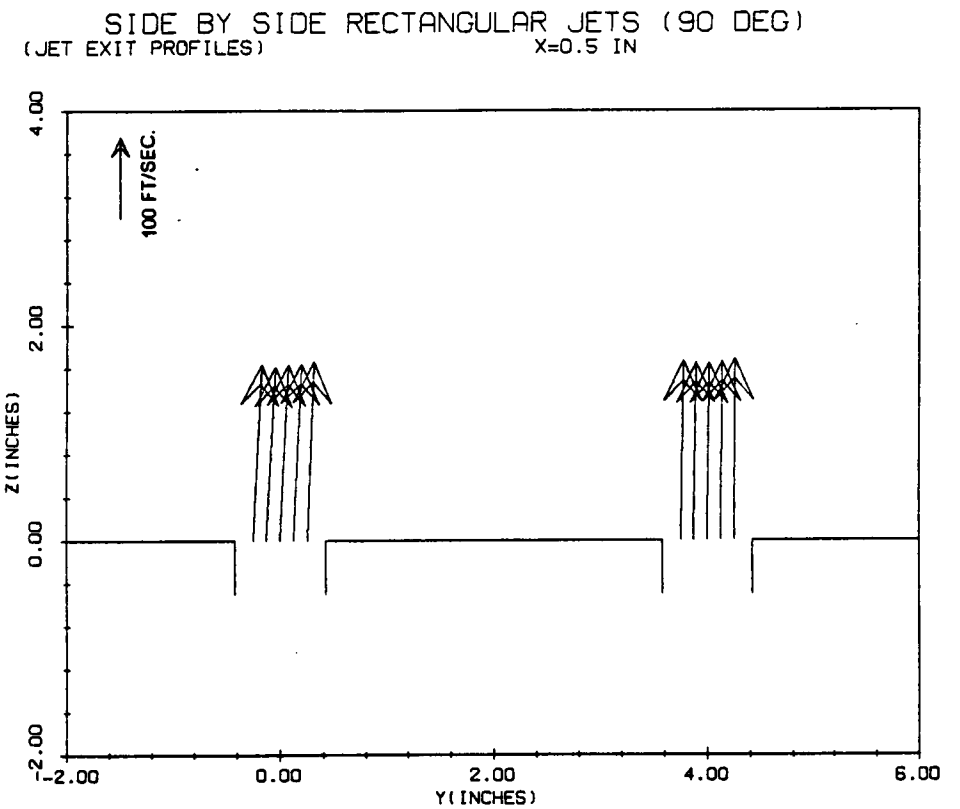

Figure 26. c) X = 0.5 in.

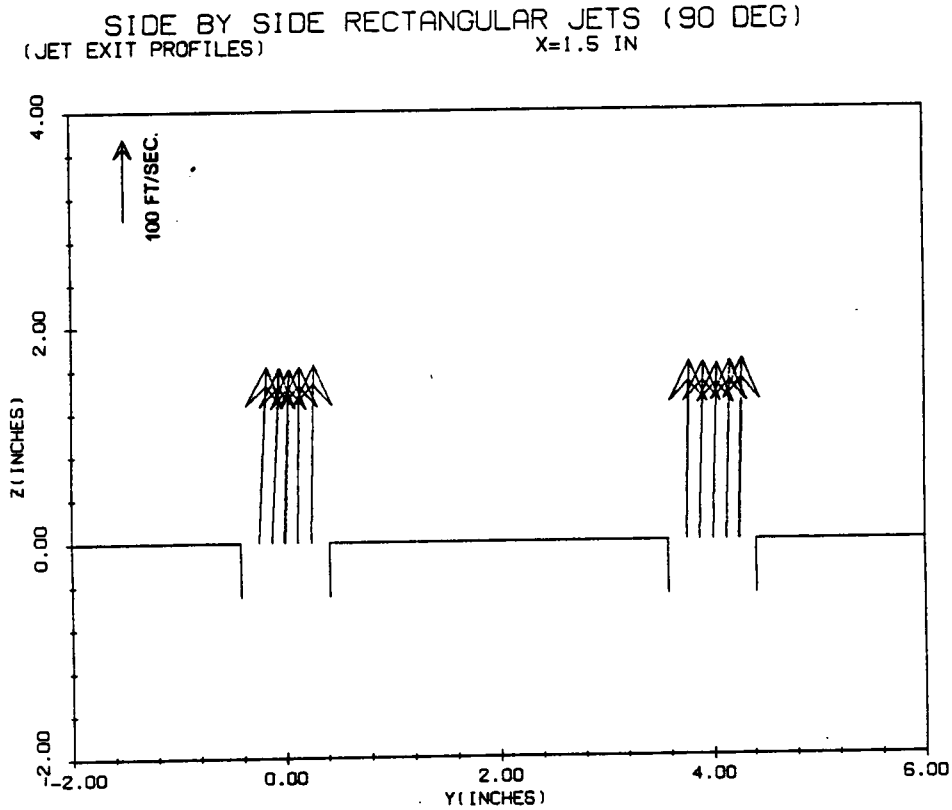

Figure 26. d) X = 1.5 in.

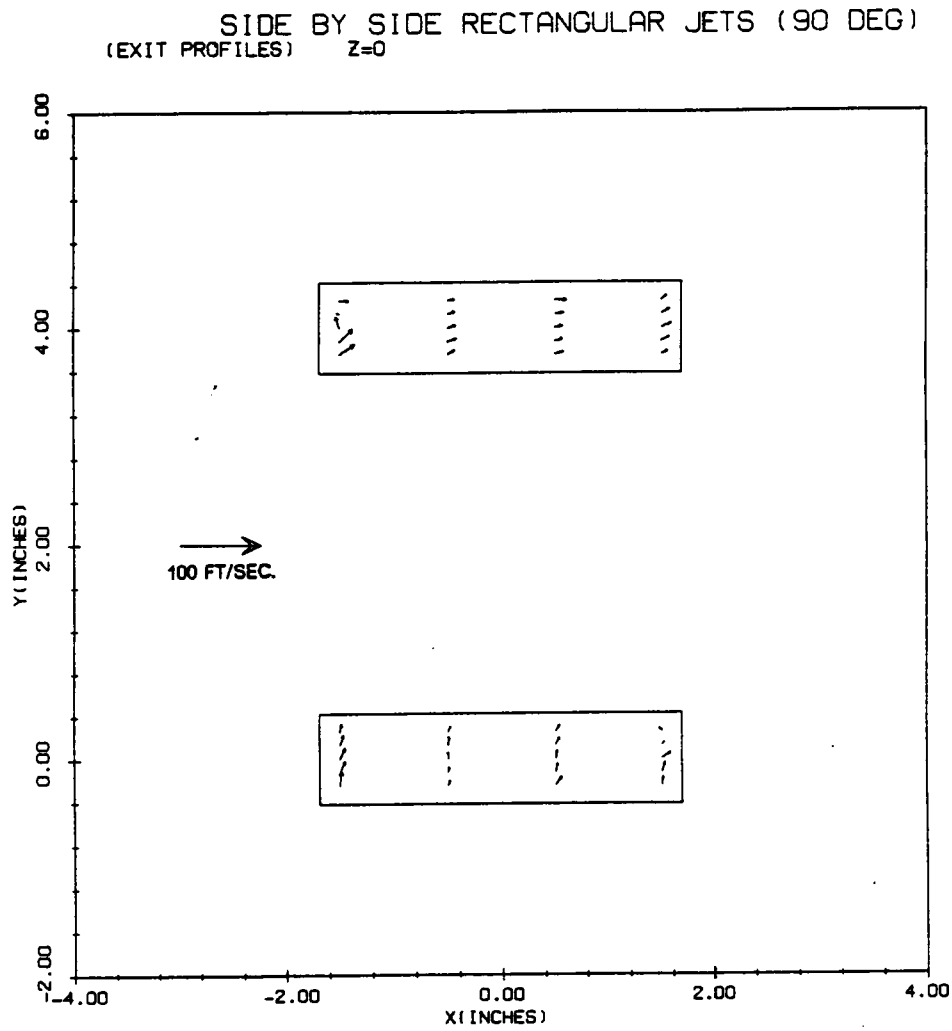

Figure 26. e) Z = 0.0 in.

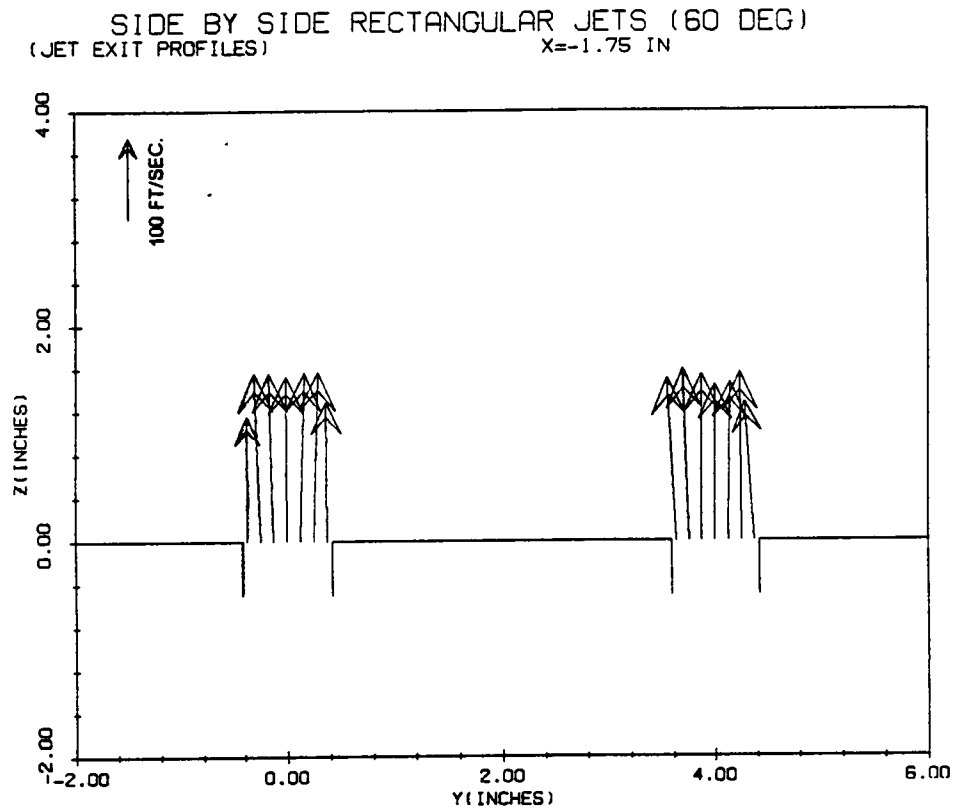

Figure 27. 60° rectangular jet exit profiles.: a) X = -1.75 in.

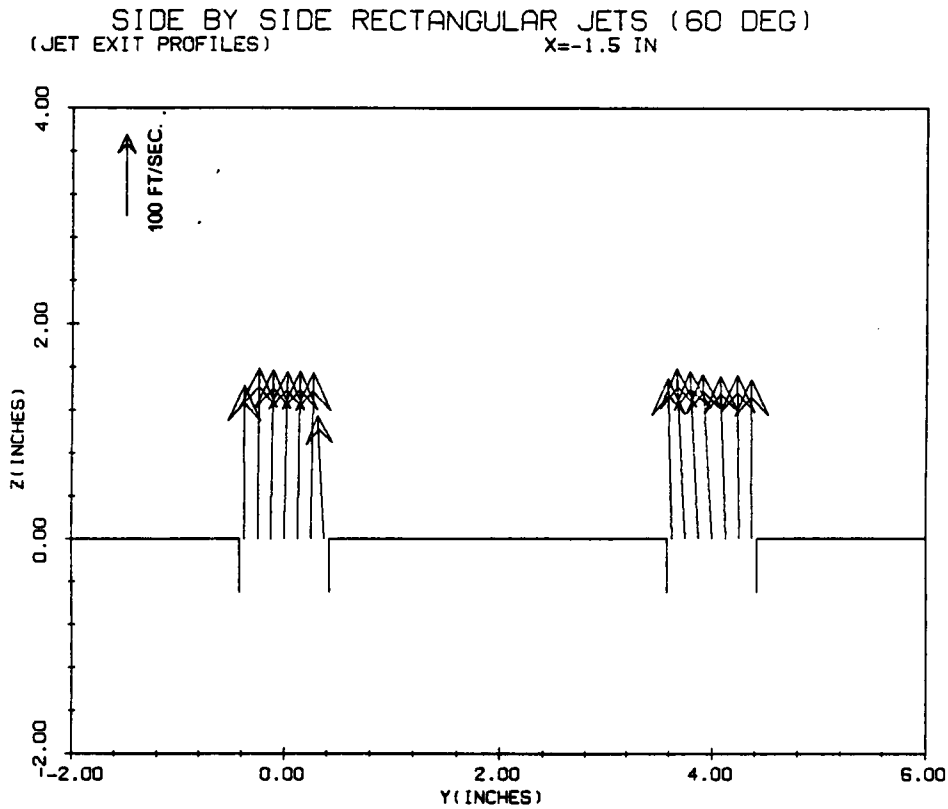

Figure 27. b) X = -1.5 in.

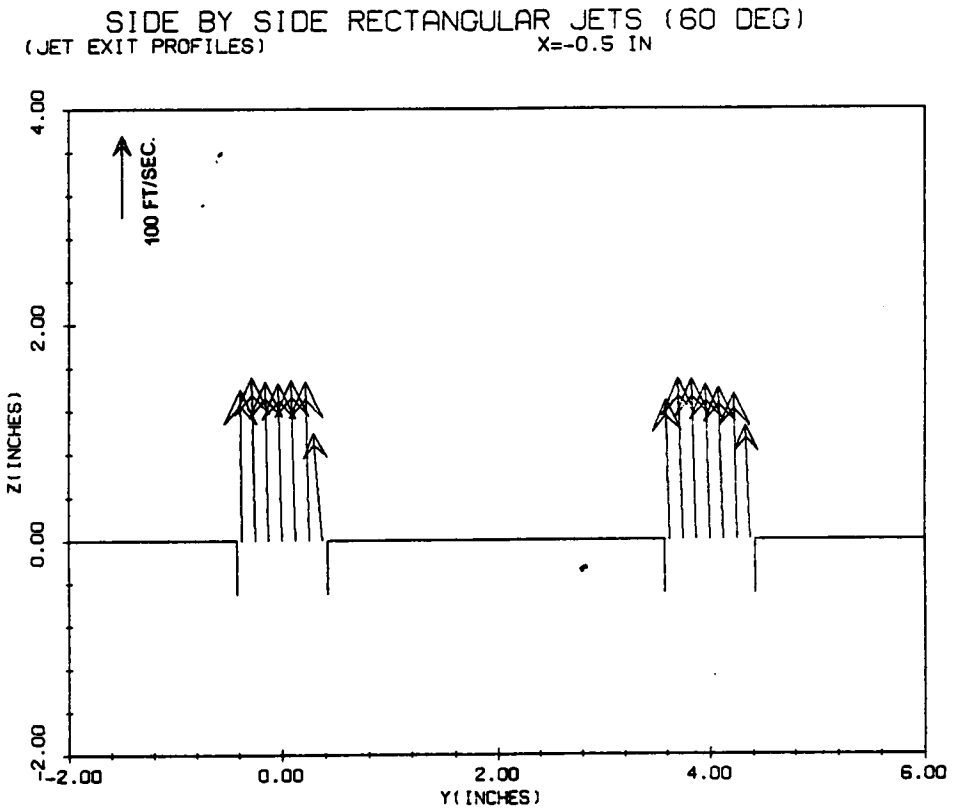

Figure 27. c) X = -0.5 in.

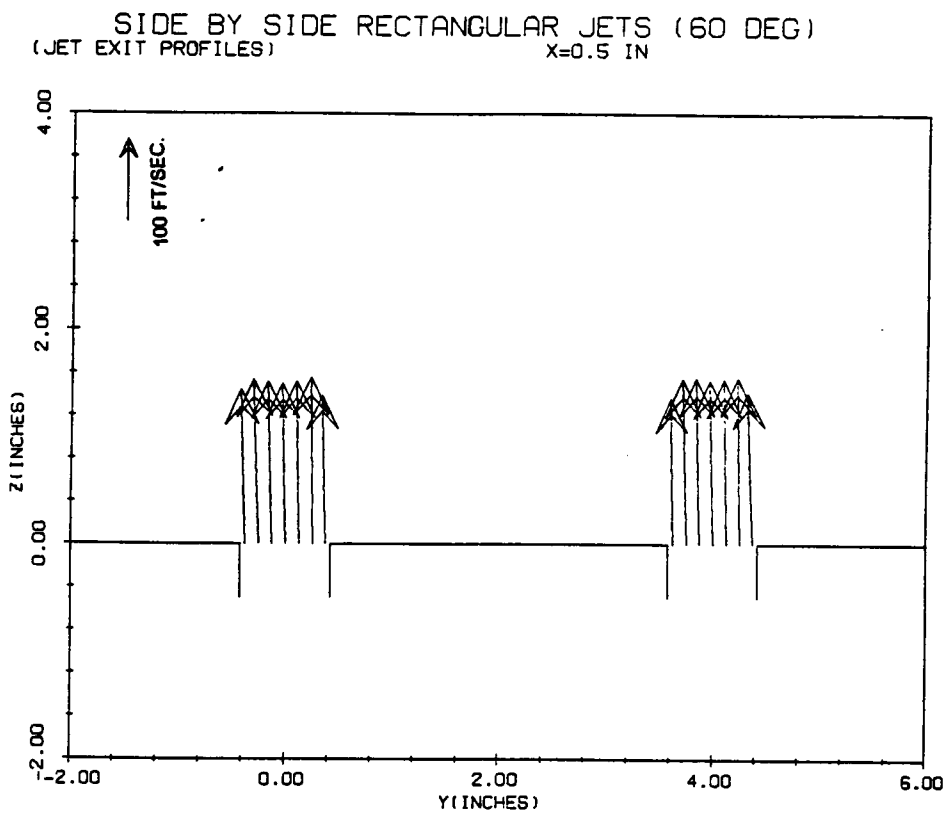

Figure 27. d) X = 0.5 in.

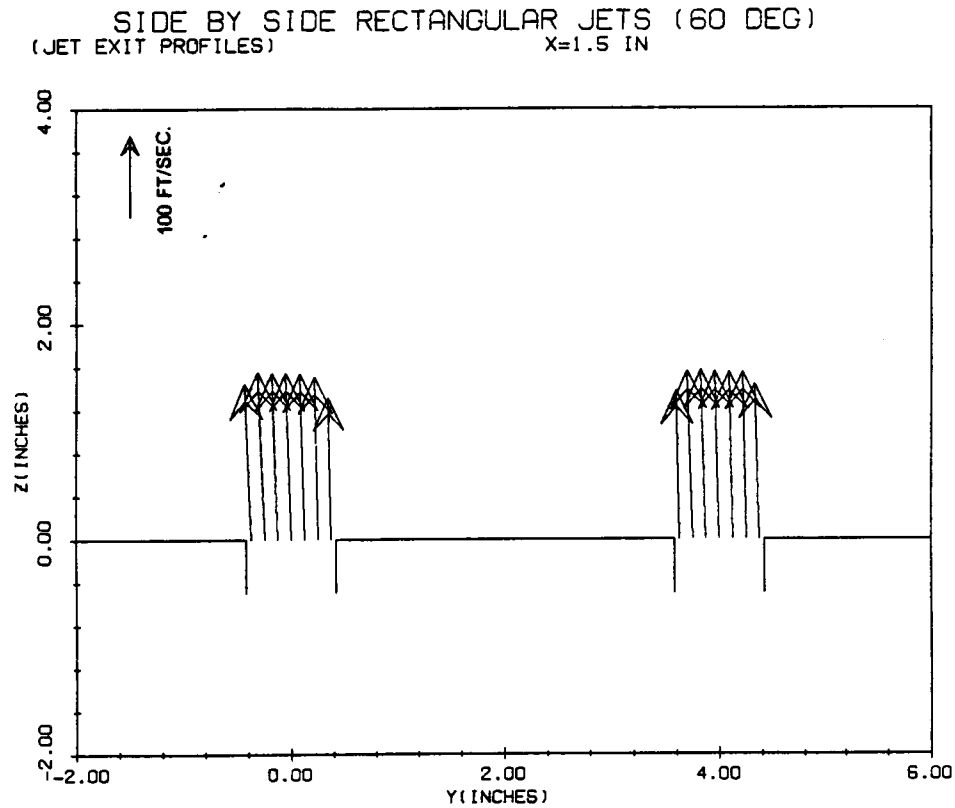

Figure 27. e) X = 1.5 in.

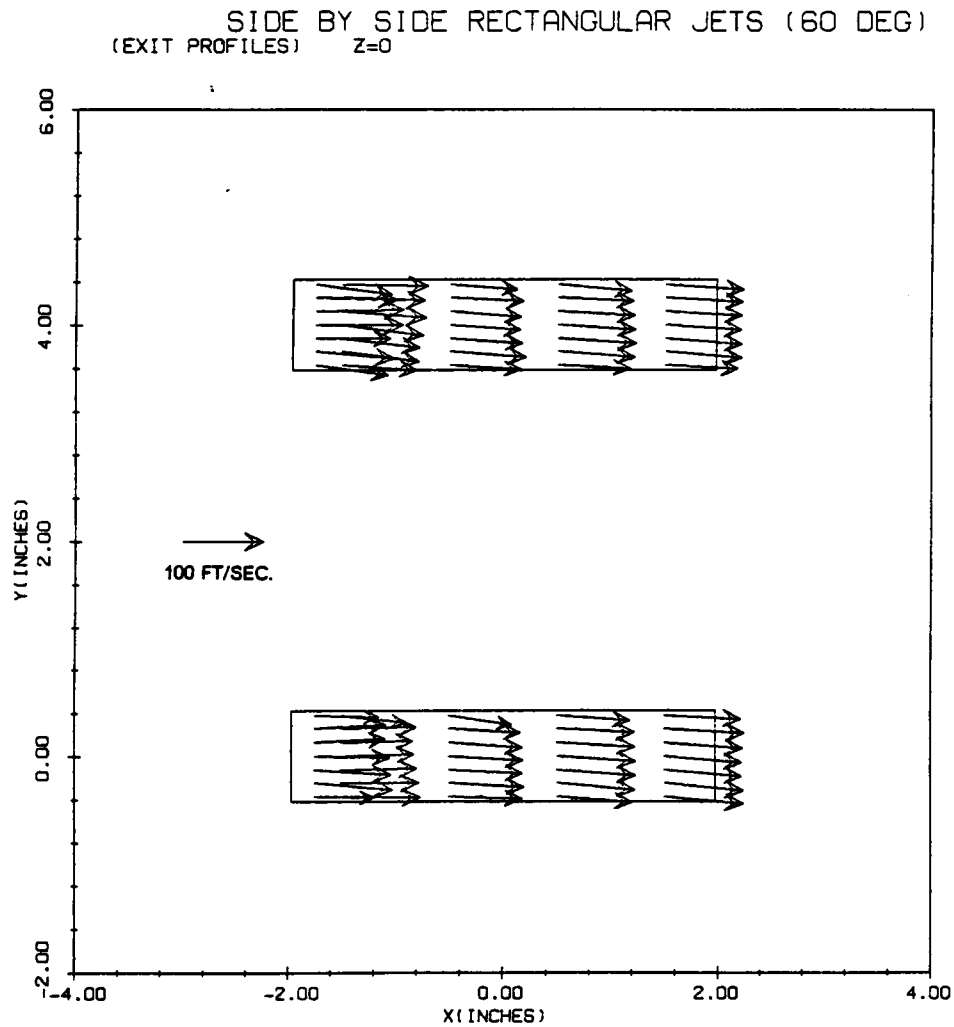

Figure 27. f) Z = 0.0 in.

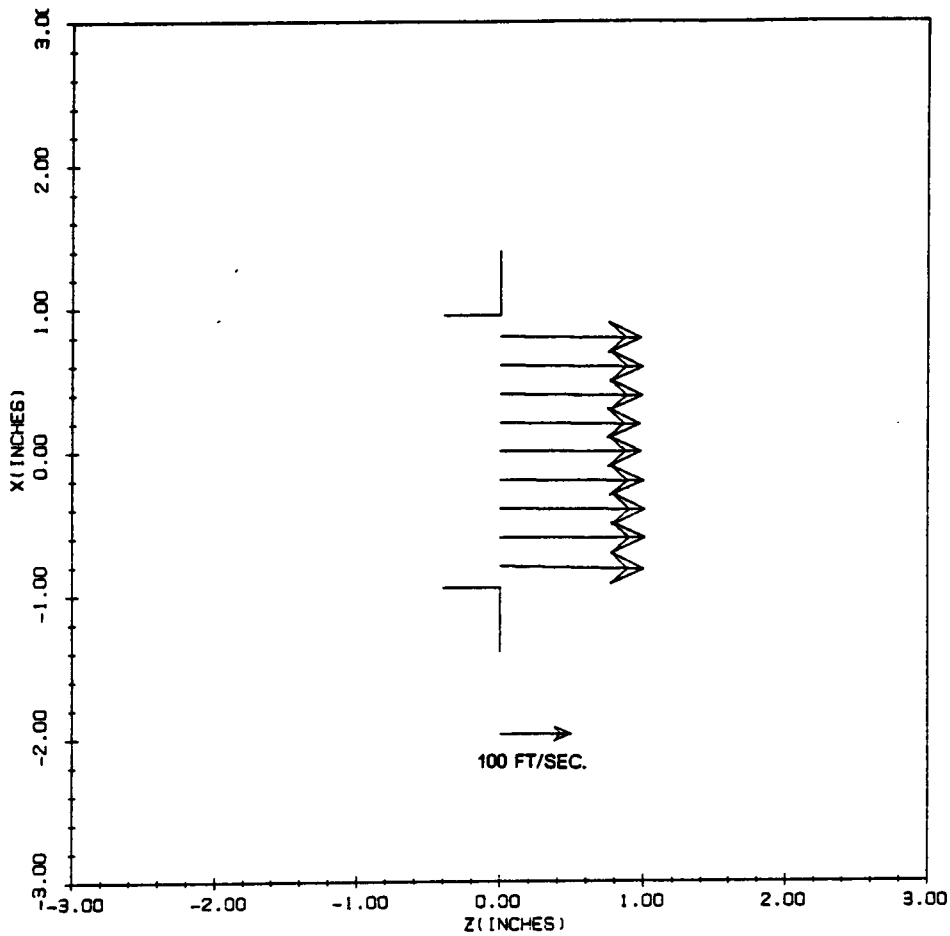

Figure 28. 90° circular jet exit velocity profiles.

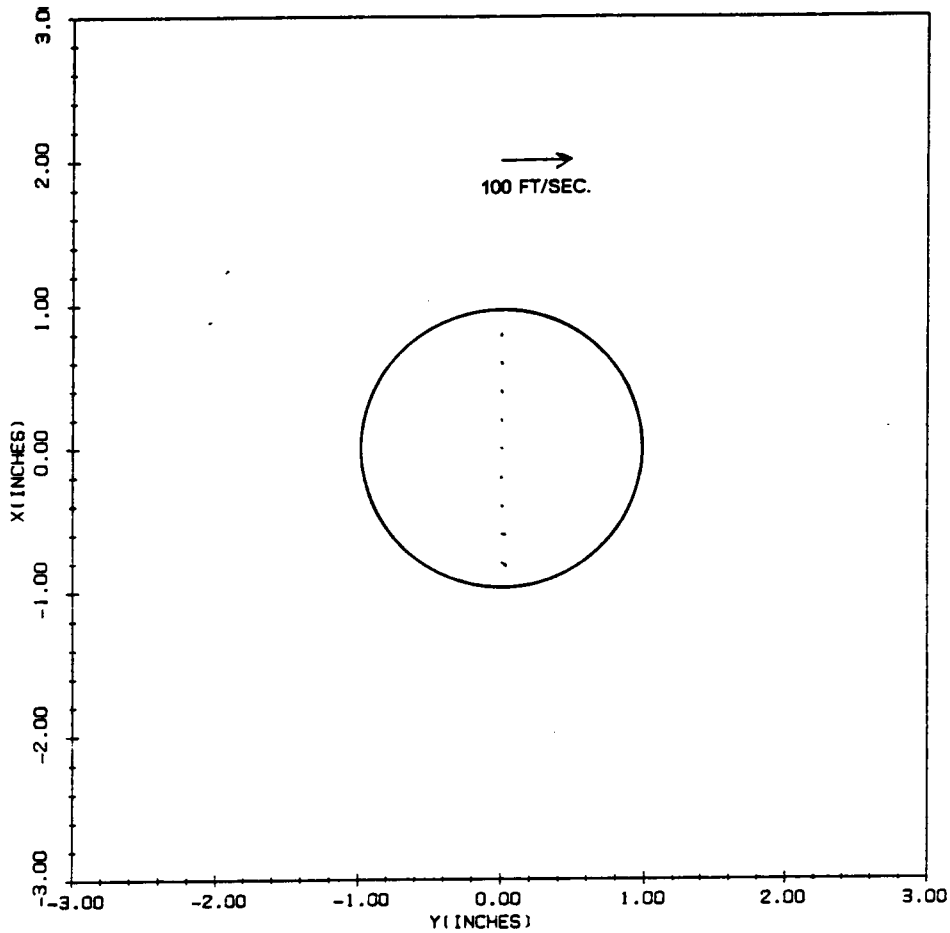

Figure 28. (continued)

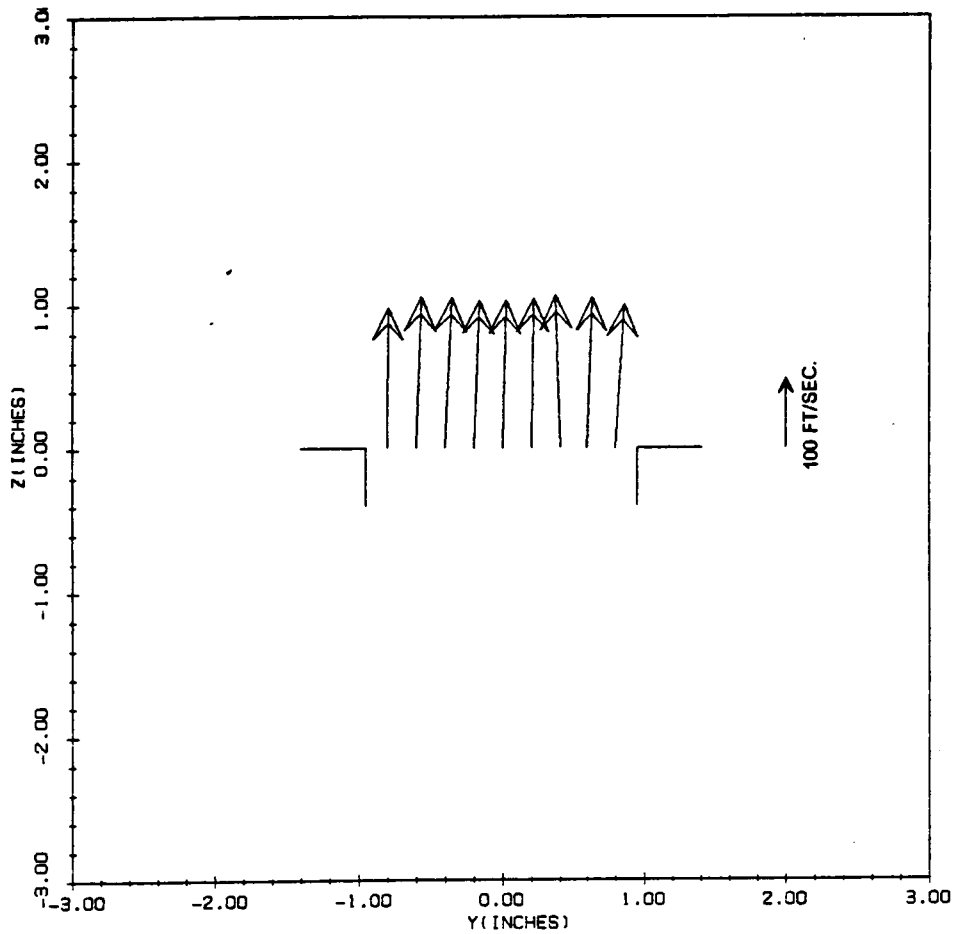

Figure 29. 90° circular jet exit profiles, 40 % swirl.

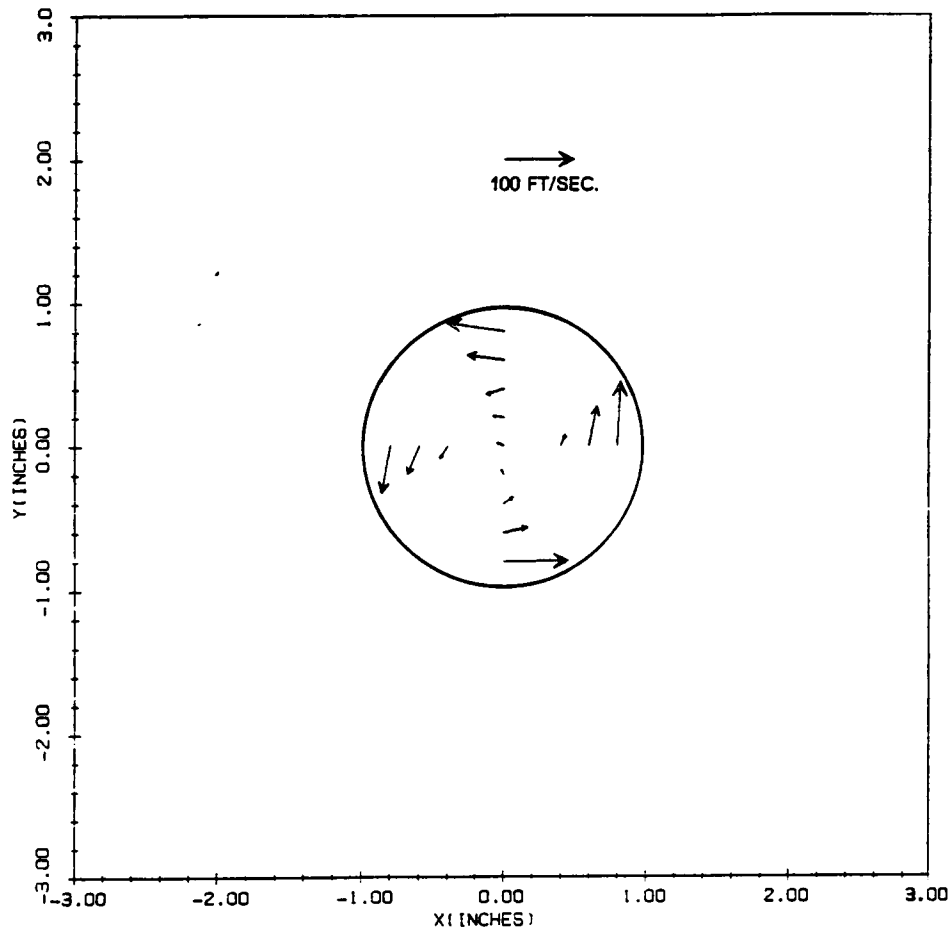

Figure 29. (continued)

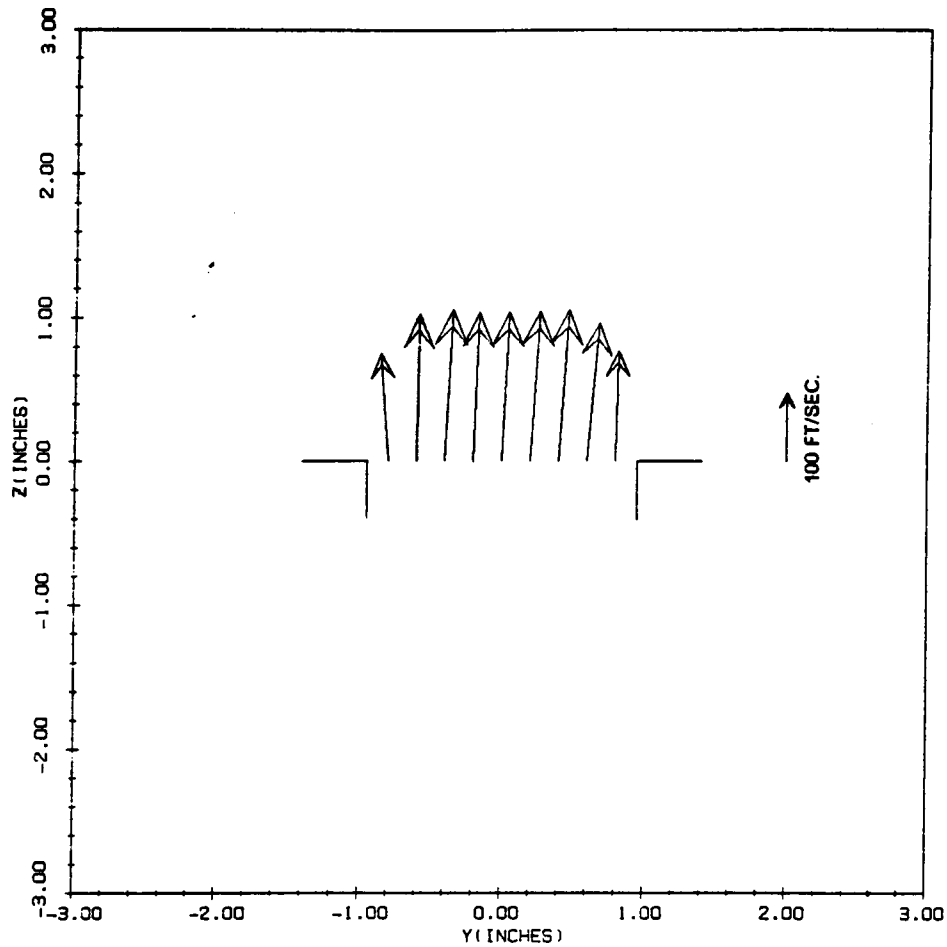

Figure 30. 90° circular jet exit profiles, 58 % swirl.

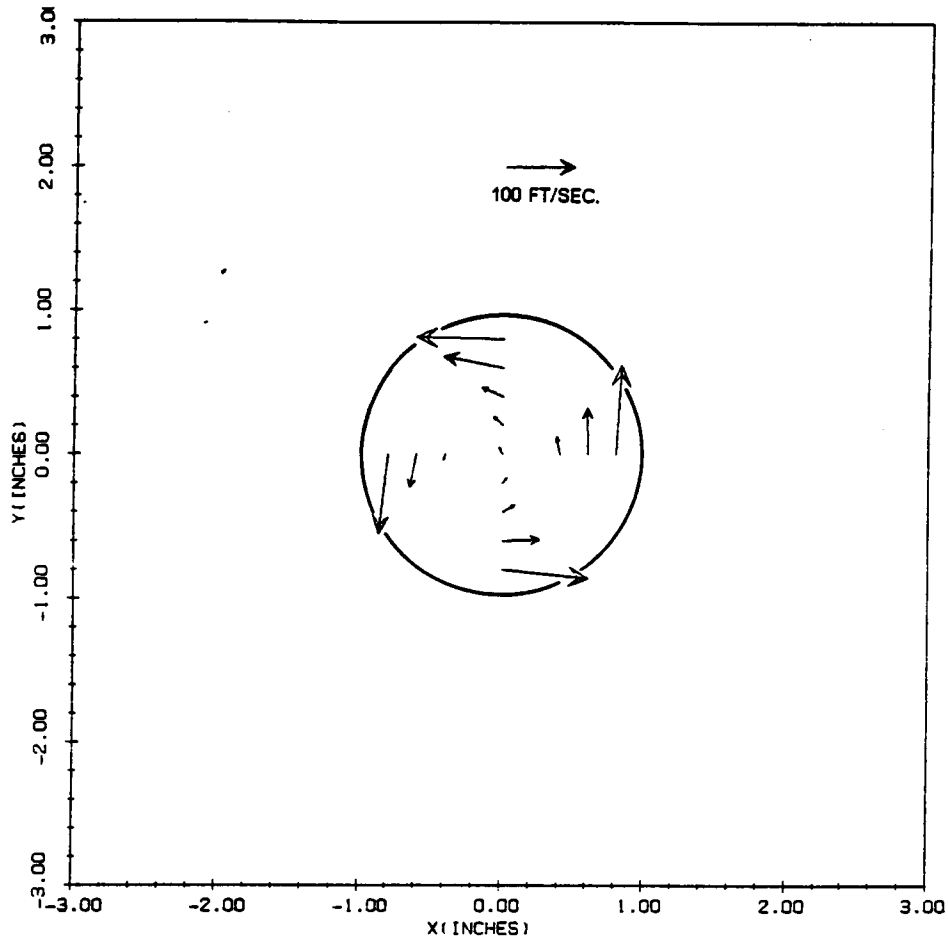

Figure 30. (continued)

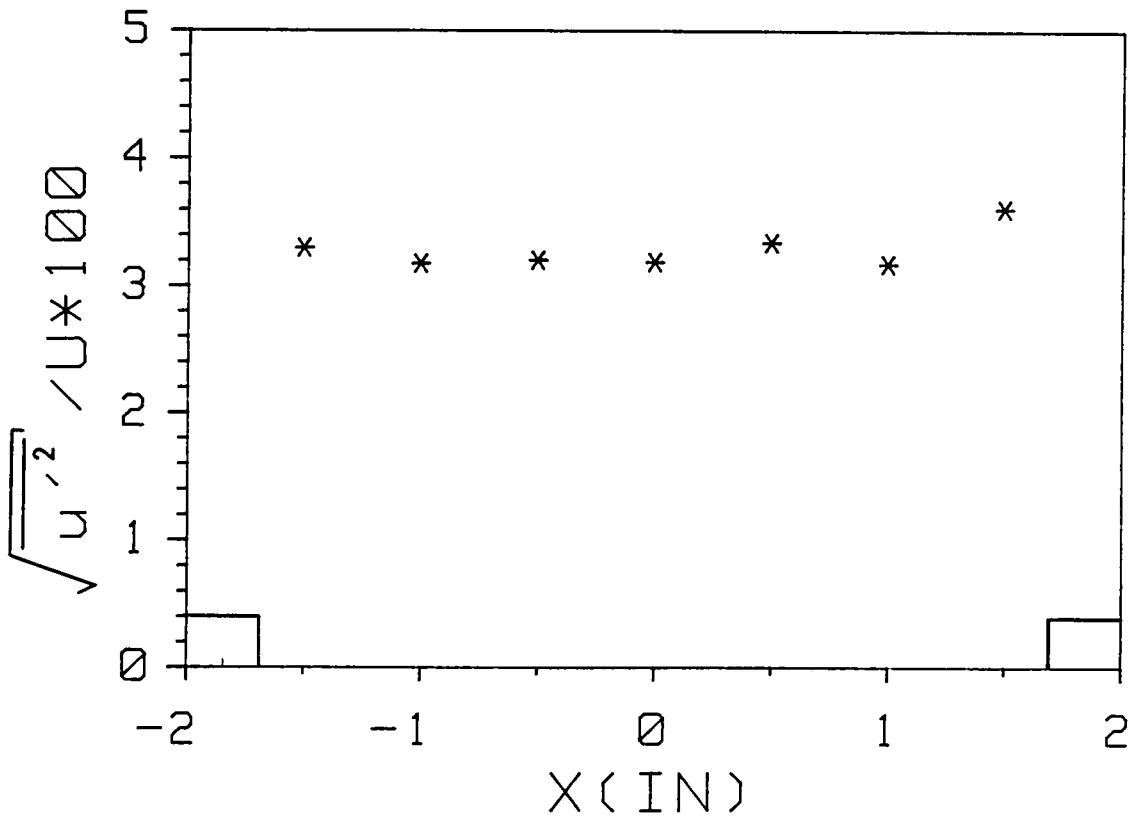

Figure 31. 90° circular jet exit profiles, high turbulence.

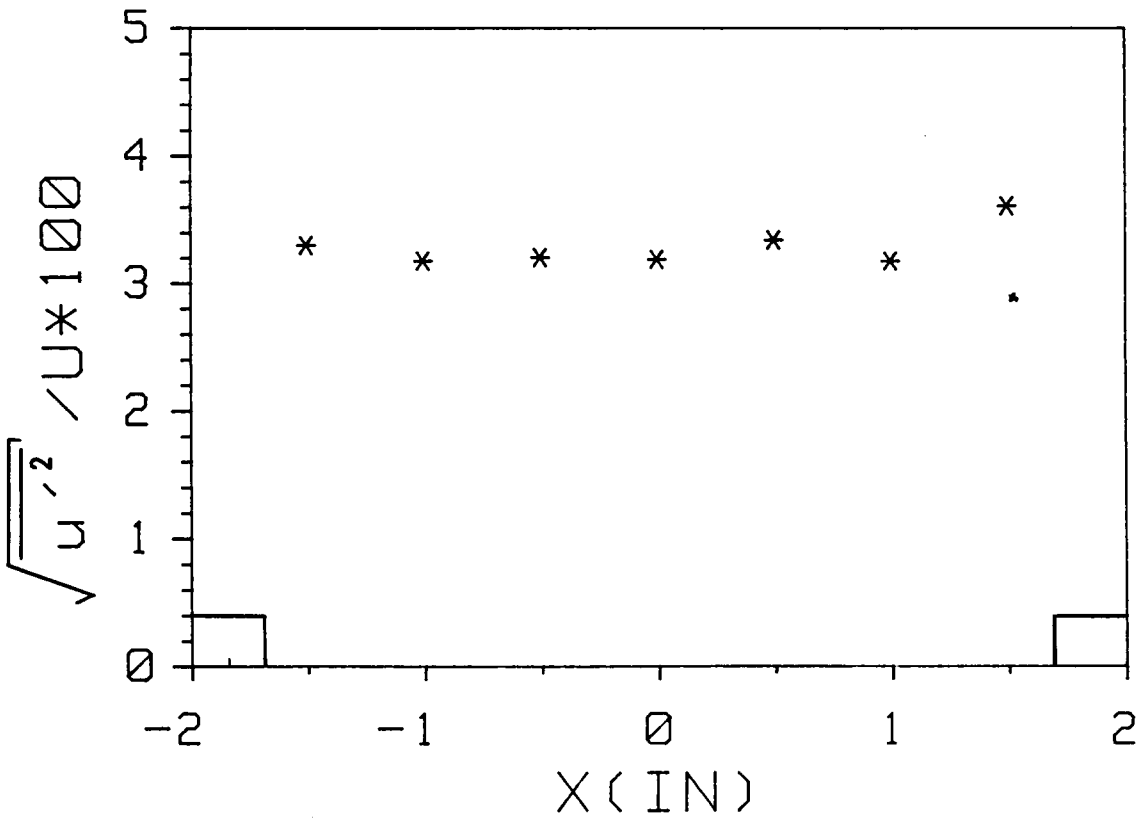

Figure 32. 90° rectangular jet exit turbulence profile.

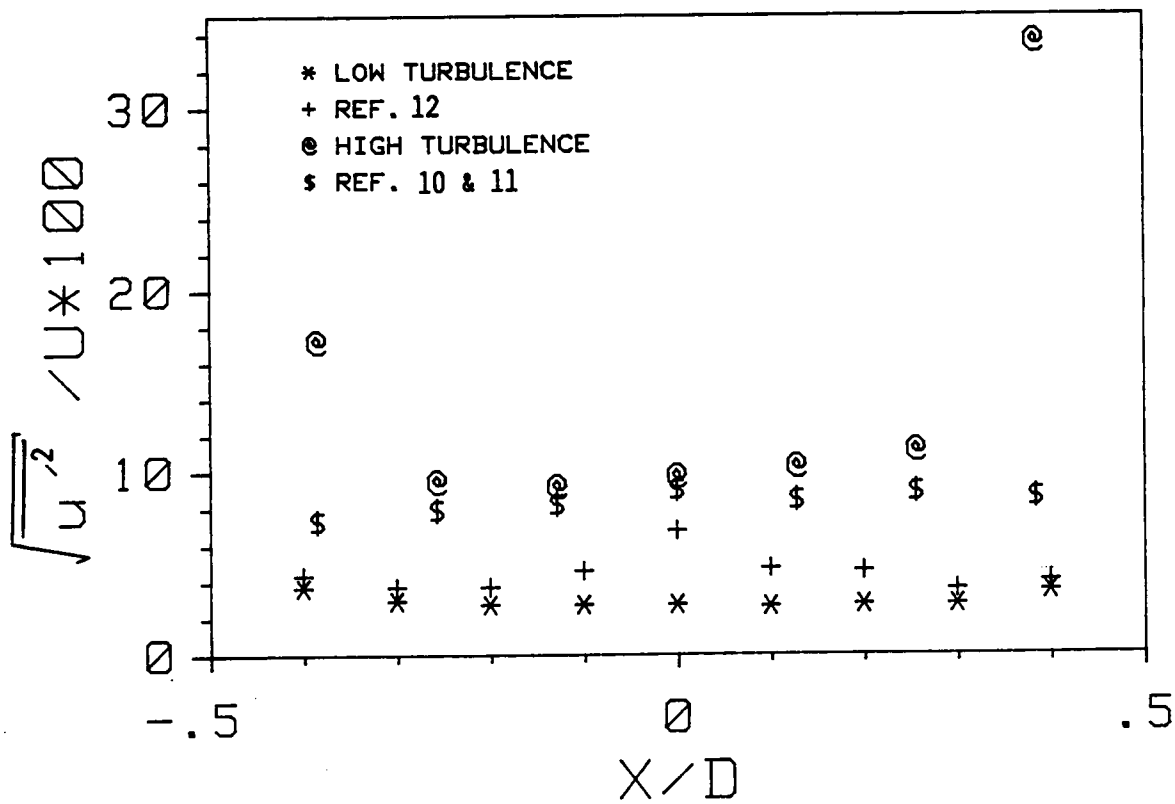

Figure 33. 90° circular jet exit turbulence profiles.

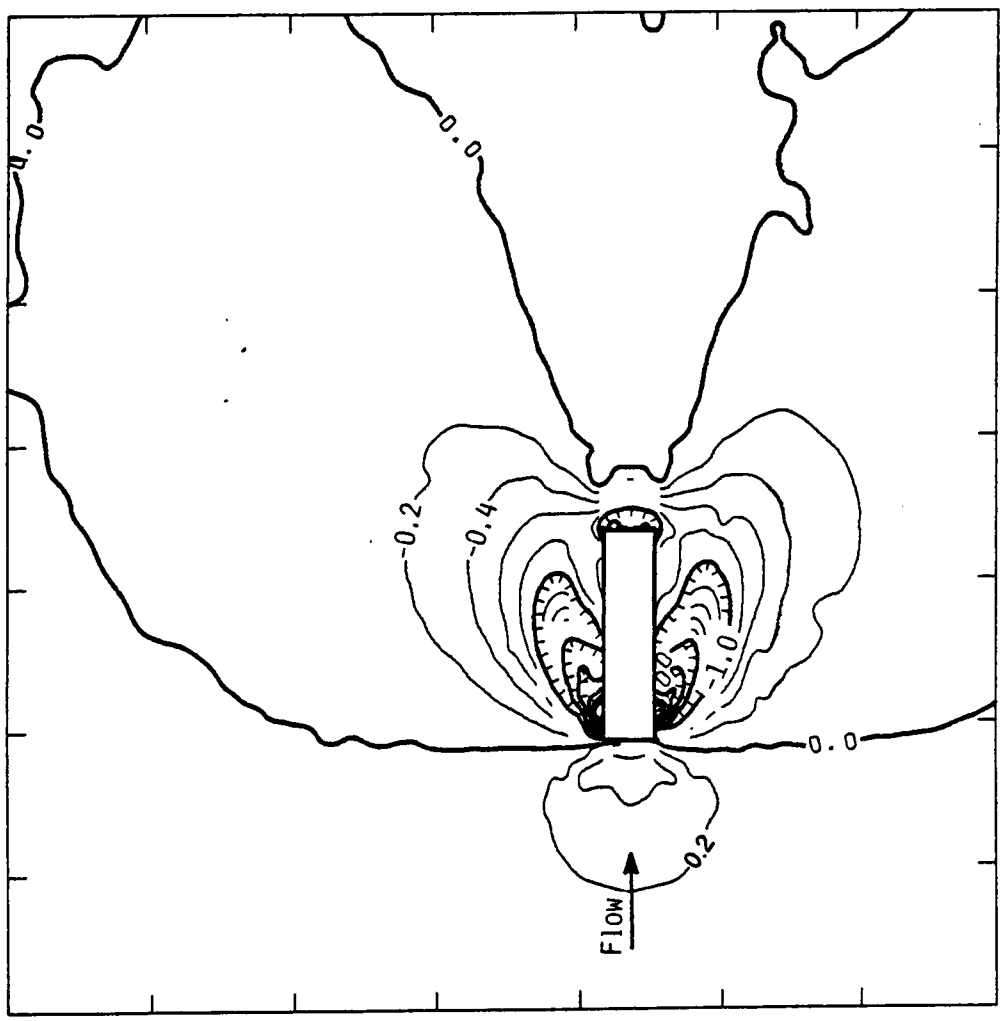

Figure 34. Surface pressures, 90° single rectangular jet, R = 2.2.

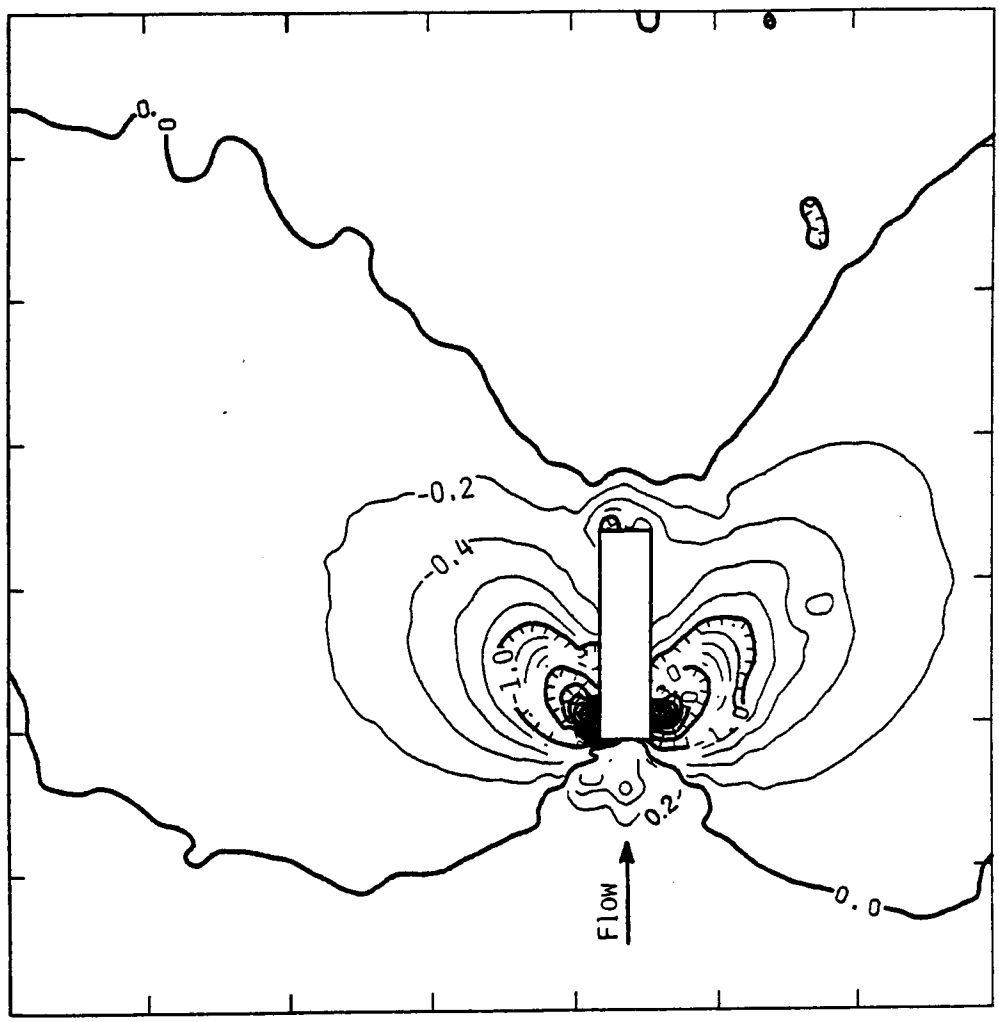

Figure 35. Surface pressures, 90° single rectangular jet, R = 4.0.

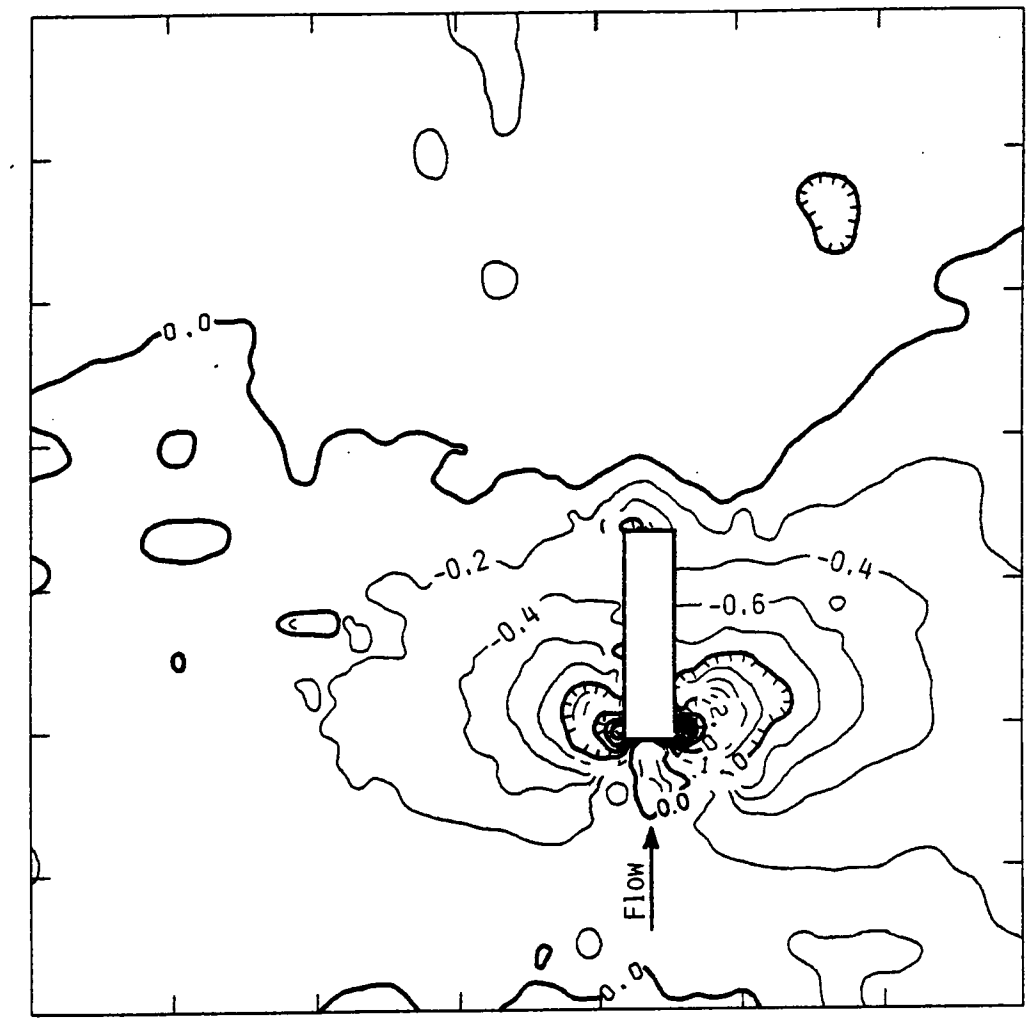

Figure 36. Surface pressures, 90° single rectangular jet, R = 8.0.

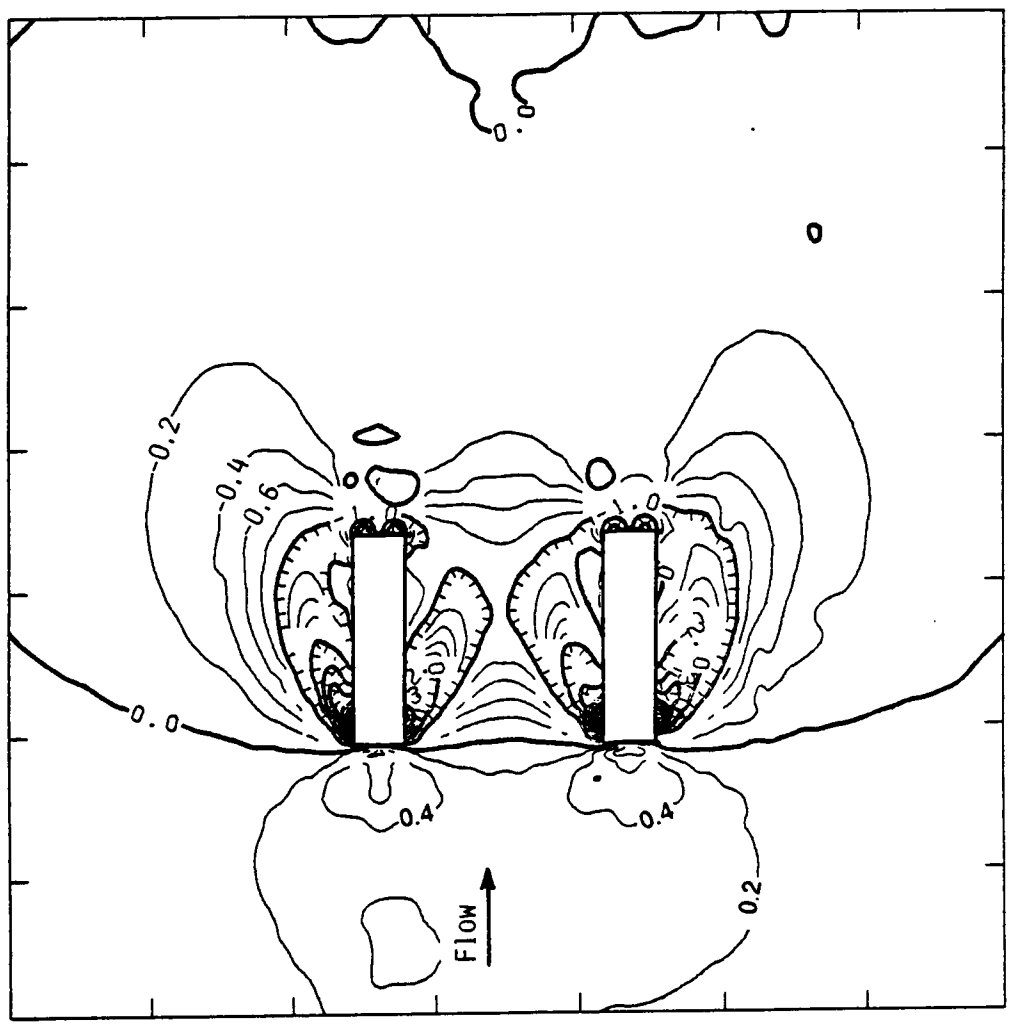

Figure 37. Surface pressures, 90° side-by-side rectangular, R = 2.2.

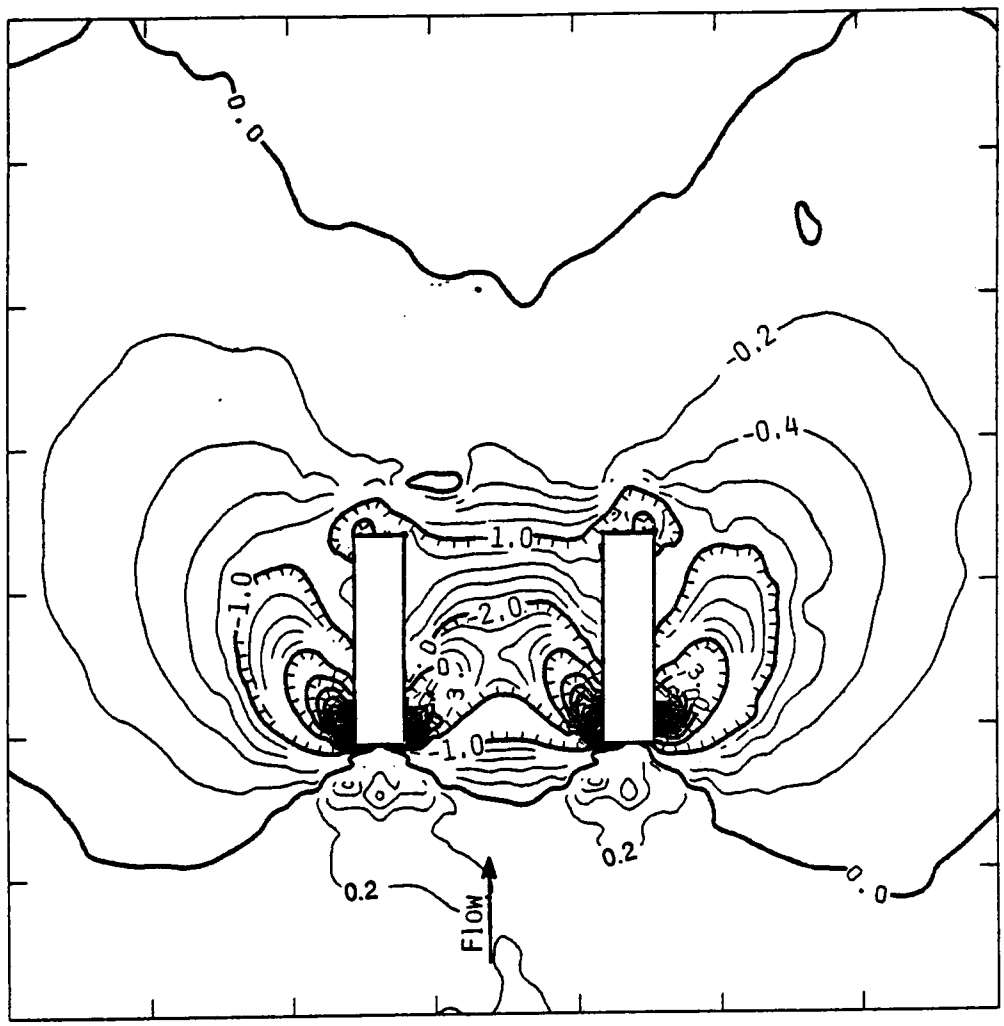

Figure 38. Surface pressures, 90° side-by-side rectangular, R = 4.0.

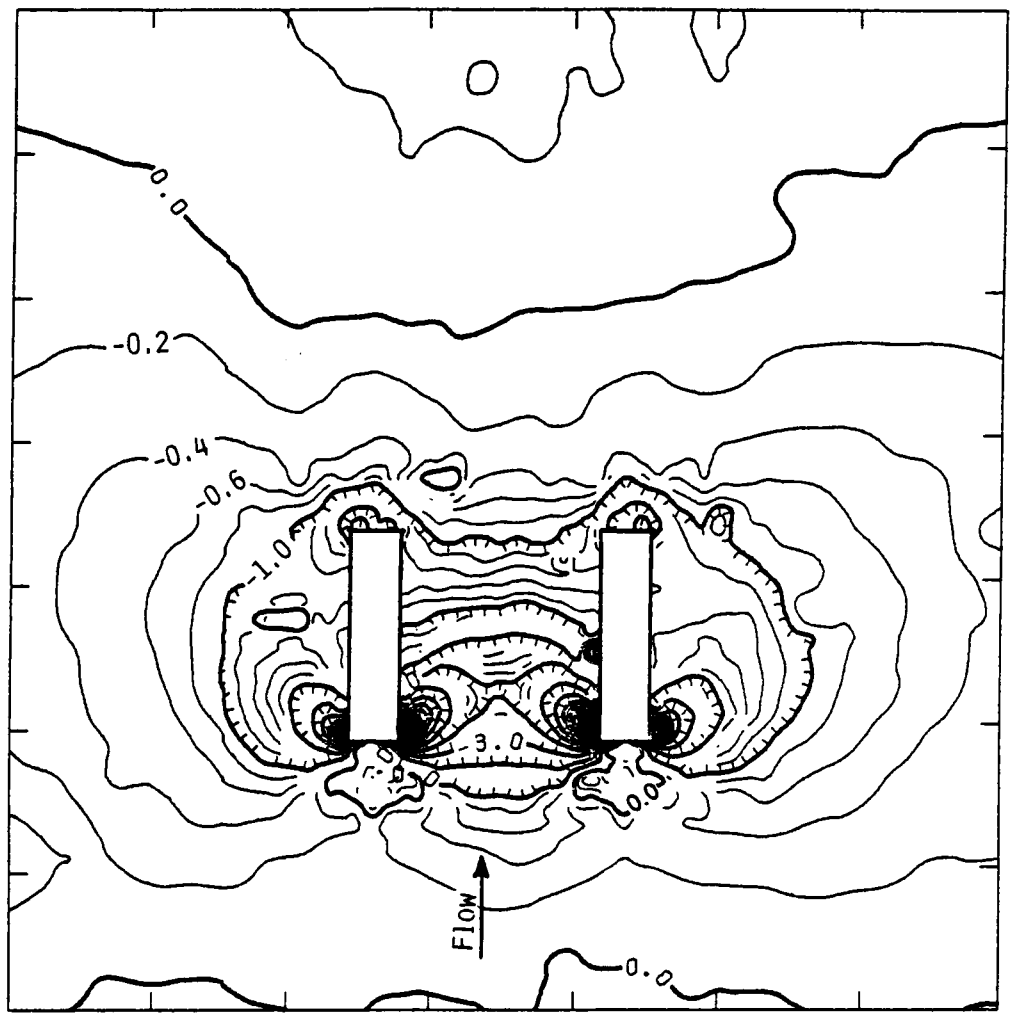

Figure 39. Surface pressures, 90° side-by-side rectangular, R = 8.0.

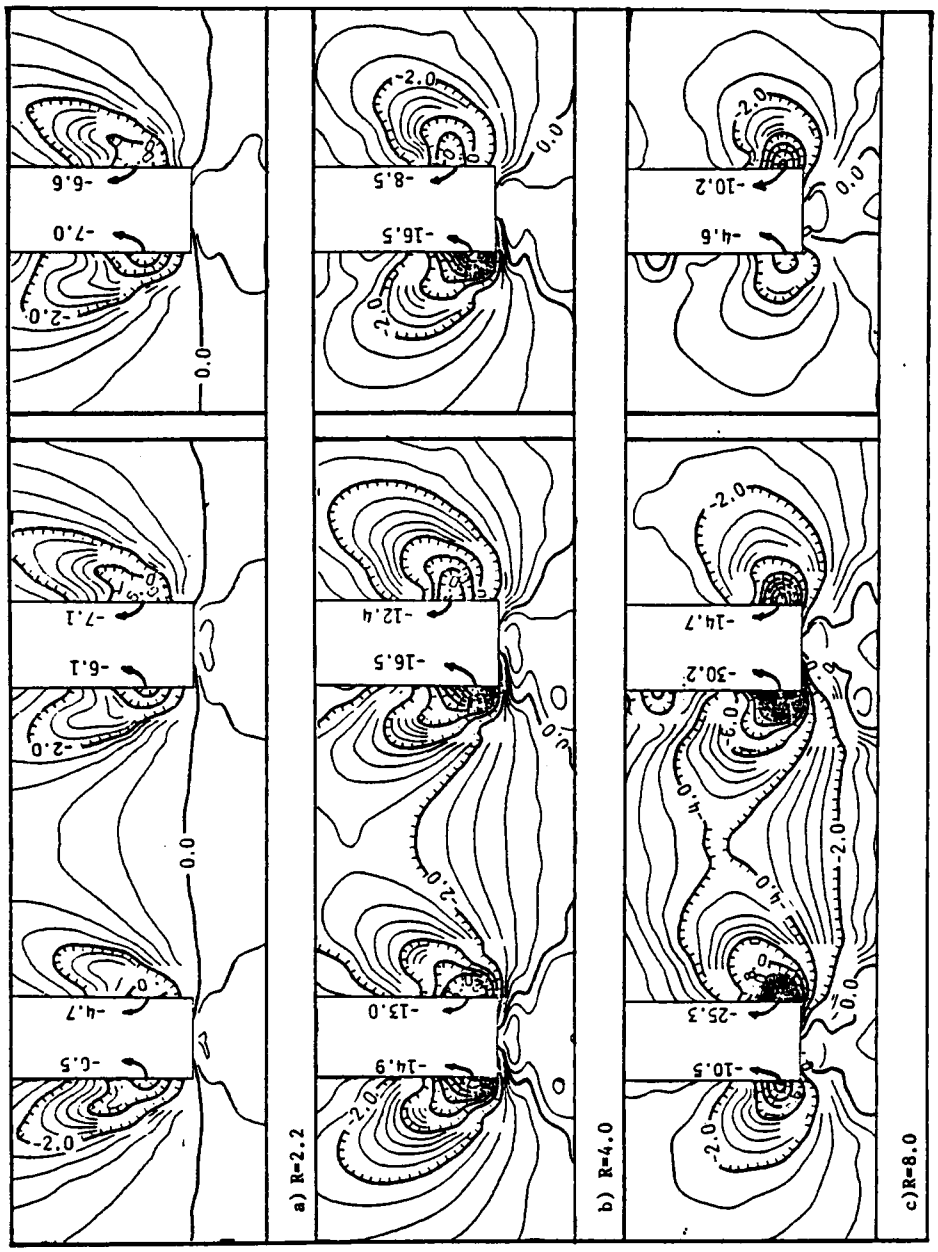

Figure 40. Surface pressures, 90° rectangular jets, enlarged front.

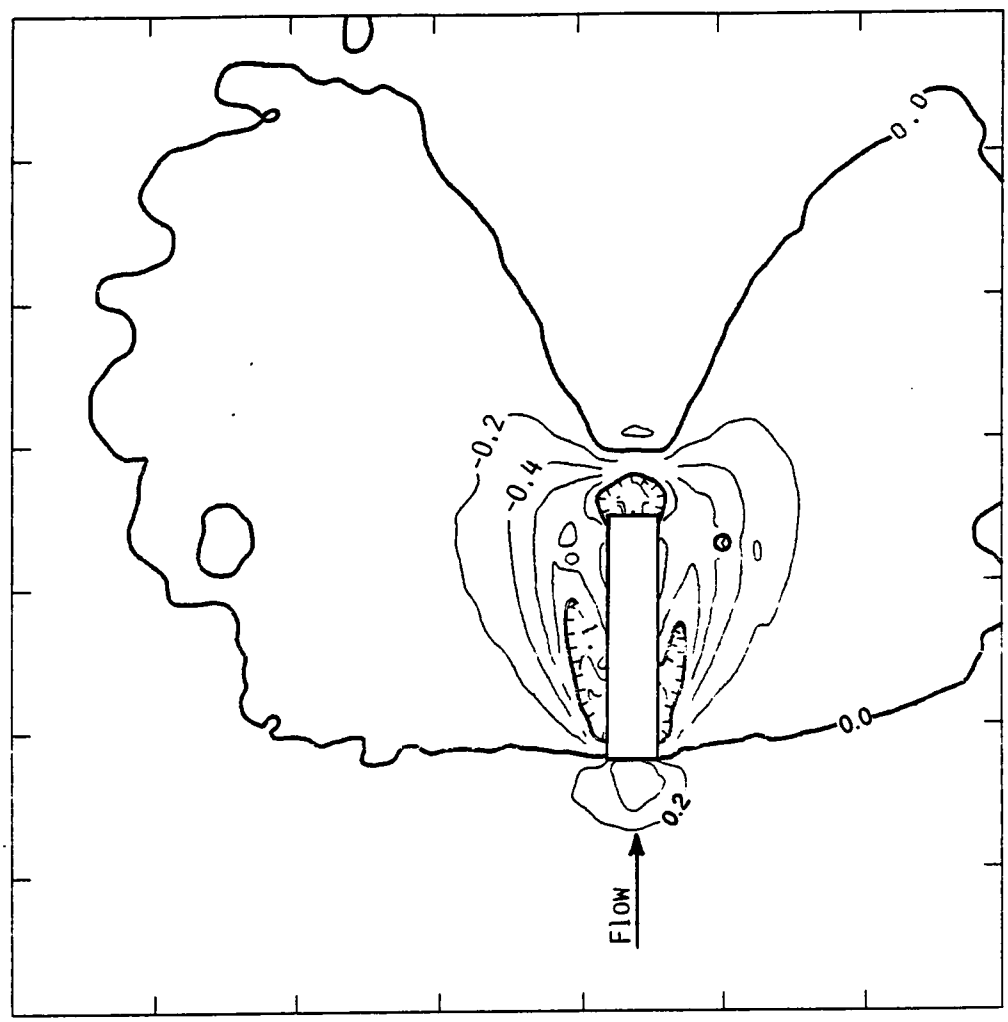

Figure 41. Surface pressures, 60° single rectangular jet, R = 2.2.

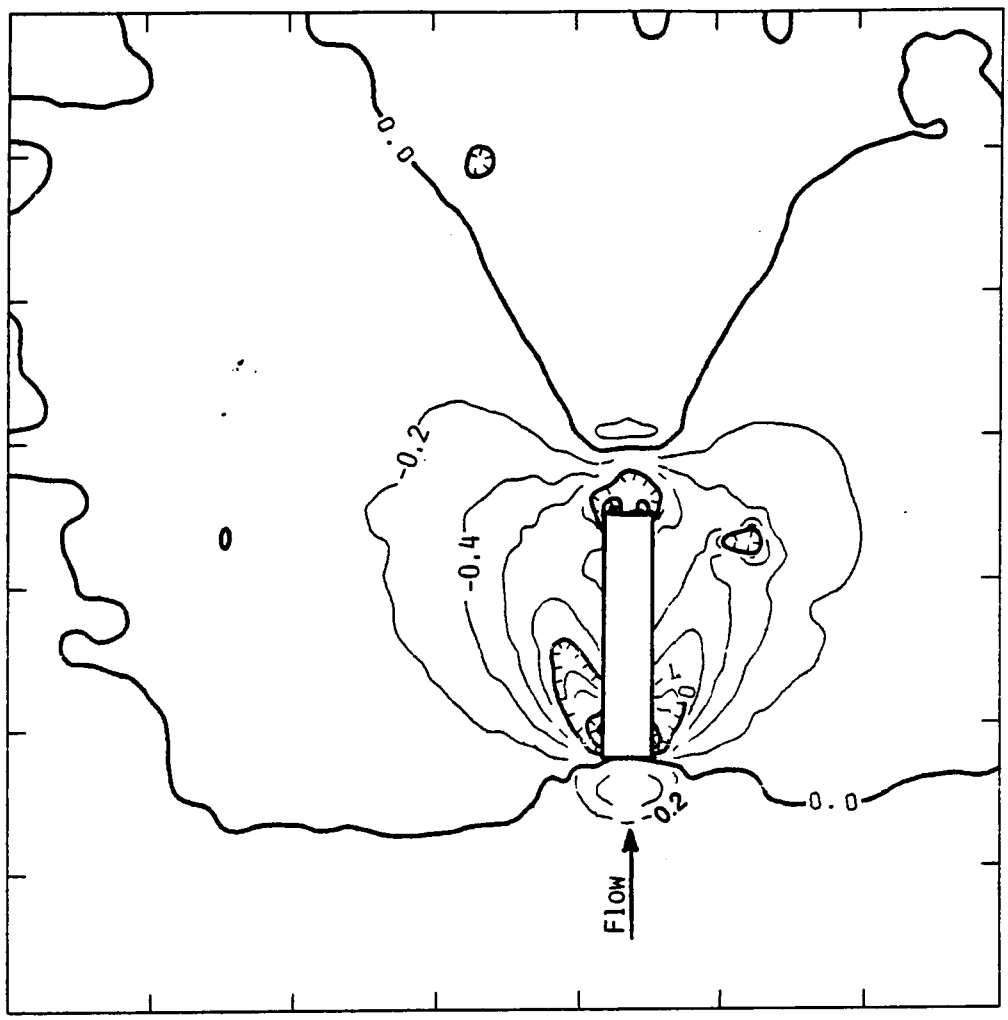

Figure 42. Surface pressures, 60° single rectangular jet, R = 4.0.

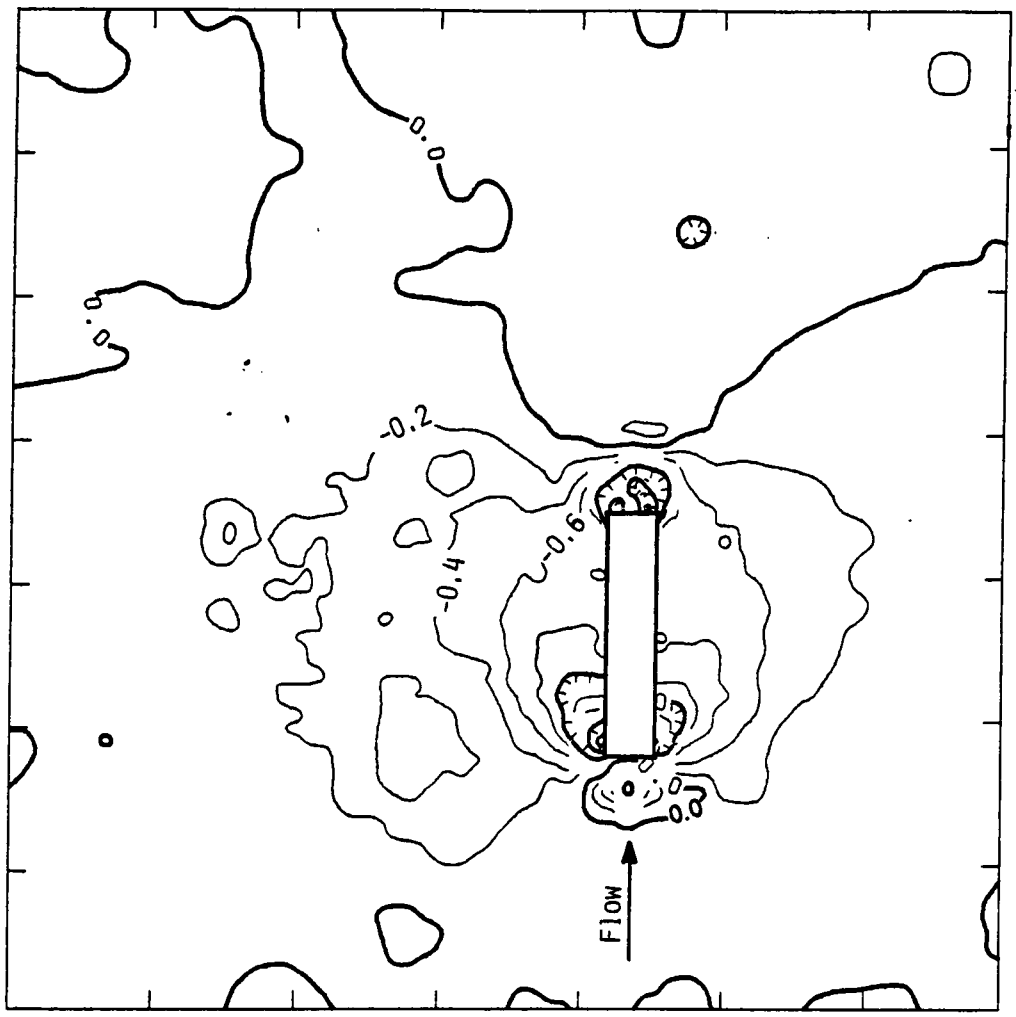

Figure 43. Surface pressures, 60° single rectangular jet, R = 8.0.

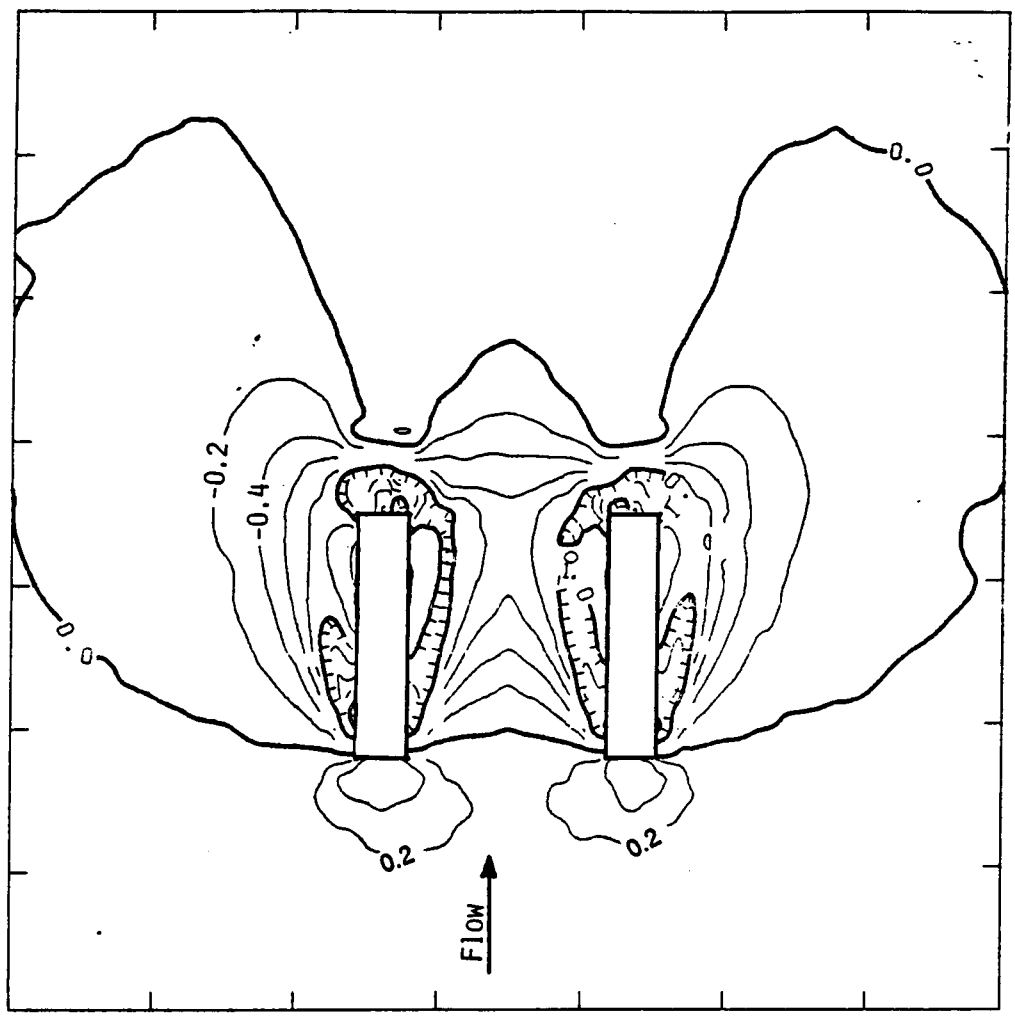

Figure 44. Surface pressures, 60° side-by-side rectangular, R = 2.2.

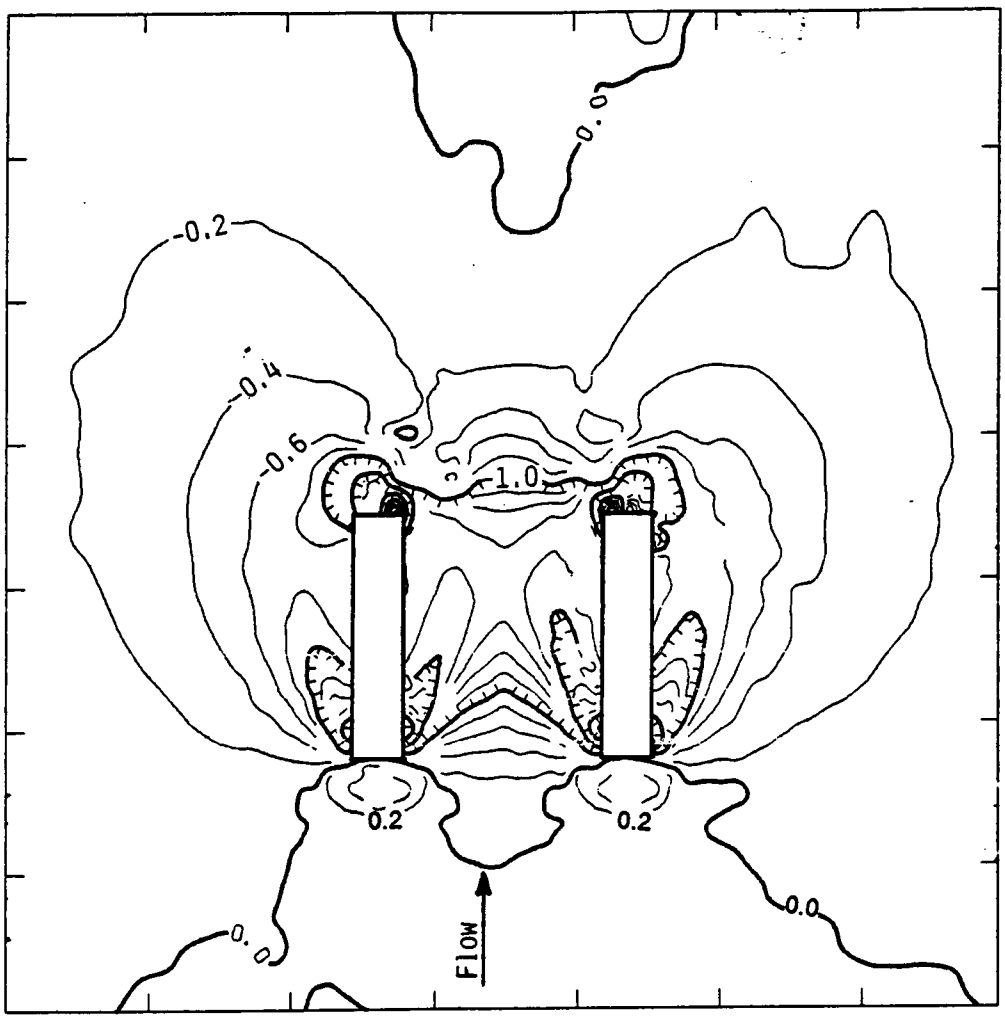

Figure 45. Surface pressures, 60° side-by-side rectangular, R = 4.0.

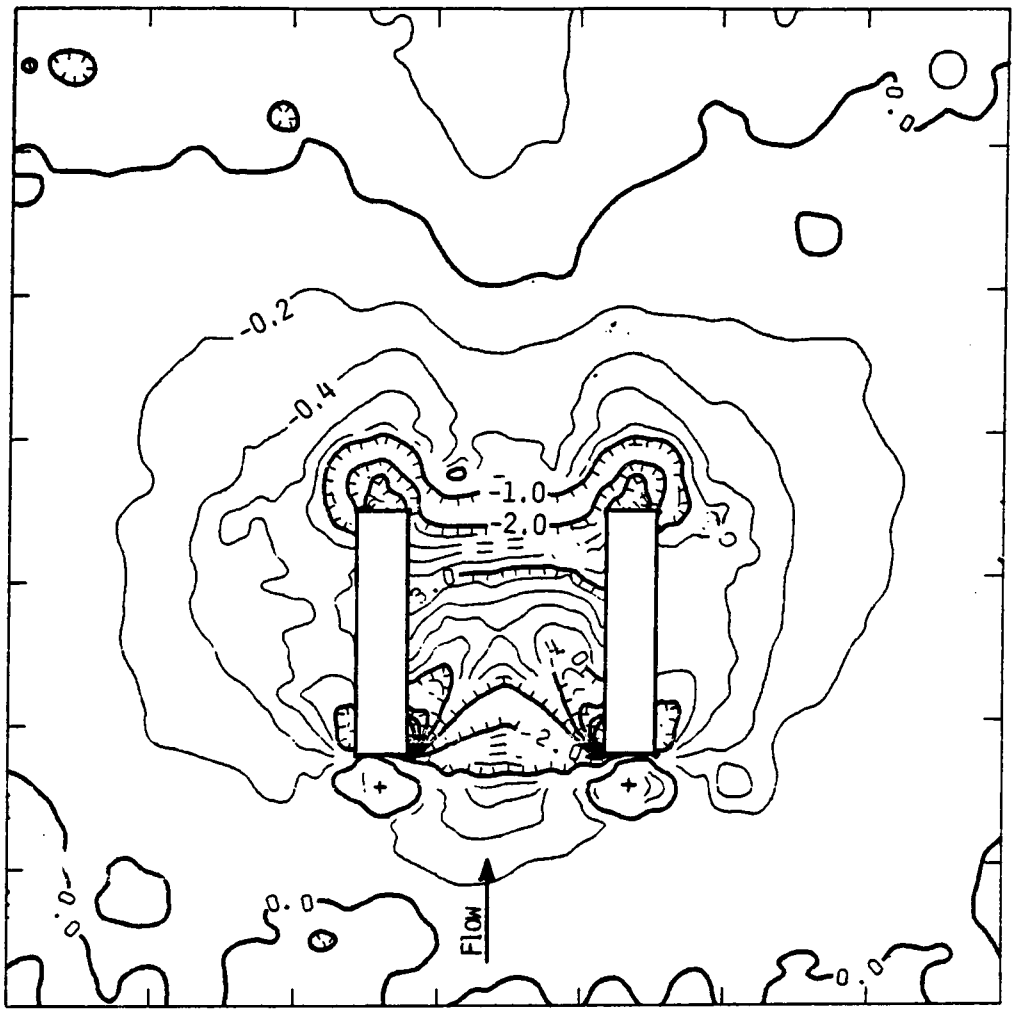

Figure 46. Surface pressures, 60° side-by-side rectangular, R = 8.0.

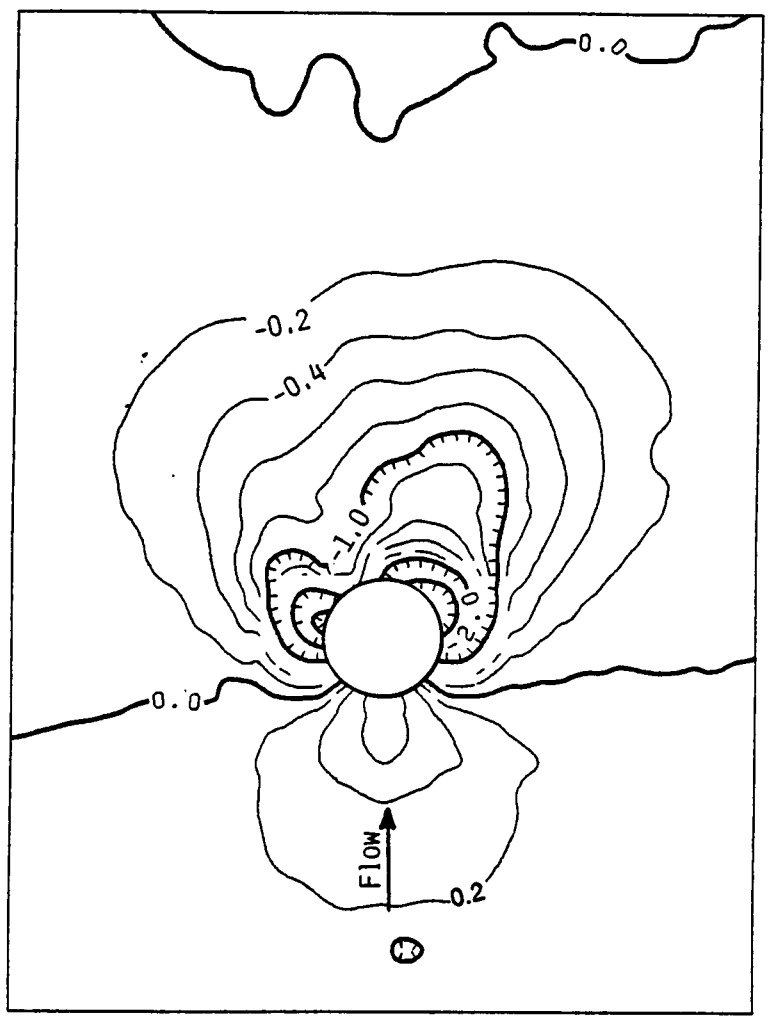

Figure 47. Surface pressures, 90° circular jet, R = 2.2.

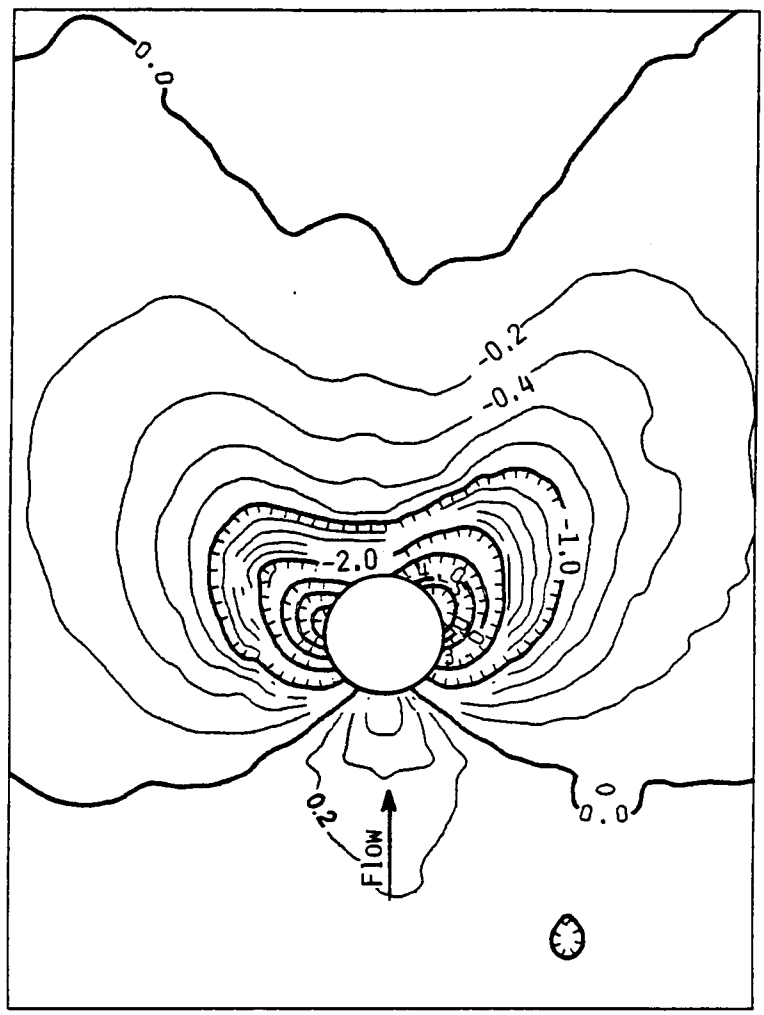

Figure 48. Surface pressures, 90° circular jet, R = 4.0.

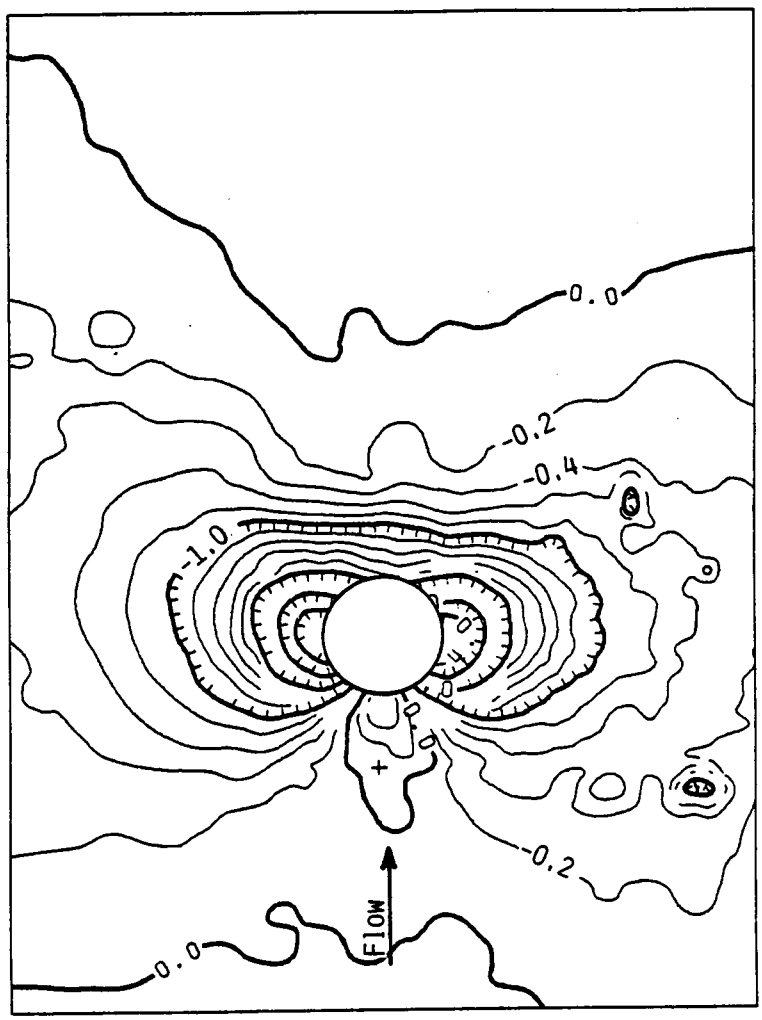

Figure 49. Surface pressures, 90° circular jet, R = 8.0.

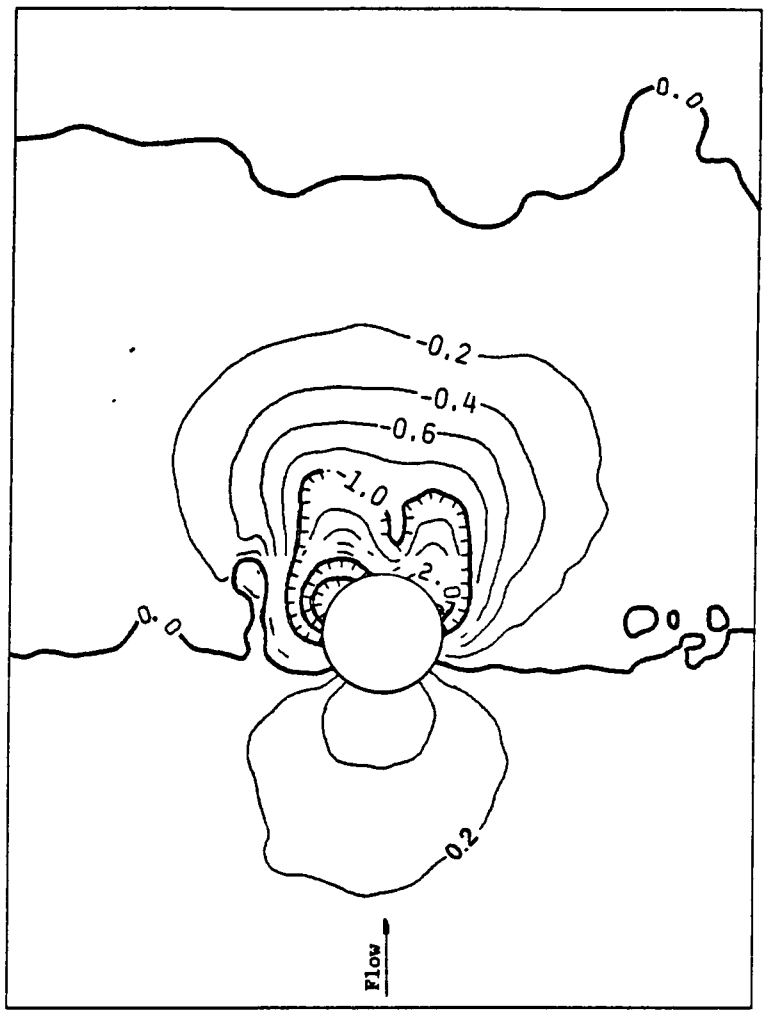

Figure 50. Surface pressures, 90° circular, high turbulence, R = 2.2.

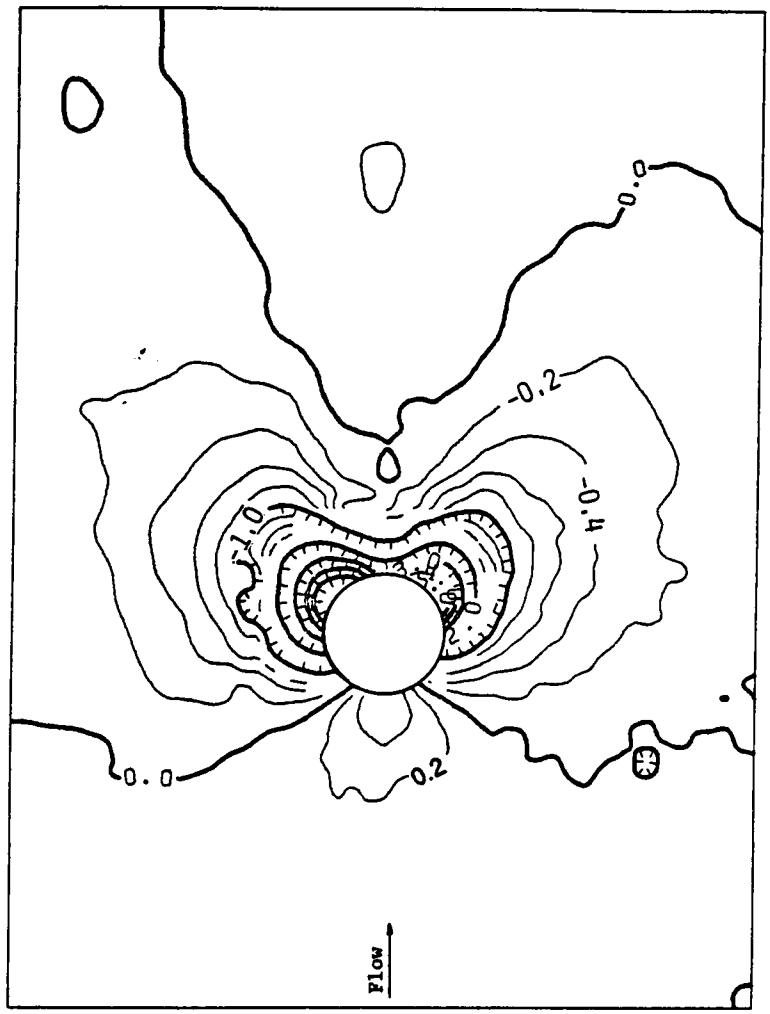

Figure 51. Surface pressures, 90° circular, high turbulence, R = 4.0.

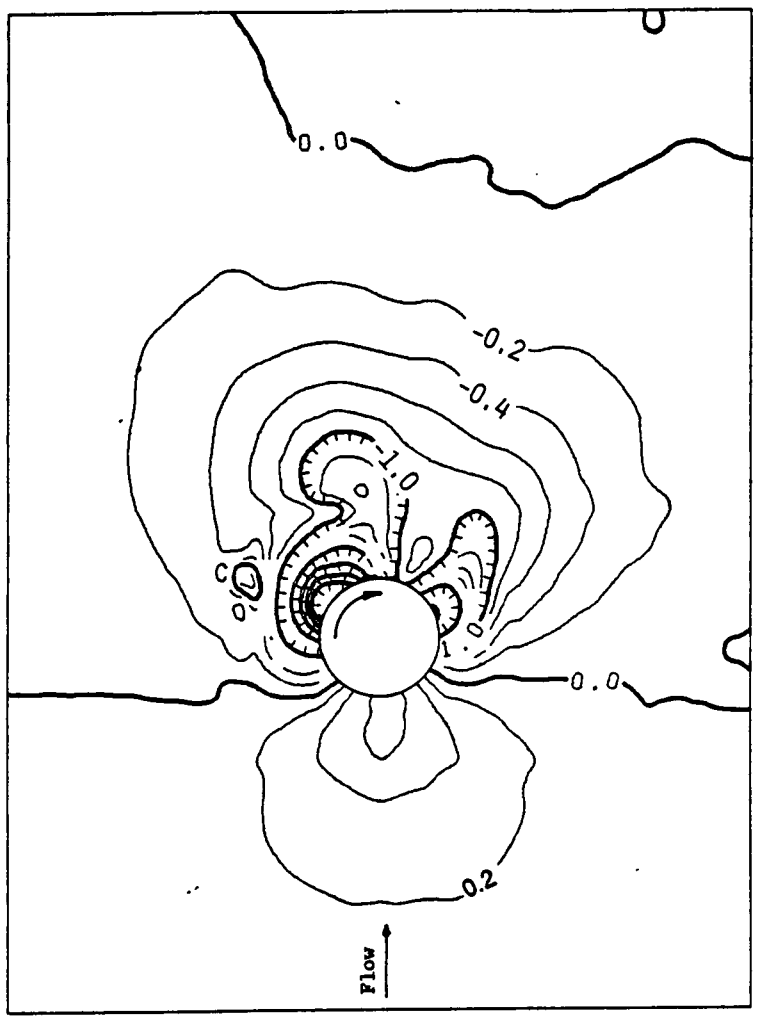

Figure 52. Surface pressures, 90° circular jet, 40 % swirl, R = 2.2.

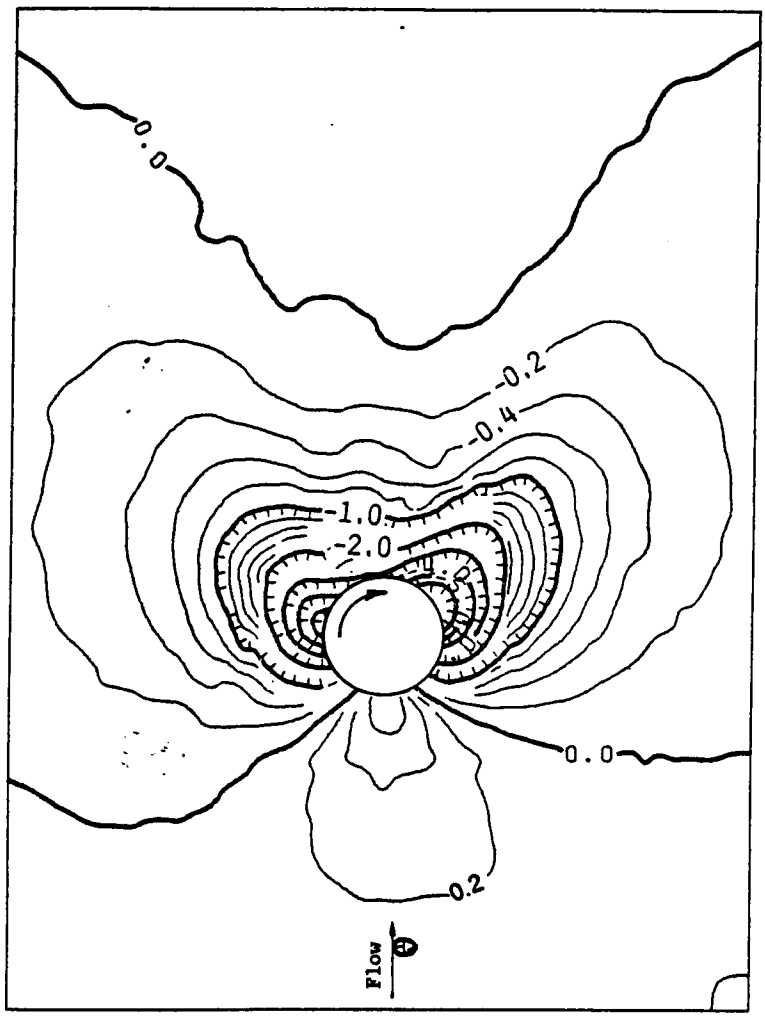

Figure 53. Surface pressures, 90° circular jet, 40 % swirl, R = 4.0.

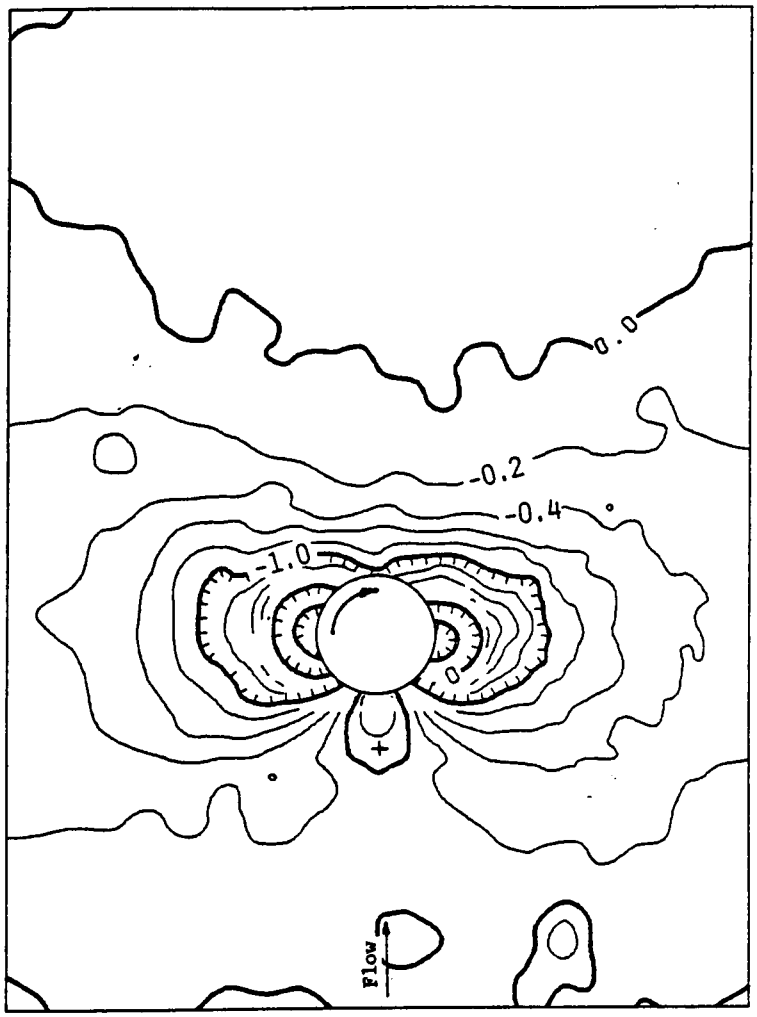

Figure 54. Surface pressures, 90° circular jet, 40 % swirl, R = 8.0.

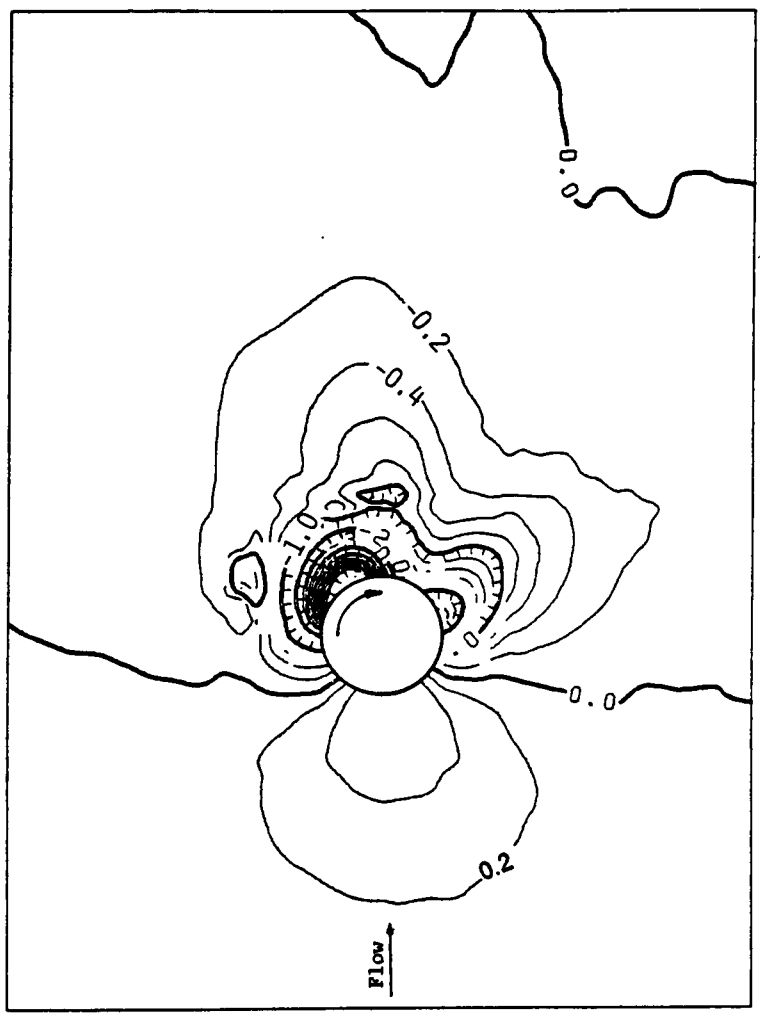

Figure 55. Surface pressures, 90° circular jet, 58 % swirl, R = 2.2.

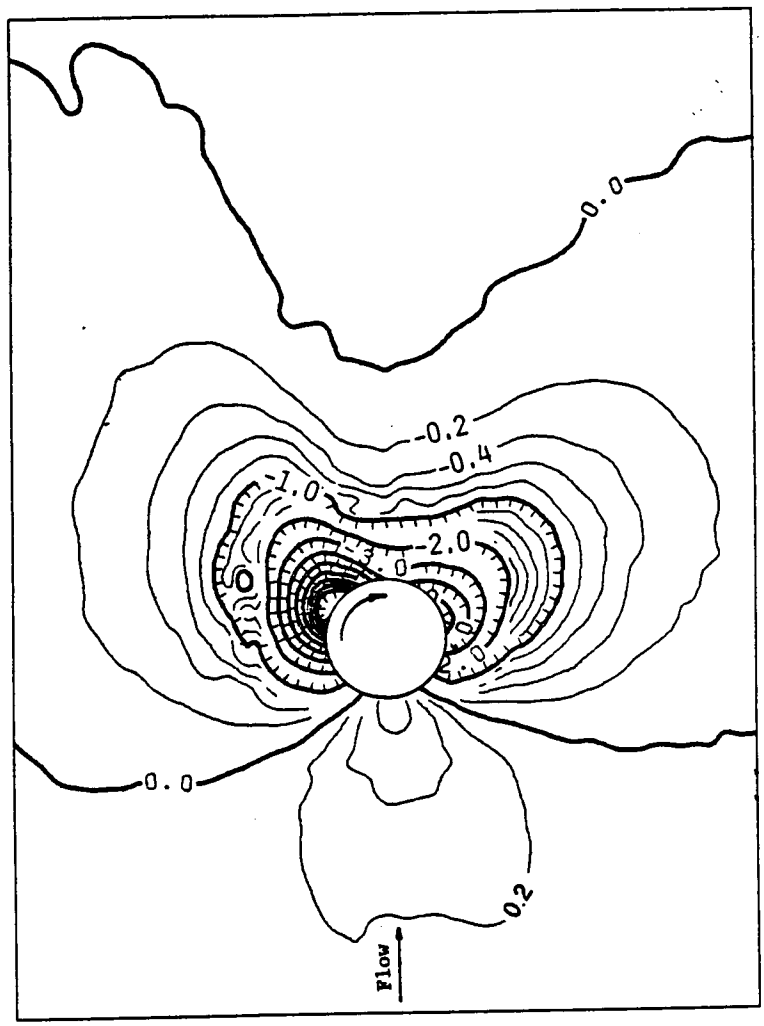

Figure 56. Surface pressures, 90° circular jet, 58 % swirl, R = 4.0.

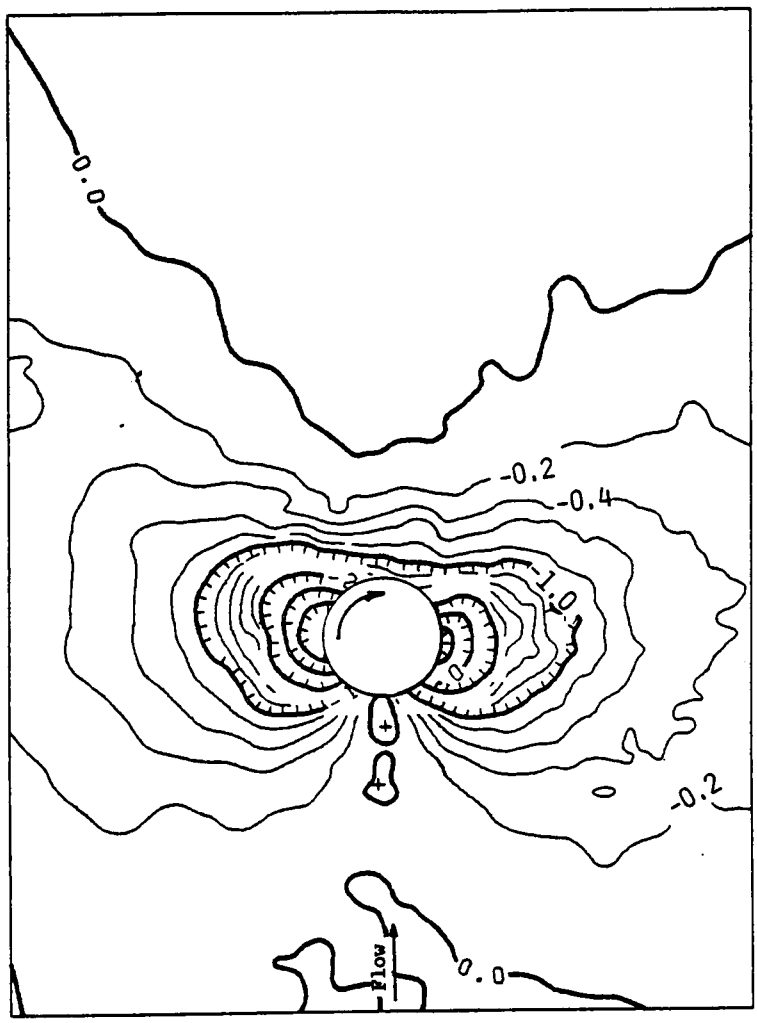

Figure 57. Surface pressures, 90° circular jet, 58 % swirl, R = 8.0.

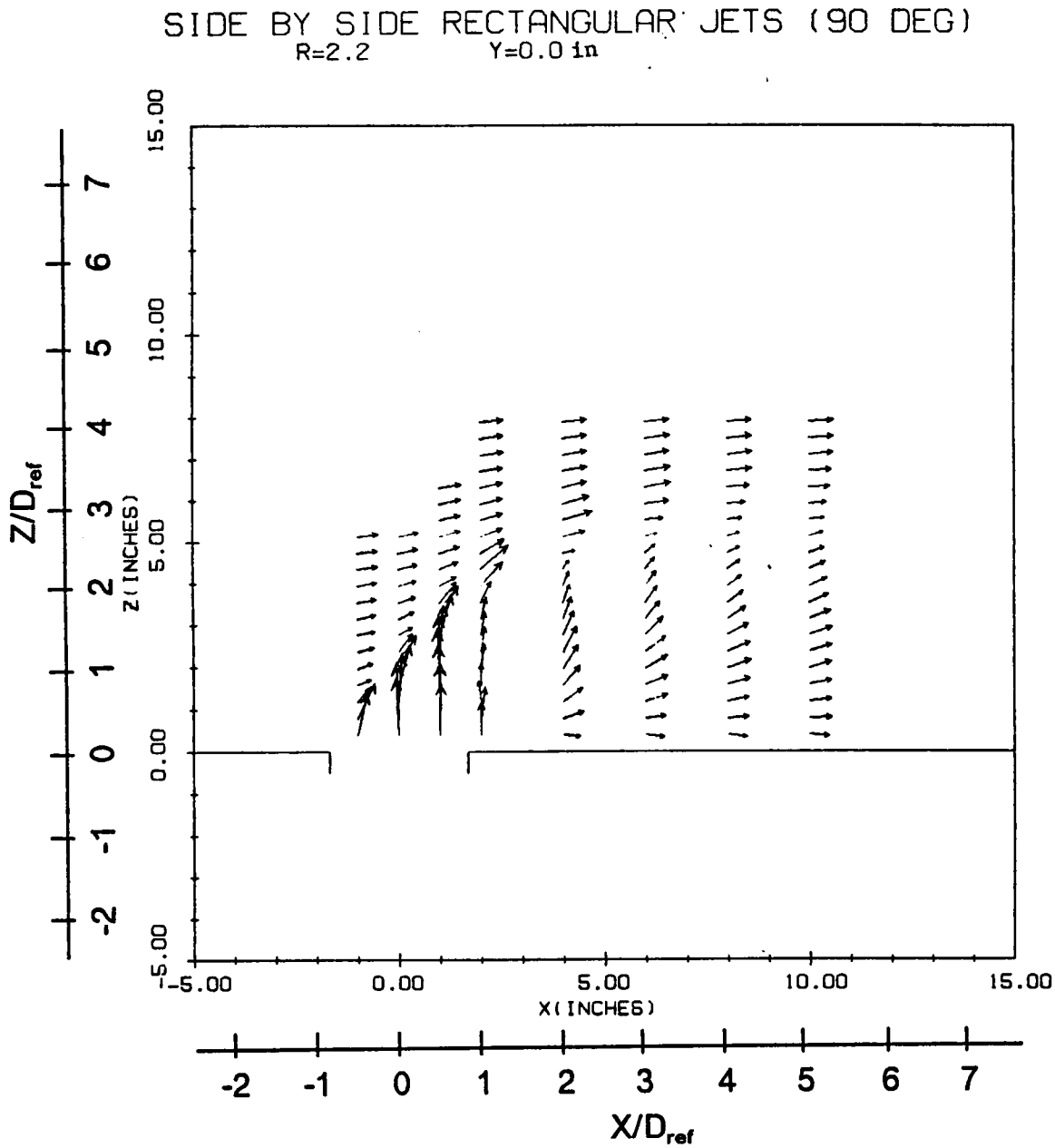

Figure 58. Mean flowfield, 90° side-by-side dual rectangular, R = 2.2.: $Y/D_{ref} = 0.0$.

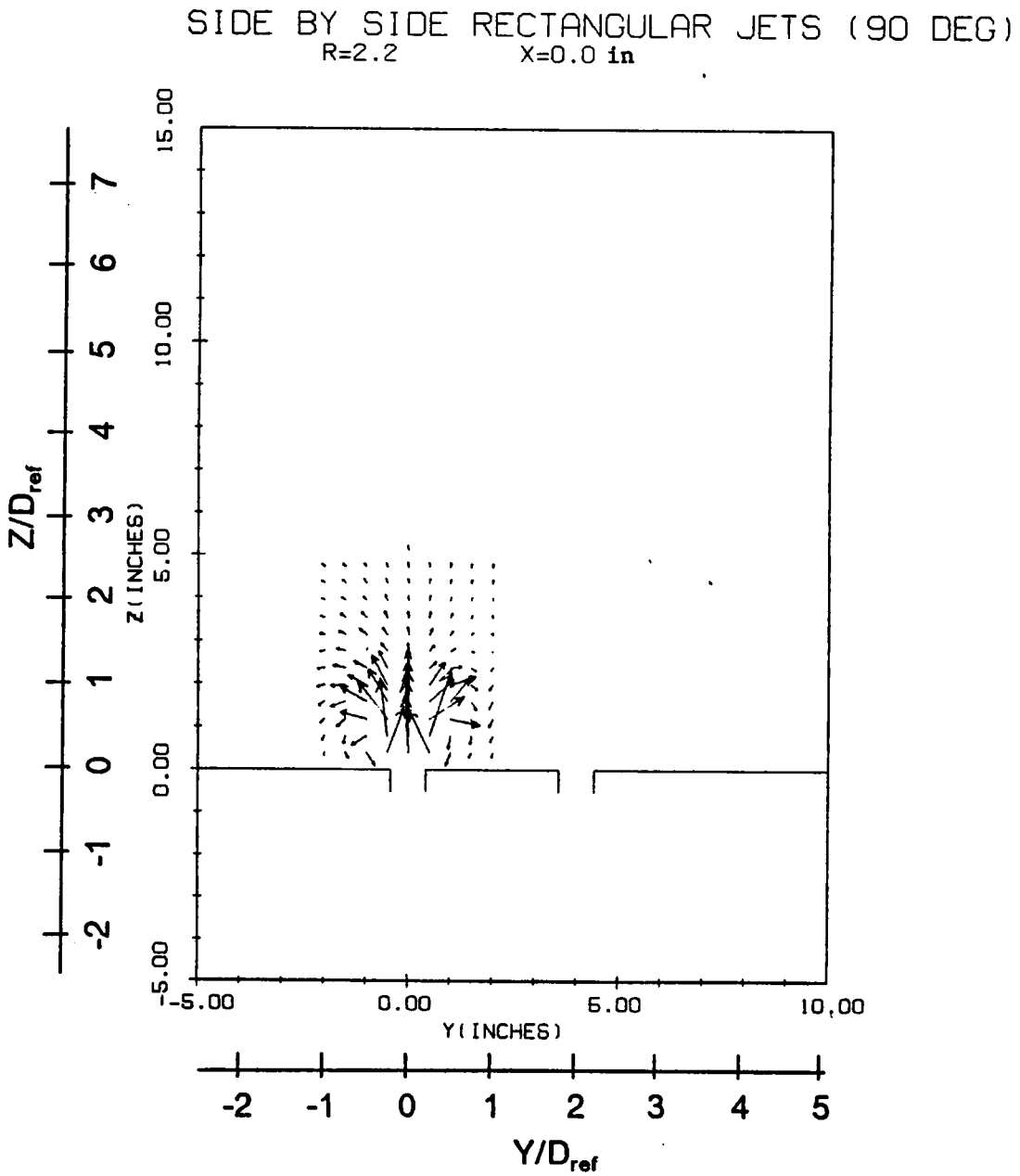

Figure 59. Mean flowfield, 90° side-by-side dual rectangular, R=2.2.: X/D_{ref} =0.0.

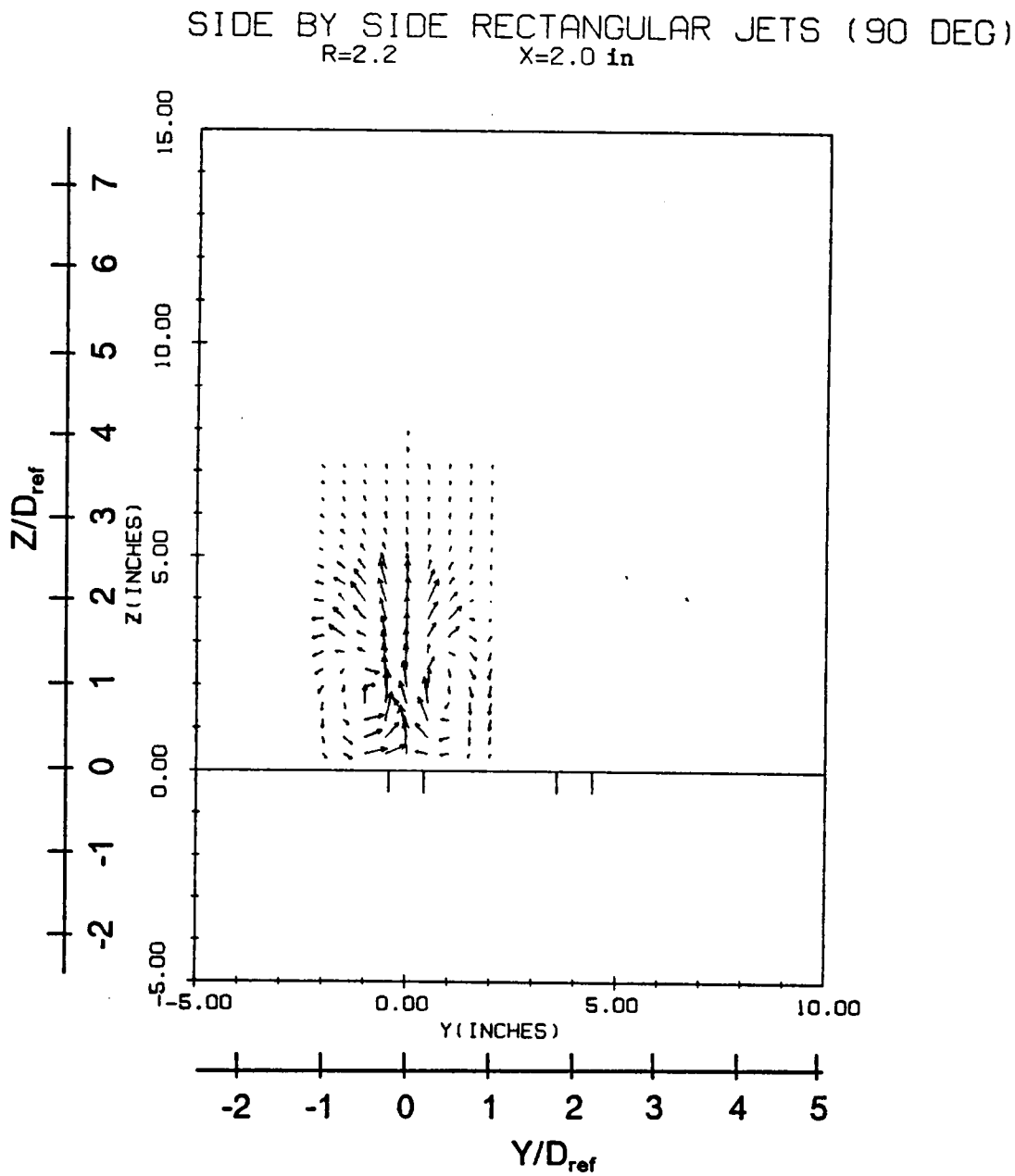

Figure 60. Mean flowfield, 90° side-by-side dual rectangular, R = 2.2.: $X/D_{ref} = 1.026$.

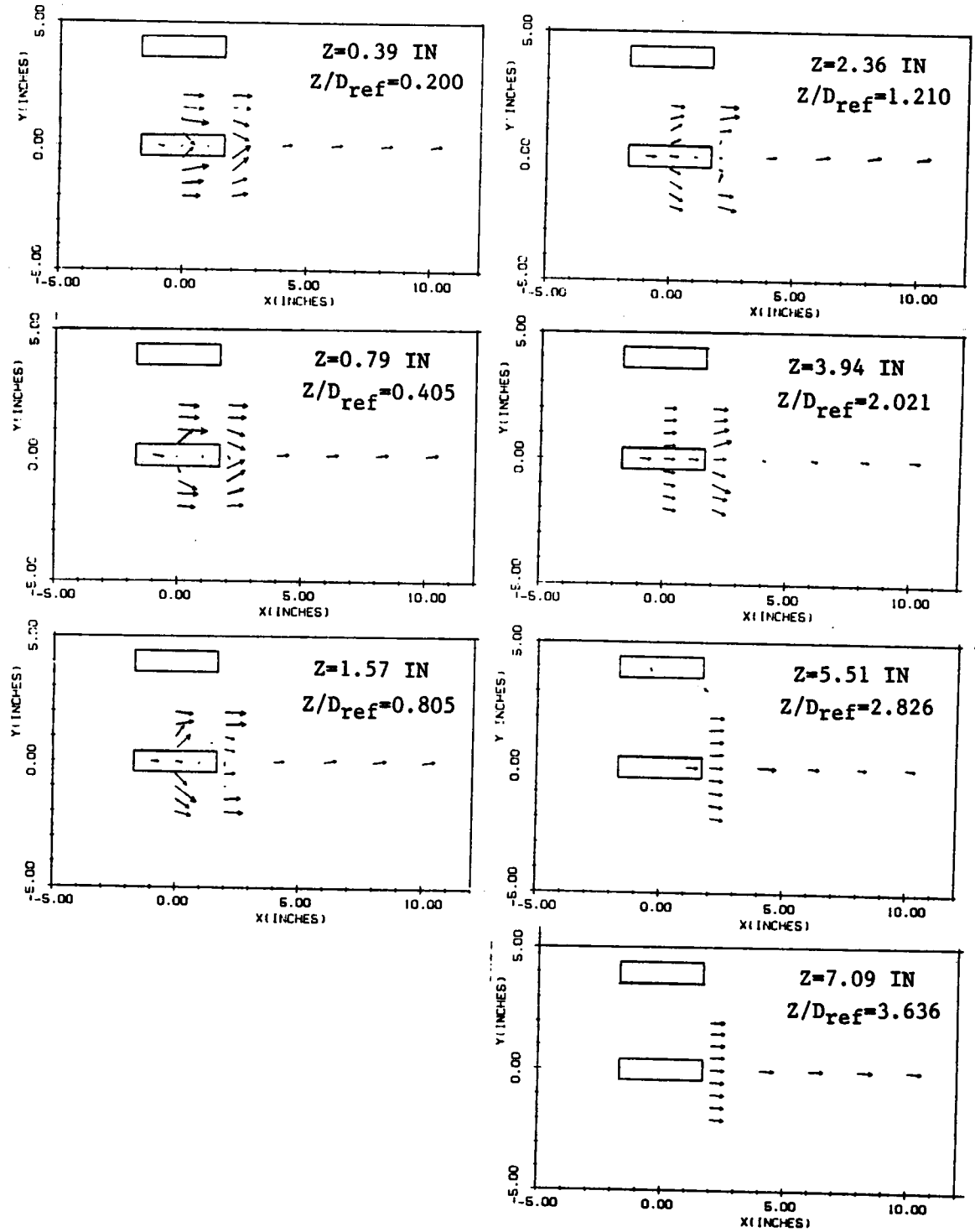

Figure 61. Mean flowfield, 90° side-by-side dual rectangular, R = 2.2.: Z/D_{ref} = const.

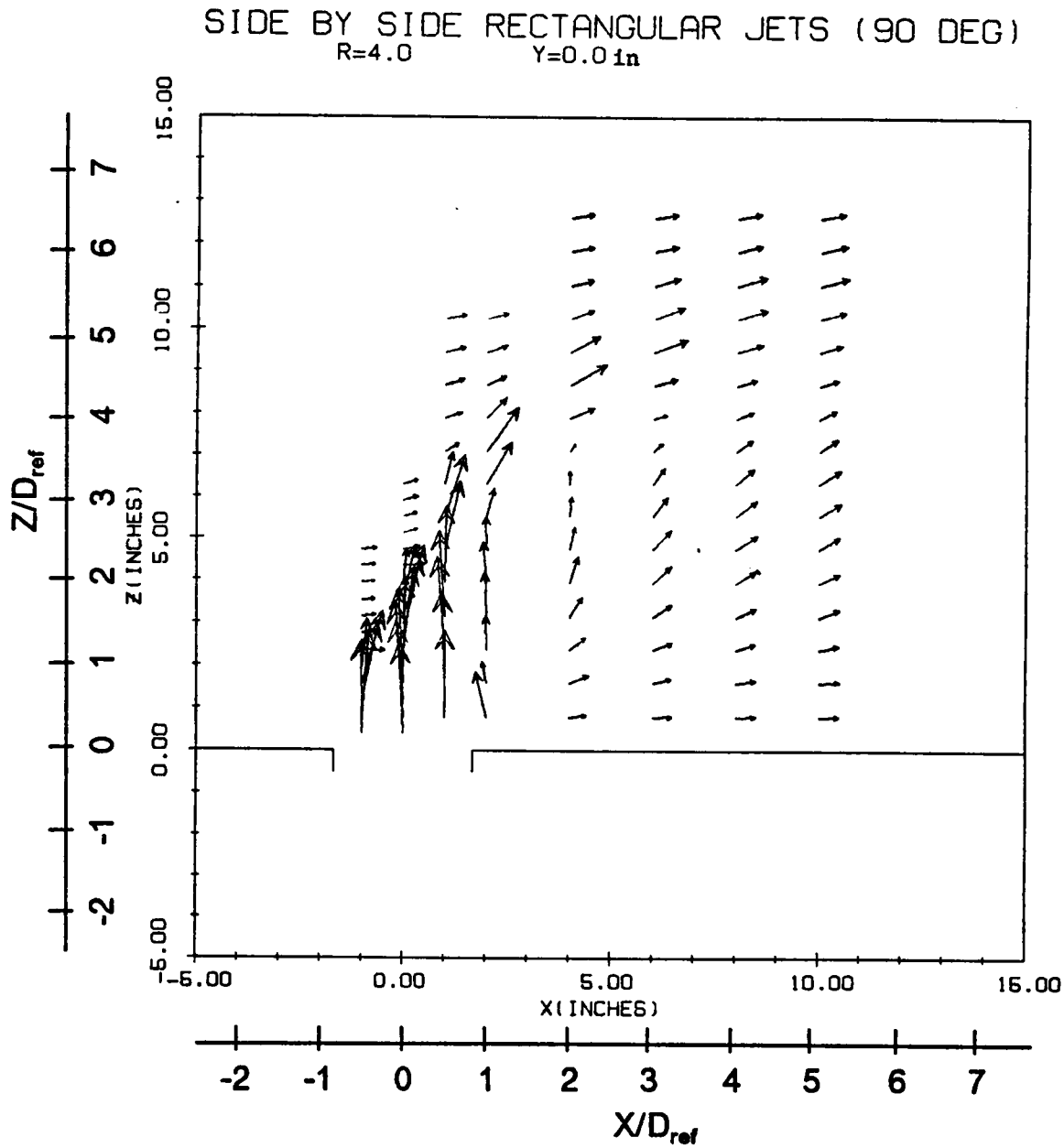

Figure 62. Mean flowfield, 90° side-by-side dual rectangular, R = 4.0.: $Y/D_{ref} = 0.0$.

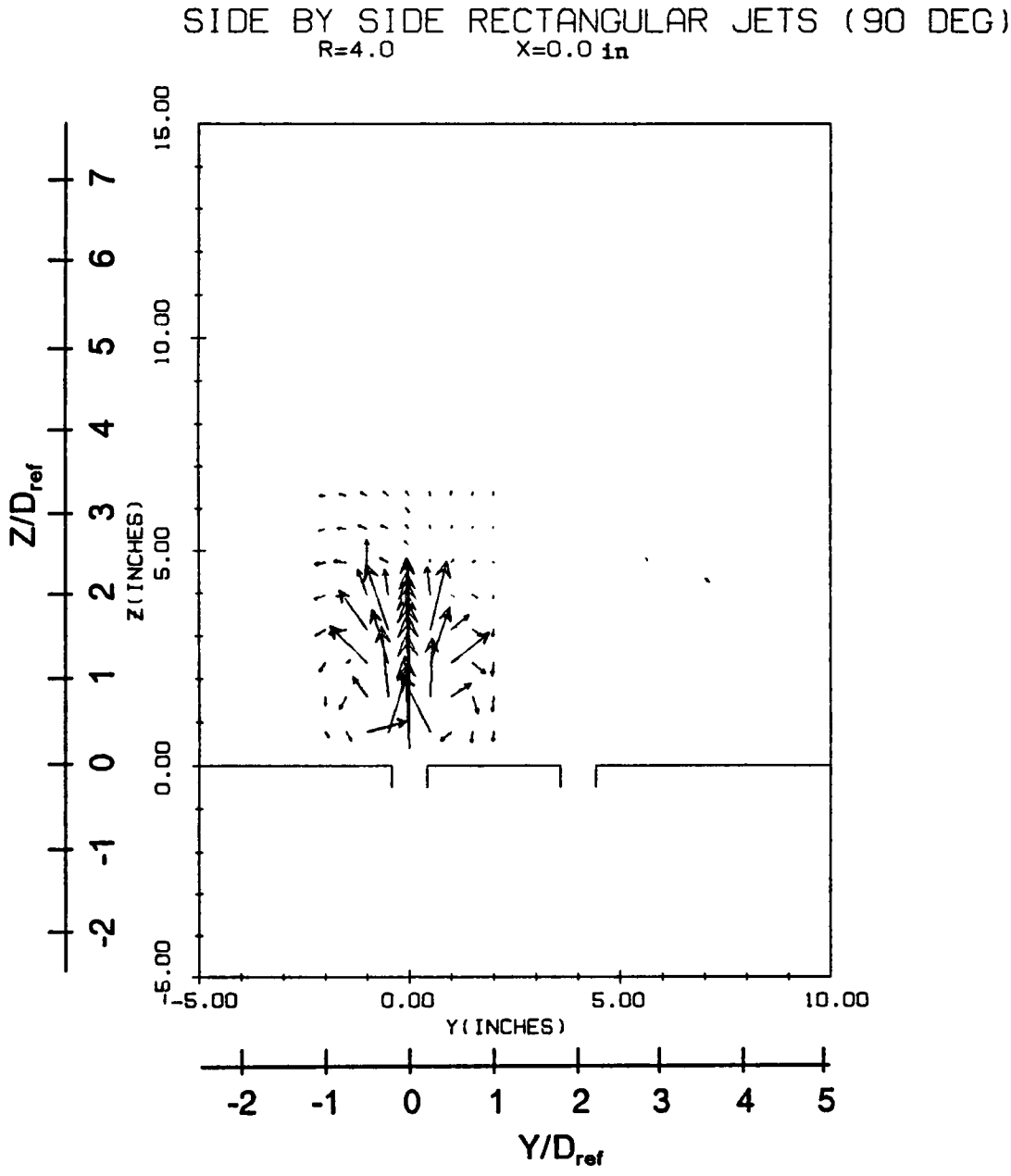

Figure 63. Mean flowfield, 90° side-by-side dual rectangular, R = 4.0.: $X/D_{ref} = 0.0$.

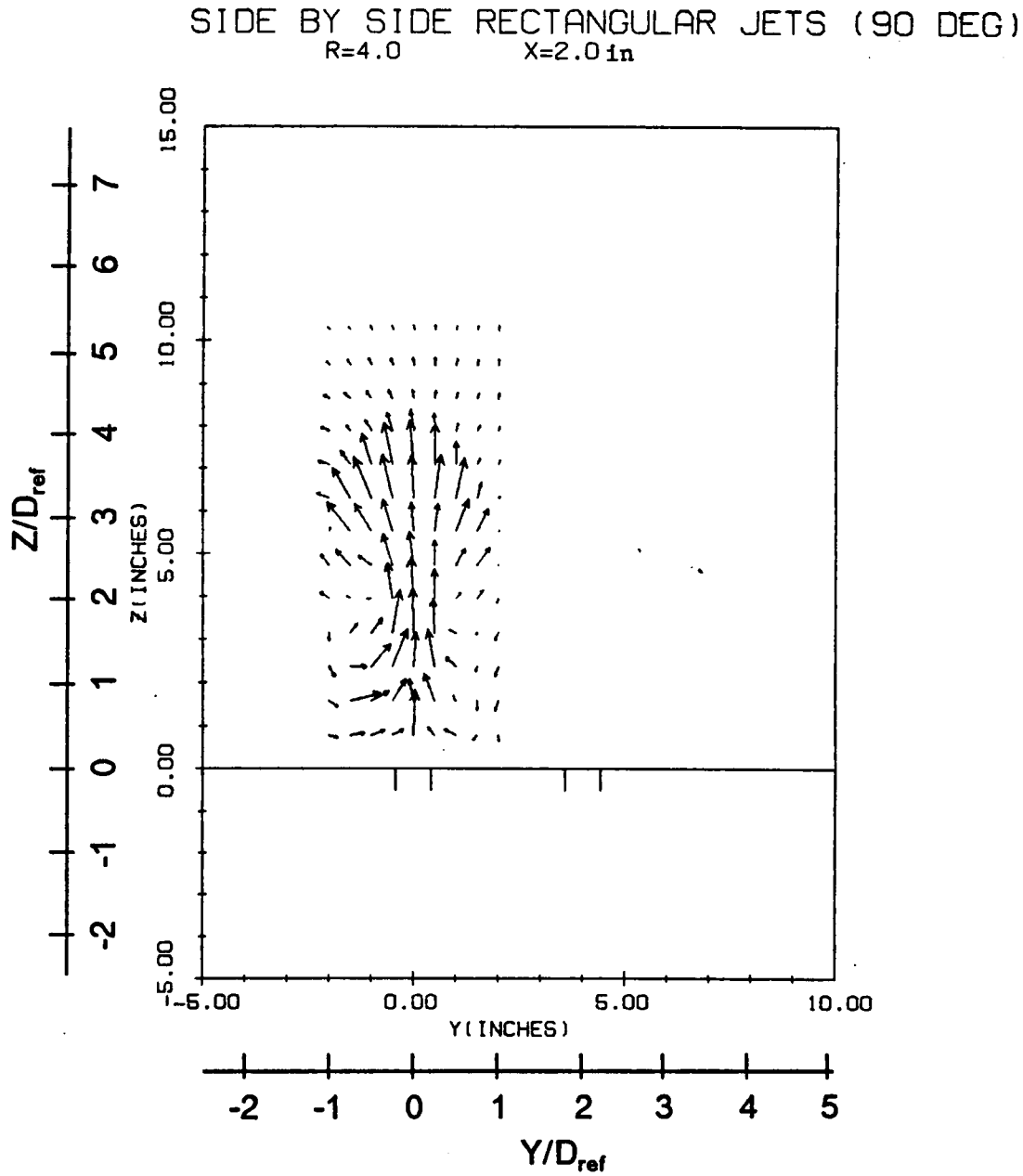

Figure 64. Mean flowfield, 90° side-by-side dual rectangular, R = 4.0.: $X/D_{ref} = 1.026$.

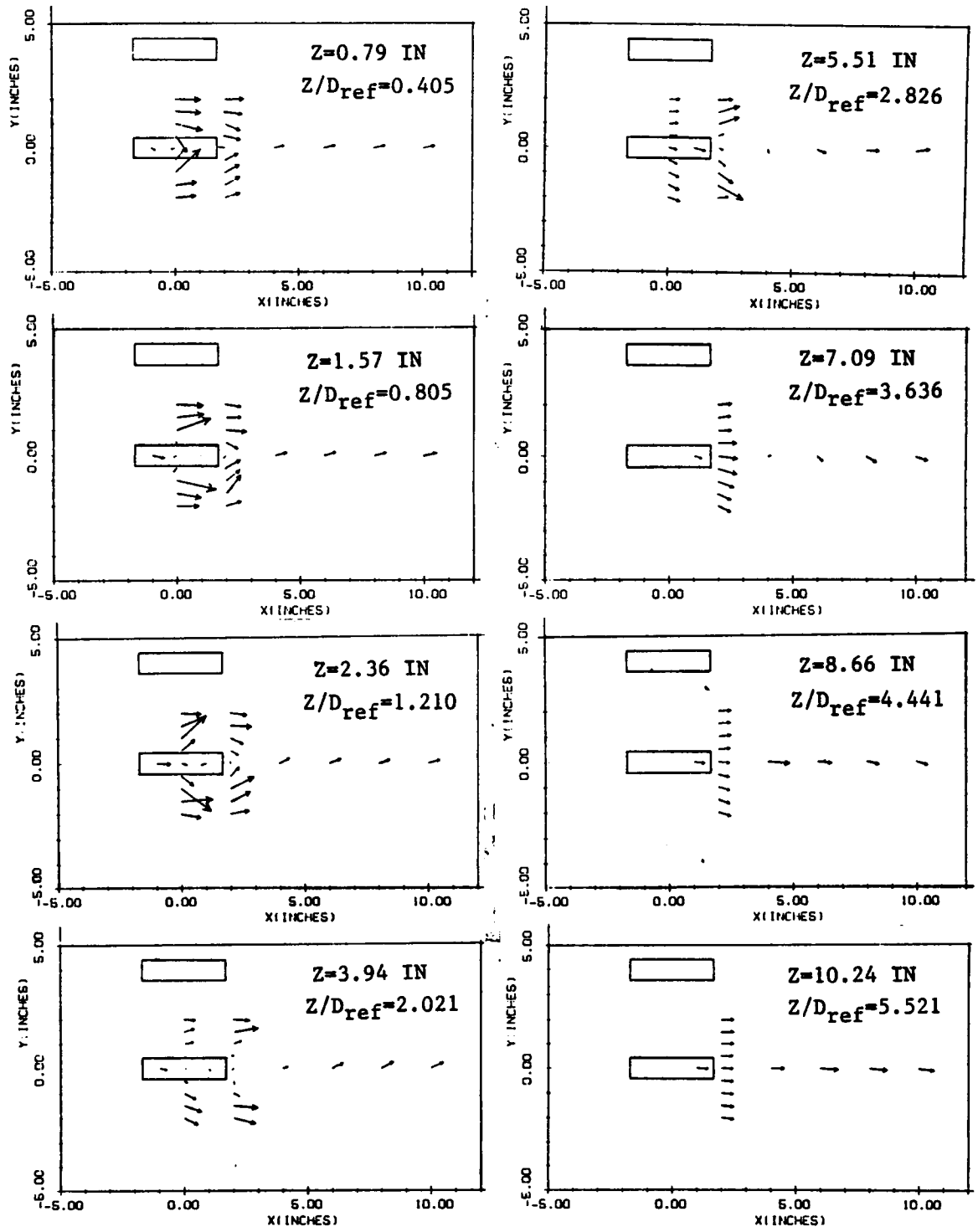

Figure 65. Mean flowfield, 90° side-by-side dual rectangular, R = 4.0.: Z/D_{ref} = const.

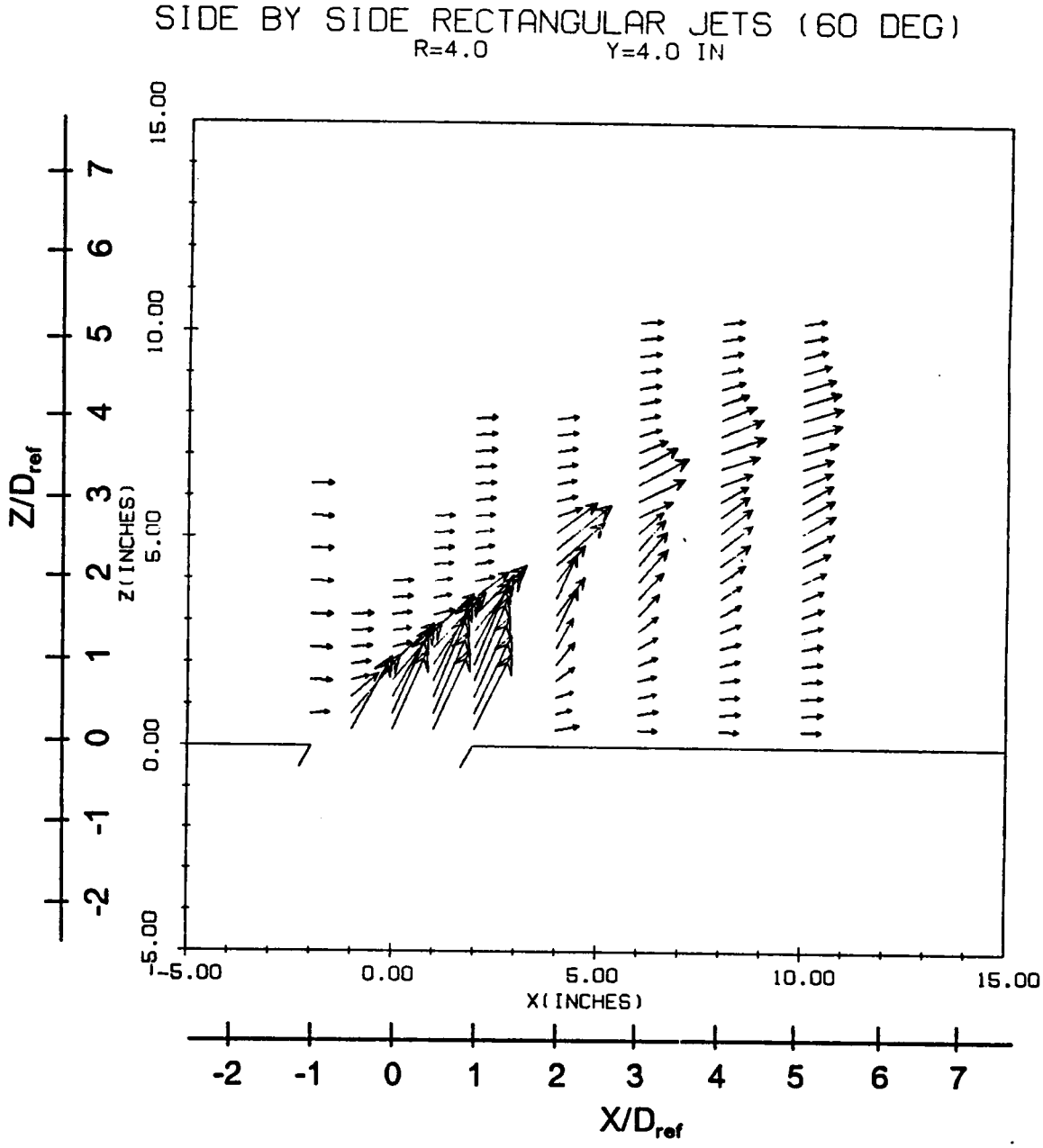

Figure 66. Mean flowfield, 60° side-by-side dual rectangular, R = 4.0.: Y/D_{ref} = 2.051.

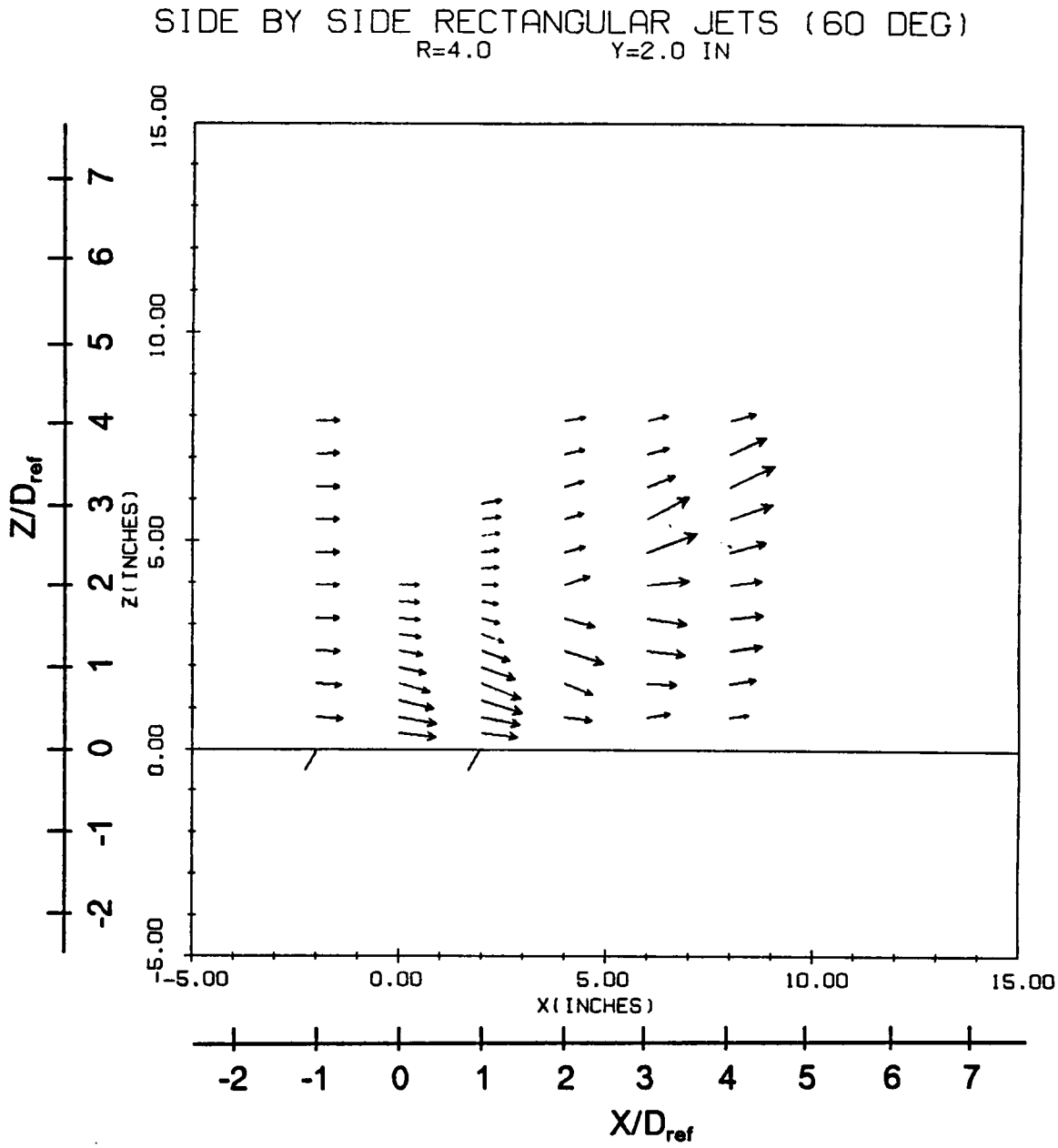

Figure 67. Mean flowfield, 60° side-by-side dual rectangular, R = 4.0.: $Y/D_{ref} = 1.026$.

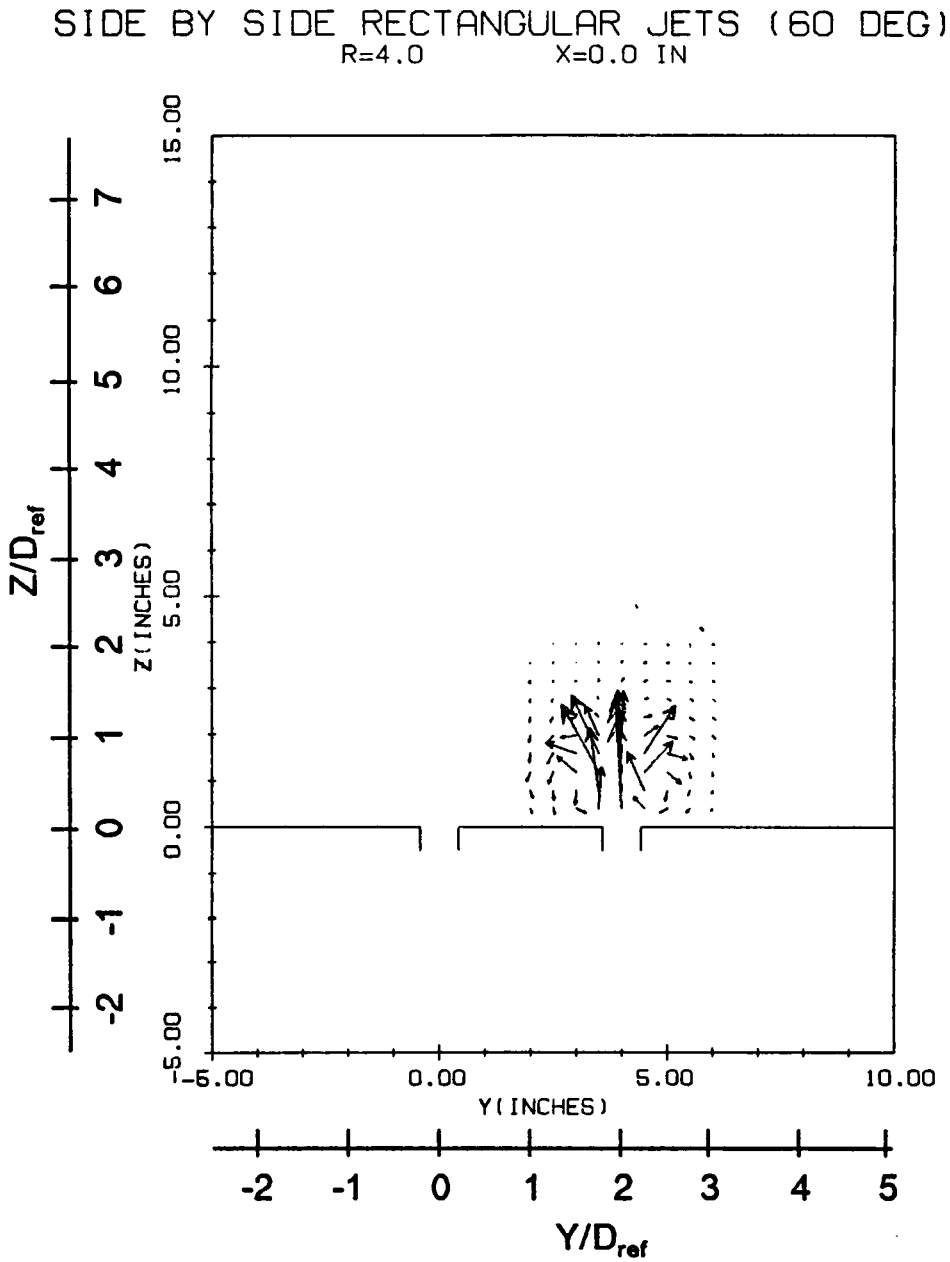

Figure 68. Mean flowfield, 60° side-by-side dual rectangular, R = 4.0.: $X/D_{ref} = 0.0$.

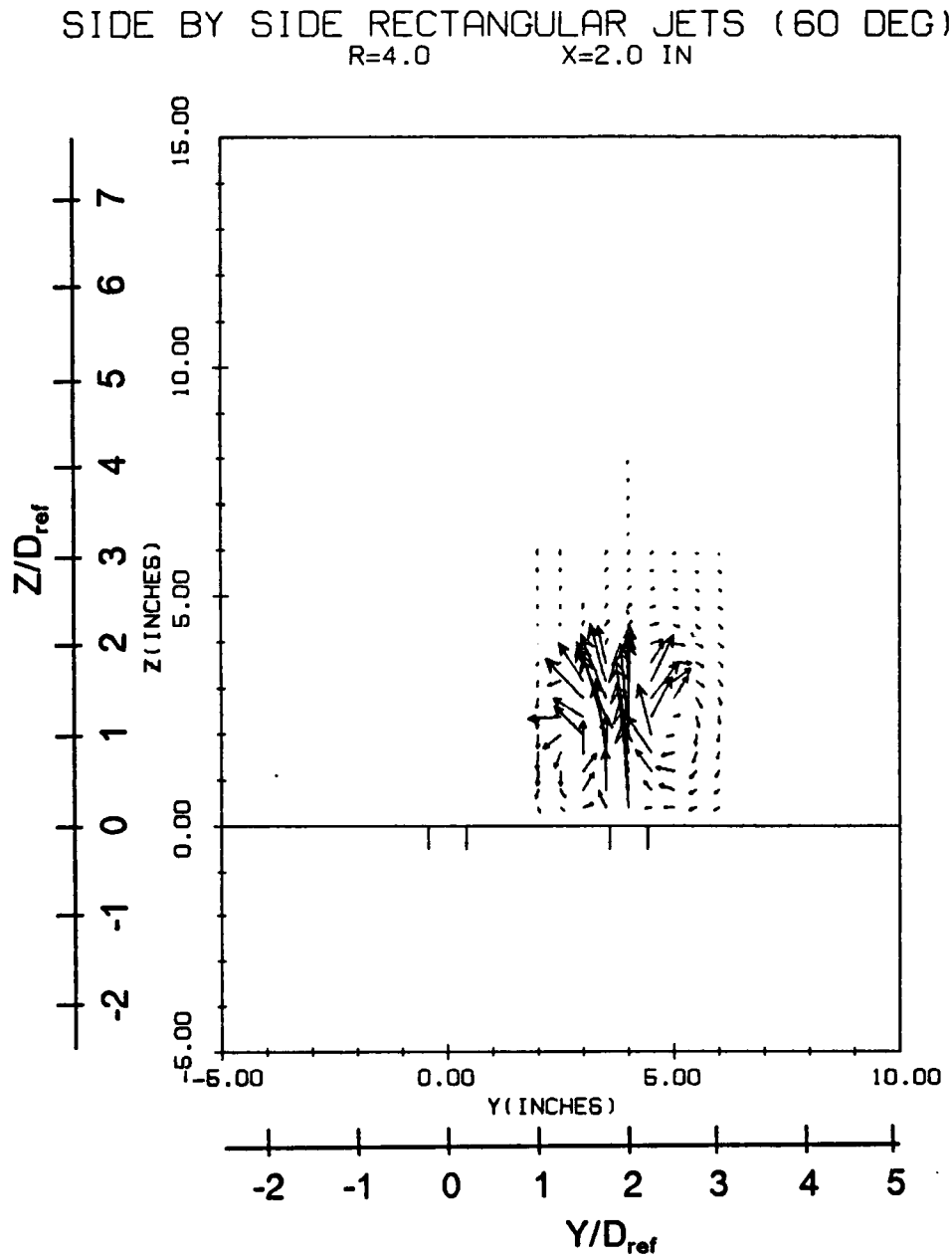

Figure 69. Mean flowfield, 60° side-by-side dual rectangular, R = 4.0.: $X/D_{ref} = 1.026$.

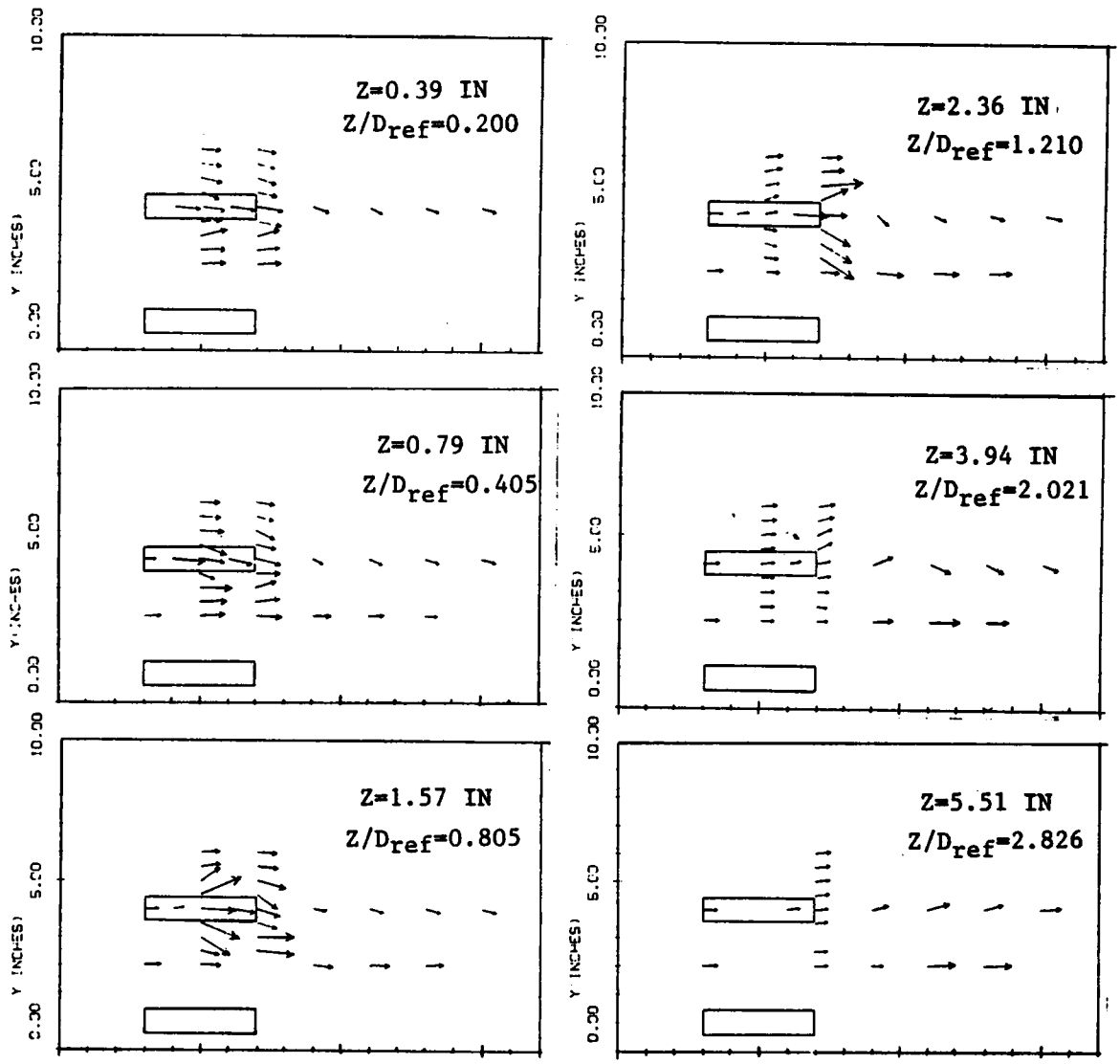

Figure 70. Mean flowfield, 60° side-by-side dual rectangular, R = 4.0.: Z/D_{ref} = const.

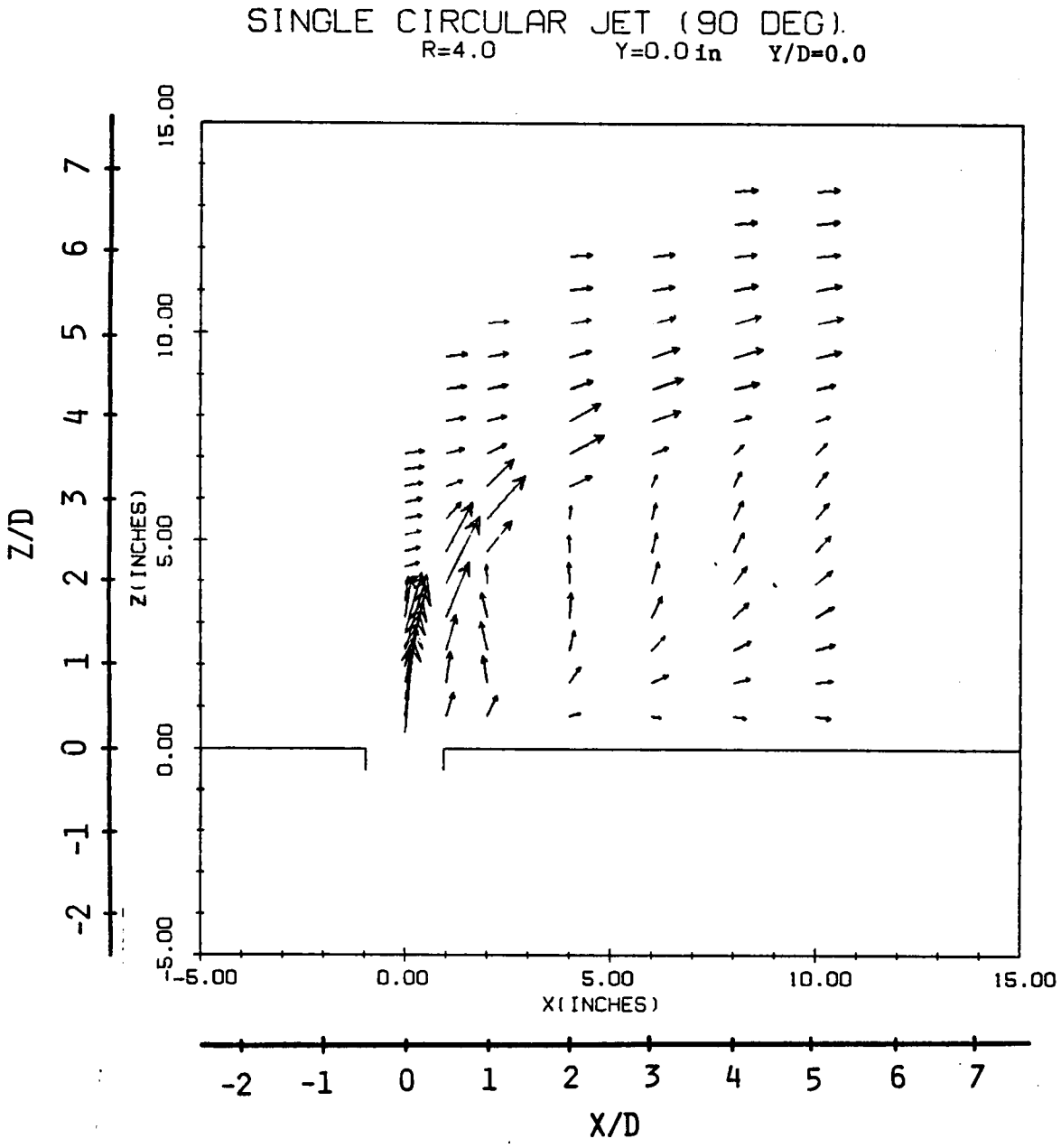

Figure 71. Mean flowfield, 90° circular jet, R = 4.0.: Y/D = 0.0.

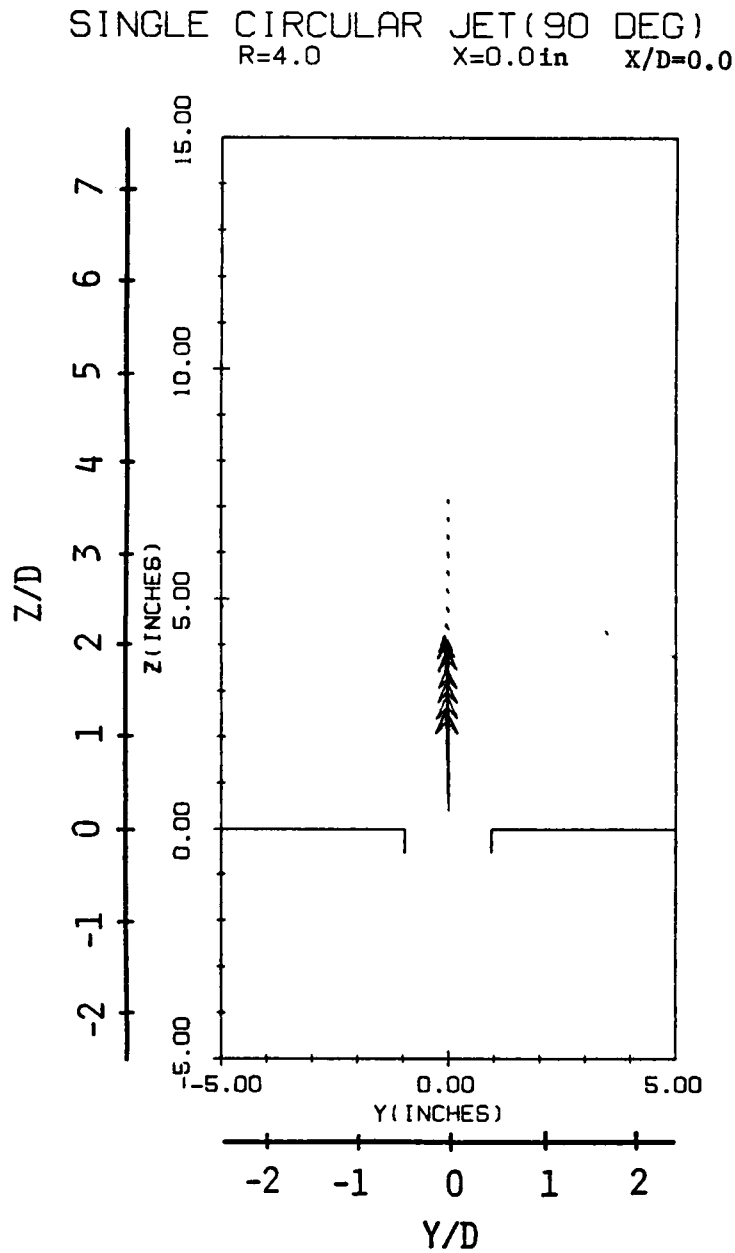

Figure 72. Mean flowfield, 90° circular jet, R = 4.0.: X/D = 0.0.

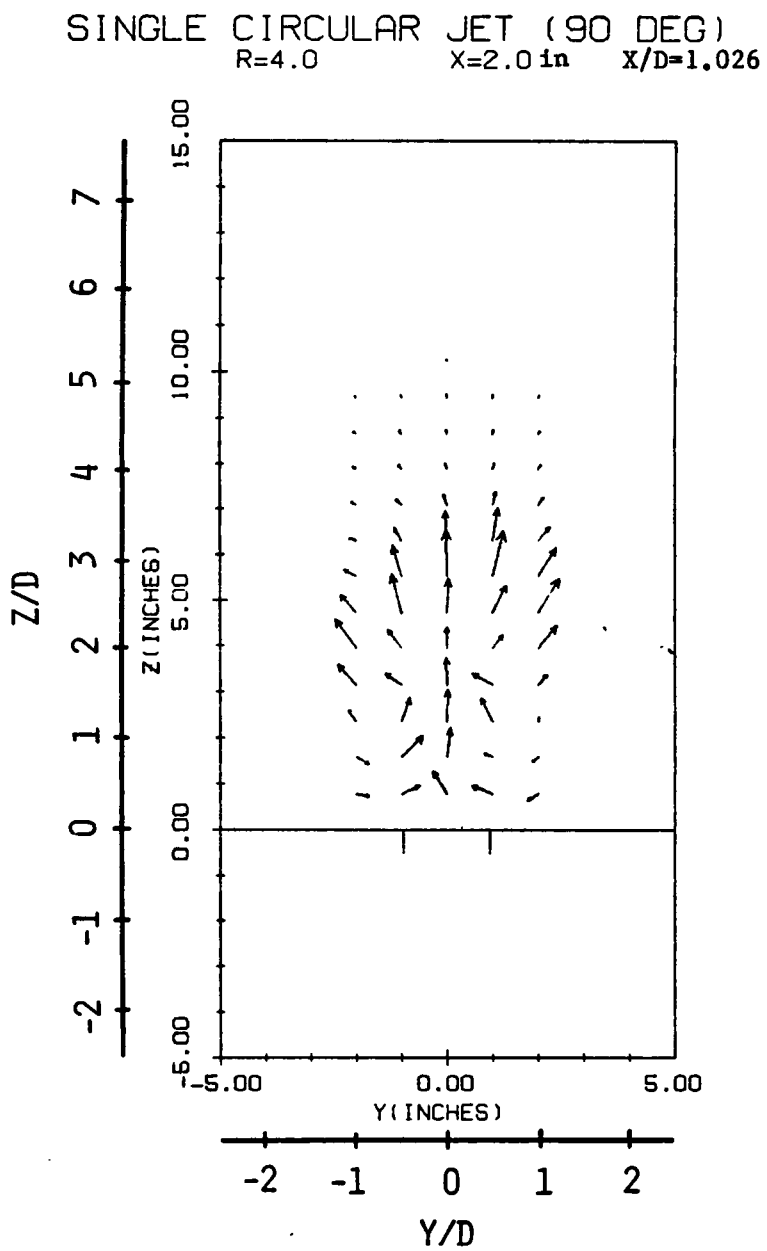

Figure 73. Mean flowfield, 90° circular jet, R = 4.0.: X/D = 1.026.

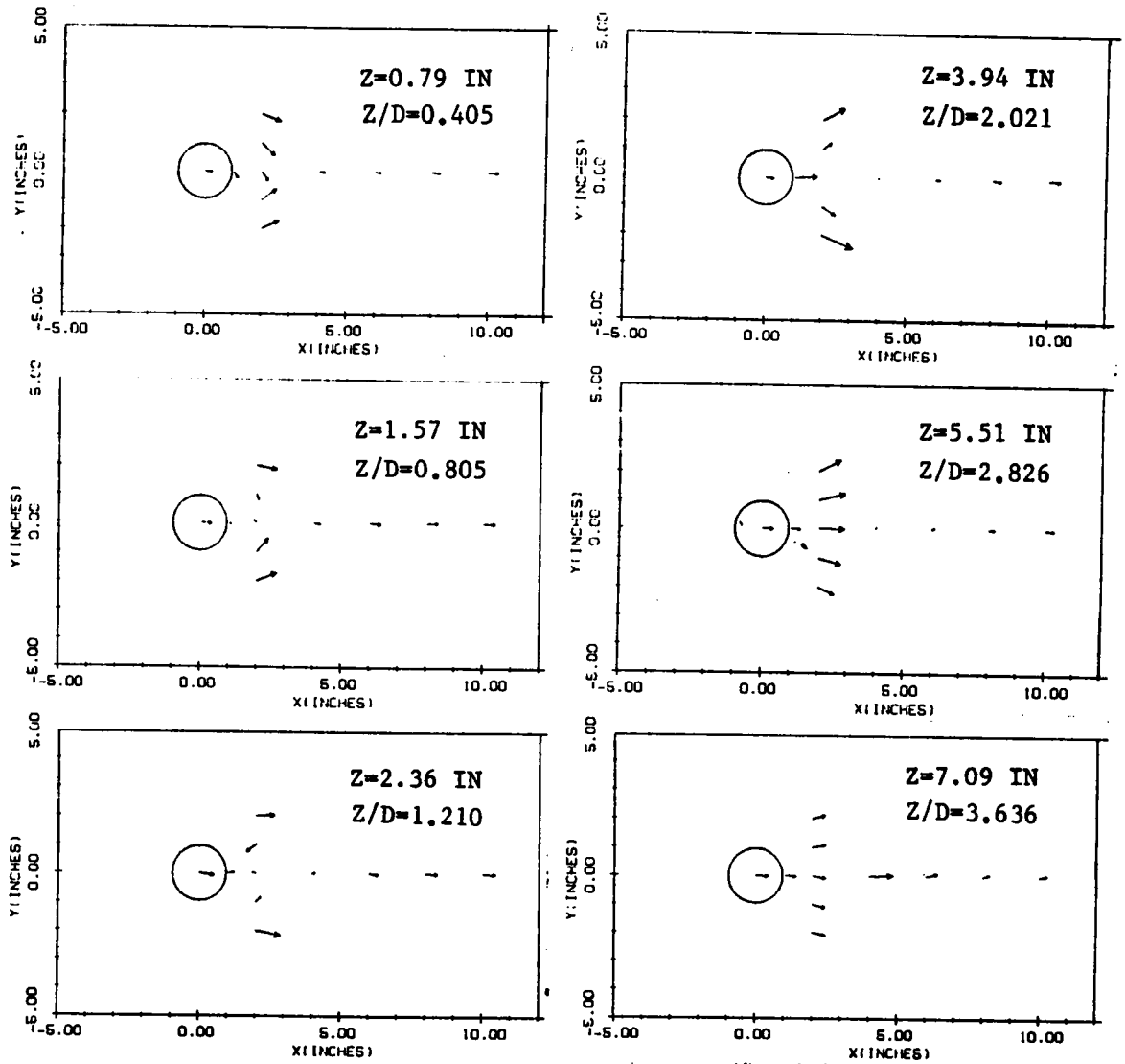

Figure 74. Mean flowfield, 90° circular jet, R = 4.0.: Z/D = const.

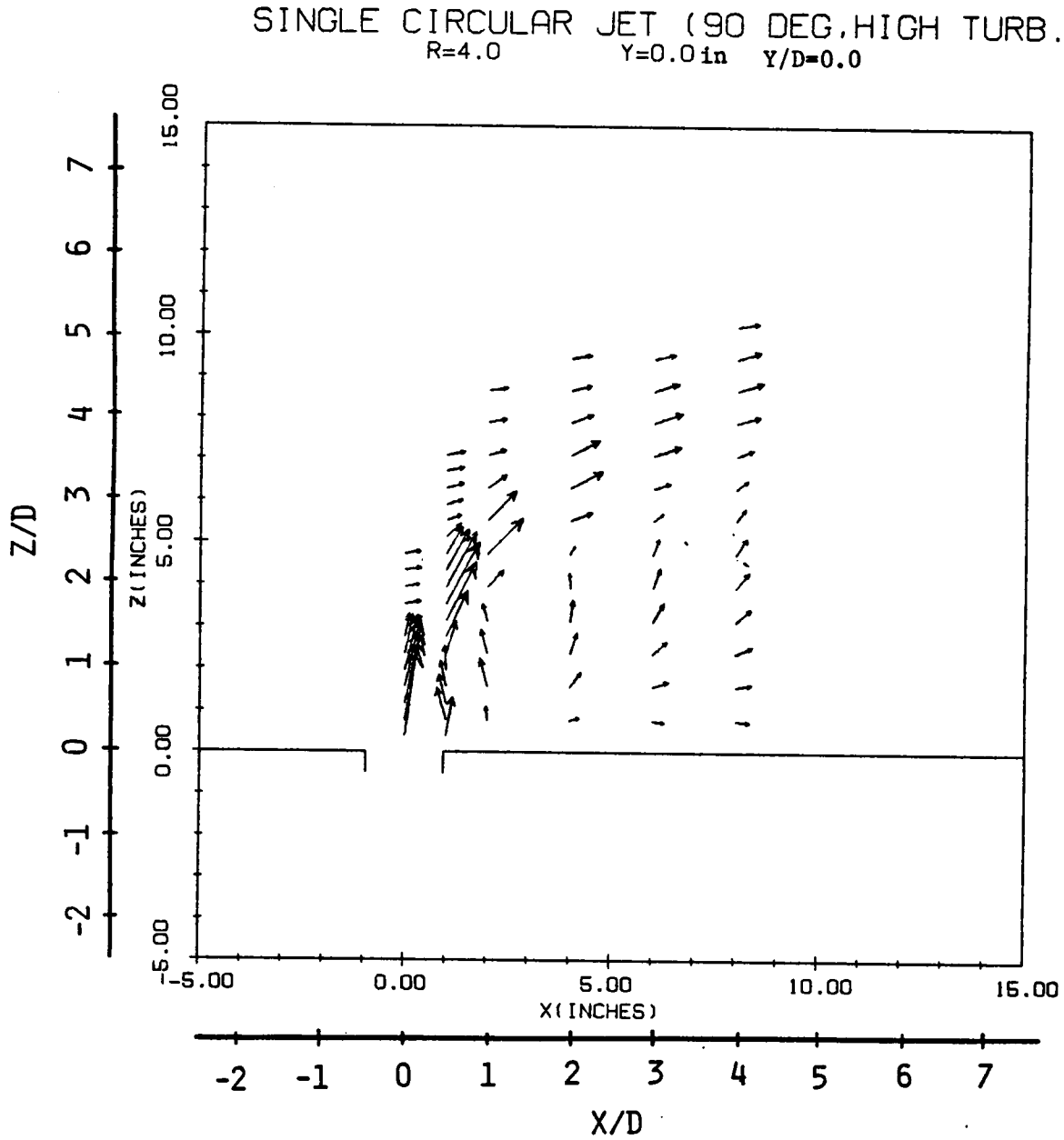

Figure 75. Mean flowfield, 90° circular jet, high turbulence, R = 4.0.: Y/D = 0.0.

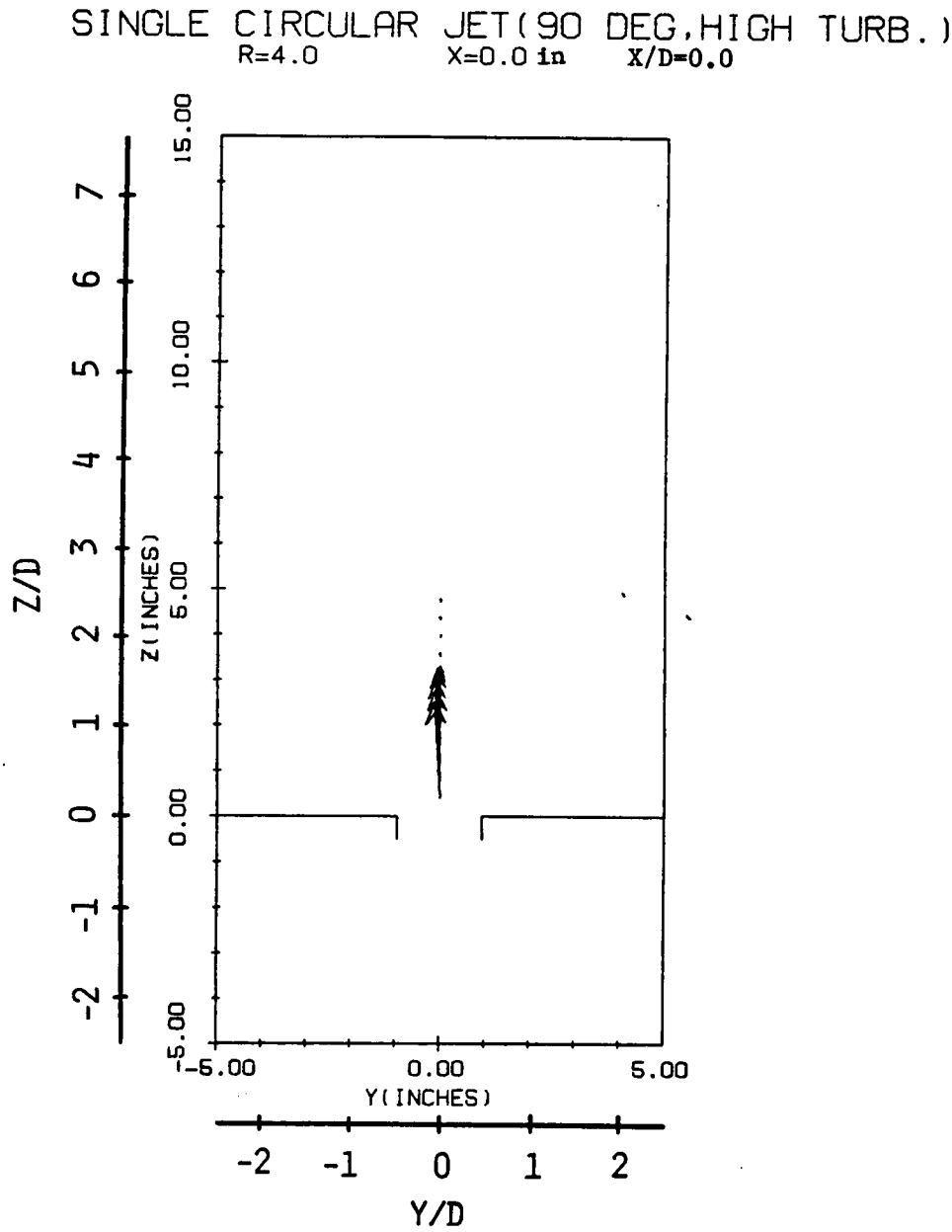

Figure 76. Mean flowfield, 90° circular jet, high turbulence, R = 4.0.: X/D = 0.0.

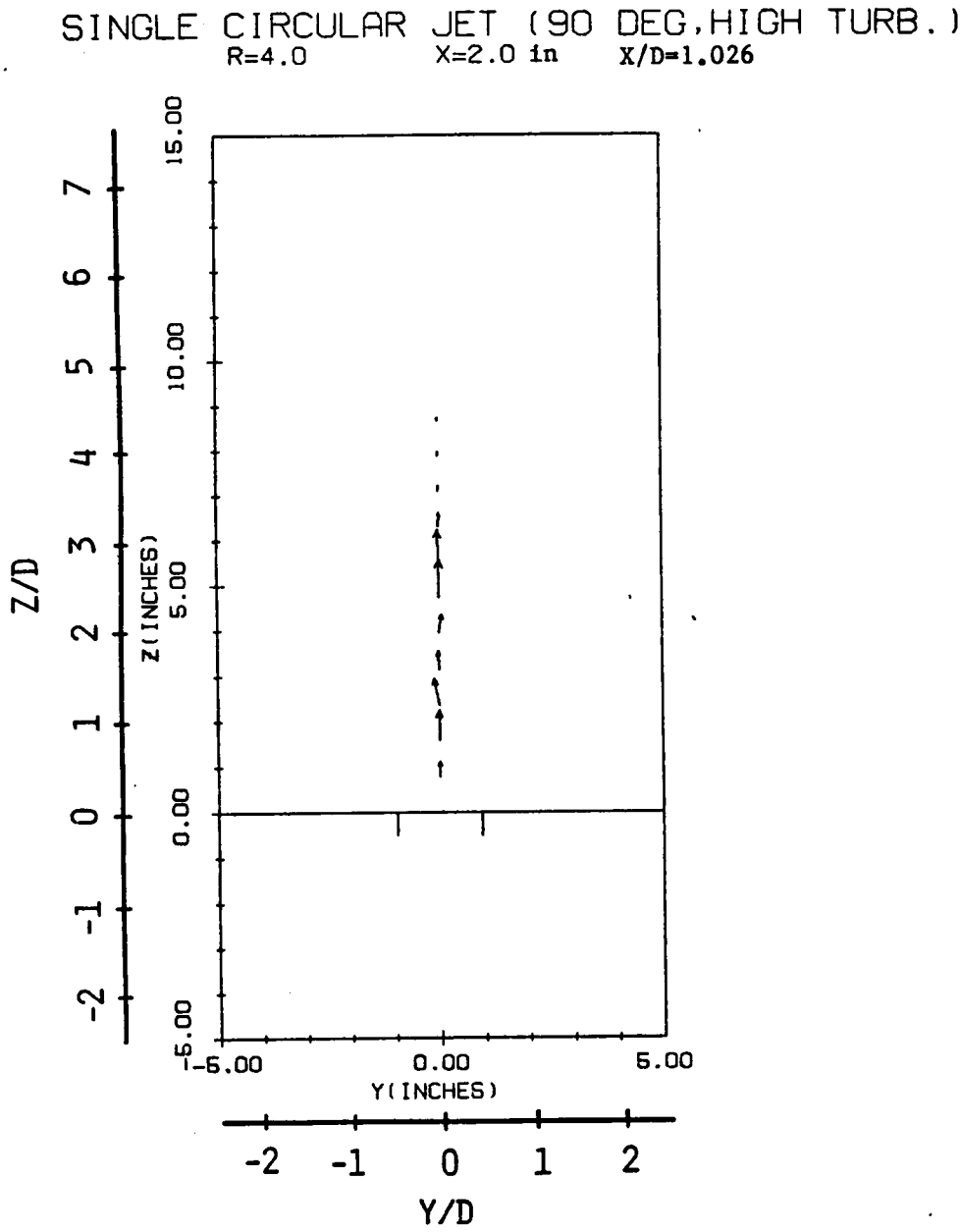

Figure 77. Mean flowfield, 90° circular jet, high turbulence, R = 4.0.: X/D = 1.026.

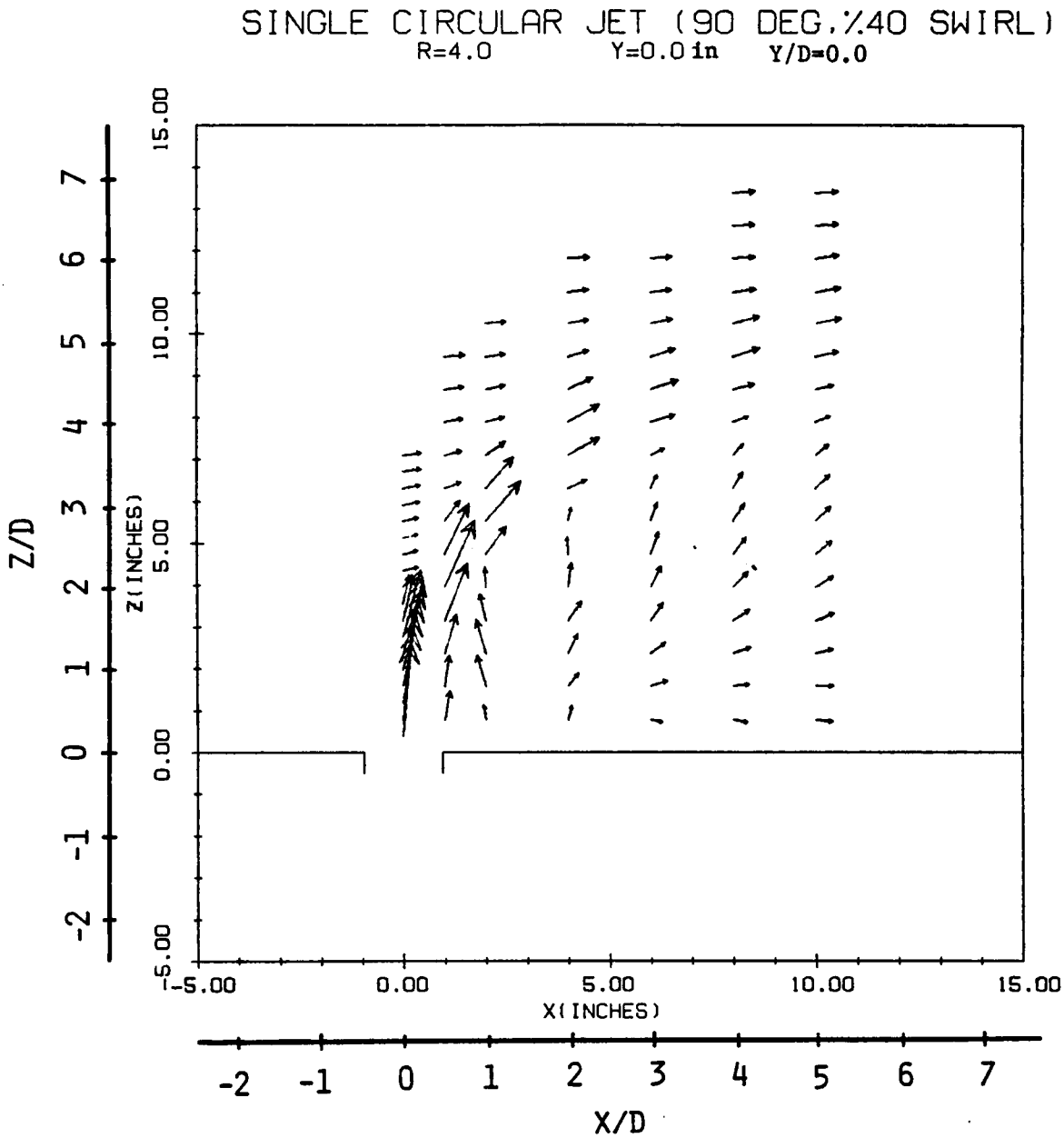

Figure 78. Mean flowfield, 90° circular jet, 40 % swirl, R=4.0.: Y/D=0.0.

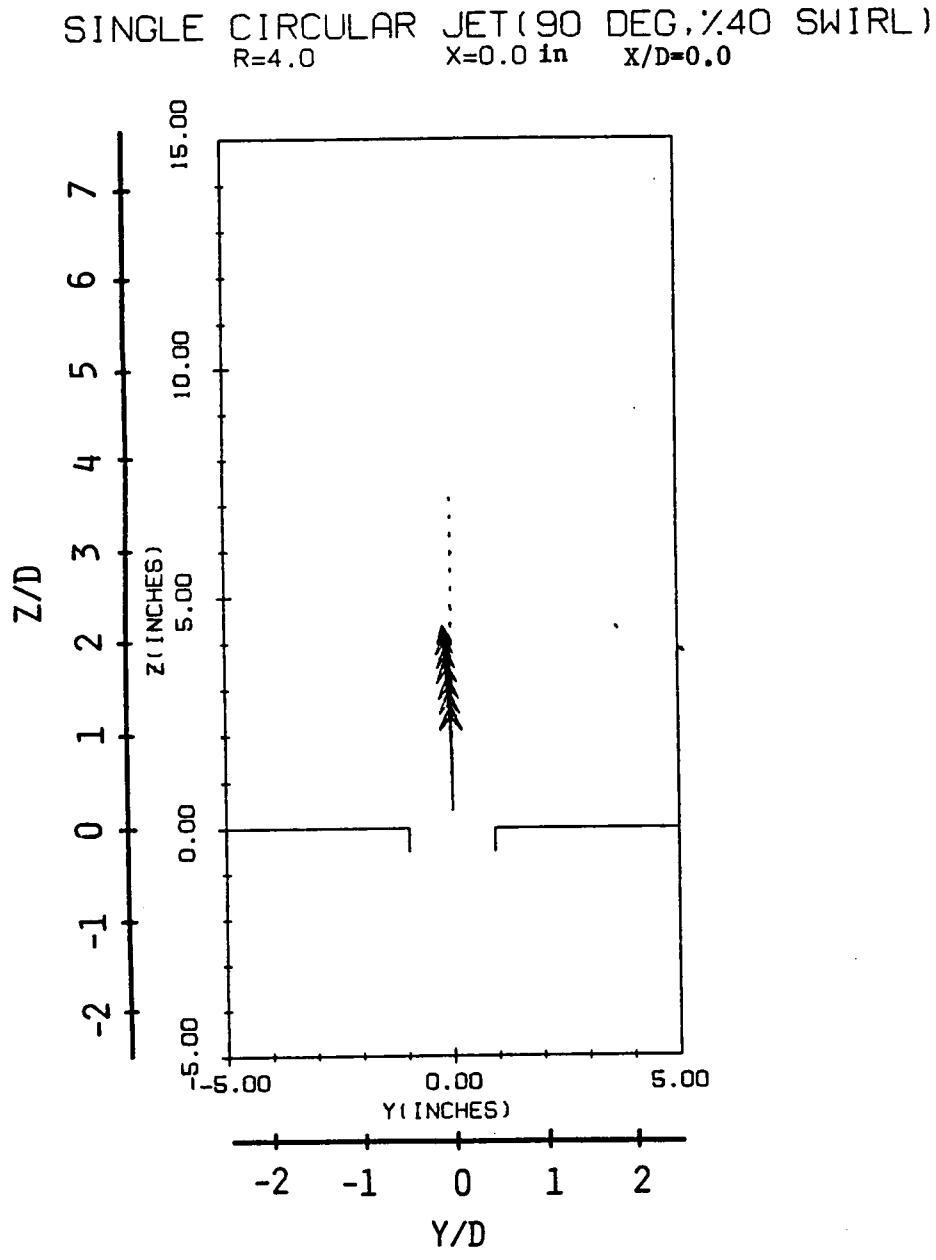

Figure 79. Mean flowfield, 90° circular jet, 40 % swirl, R = 4.0.: X/D = 0.0.

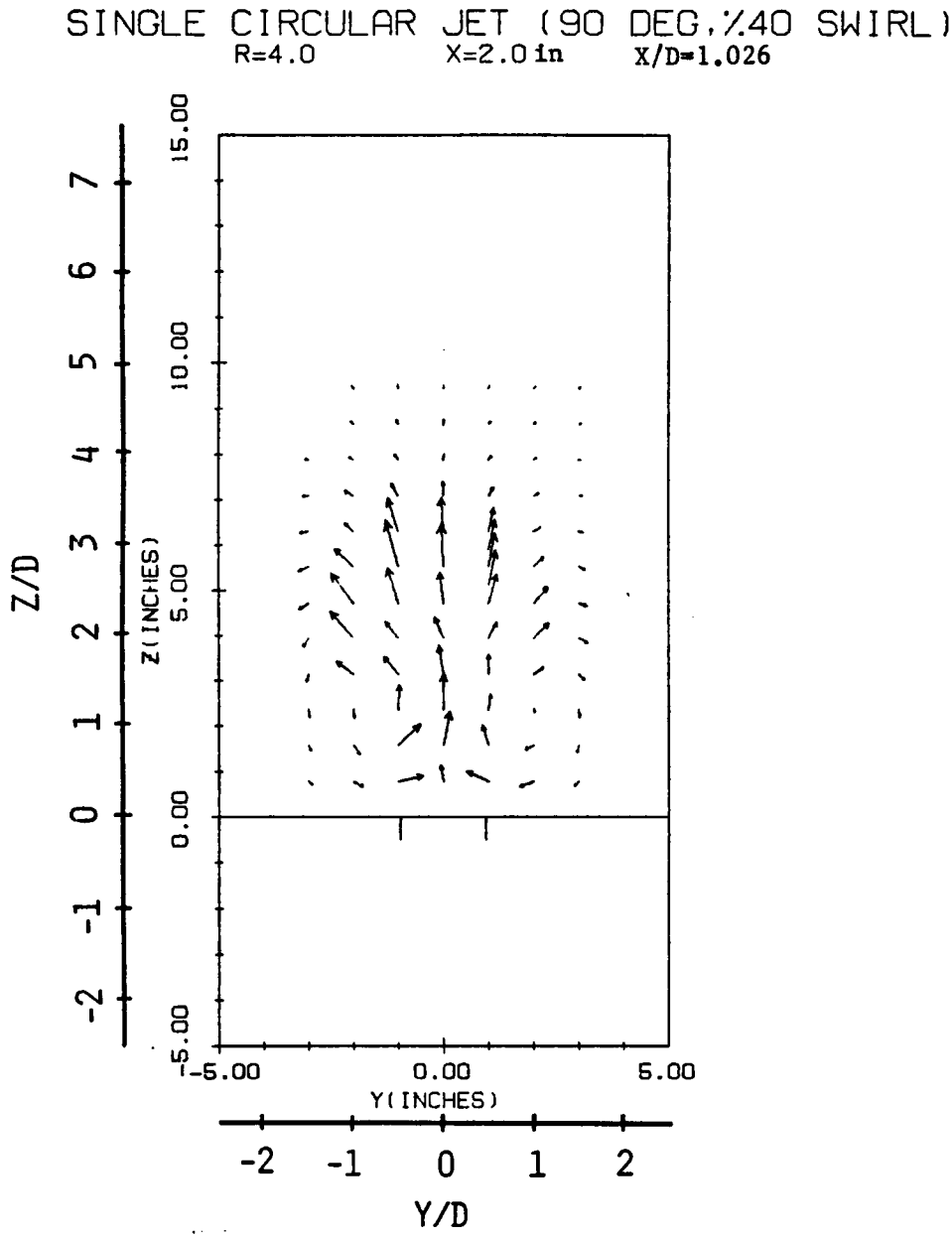

Figure 80. Mean flowfield, 90° circular jet, 40 % swirl, R = 4.0.: X/D = 1.026.

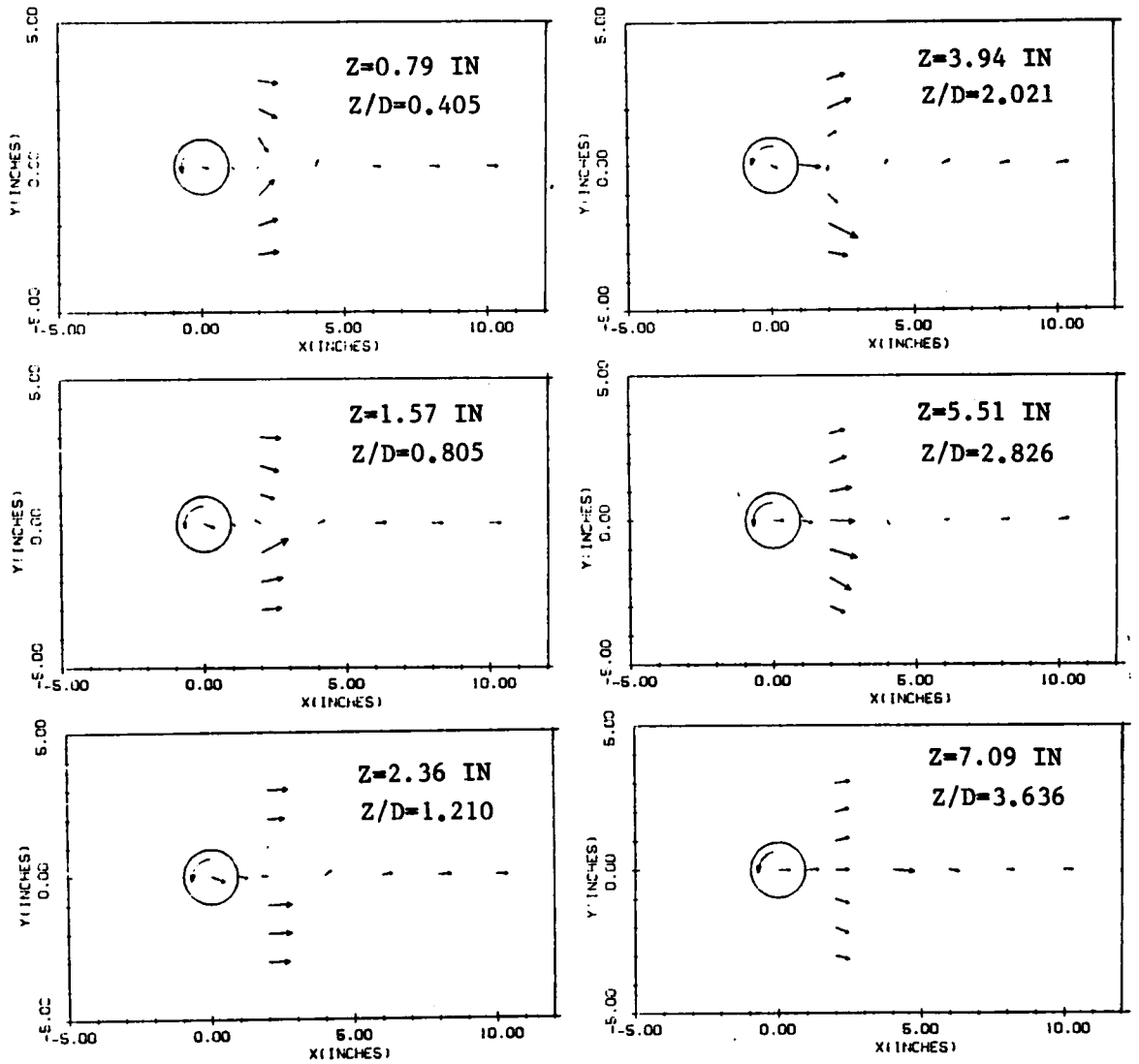

Figure 81. Mean flowfield, 90° circular jet, 40 % swirl, R = 4.0.: Z/D = const.

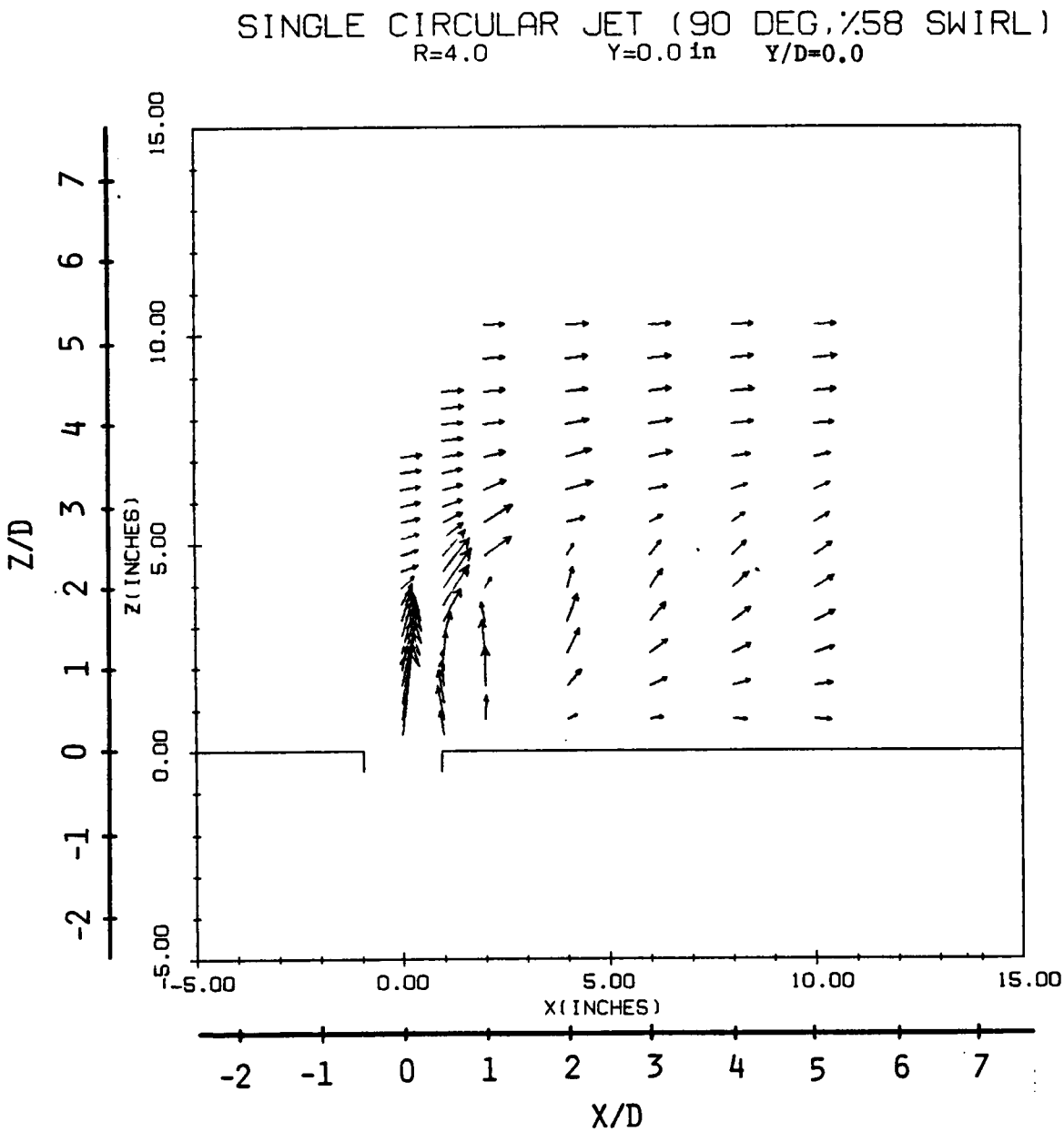

Figure 82. Mean flowfield, 90° circular jet, 58 % swirl, R=4.0.: Y/D=0.0.

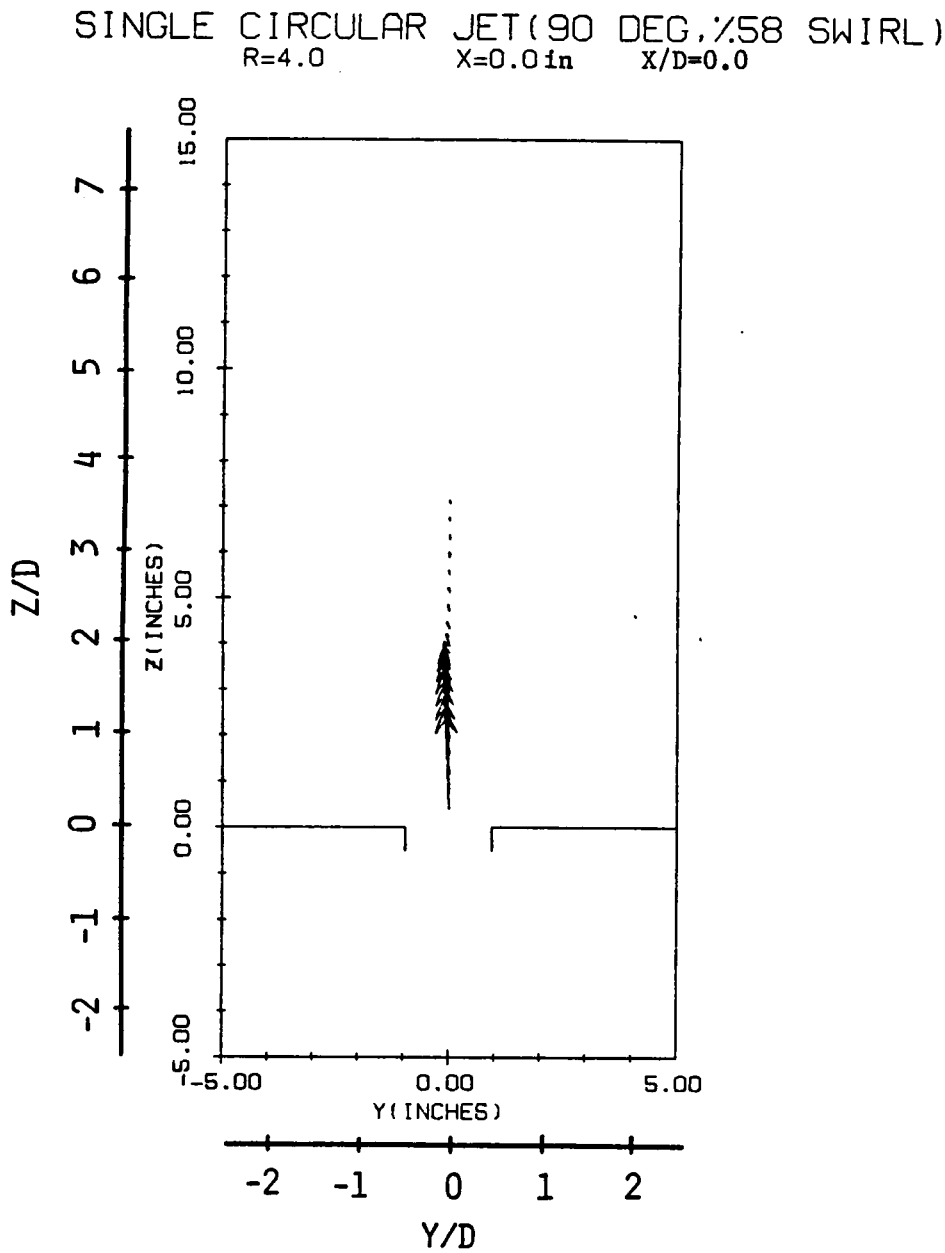

Figure 83. Mean flowfield, 90° circular jet, 58 % swirl, R=4.0.: X/D=0.0.

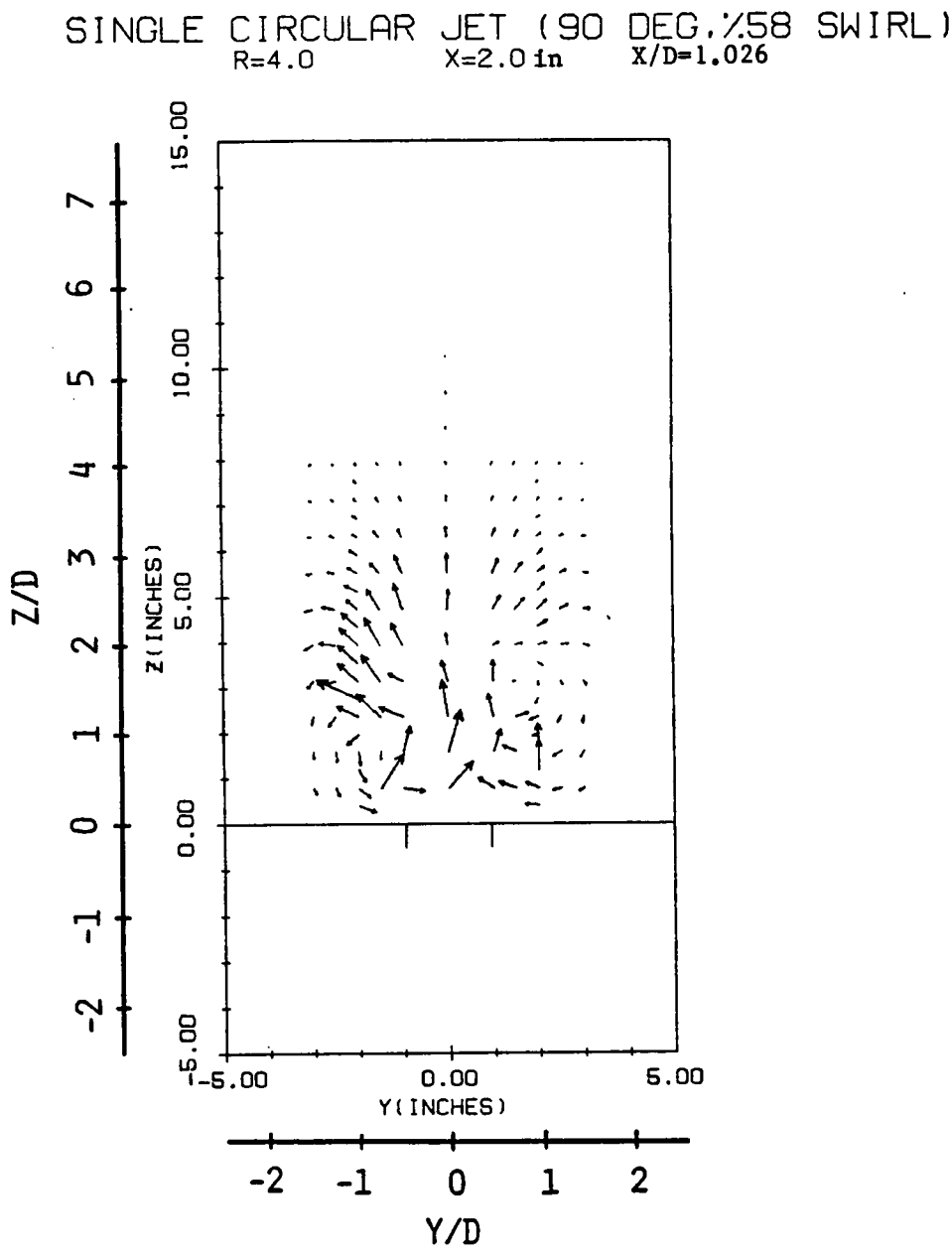

Figure 84. Mean flowfield, 90° circular jet, 58 % swirl, R = 4.0.: X/D = 1.026.

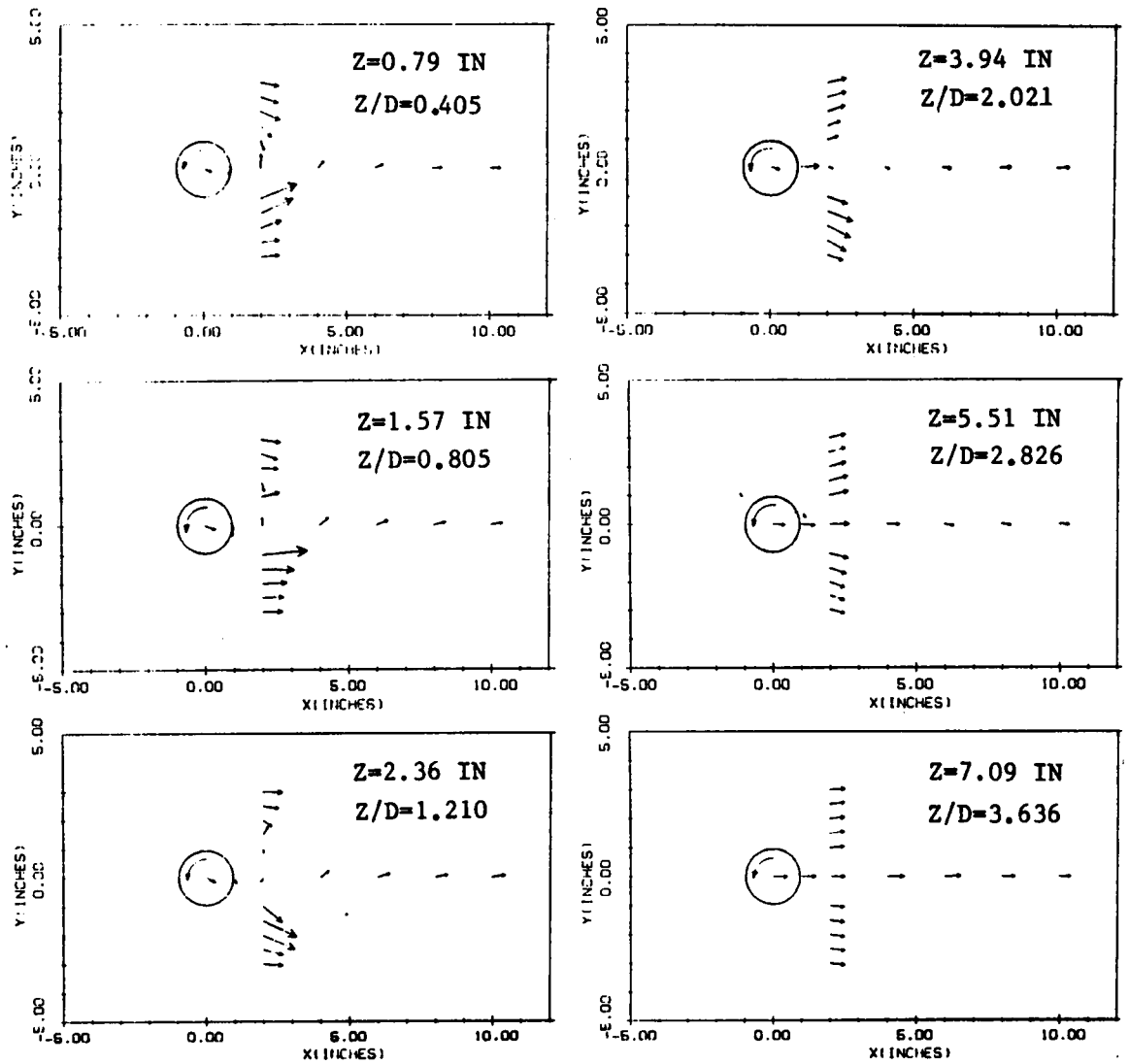

Figure 85. Mean flowfield, 90° circular jet, 58 % swirl, R = 4.0.: Z/D = const.

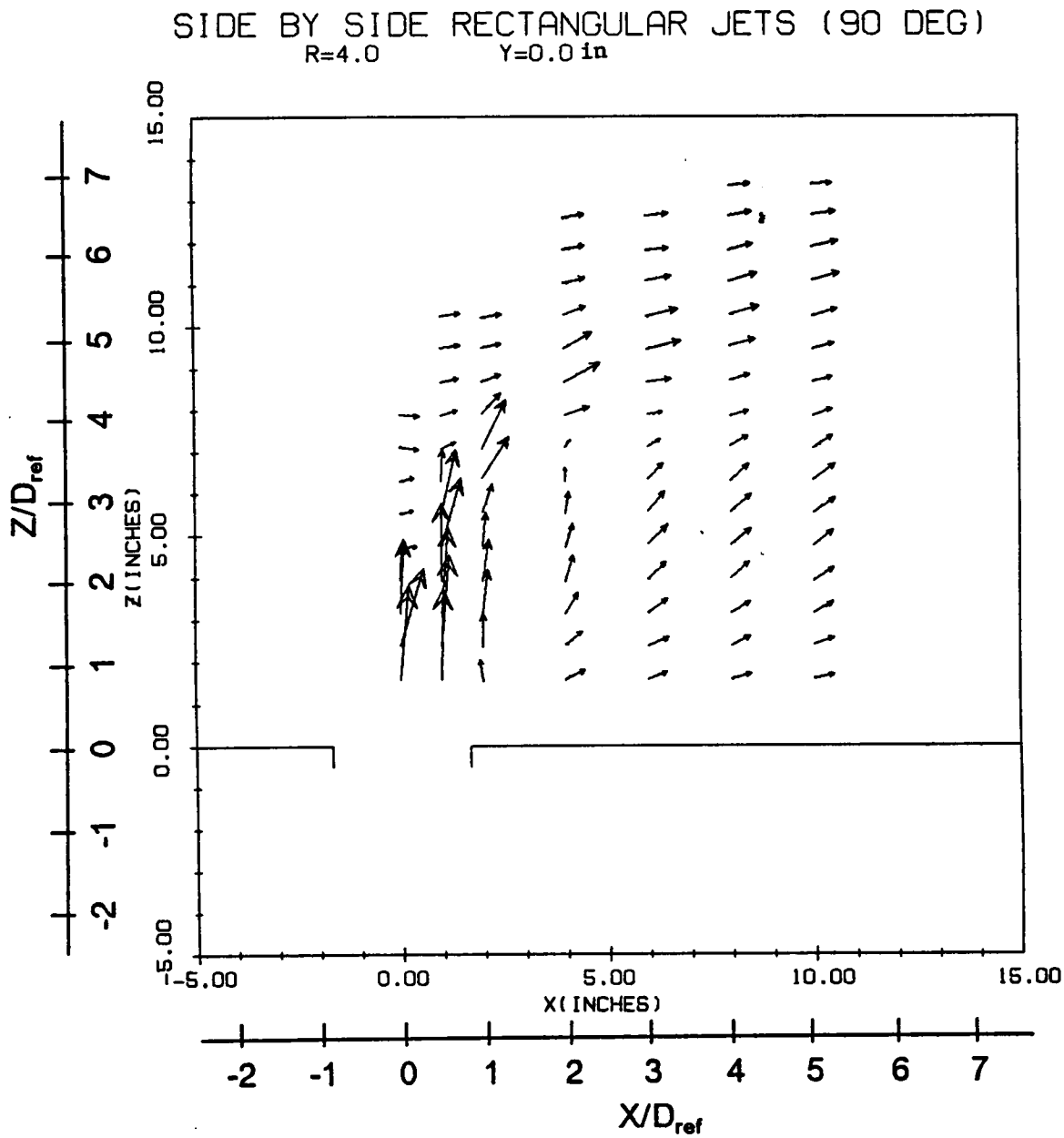

Figure 86. Mean flowfield, 90° side-by-side dual rectangular, R = 4.0.: $Y/D_{ref} = 0.0$.

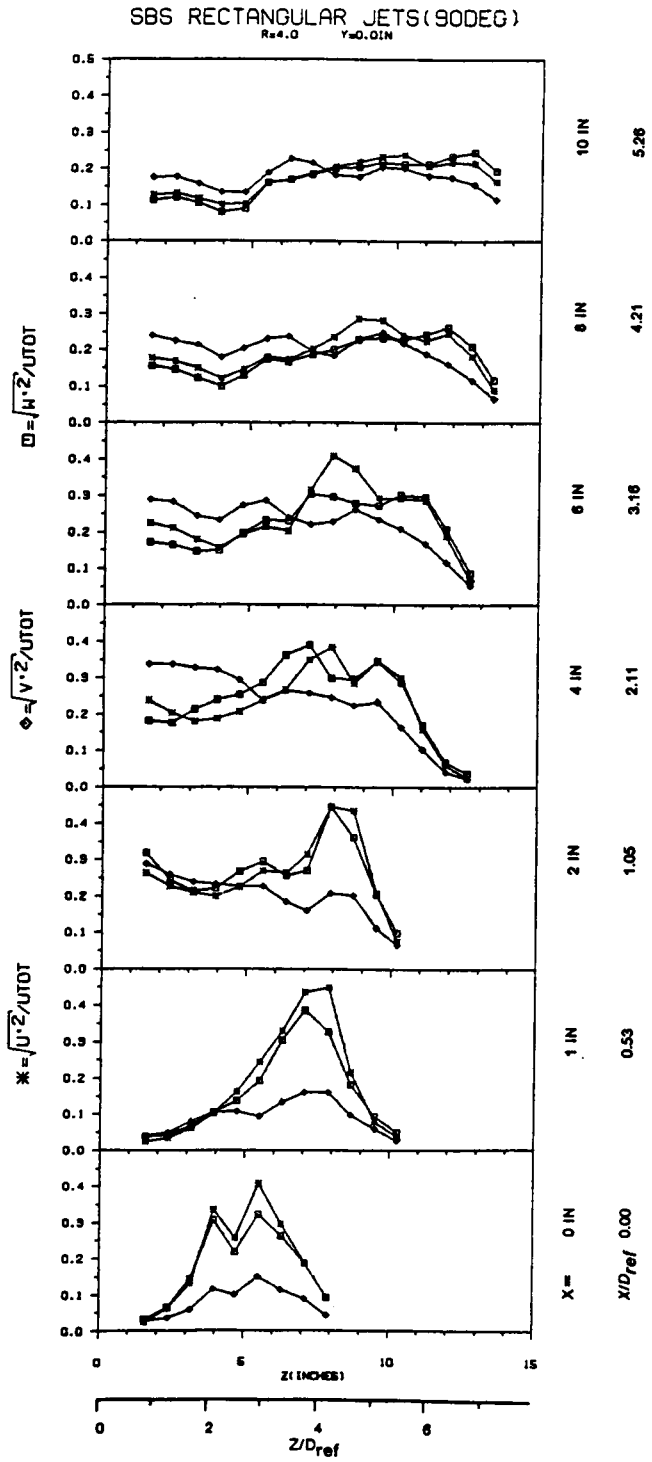

Figure 87. Turbulence, 90° side-by-side dual rectangular jets, R = 4.0.

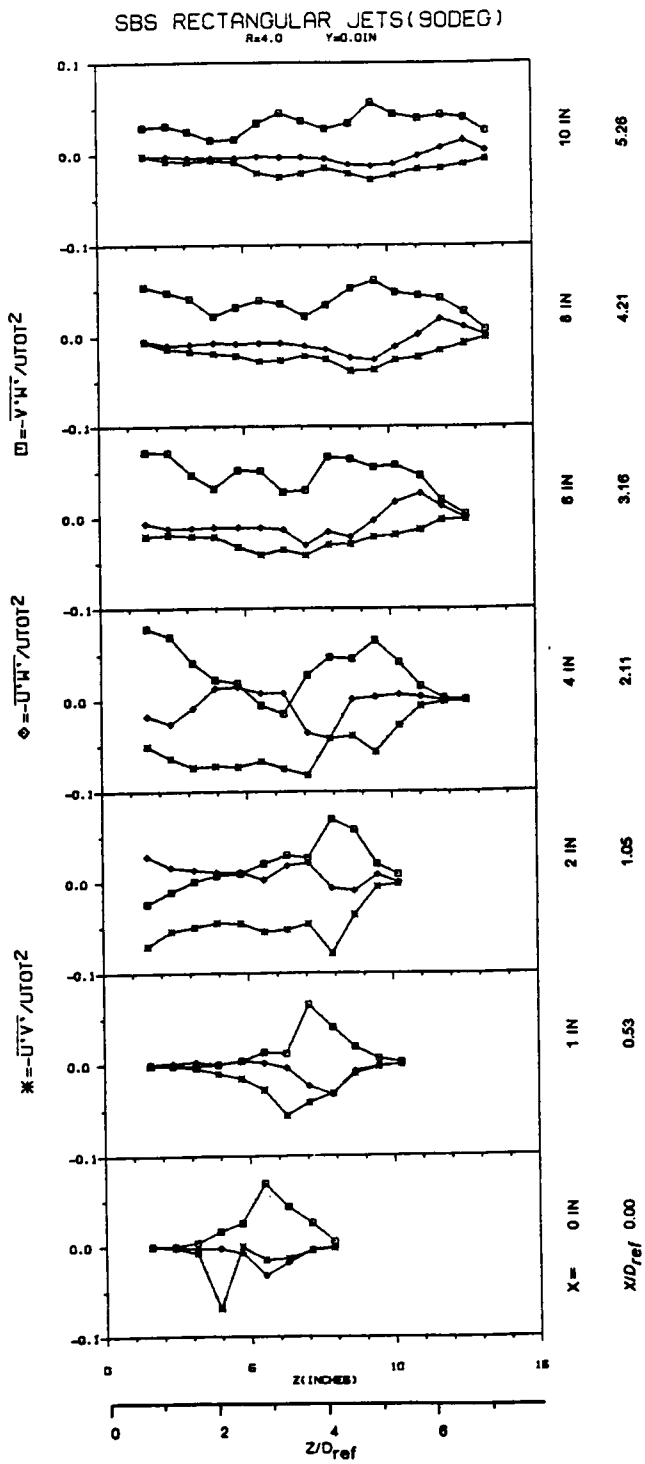

Figure 88. Turbulence, 90° side-by-side dual rectangular jets, R = 4.0.

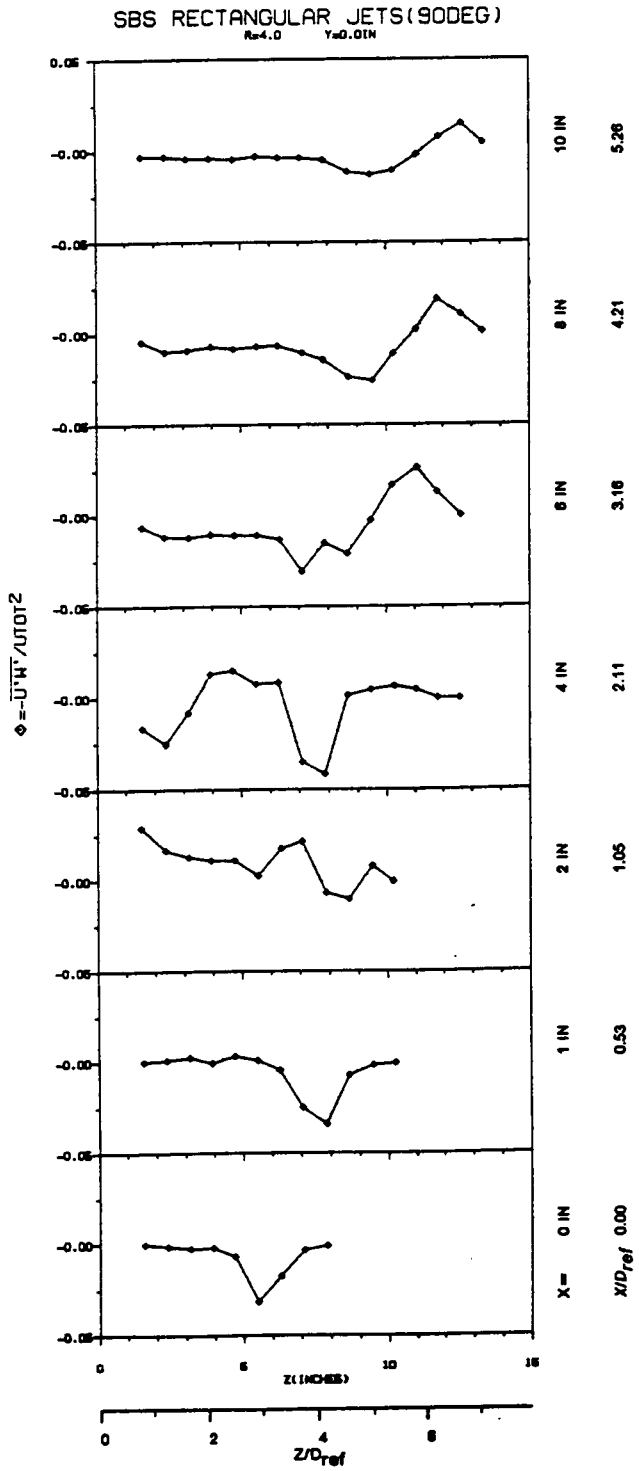

Figure 89. Turbulence, 90° side-by-side dual rectangular jets, R = 4.0.

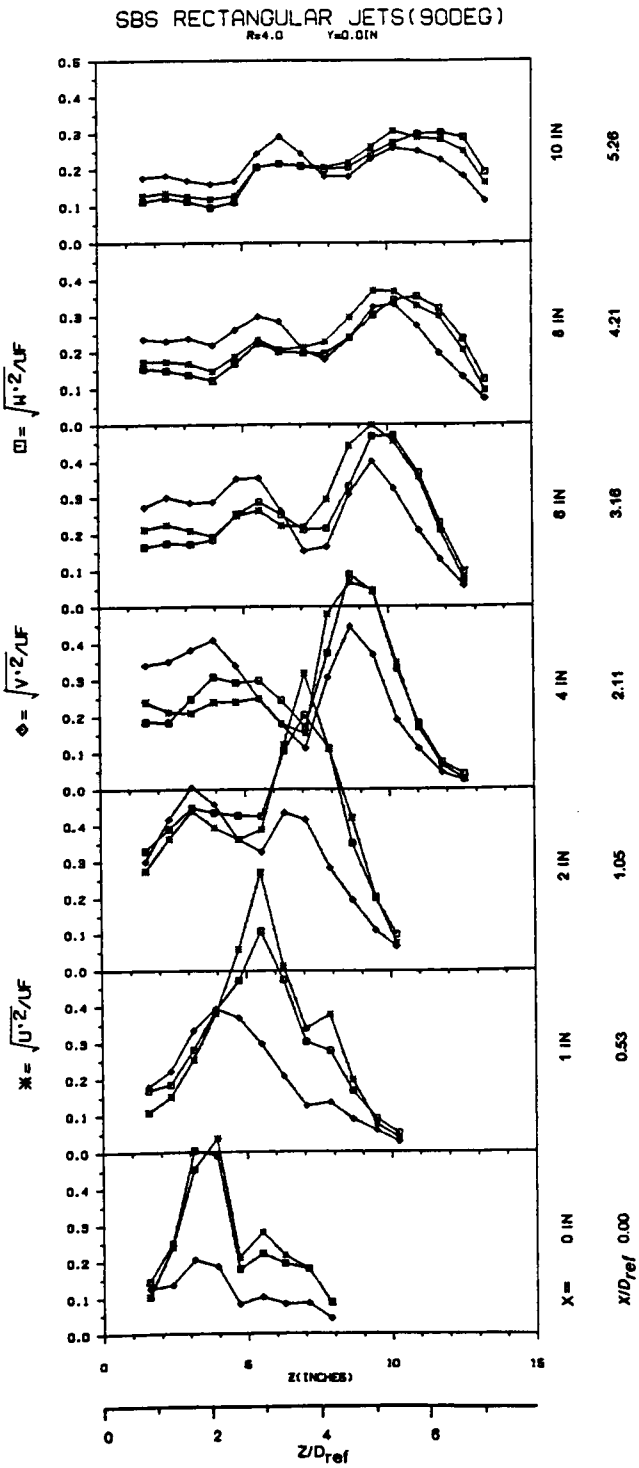

Figure 90. Turbulence, 90° side-by-side dual rectangular jets, R = 4.0.

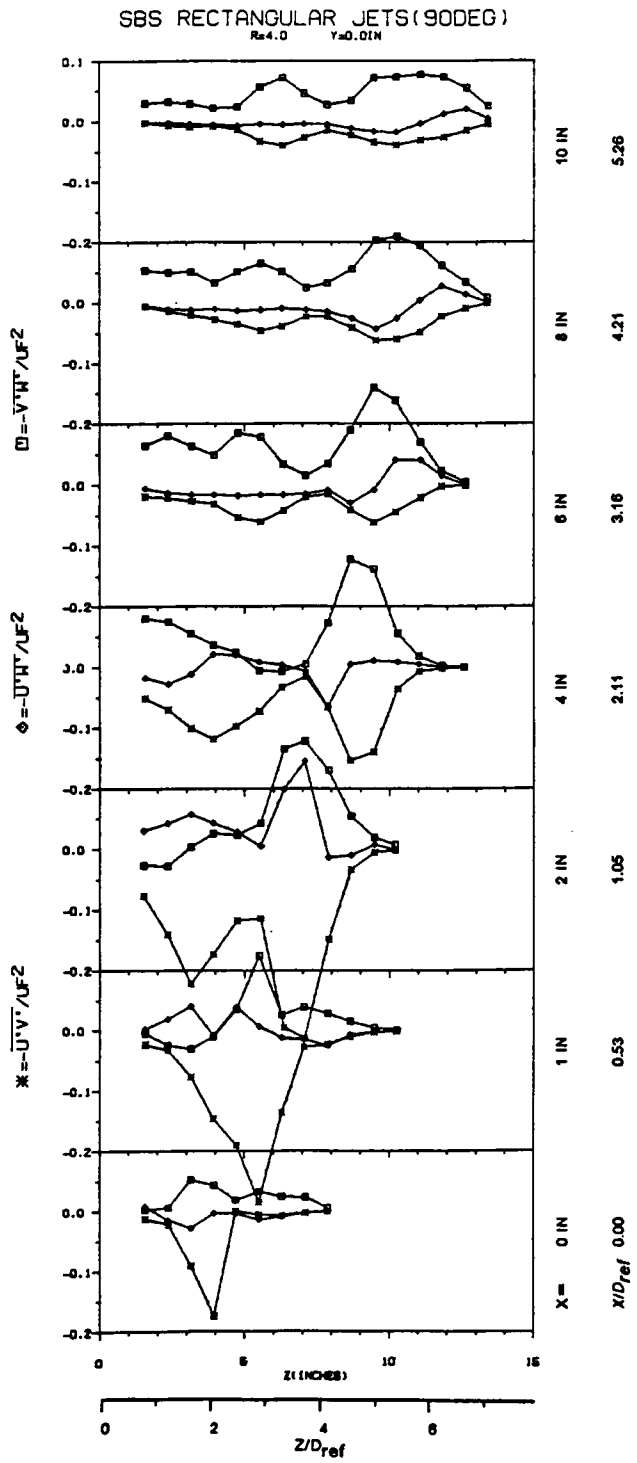

Figure 91. Turbulence, 90° side-by-side dual rectangular jets, R = 4.0.

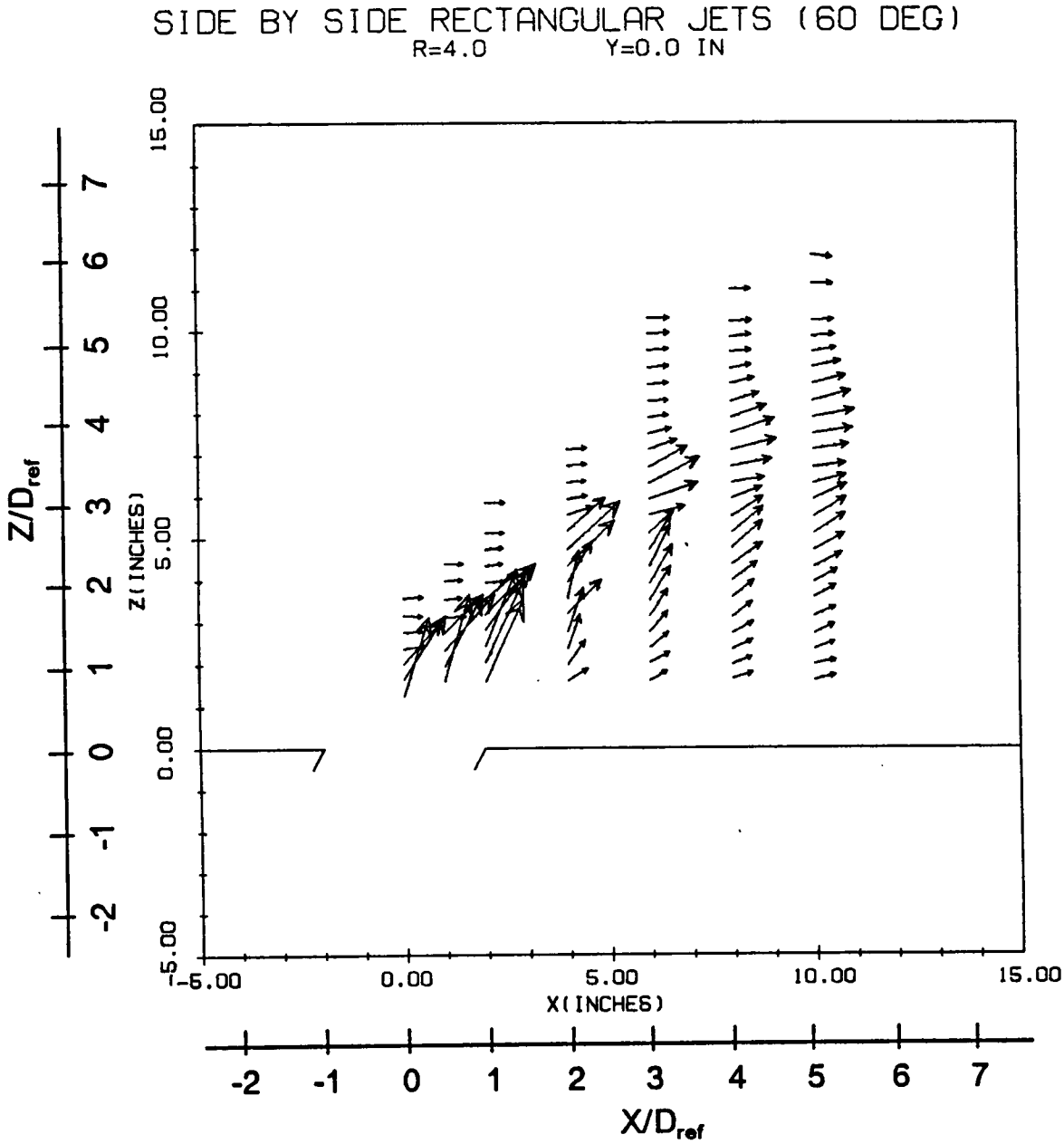

Figure 92. Mean flowfield, 60° side-by-side dual rectangular, R = 4.0.: $Y/D_{ref} = 0.0$.

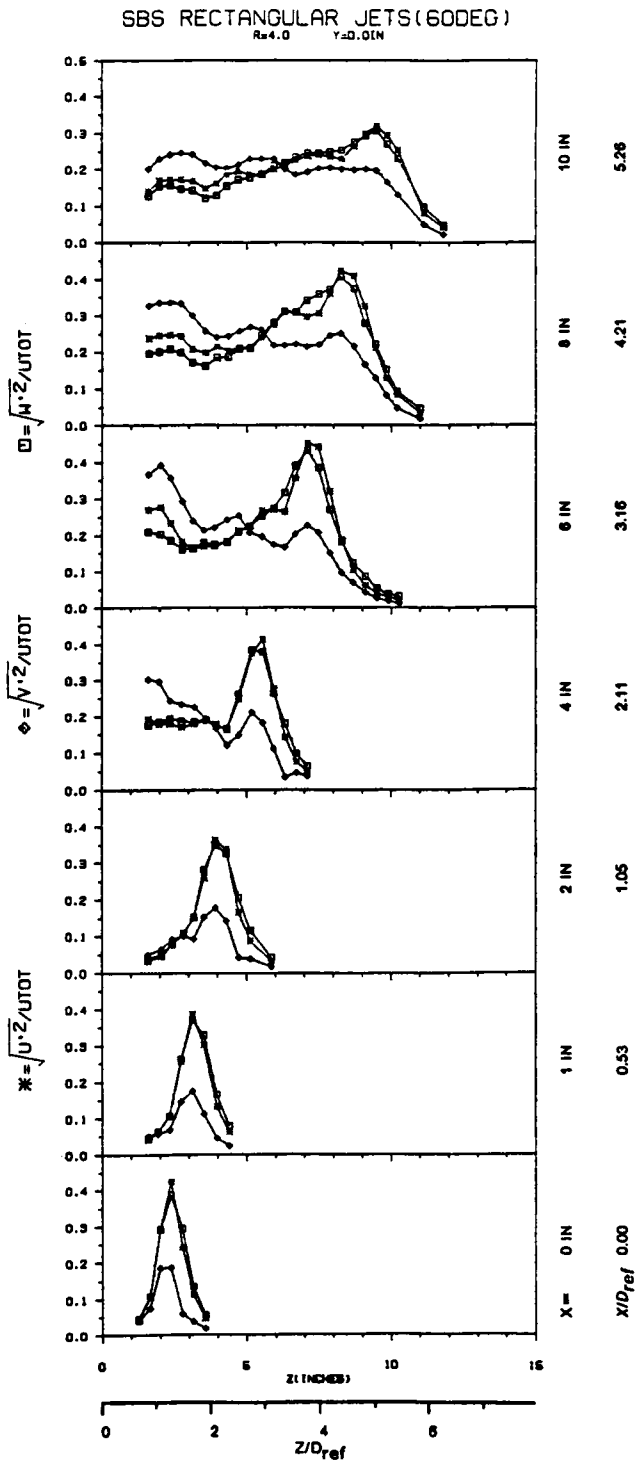

Figure 93. Turbulence, 60° side-by-side dual rectangular jets, R = 4.0.

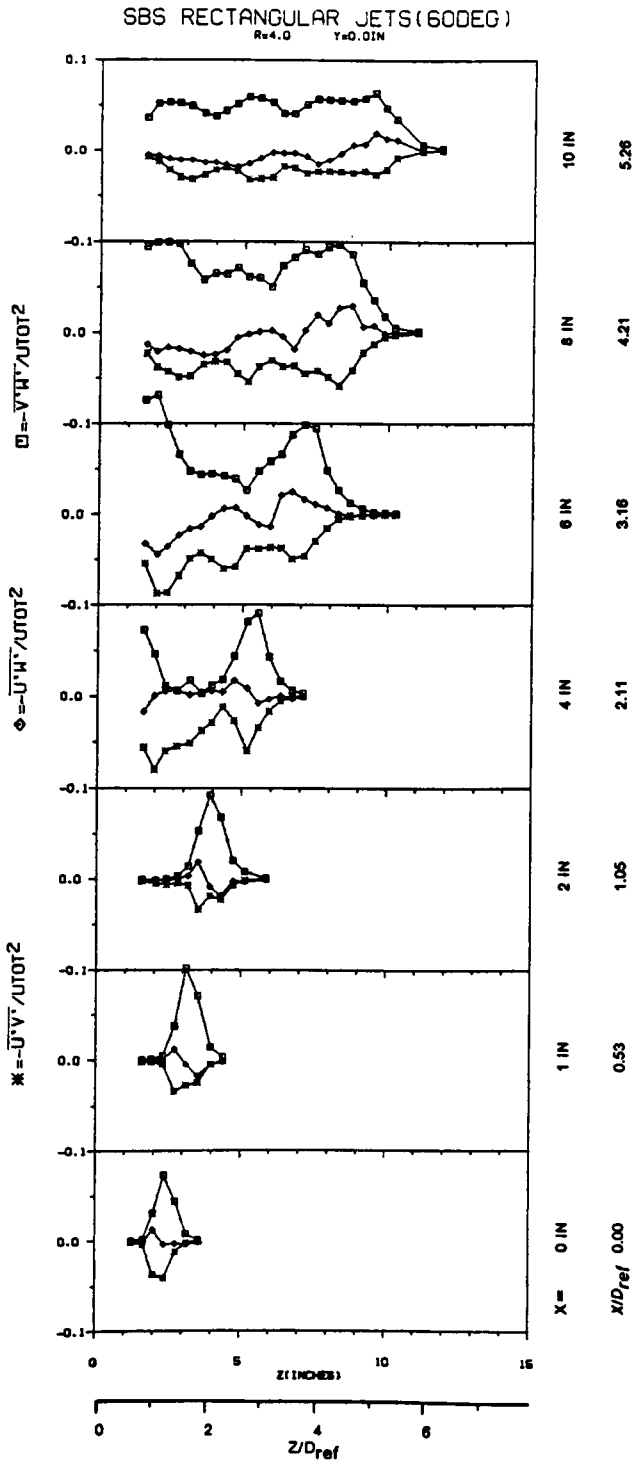

Figure 94. Turbulence, 60° side-by-side dual rectangular jets, R = 4.0.

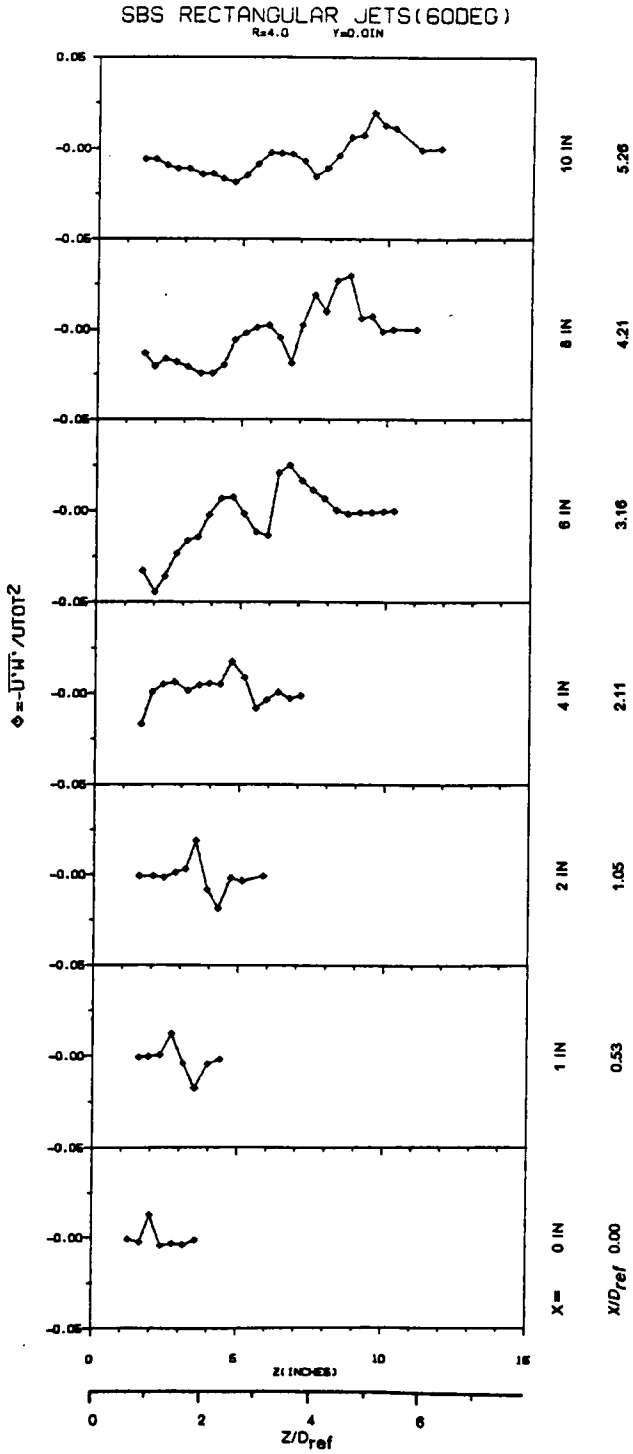

Figure 95. Turbulence, 60° side-by-side dual rectangular jets, R = 4.0.

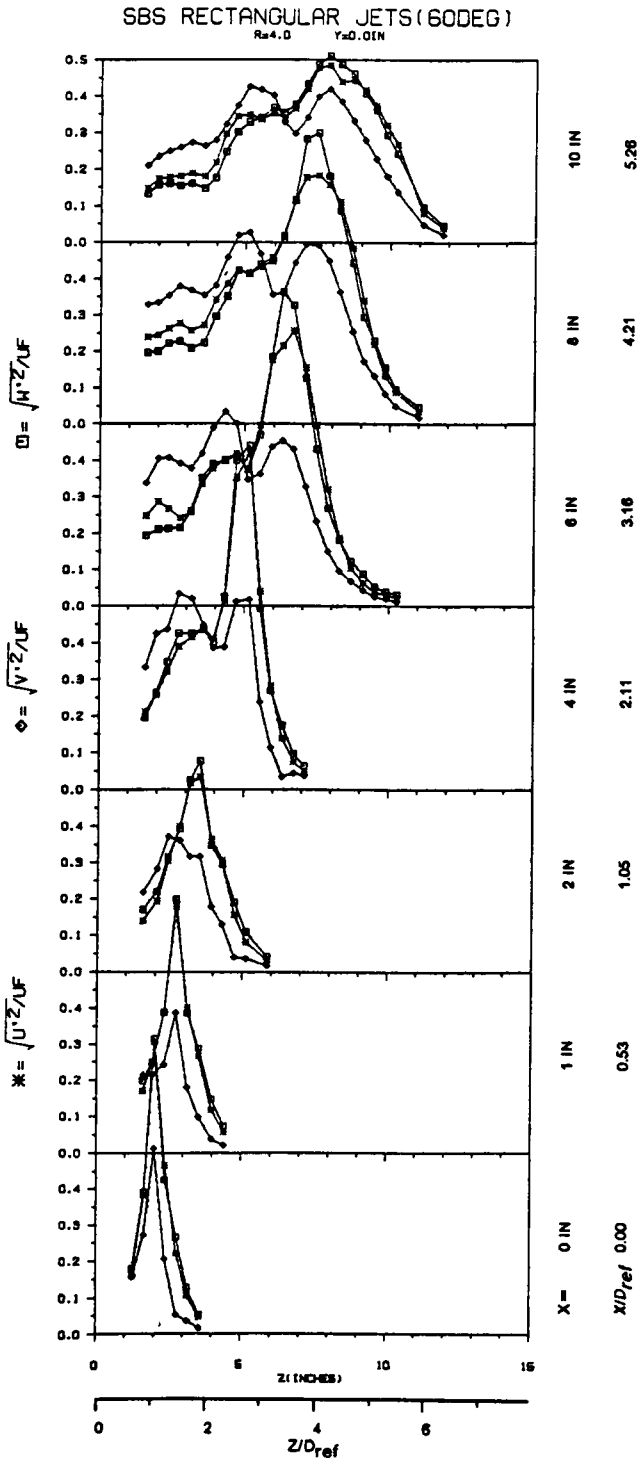

Figure 96. Turbulence, 60° side-by-side dual rectangular jets, R = 4.0.

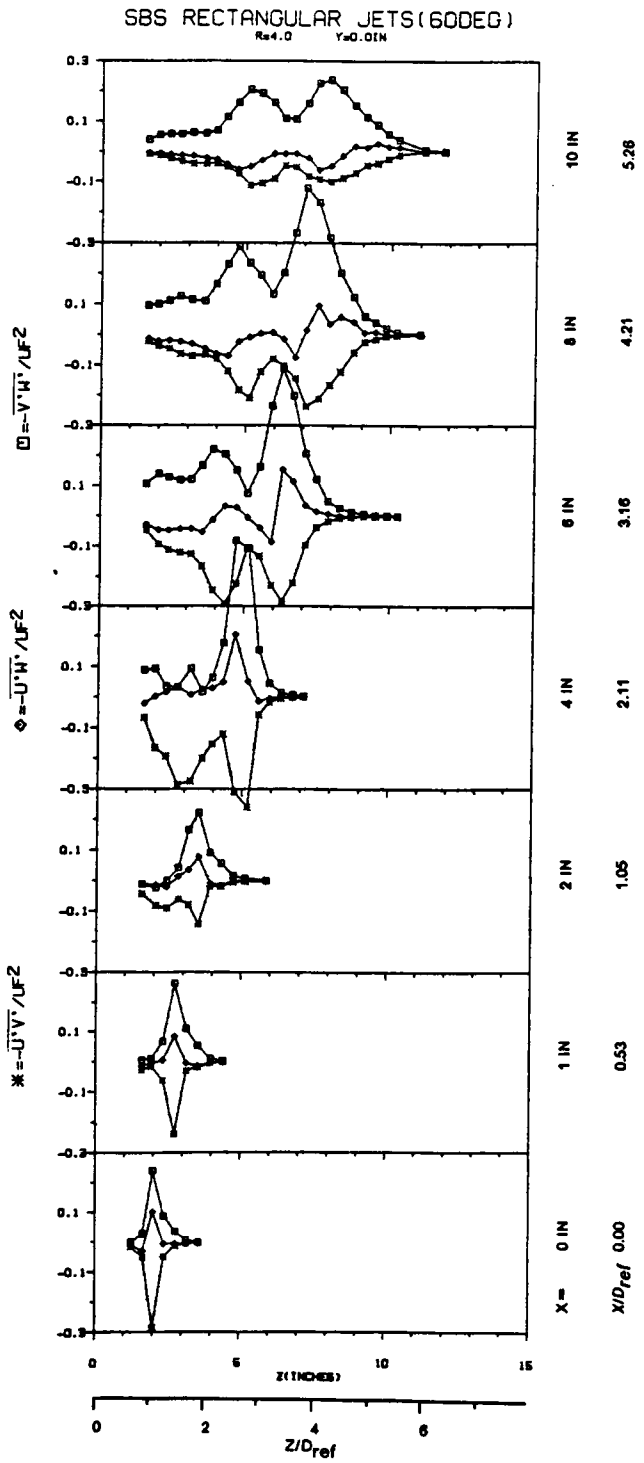

Figure 97. Turbulence, 60° side-by-side dual rectangular jets, R = 4.0.

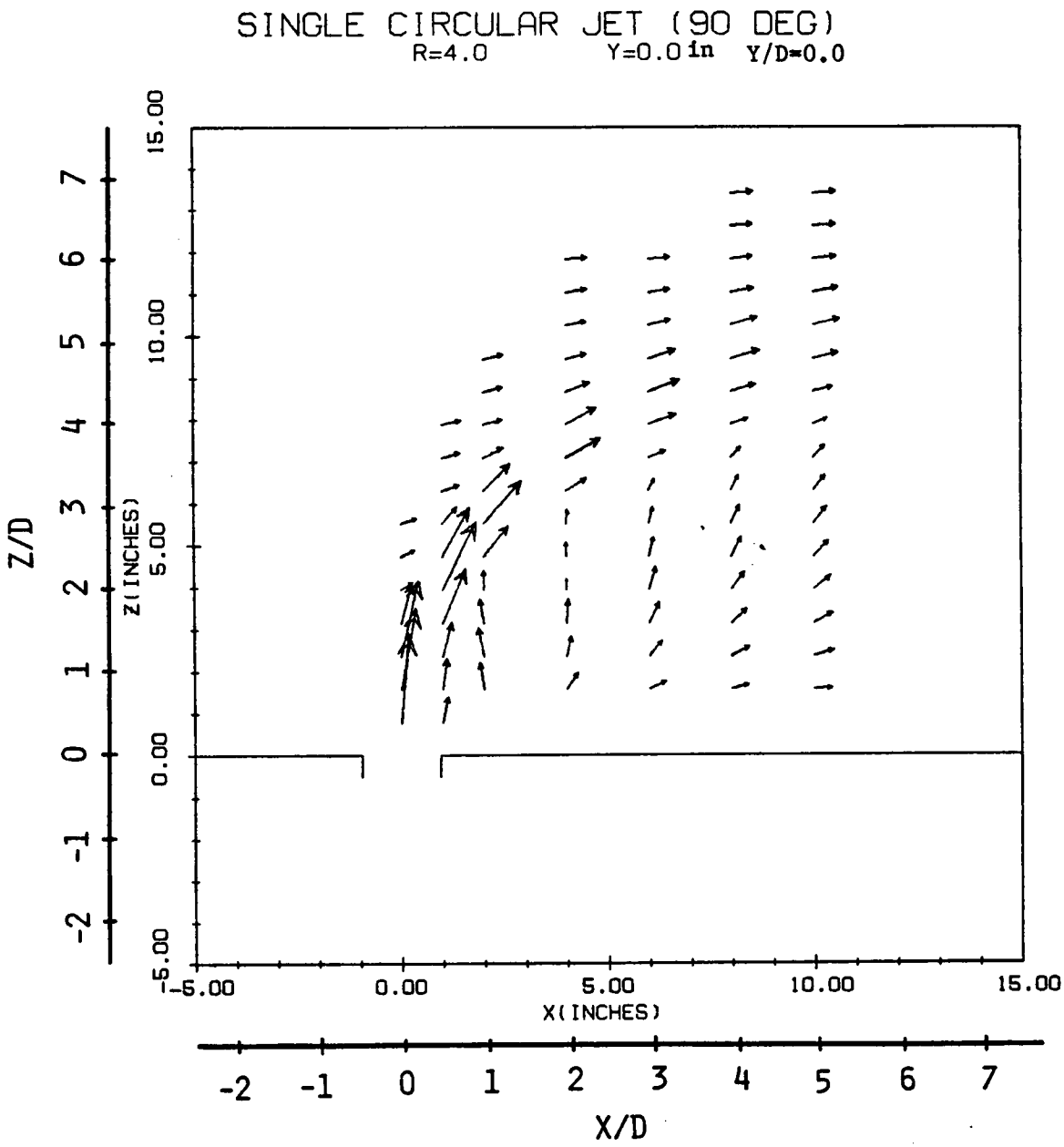

Figure 98. Mean flowfield, 90° circular jet, R = 4.0.: Y/D = 0.0.

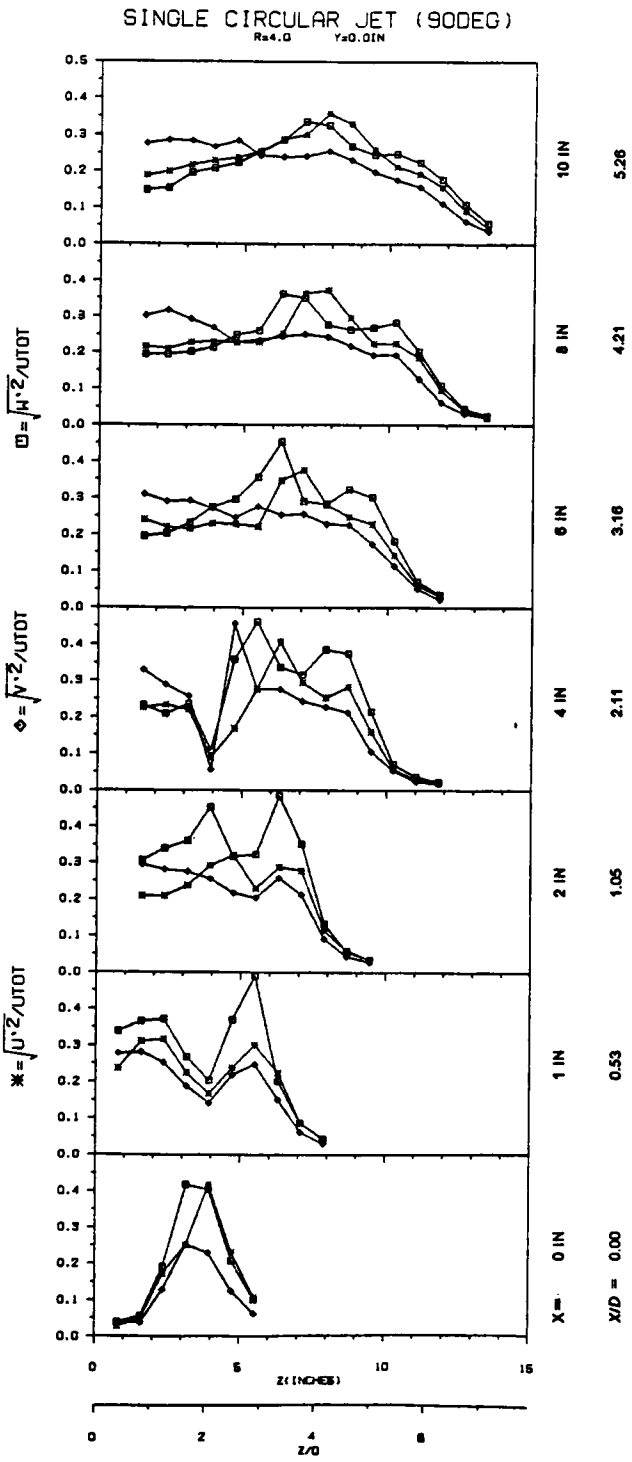

Figure 99. Turbulence, 90° circular jet, R = 4.0.

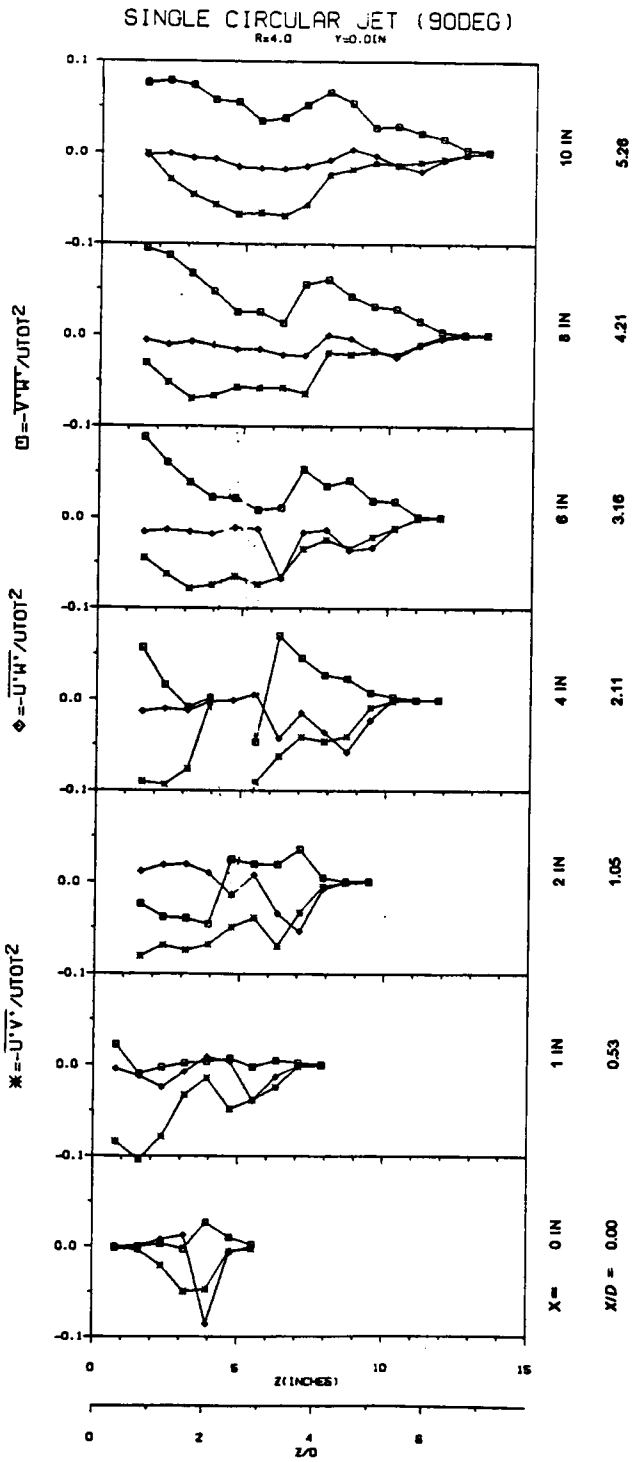

Figure 100. Turbulence, 90° circular jet, R = 4.0.

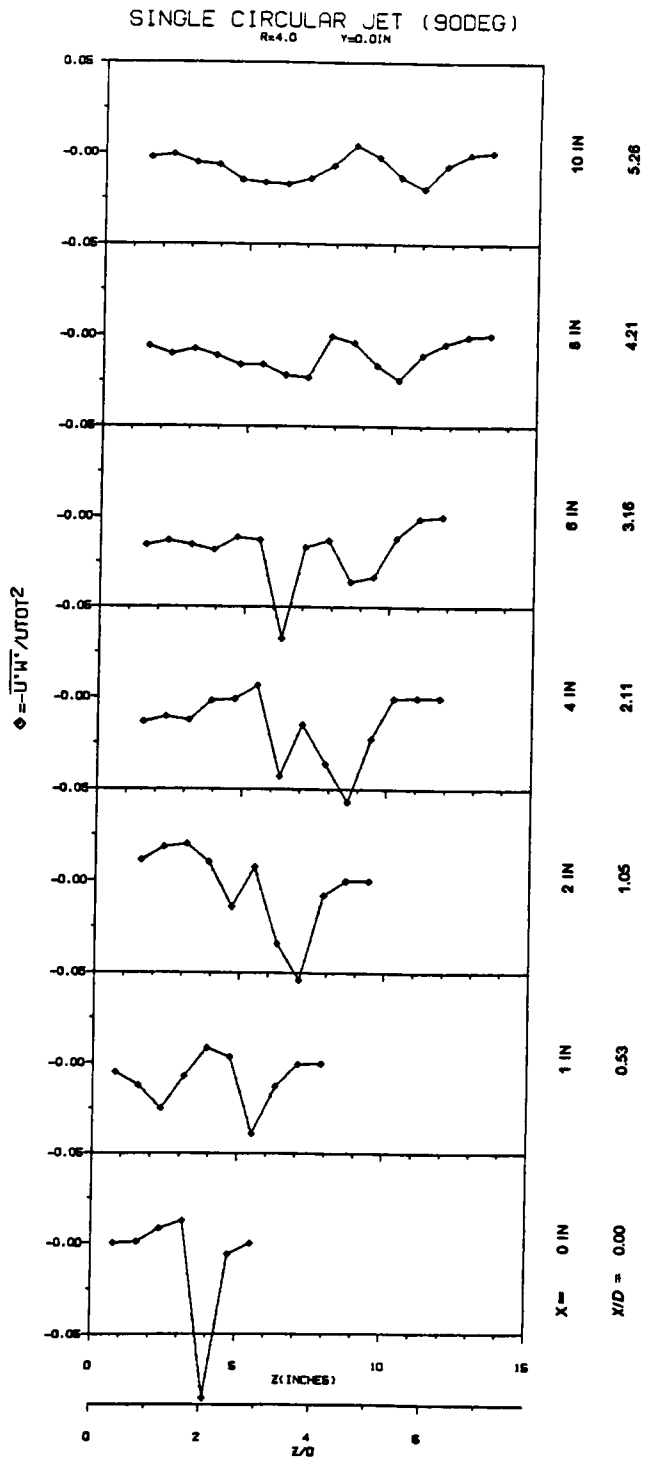

Figure 101. Turbulence, 90° circular jet, R = 4.0.

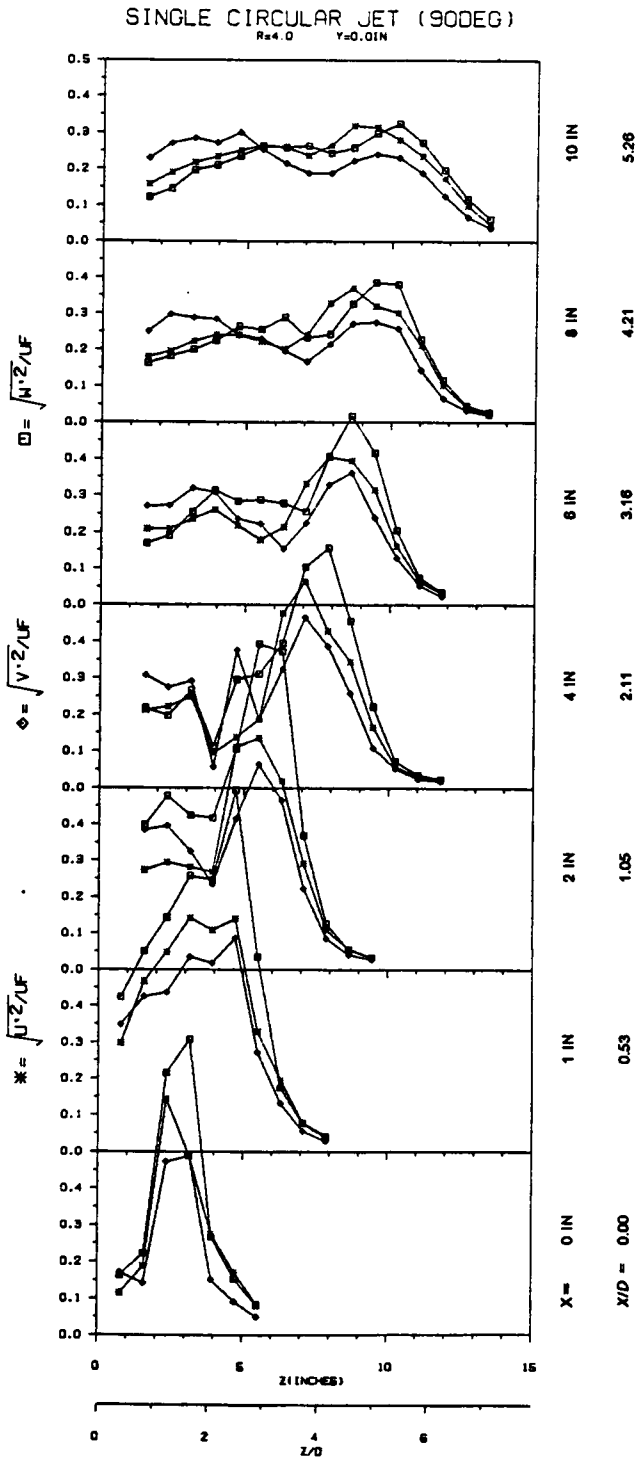

Figure 102. Turbulence, 90° circular jet, R = 4.0.

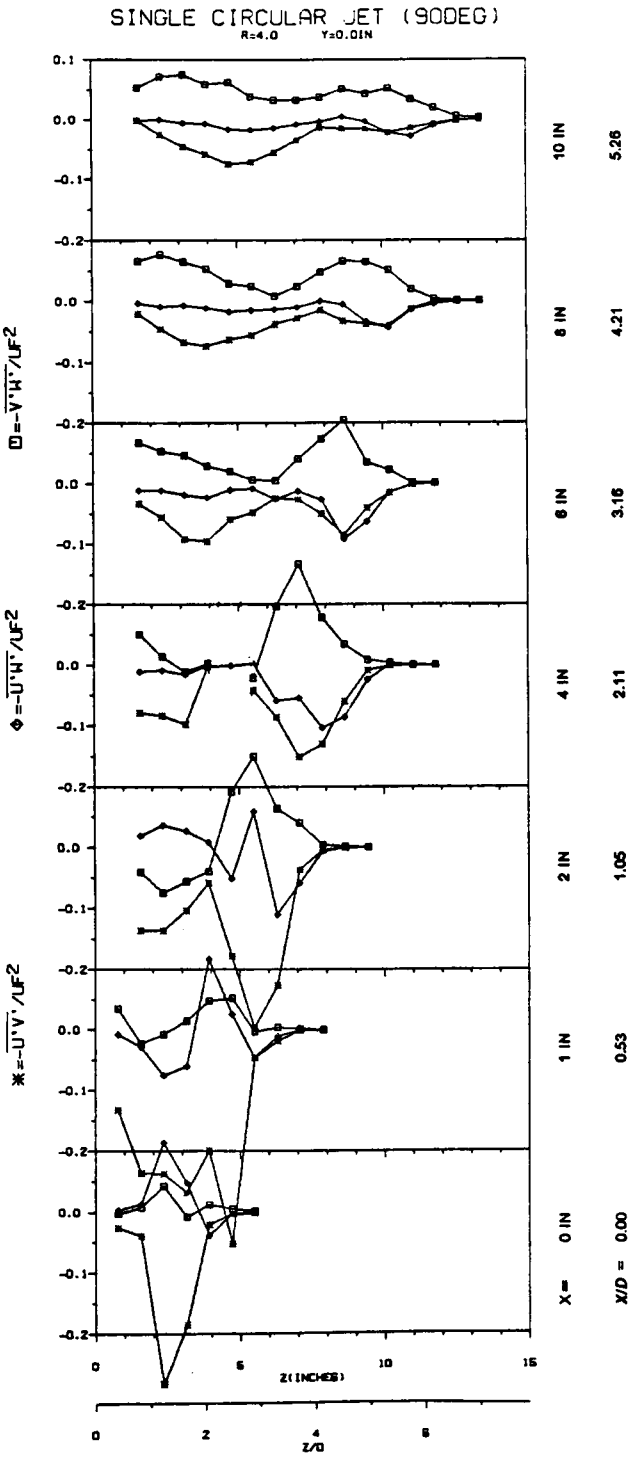

Figure 103. Turbulence, 90° circular jet, R = 4.0.

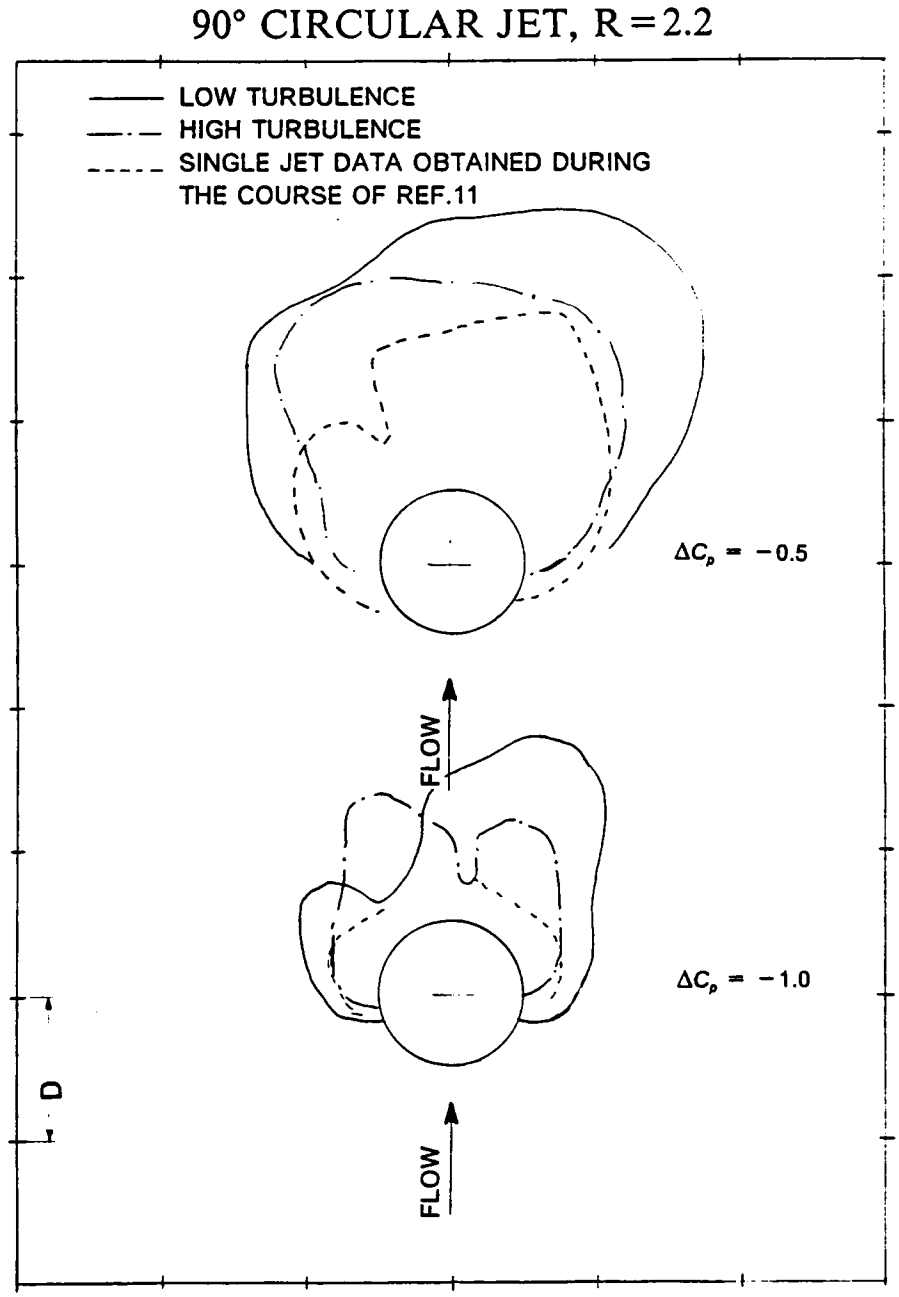

Figure 104. Surface pressures comparison with Ref.11, circular jet, R=2.2

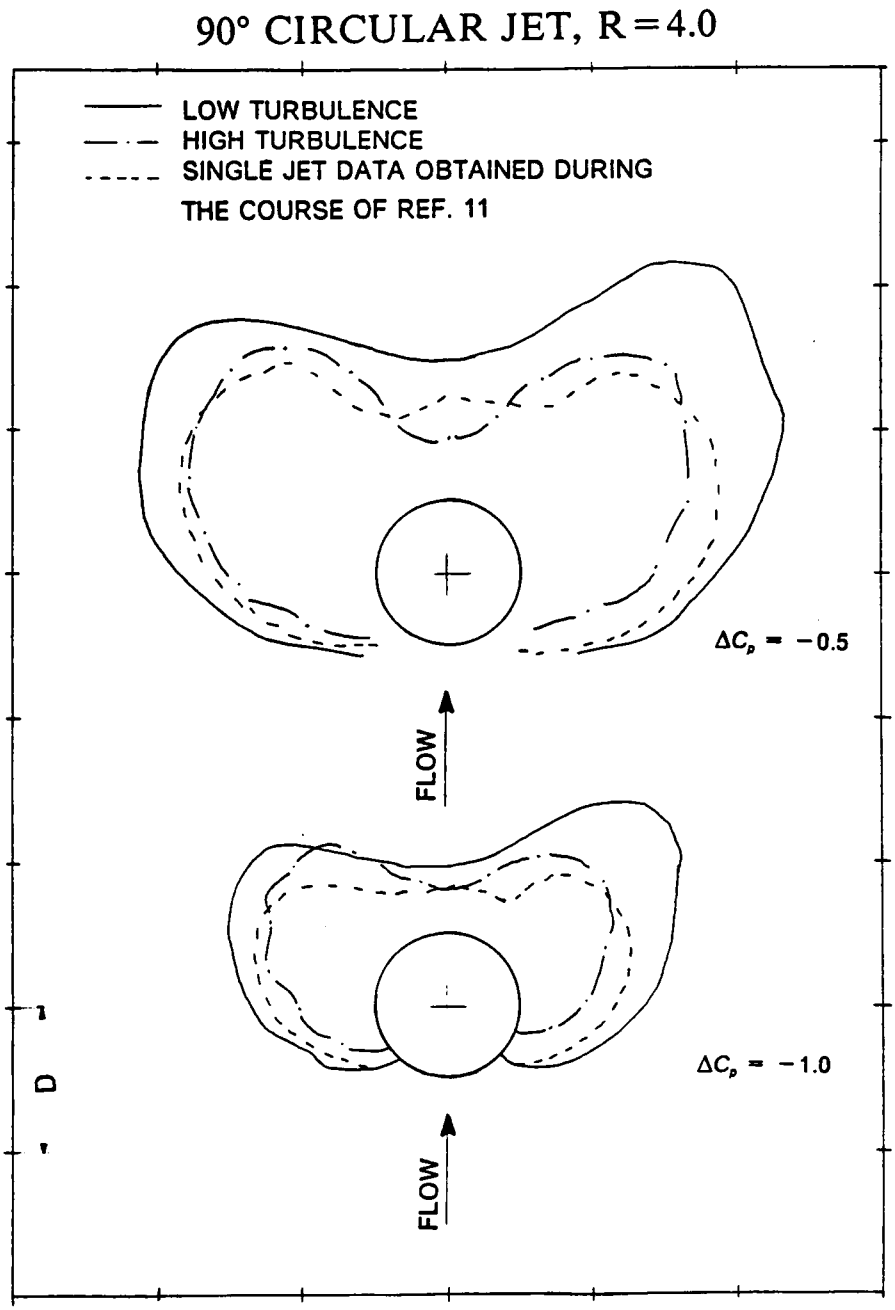

Figure 105. Surface pressures comparison with Ref.11, circular jet, R=4.0

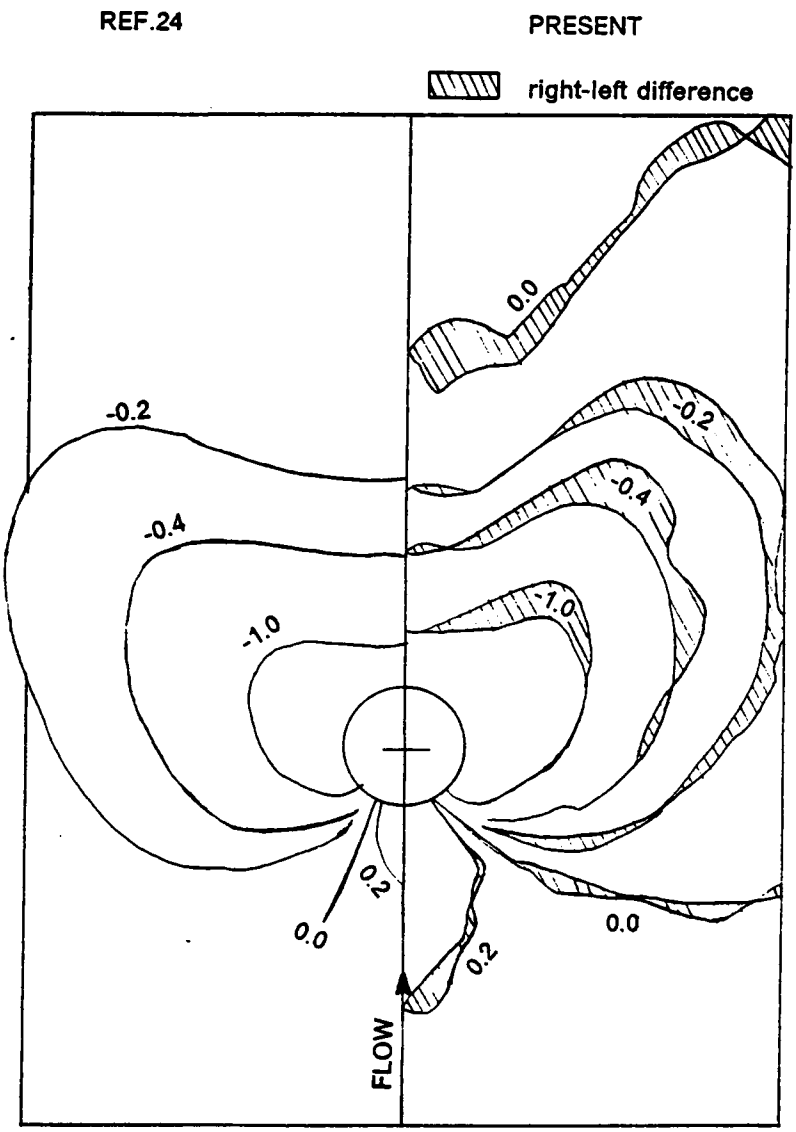

Figure 106. Surface pressures comparison with Ref.24, circular jet, R = 4.0

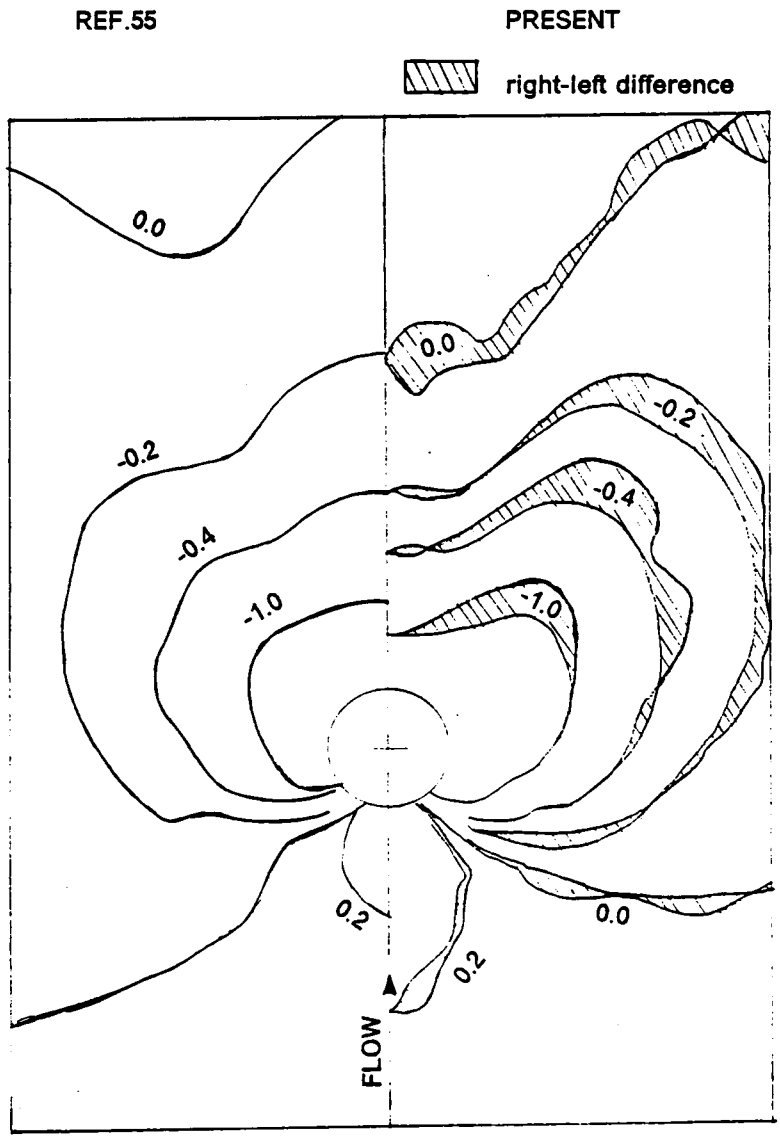

Figure 107. Surface pressures comparison with Ref.55, circular jet, R = 4.0

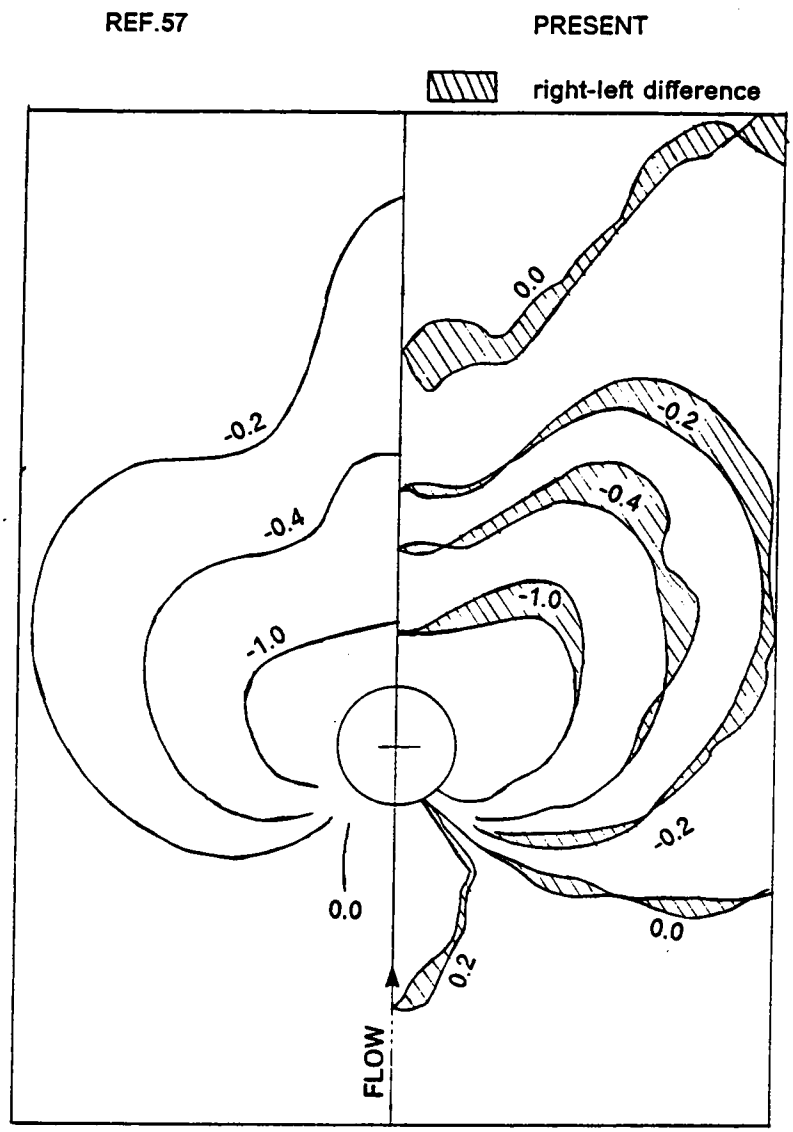

Figure 108. Surface pressures comparison with Ref.57, circular jet, R = 4.0

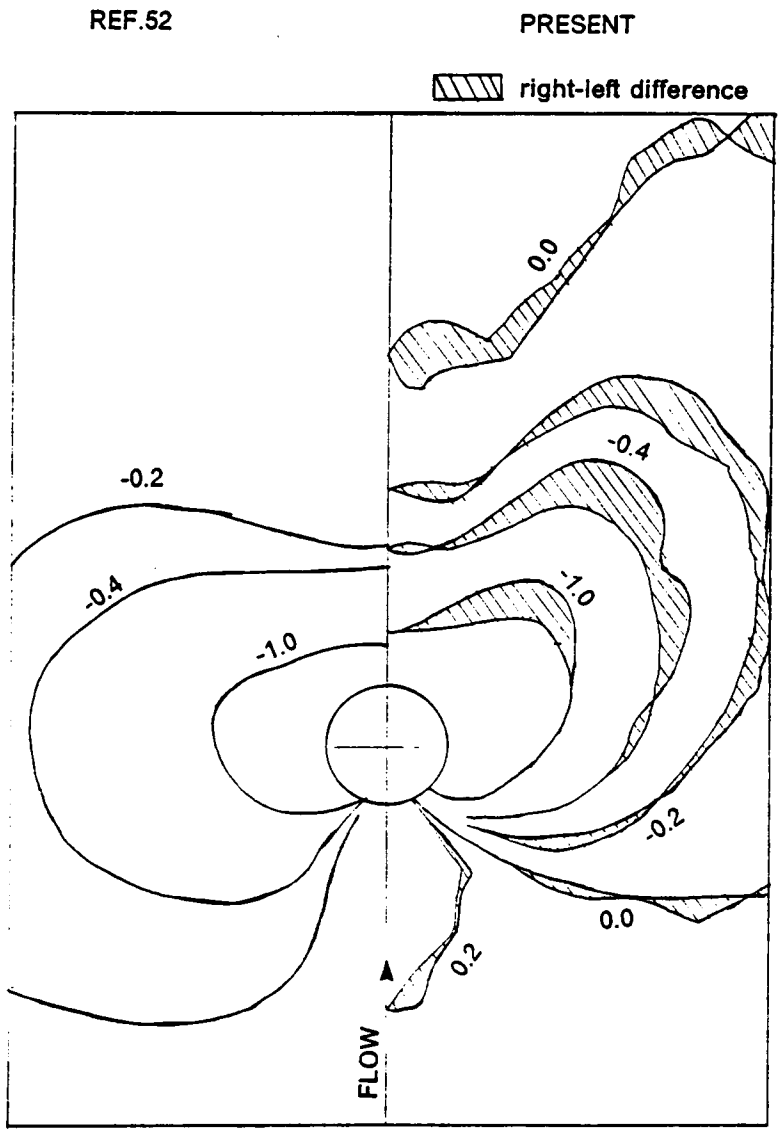

Figure 109. Surface pressures comparison with Ref.52, circular jet, R = 4.0

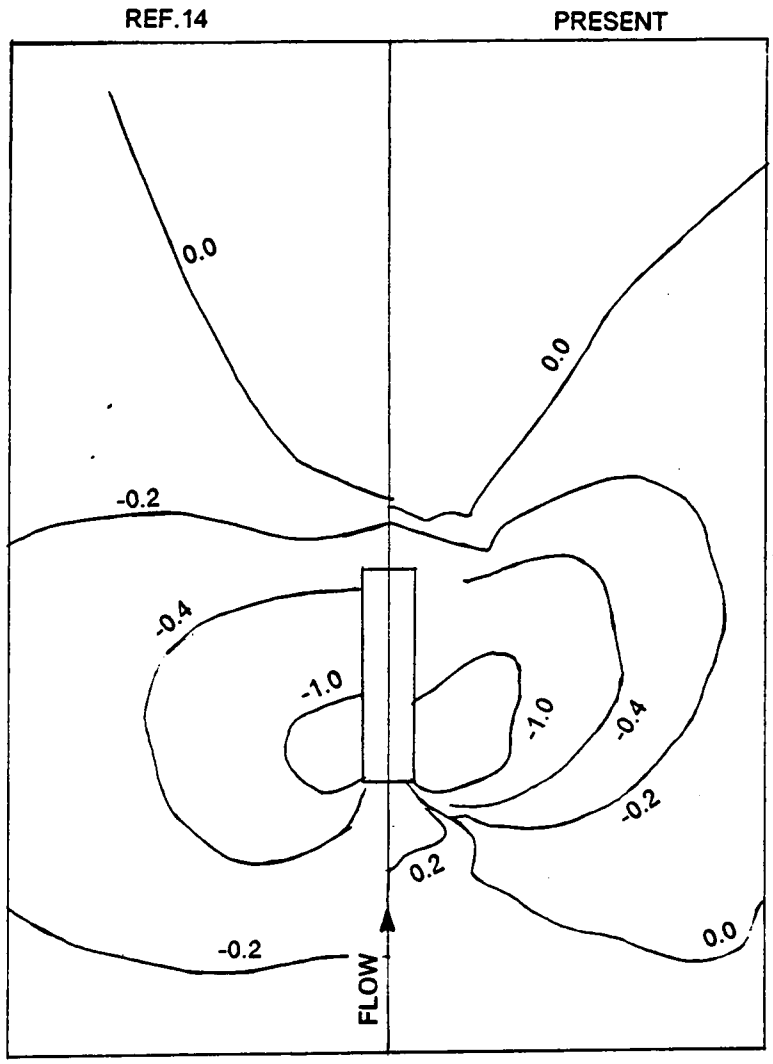

Figure 110. Surface pressures comparison with Ref.14, rectangular jet, R = 4.0.

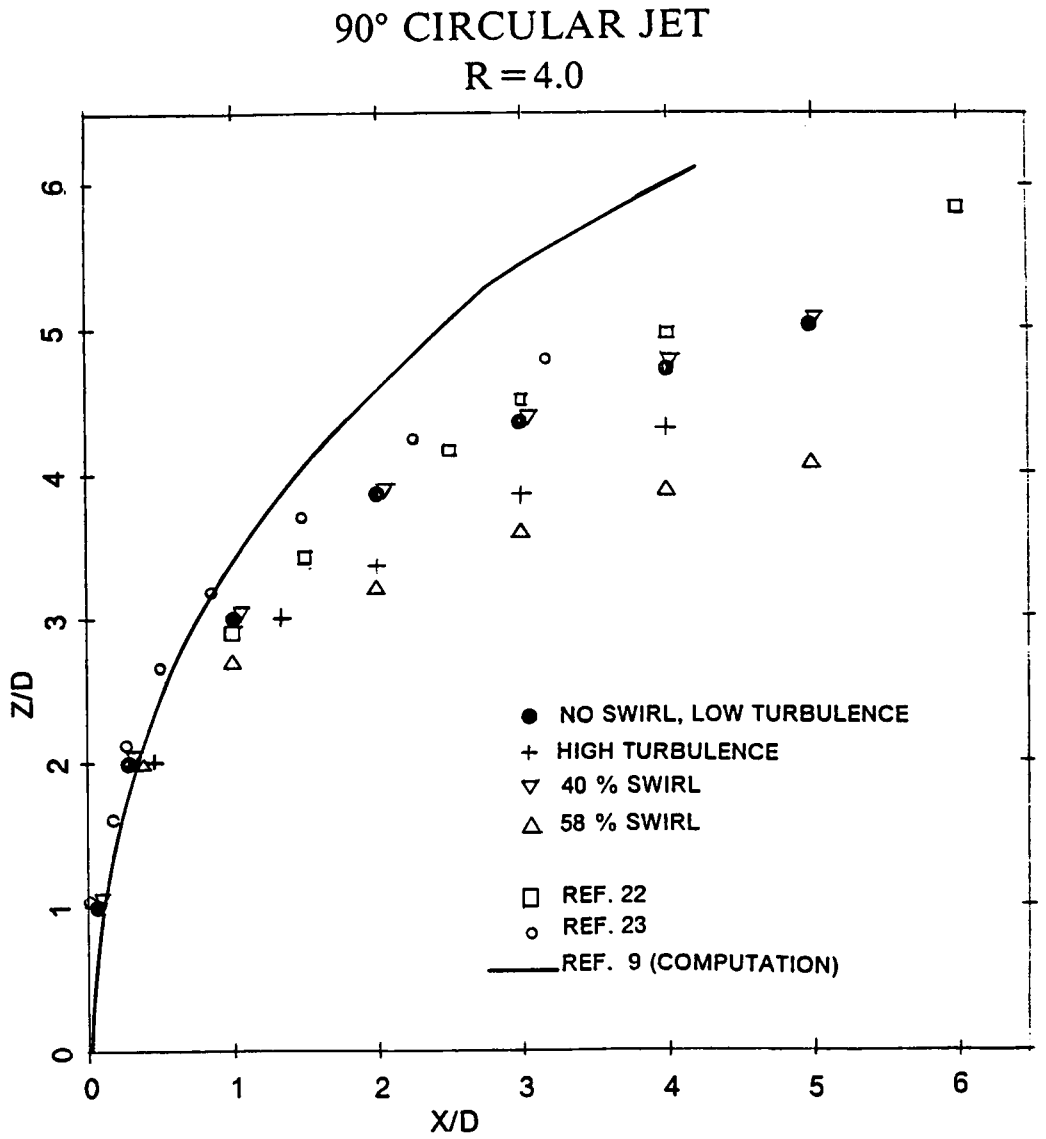

Figure 111. Trajectory comparisons with Refs.22, 23 and 9, circular jets, R = 4

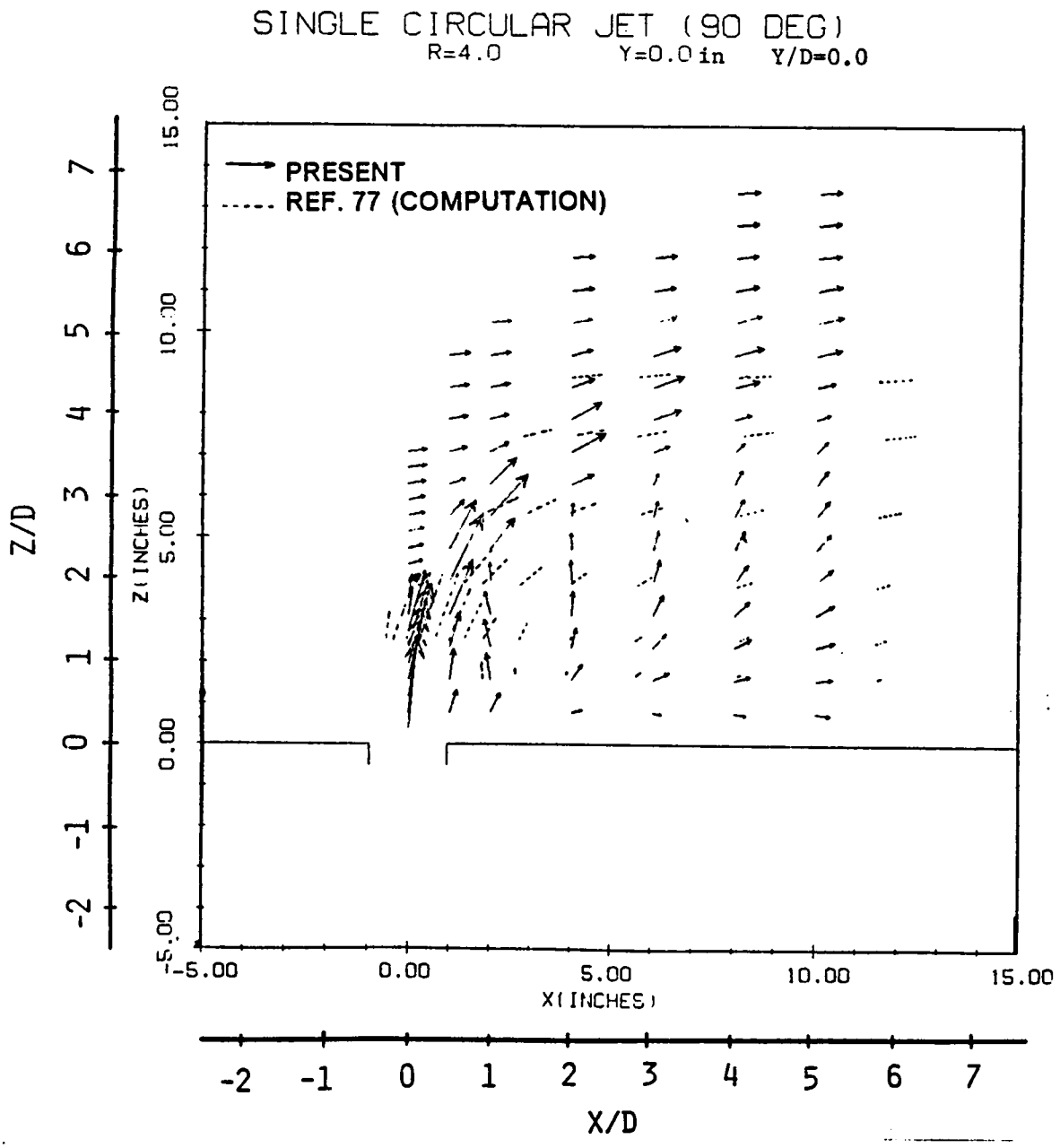

Figure 112. Mean flowfield comparison with Ref.77, circular jet, R = 4.0.

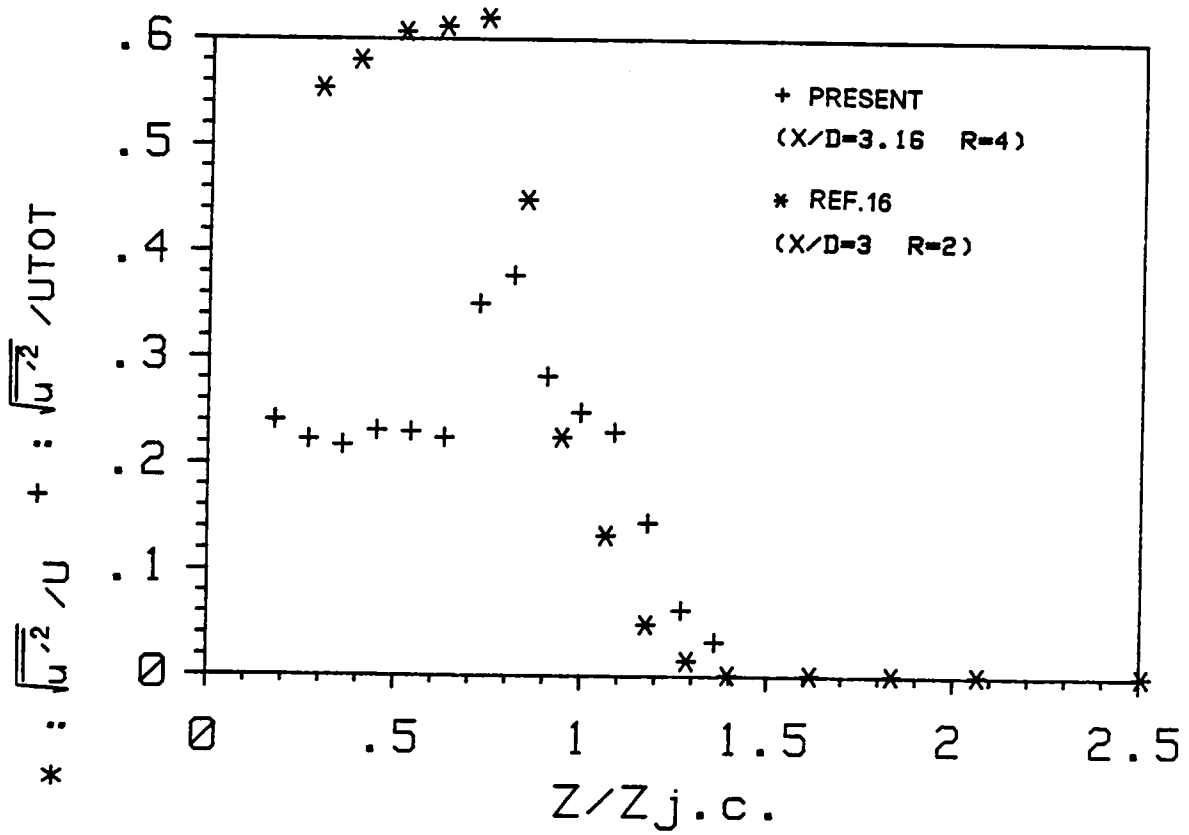

Figure 113. Turbulence comparison with Ref.16, circular jet.

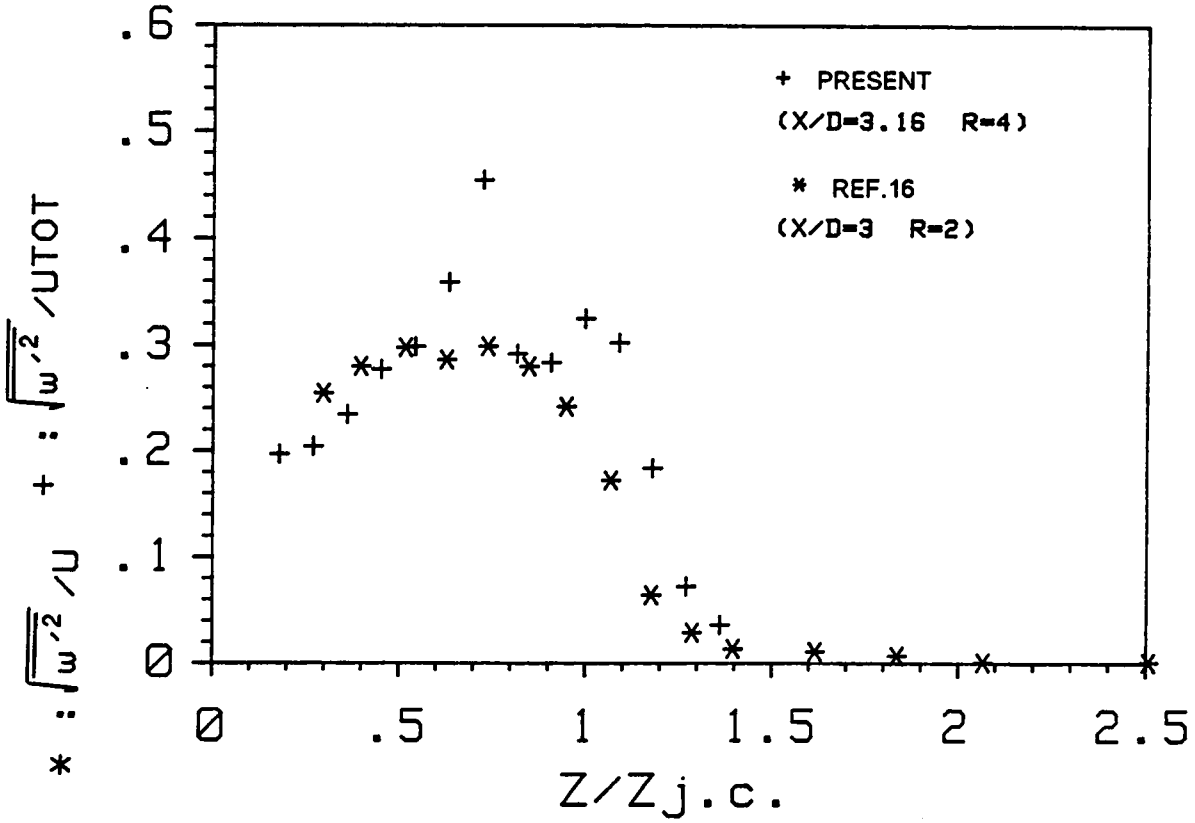

Figure 114. Turbulence comparison with Ref.16, circular jet.

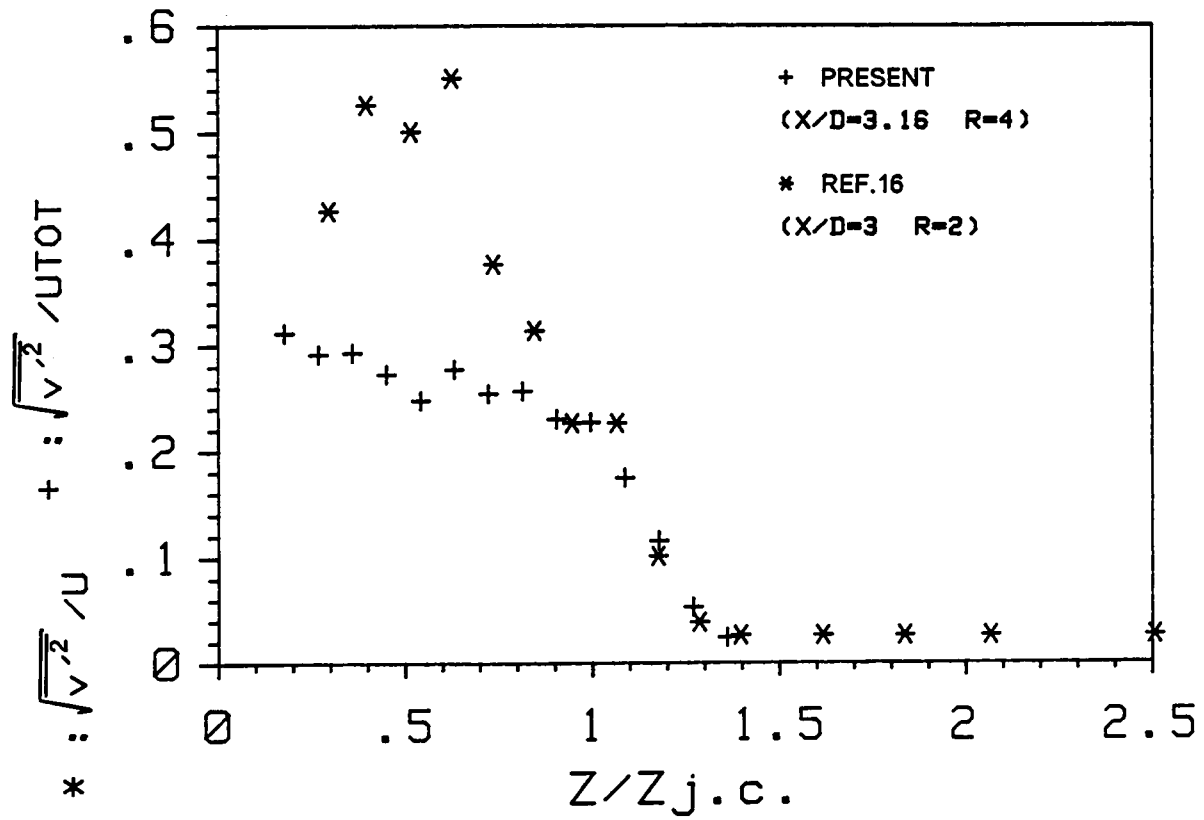

Figure 115. Turbulence comparison with Ref.16, circular jet.

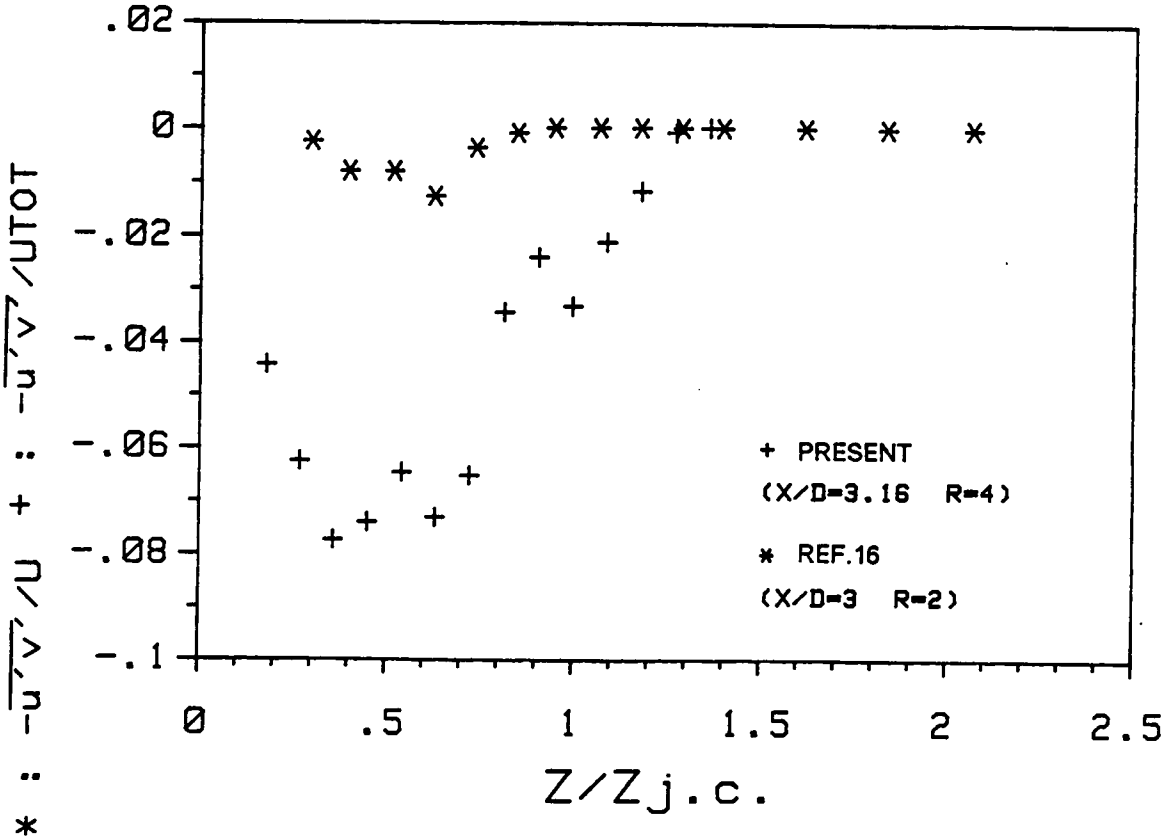

Figure 116. Turbulence comparison with Ref.16, circular jet.

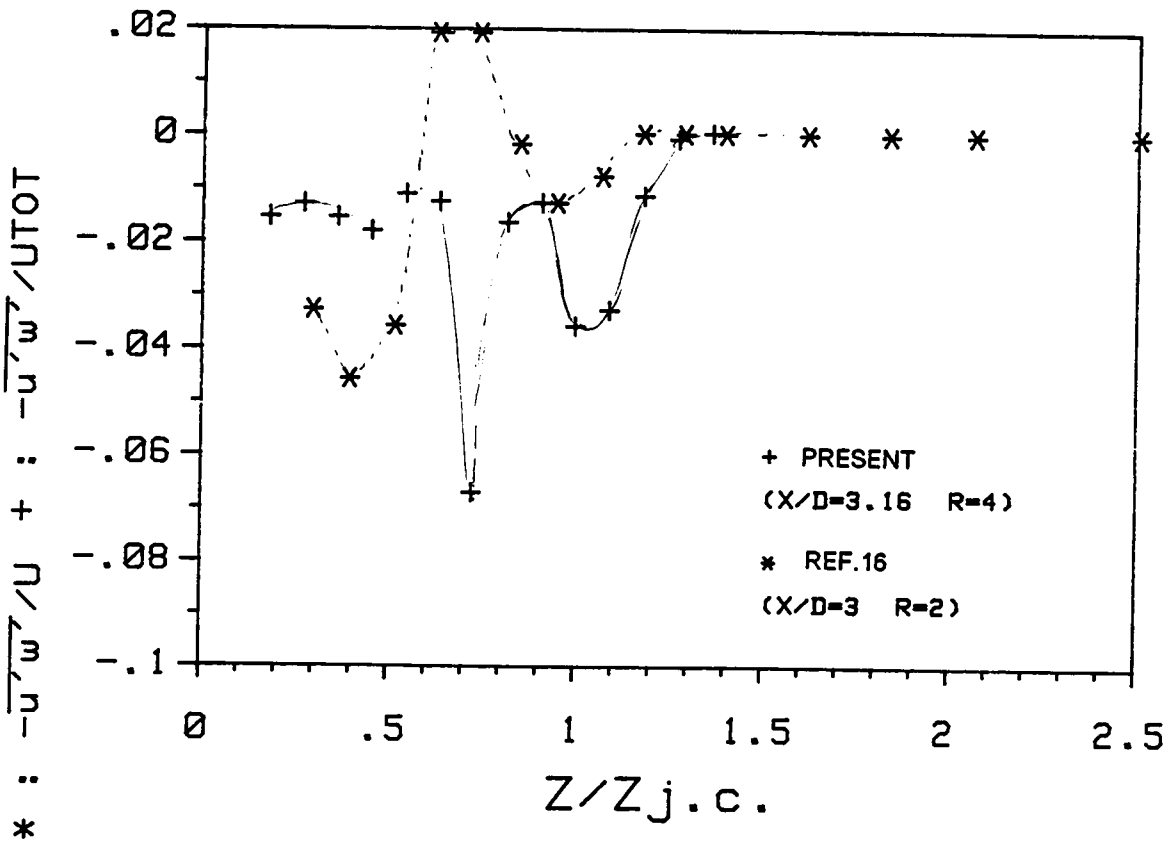

Figure 117. Turbulence comparison with Ref.16, circular jet.

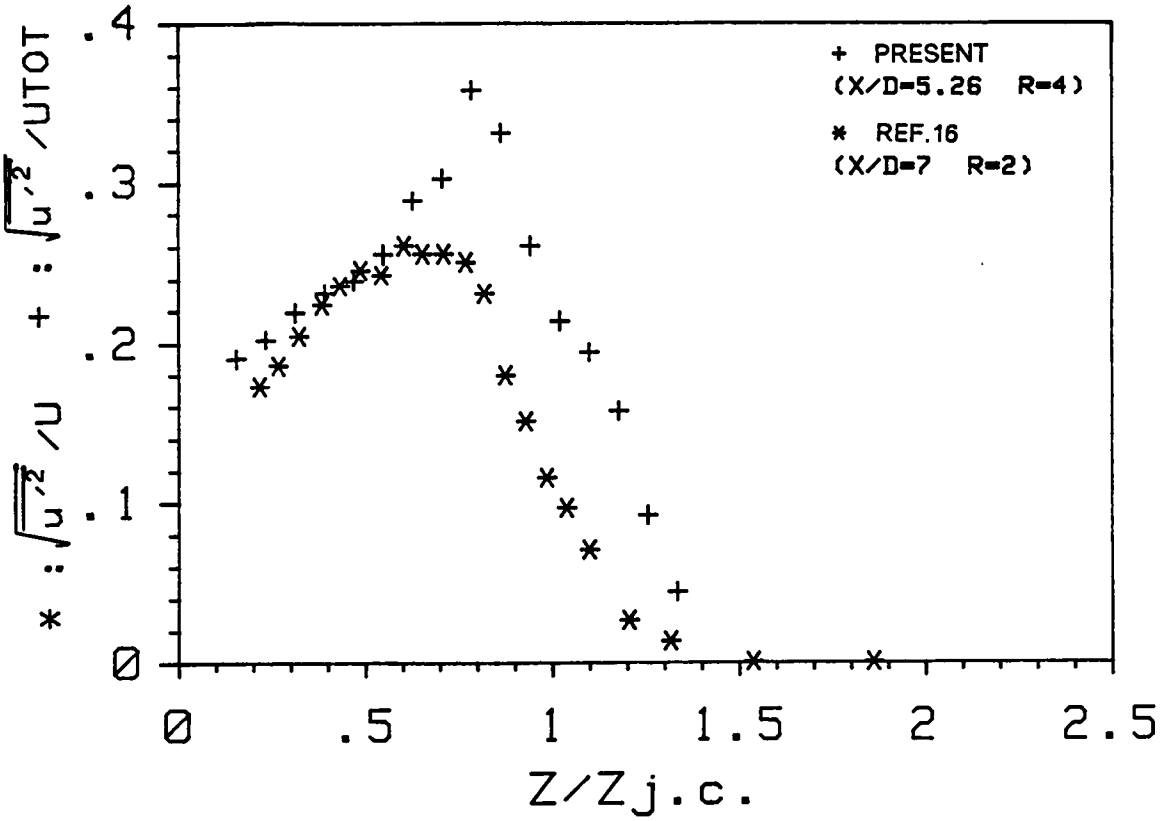

Figure 118. Turbulence comparison with Ref.16, circular jet.

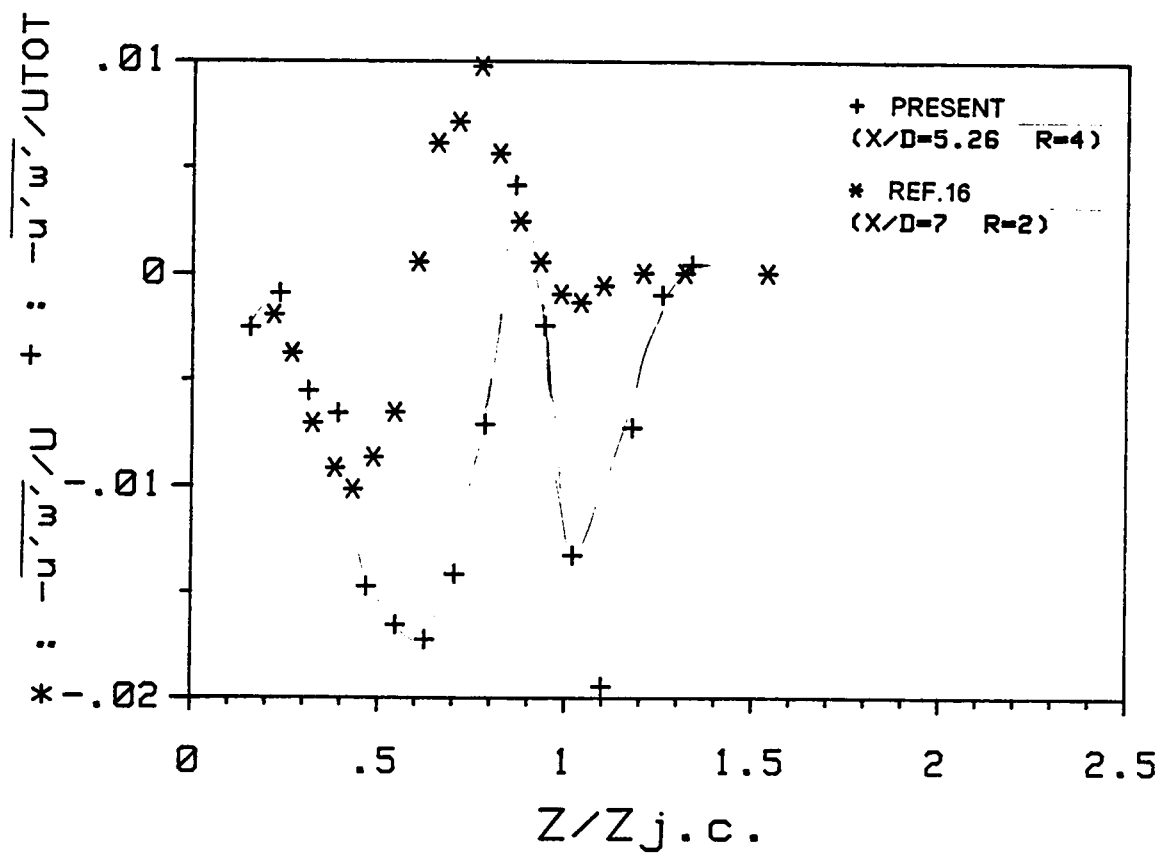

Figure 119. Turbulence comparison with Ref.16, circular jet.

Appendix A

THE COMPUTER PROGRAMS USED FOR PRESSURE DISTRIBUTION MEASUREMENTS

In this appendix two programs and one sample data file will be presented. The programs were written for the HP 9836 computer in BASIC language. The data file was prepared for the GPCP plotting program (Ref.83). The first program (SCANNER1) was used during experiments for rotation of the Scanivalves, data gathering and storage. The first six Scanivalves were rotated by a common motor, and the first six transducers were connected to the channels 21 through 26 of the channel selector. The second six Scanivalves were rotated by another common motor, and the second six transducers were connected to the channels 27 through 32 of the channel selector. In this program device numbers 709, 722,

and 716 correspond to channel selector, digital voltmeter and relay actuator respectively. A command like OUTPUT 716;"A1" activates the channel 1 of the relay actuator and another command like OUTPUT 716;"B1" deactivates the same channel, etc.. The second program (CPP) was used for the calculation of $\Delta C_p = C_{Pjet\ on} - C_{Pjet\ off}$.

```
10    !   SKINNER1
20    ON KEY 4 LABEL "STOP" GOTO Finito
30     DIM Pressure(600)
40  !  CREATE ASCII "DATA:INTERNAL,4,1",25
50     CREATE ASCII "DATA:INTERNAL,4,1",75
60     ASSIGN @File1 TO "DATA:INTERNAL,4,1"
70     I=1
80     FOR N=1 TO 50
90     CALL Adv1(0)
100    NEXT N
110    FOR K=21 TO 26
120 !  IF K>24 THEN GOTO Datastore
130    C$=VAL$(K)
140    CALL Adv1(1)
150    OUTPUT 709;C$
160    CALL Trig1(I,Pressure(*))
170    NEXT K
180    FOR N=1 TO 50
190    CALL Adv2(0)
200    NEXT N
210    FOR K=27 TO 32
220    C$=VAL$(K)
230    CALL Adv2(1)
240    OUTPUT 709;C$
250    CALL Trig2(I,Pressure(*))
260    NEXT K
270 Datastore:    !
280    ON ERROR GOTO 340
290    FOR N=1 TO I-1
300    OUTPUT @File1;N,Pressure(N)
310    NEXT N
320    ASSIGN @File1 TO *
330    GOTO Finito
340    ASSIGN @File1 TO *
350    PURGE "DATA:INTERNAL,4,1"
360    INPUT "PUT A NEW DISC AND HIT RETURN",A$
370    CREATE ASCII "DATA:INTERNAL,4,1",75
380    ASSIGN @File1 TO "DATA:INTERNAL,4,1"
390    GOTO 290
400 Finito:!
410    OFF KEY 4
420    OFF ERROR
430    END
440    SUB Trig1(I,Pressure(*))
450    FOR J=1 TO 48
460    Sum=0
470    WAIT 1
480    TRIGGER 722
490    ENTER 722;A
500    FOR K=1 TO 25
510    TRIGGER 722
520    ENTER 722;C
530    Sum=Sum+C
540    NEXT K
550    Pressure(I)=Sum/25.
560    I=I+1
570    CALL Adv1(0)
580    NEXT J
590    SUBEND
```

```
600   SUB Trig2(I,Pressure(*))
610   FOR J=1 TO 48
620   Sum=0
630   WAIT 1
640   TRIGGER 722
650   ENTER 722;A
660   FOR K=1 TO 25
670   TRIGGER 722
680   ENTER 722;C
690   Sum=Sum+C
700   NEXT K
710   Pressure(I)=Sum/25.
720   I=I+1
730   CALL Adv2(0)
740   NEXT J
750   SUBEND
760   SUB Adv1(P)
770   IF P THEN OUTPUT 716;"A2"
780   OUTPUT 716;"A1"
790   WAIT .04
800   OUTPUT 716;"B1"
810   OUTPUT 716;"B2"
820   SUBEND
830   SUB Adv2(P)
840   IF P THEN OUTPUT 716;"A4"
850   OUTPUT 716;"A3"
860   WAIT .04
870   OUTPUT 716;"B3"
880   OUTPUT 716;"B4"
890   SUBEND
```

```
10 !     CPP
20 !     THIS PROGRAM READS THE PRESSURE DATA SUBTRACTS THE TARE AND
30 !     CALCULATES THE NONDIMENSIONAL PRESSURE COEFFICIENT
40       DIM A(600),B(600)
50       INPUT "PREFA(IN H2O)=?",Prefa
60       INPUT "PREFB(IN H2O)=?",Prefb
70       Prefa=Prefa*.0361111
80       Prefb=Prefb*.0361111
90 !     READ PRESSURE DATA
100      INPUT "FIRST DATA FILE AND # OF POINTS TO BE READ?",F$,N
110      INPUT "SECOND DATA FILE(TARE) ?",G$
120      INPUT "OUTPUT FILE NAME AND SIZE ?",H$,M
130      ASSIGN @Path1 TO F$&":INTERNAL,4,1"
140      FOR I=1 TO N
150      ENTER @Path1;Aa,A(I)
160      A(I)=100.*A(I)
170      NEXT I
180      ASSIGN @Path1 TO *
190 !    READ THE TARE DATA
200      ASSIGN @Path2 TO G$&":INTERNAL,4,1"
210      FOR I=1 TO N
220      ENTER @Path2;Bb,B(I)
230      B(I)=100.*B(I)
240      NEXT I
250      ASSIGN @Path2 TO *
260 !    CALCULATE CP(JET ON)
270      CALL Cp(A(*),N,Prefa)
280 !    CALCULATE CP(JET OFF)
290      CALL Cp(B(*),N,Prefb)
300 !    CALCULATE DELTA CP AND STORE
310      FOR I=1 TO N
320      A(I)=A(I)-B(I)
330      NEXT I
340      CREATE ASCII H$,M
350      ASSIGN @Path3 TO H$
360      FOR I=1 TO N
370      OUTPUT @Path3;A(I)
380      NEXT I
390      ASSIGN @Path3 TO *
400      Pa=Prefa/.036111
410      Pb=Prefb/.036111
420      PRINT F$,G$,Pa,Pb,H$
430      END
440      SUB Cp(A(*),N,Prefa)
450      N1=47
460      N2=48
470      Payda=(A(N2)-A(N1))*Prefa
480      FOR I=1 TO N
490      A(I)=(A(I)-A(N1))/Payda
500      IF I=N2 THEN GOTO Exit1
510      GOTO Exit2
520 Exit1:     !
530      N1=N1+48
540      N2=N2+48
550      IF N2>N THEN GOTO Exit2
560      Payda=(A(N2)-A(N1))*Prefa
570 Exit2:     NEXT I
580      SUBEND
```

```
//A291MEHM JOB 44EB2,MEHMET,REGION=1500K
/*PRIORITY IDLE
/*JOBPARM    LINES=8, CARDS=5000
//STEP1 EXEC GPCP
//SYSIN DD *
JOB  064C
FLEX
REF  10.0
SIZE 2.3  2.3  1.0  2.0  -6.0      0.25  6.0      -6.0      0.25 10.0
CNTL 0.02 0.04      2    6                                      8    8
CNTL (F11.7,2X,F11.7,2X,F11.7,3F8.0,I4,I2,T73,8A1)
CNTL      1         2         3
 -1.6667004    -1.6667004    -0.0740111                        1  1
 -1.3333673    -1.6667004     0.0162720                        1  2
 -1.0000334    -1.6667004     0.1675187                        1  3
     Y              X             ΔCp
 -1.6666651     8.3333321     0.0724239                       16 34
 -1.6666651     8.9999981     0.0584492                       16 35
 -1.6666651     9.6666641     0.0729440                       16 36

BEND
PRNT
PHS4
SKIP 0.03
BLEV 0.2
BRDR
LINE      1-0.95 0.0  0.0 -0.95
LINE      1 0.0 -0.95 0.95 0.0
LINE      1 0.95 0.0  0.0  0.95
LINE      1 0.0  0.95-0.95 0.0
END
STOP
/*
//
```

Subdivision no.

Port no.

optional

An example data file for the GPCP plotting program of Ref.83.

Appendix B

THE COMPUTER PROGRAM USED FOR X-WIRE MEASUREMENTS

In this appendix, the computer program named XWIRE will be presented. First there will be a description of the program. A schematic program structure, program listing and the calibration data of the pitch, roll and Z potentiometers will follow this.

DESCRIPTION OF THE PROGRAM

This program controls the pitch and roll angles and the Z location of the hot wire probe. It also reads data from the R.M.S. and D.C. voltmeters and re-

duces and stores this data. This program was written in BASIC for the HP 9836 computer.

After being started, this program first asks the current Z location, which should be used as a reference value. Then, the program creates two data files onto a floppy disc; one for storing the raw data, and the other for storing the reduced data. Before each data point, the user has access to three subroutines. He also has a choice to stop the program if all the data points have been finished. First subroutine (UP-DOWN) sets the Z location of the probe. The Z traverse goes down for increasing Z. The user chooses if he wants to go up or down. Then he inputs a time interval in seconds for which the electric current will be applied to the traverse motor. Before this he must be sure that a special switch was set to correct position (up or down). Then the computer activates the traverse motor and at the end of the specified time, reads the new Z location from the Z potentiometer and informs the user. If the user is satisfied with this value, he can go out of this subroutine. This procedure was necessary because there was only one relay available for Z traverse, and a drill motor was used to power this mechanism rather than an expensive step motor.

The second subroutine (PITCH) sets the pitch angle of the probe. It first asks the required pitch angle. Then it decides the direction of the movement and activates the pitch motor. During the motor run, the program continuosly triggers the pitch potentiometer and stops the motor when the required pitch angle is set. This ends the run of this subroutine. Subroutine PITCH should be called before the first data point, even if the pitch angle was set correctly because, this is the

way to input the pitch angle to the computer. For other data points, if the user doesn't want to change the pitch angle, he can omit calling this subroutine. The required pitch angle for each data point was known from the previously made yawhead measurements.

The third subroutine (READDATA) reads and reduces the X-Wire data. This subroutine can be called if the Z location and the pitch angle is set correctly. This subroutine first asks the user a parameter called UUF. This parameter, which is the ratio of U_{TOTAL} to U_{∞} and is known from the previously made yawhead measurements, will be used during the data reduction. Subroutine READDATA uses a fourth subroutine (SETROLL) for setting the roll angle of the probe. Subroutine READDATA calls the subroutine SETROLL with the required potentiometer output for the specified roll angle. After receiving the information, the subroutine SETROLL decides on the direction of the movement and gives power to the roll motor for a certain time interval. After each step, this subroutine checks the roll angle from the roll potentiometer. If the specified roll angle is not reached, it commands another step with the same time interval and direction. If the specified roll angle is passed, then the next step will be in the opposite direction with the time interval reduced by half. Therefore, this subroutine uses the interval halving method until the roll angle is set with the required accuracy. Subroutine READDATA actually sets the roll angle of the probe as 0°, 90°, 45° and for each roll angle reads data. If one calls the D.C. output of sensor#1 as "A" and of sensor#2 as "B", and if one calls the R.M.S. output of the sensor#1 as "a" and of sensor#2 as "b", for each roll angle the program reads a,

b, (A + B), (a + b), (A-B), (a-b). After setting each roll angle the program tells the user to switch the correlator to "A" and asks the range of the R.M.S. voltmeter in volts. If the range was not changed since the previous reading, he can just hit the ENTER key. However, before hitting this key he should be careful about seeing that both voltmeters, particularly the R.M.S. voltmeter, has stable output and the range is the one which gives the best accuracy. Entering the range of the R.M.S. voltmeter is important because, for all the ranges the R.M.S. voltmeter gives 1 volt output at the maximum deflection. Therefore, if the range is 1 volt no correction will be necessary but, if the range is different than 1 volt, then the output of the R.M.S. voltmeter should be multiplied by the range. After "A" this procedure will be repeated for "B", "A + B" and "A-B". The program assumes the output of the D.C. voltmeter is connected to channel 11, and the output of the R.M.S. voltmeter is connected to channel 12 of the channel selector. After one of these channels is connected to the digital voltmeter, the program first waits three seconds, then takes a sample and throws it away. Then it takes 20 more samples, takes their average and stores in the memory. When all the data is read for all three roll angles, the program asks the user if he wants to store data. If the answer is no, the subroutine returns to the main program. If the answer is yes, the program stores the raw data in the first file then makes data reduction with the formulas given in chapter 3 and stores the reduced data in the second file. Then it returns back to the main program where the user can call one of the three subroutines (UP-DOWN, PITCH, READDATA) for another data point or stop

the program. Raw data is stored only for security reasons, and the reduced data is ready to be transferred to the mainframe computer for plotting.

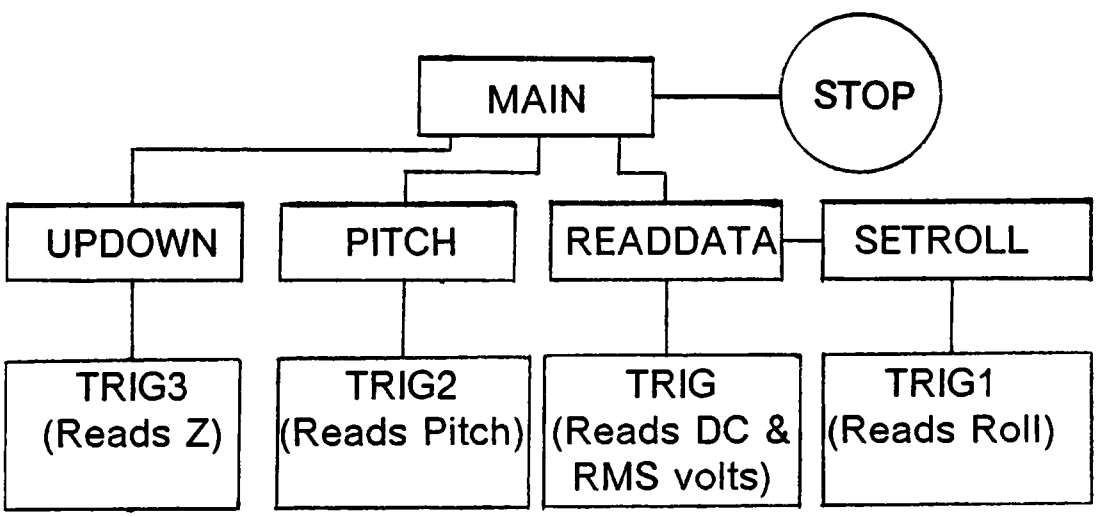

Schematic program structure.

```
10 !  XWIRE
20 !  JULY 8 1990, MEHMET SERIF KUNSEOGLU
30    INPUT "PRINTER=?",A
40    INPUT "BEGINING RUN #?",N
50    INPUT "Z0(MM)=?",Z0
60    Z=Z0
70    CALL Trig3(R0)
80    INPUT "DO YOU WANT TO STORE DATA?(Y/N)",A$
90    IF A$="N" THEN GOTO 150
100   INPUT "FILE NAME AND SIZE?",F$,M
110   CREATE ASCII F$&":INTERNAL,4,1",M
120   CREATE ASCII F$&"DR"&":INTERNAL,4,1",M
130   ASSIGN @File1 TO F$&":INTERNAL,4,1"
140   ASSIGN @File2 TO F$&"DR"&":INTERNAL,4,1"
150   PRINTER IS A
160   ON KEY 0 LABEL "UP-DOWN" GOTO 210
170   ON KEY 4 LABEL "PITCH" GOTO 230
180   ON KEY 5 LABEL "READ DATA" GOTO 250
190   ON KEY 9 LABEL "STOP" GOTO Finito
200   GOTO 200
210   CALL Updown(Z0,A0,Z)
220   GOTO 150
230   CALL Pitch(Gama)
240   GOTO 150
250   CALL Readdata(N,@File1,Gama,Z,@File2,R2)
260   GOTO 150
270 Finito:  !
280   ASSIGN @File1 TO *
290   END
300   SUB Readdata(N,@File1,Gama,Z,@File2,R2)
310   OFF KEY
320   DIM Aapbb(3),Aambb(3),Apb(3),Amb(3),A(3),D(3),R(3),Rx(3)
330   OPTION BASE 1
340   R(1)=30
350   R(2)=70
360   R(3)=47
370   Rx(1)=1
380   Rx(2)=90
390   Rx(3)=45
400 !  INPUT "Z(MM)=?",Z
410   INPUT "UUF=?",Uuf !TOTAL VEL TO FREESTREAM RATIO FROM YAWHEAD
420   Uuf2=Uuf*Uuf
430   CALL Trig("02",Temp)
440   Temp=Temp*100.
450   Temp=ABS(Temp)
460   Temp=Temp/.0556
470   FOR I=1 TO 3
480   CALL Setroll(R(I))
490   PRINT "ROLL=",Rx(I)
500   R1=10
510   INPUT "SWITCH A AND ENTER RANGE(RMS VOLTS)",Rr
520   IF Rr<>0 THEN R2=Rr
530   CALL Trig("12",A(I))
540   A(I)=A(I)*R2
550   INPUT "SWITCH B AND ENTER RANGE(RMS VOLTS)",Rr
560   CALL Trig("12",B(I))
570   IF Rr<>0 THEN R2=Rr
580   B(I)=B(I)*R2
590   INPUT "SWITCH A+B AND ENTER RANGE(RMS VOLTS)",Rr
600   IF Rr<>0 THEN R2=Rr
610   CALL Trig("11",Aapbb(I))
```

```
620  CALL Trig("12",Apb(I))
630  Aapbb(I)=Aapbb(I)*R1
640  Apb(I)=Apb(I)*R2
650  INPUT "SWITCH A-B AND  ENTER RANGE(RMS VOLTS)",Rr
660  IF Rr<>0 THEN R2=Rr
670  CALL Trig("11",Aambb(I))
680  CALL Trig("12",Amb(I))
690  Aambb(I)=Aambb(I)*R1
700  Amb(I)=Amb(I)*R2
710  NEXT I
720  PRINT "RUN# =",N,"Z(MM)=",Z,"TEMP=",Temp,"PITCH=",Gama,"UUF=",Uuf
730  FOR I=1 TO 3
740  PRINT USING "SDD.DDE,X,SDD.DDE,X,SDD.DDE,X,SDD.DDE,X,SDD.DDE,X,SDD.DDE";Aapbb(I),Aambb(I),Apb(I),Amb(I),
750  NEXT I
760  INPUT "DO YOU WANT TO STORE DATA?(Y/N)",A$
770  IF A$="N" THEN GOTO 1450
780  OUTPUT @File1;N,Z,Temp,Gama,Uuf
790  FOR I=1 TO 3
800  OUTPUT @File1;Aapbb(I),Aambb(I),Apb(I),Amb(I),A(I),B(I)
810  NEXT I
820 ! DATA REDUCTION
830 ! ---------------------------------------------------
840  Uddcp=(Aapbb(1)+Aapbb(2)+Aapbb(3))/3.
850  Vddcp=Aambb(1)
860  Hddcp=Aambb(2)
870  Uudcp2=Uddcp^2+Vddcp^2+Hddcp^2
880  Uudcp=SQR(Uudcp2)
890  Up=(Apb(1)+Apb(2)+Apb(3))/3.
900  Vp=Amb(1)
910  Hp=Amb(2)
920  Uvp=A(1)*A(1)-B(1)*B(1)
930  Uwp=A(2)*A(2)-B(2)*B(2)
940  Vwp=-Vp*Vp-Hp*Hp+Amb(3)*Amb(3)
950  Up=Up/Uudcp
960  Vp=Vp/Uudcp
970  Hp=Hp/Uudcp
980  Uvp=Uvp/Uudcp2
990  Uwp=Uwp/Uudcp2
1000 Vwp=Vwp/Uudcp2
1010 Cg=COS(Gama)
1020 Sg=SIN(Gama)
1030 U=SQR((Up*Cg)^2+(Hp*Sg)^2-2*Uwp*Sg*Cg)
1040 V=Vp
1050 W=SQR((Up*Sg)^2+(Hp*Cg)^2-2*Uwp*Sg*Cg)
1060 Uv=Uvp*Cg-Vwp*Sg
1070 Uw=Up*Up*Cg*Sg+Uwp*(Cg*Cg-Sg*Sg)-Hp*Hp*Cg*Sg
1080 Vw=Uvp*Sg+Vwp*Cg
1090 Uv=-Uv
1100 Uw=-Uw
1110 Vw=-Vw
1120 PRINT
1130 ! PRINT TURB. DATA NORMALIZED WITH LOCAL TOTAL VELOCITY
1140 ON ERROR GOTO 1160
1150 PRINT USING "3D.5D,X,3D.5D,X,3D.5D,X,3D.5D,X,3D.5D,X,3D.5D,X,3D.5D";U,V,W,Uv,Uw,Vw
1160 OFF ERROR
1170 OUTPUT @File2;N,Z,U,V,W,Uv,Uw,Vw
1180 U=U*Uuf
1190 V=V*Uuf
1200 W=W*Uuf
1210 Uv=Uv*Uuf2
1220 Uw=Uw*Uuf2
```

```
1230  Uw=Uw*Uuf^2
1240  !    PRINT TURB DATA NORMALIZED WITH FREESTREAM VEL.
1250  ON ERROR GOTO 1270
1260  PRINT USING "3D.5D,X,3D.5D,X,3D.5D,X,3D.5D,X,3D.5D,X,3D.5D,X,3D.5D";U,V,W,Uv,Uw,Vw
1270  OFF ERROR
1280  OUTPUT @File2;U,V,W,Uv,Uw,Vw
1290  Udcp=Udcp/Uudc
1300  Vdcp=Vdcp/Uudcp
1310  Wdcp=Wdcp/Uuncp
1320  Udc=Udcp*Cg-Wdcp*Sg
1330  Vdc=Vdcp
1340  Wdc=Udcp*Sg+Wdcp*Cg
1350  Udc=Udc*Uuf
1360  Vdc=Vdc*Uuf
1370  Wdc=Wdc*Uuf
1380  !  PRINT MEAN VELOCITIES NORMALIZED WITH FREESTREAM VEL.
1390  ON ERROR GOTO 1410
1400  PRINT USING "3D.5D,X,3D.5D,X,3D.5D";Udc,Vdc,Wdc
1410  OFF ERROR
1420  OUTPUT @File2;Udc,Vdc,Wdc
1430  PRINT
1440  N=N+1
1450  SUBEND
------------------------------------------------------------
1460  SUB Trig(A$,B)
1470  OUTPUT 722;"F1"
1480  OUTPUT 709;A$
1490  TRIGGER 722
1500  ENTER 722;Dum
1510  B=0
1520  WAIT 3
1530  FOR I=1 TO 20
1540  TRIGGER 722
1550  ENTER 722;C
1560  B=B+C
1570  NEXT I
1580  B=B/20
1590  SUBEND
------------------------------------------------------------
1600  SUB Setroll(R)
1610  OUTPUT 722;"F4"
1620  OUTPUT 709;"21"
1630  CALL Trig1(R2,R,Diff)
1640  IF ABS(Diff)<1 THEN GOTO Finito
1650  Dt=.2
1660  IF R2>R THEN GOTO Decrease
1670 Increase:     !
1680  OUTPUT 716;"A2"
1690  WAIT Dt
1700  OUTPUT 716;"B2"
1710  CALL Trig1(R2,R,Diff)
1720  IF ABS(Diff)<1 THEN GOTO Finito
1730  IF R2>R THEN
1740  Dt=Dt/2
1750  GOTO Decrease
1760  END IF
1770  GOTO Increase
1780 Decrease:     !
1790  OUTPUT 716;"A1"
1800  WAIT Dt
1810  OUTPUT 716;"B1"
1820  CALL Trig1(R2,R,Diff)
1830  IF ABS(Diff)<1 THEN GOTO Finito
```

```
1840  IF R2<R THEN
1850  Dt=Dt/2
1860  GOTO Increase
1870  END IF
1880  GOTO Decrease
1890 Finito:      !
1900  SUBEND
1910  SUB Trig1(R2,R,Diff)
1920  R2=0
1930  FOR N=1 TO 20
1940  TRIGGER 722
1950  ENTER 722;X
1960  R2=R2+X
1970  NEXT N
1980  R2=R2/20
1990  R2=R2/1000
2000  Diff=R2-R
2010  SUBEND
2020  SUB Updown(Z0,R0,Z)
2030  OFF KEY
2040  PRINTER IS 1
2050  ON KEY 0 LABEL "UP" GOTO Up
2060  ON KEY 4 LABEL "DOWN" GOTO Down
 2070  ON KEY 7 LABEL "STOP" GOTO Finito
 2080  GOTO 2080
 2090 Up:       !
 2100           OFF KEY
 2110           INPUT "SWITCH UP AND ENTER TIME",Dt
 2120           ON KEY 0 LABEL "STOPUP" GOTO Stopup
 2130           OUTPUT 716;"PS"
 2140           N=INT(Dt/.02)
 2150           FOR I=1 TO N
 2160           WAIT .02
 2170           NEXT I
 2180 Stopup:   OUTPUT 716;"BS"
 2190           OFF KEY
 2200           CALL Trig3(R)
 2210           Z=Z0-118.54136*(R-R0)
 2220           PRINT "Z(MM)=",Z
 2230           GOTO 2050
 2240 Down:             !
 2250           OFF KEY
 2260           INPUT "SWITCH DOWN AND ENTER TIME",Dt
 2270           ON KEY 4 LABEL "STOPDOWN" GOTO Stopdown
 2280           OUTPUT 716;"PS"
 2290           N=INT(Dt/.02)
 2300           FOR I=1 TO N
 2310           WAIT .02
 2320           NEXT I
 2330 Stopdown: OUTPUT 716;"BS"
 2340           OFF KEY
 2350           CALL Trig3(R)
 2360           Z=Z0-118.54136*(R-R0)
 2370           PRINT "Z(MM)=",Z
 2380           GOTO 2050
 2390 Finito:           !
 2400           OFF KEY
 2410           SUBEND
 2420           SUB Pitch(Gamma)
 2430           OFF KEY
 2440           PRINTER IS 1
```

```
2450          OUTPUT 722;"F4"
2460          OUTPUT 709;"22"
2470          INPUT "PITOT ANGLE=?",Gama
2480          IF Gama<=25 THEN R=-.168*Gama+24.40
2490          IF Gama>25 THEN R=-.24*Gama+26.2
2500          PRINT "R=",R
2510          CALL Trig1(R2,R,Diff)
2520          IF ABS(Diff)<.2 THEN GOTO Finito
2530          IF R2>R THEN GOTO Decrease
2540 Increase:                !
2550          ON KEY 4 LABEL "STOPINC" GOTO Stopinc
2560          OUTPUT 716;"A4"
2570          CALL Trig2(R2,R,Diff)
2580          IF R2>R THEN GOTO Stopinc
2590          GOTO 2570
2600 Stopinc:          !
2610          OFF KEY
2620          OUTPUT 716;"B4"
2630          GOTO Finito
2640 Decrease:                !
2650          ON KEY 4 LABEL "STOPDEC" GOTO Stopdec
2660          OUTPUT 716;"A3"
2670          CALL Trig2(R2,R,Diff)
2680          IF R2<R THEN GOTO Stopdec
2690          GOTO 2670
2700 Stopdec:                 !
2710          OFF KEY
2720          OUTPUT 716;"B3"
2730 Finito:          !
2740          PRINT "R2=",R2
2750          SUBEND
2760          SUB Trig2(R2,R,Diff)
2770          R2=0
2780          FOR N=1 TO 10
2790          TRIGGER 722
2800          ENTER 722;X
2810          R2=R2+X
2820          NEXT N
2830          R2=R2/10
2840          R2=R2/1000
2850          Diff=R2-R
2860          SUBEND
2870          SUB Trig3(R)
2880    !     TRIGGERS UP-DOWN POTANTIOMETER
2890          OUTPUT 722;"F4"
2900          OUTPUT 709;"23"
2910          TRIGGER 722
2920          ENTER 722;R
2930          Sum=0
2940          FOR I=1 TO 20
2950          TRIGGER 722
2960          ENTER 722;R
2970          Sum=Sum+R
2980          NEXT I
2990          R=Sum/20
3000          R=R/1000
3010          SUBEND
```

for $\gamma \leq 25°$.....$R(K\Omega) = -0.168 \times \gamma + 24.40$

for $\gamma > 25°$.....$R(K\Omega) = -0.240 \times \gamma + 26.20$

Calibration of the Pitch potentiometer.

$\varphi(°)$	$R(K\Omega)$
0	30
45	47
90	70

Calibration of the Roll potentiometer.

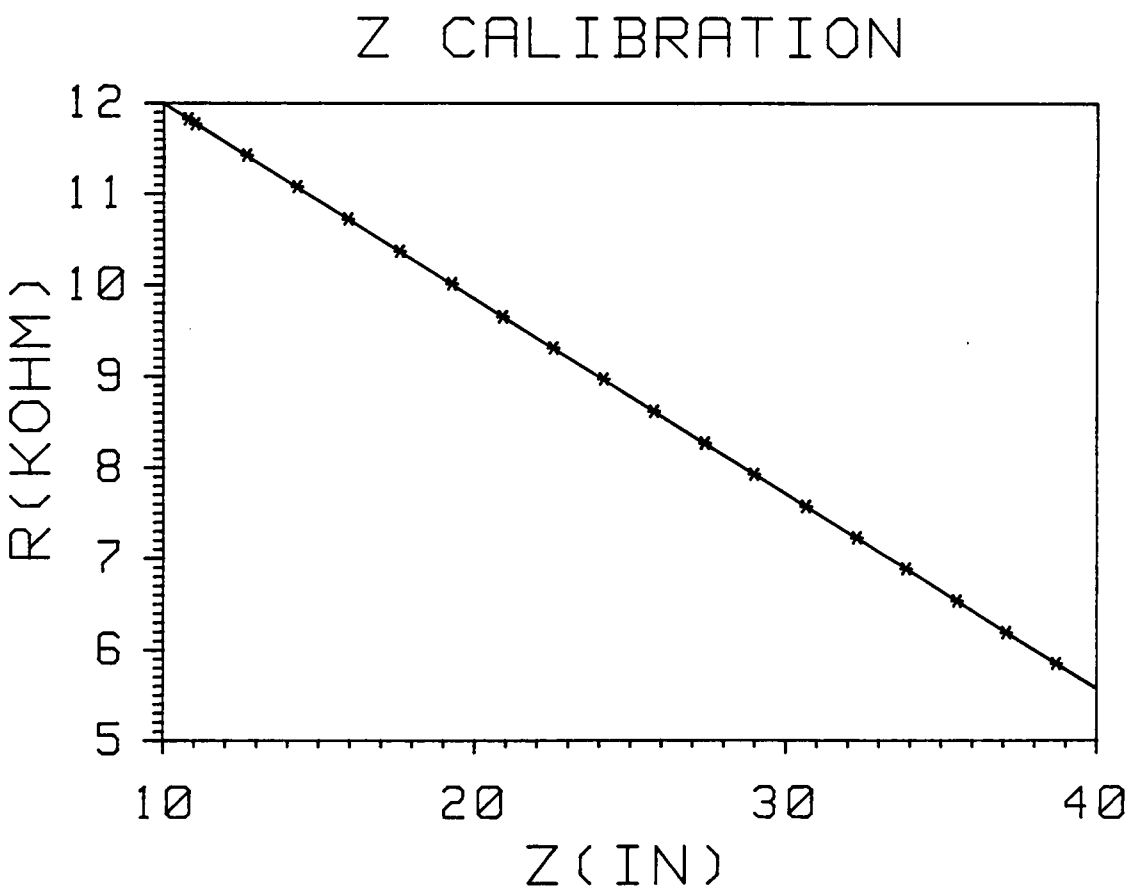

Calibration of the Z potentiometer.

Appendix C

DETAILS OF THE PROBE ROTATOR MECHANISM

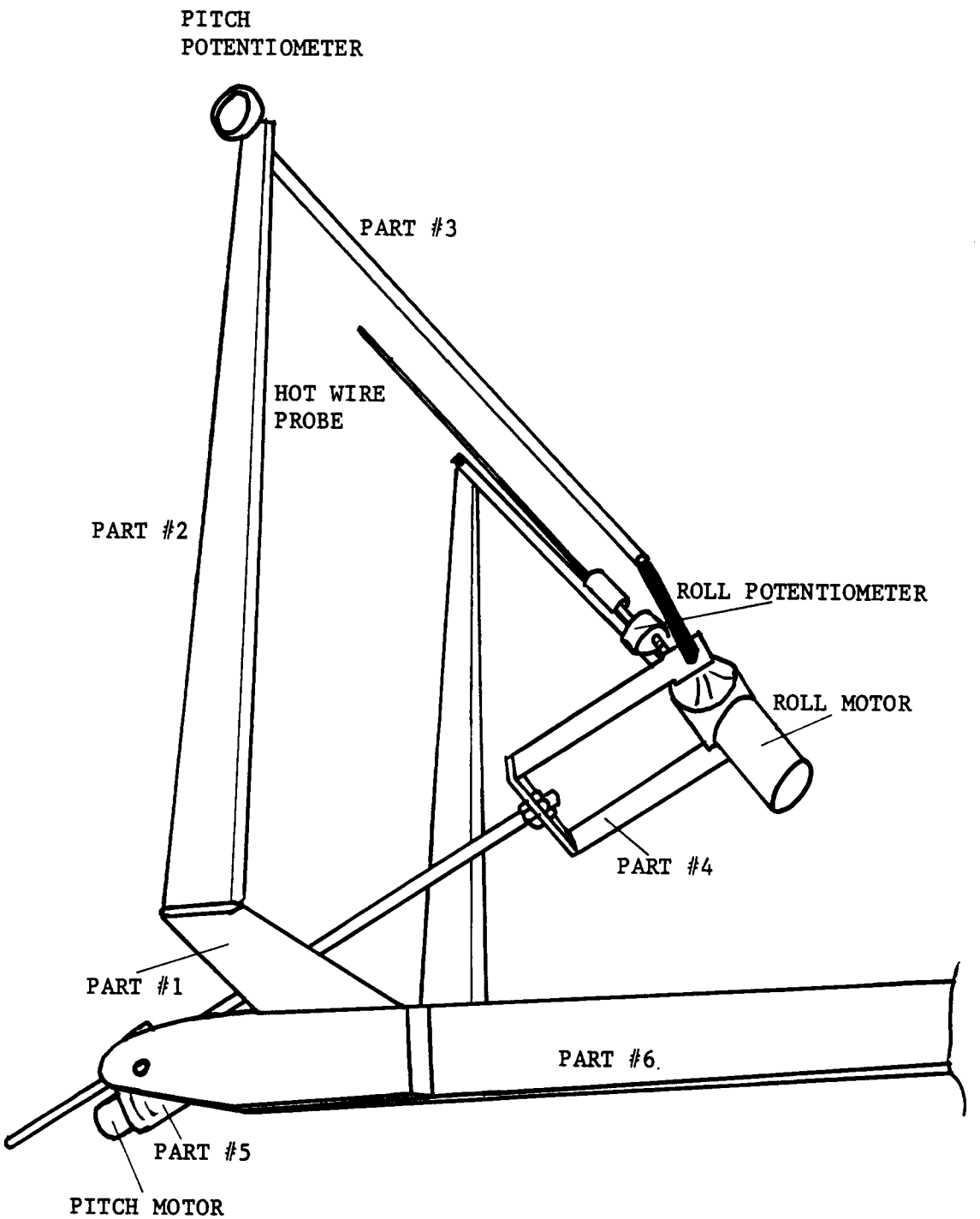

DETAILS OF THE PROBE ROTATOR MECHANISM

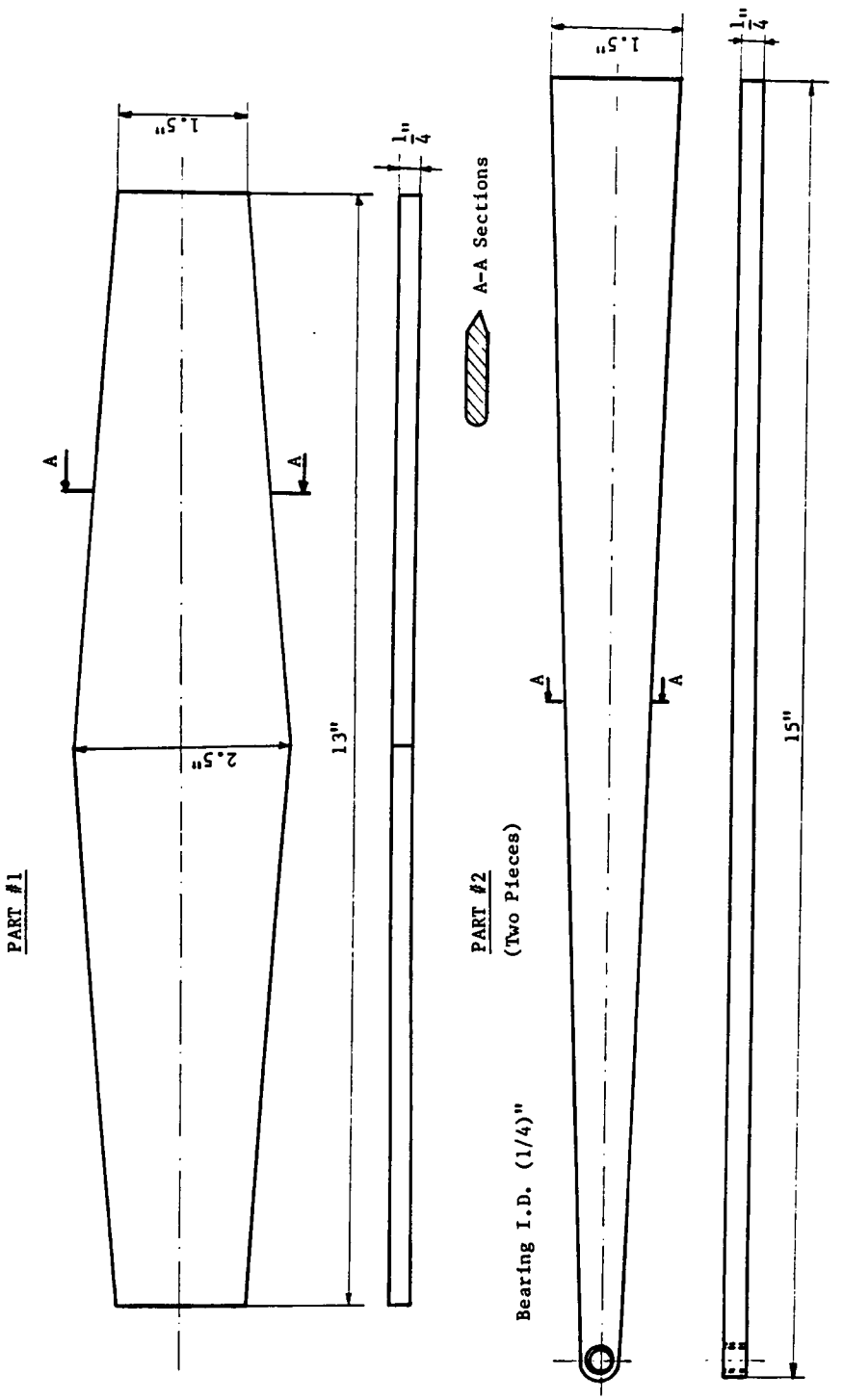

DETAILS OF THE PROBE ROTATOR MECHANISM

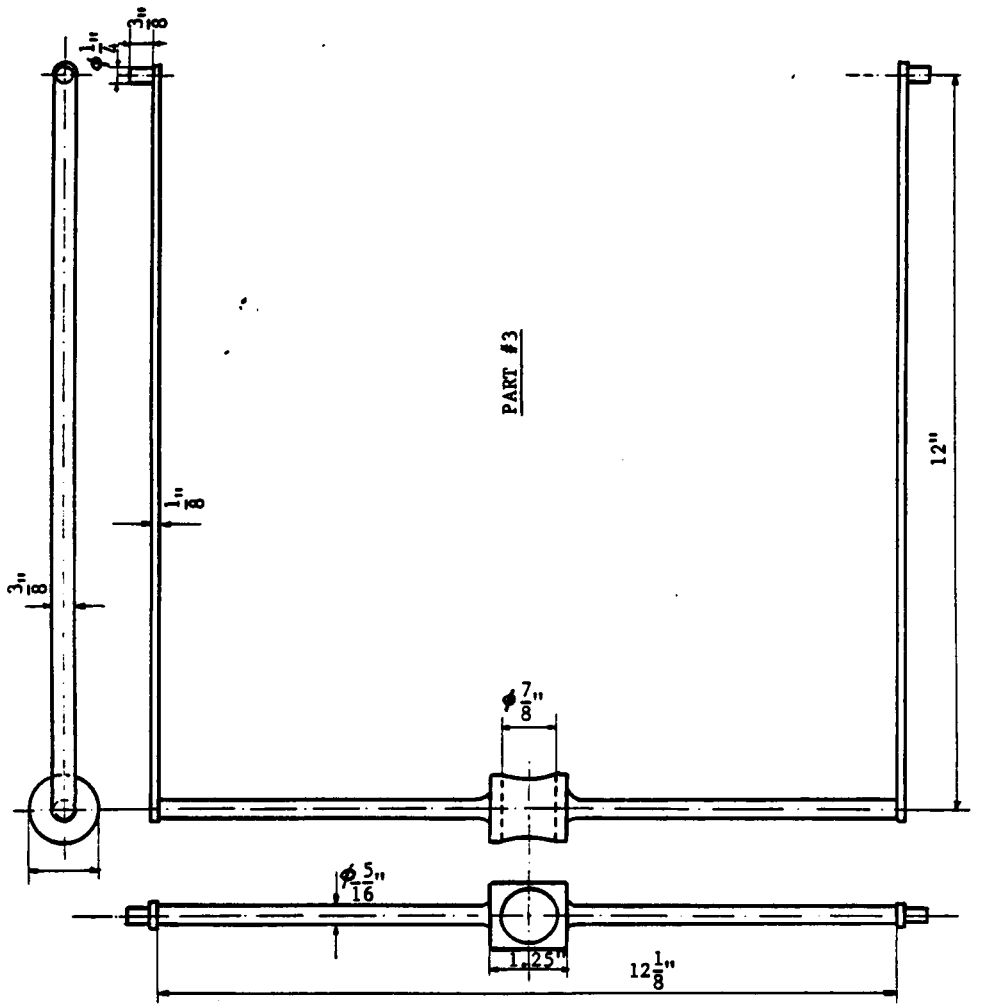

DETAILS OF THE PROBE ROTATOR MECHANISM

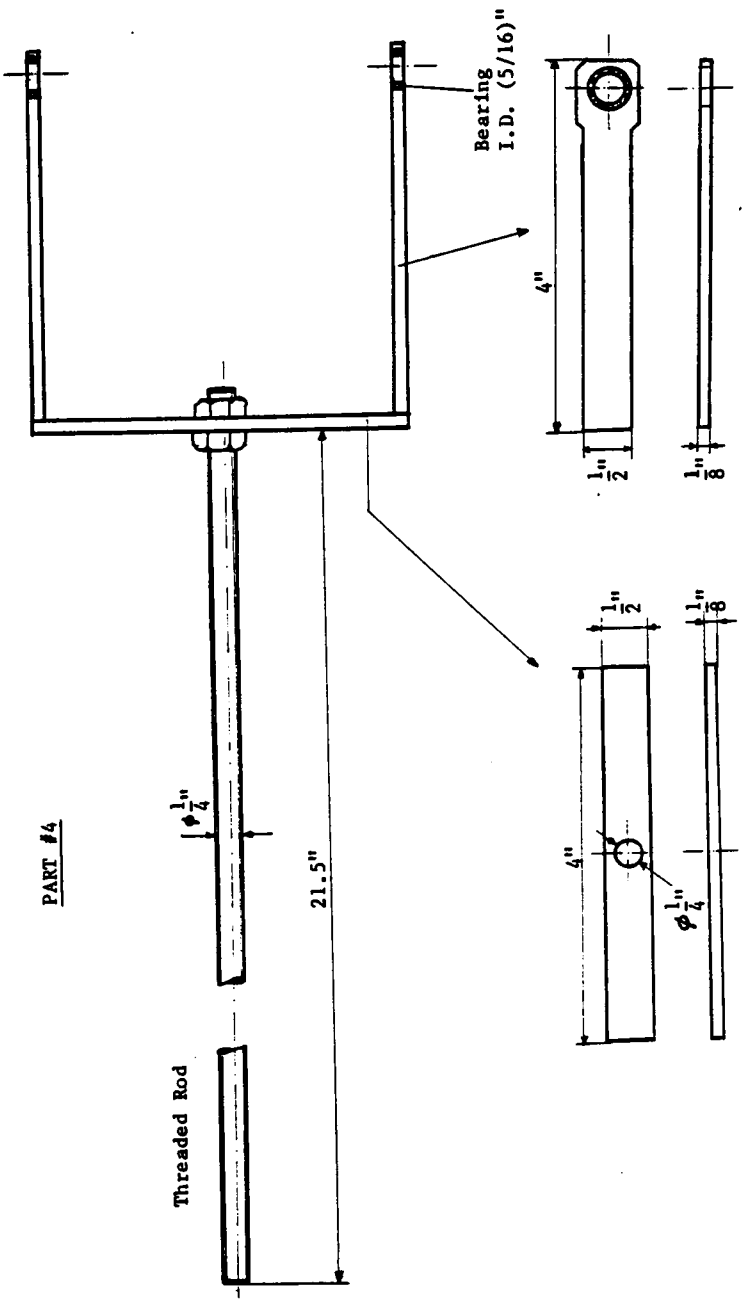
Bearing
I.D. (5/16)"
4"
1/2"
1/8"
1/2"
1/8"
4"
Ø 1/4"
PART #4
Ø 1/4"
21.5"
Threaded Rod

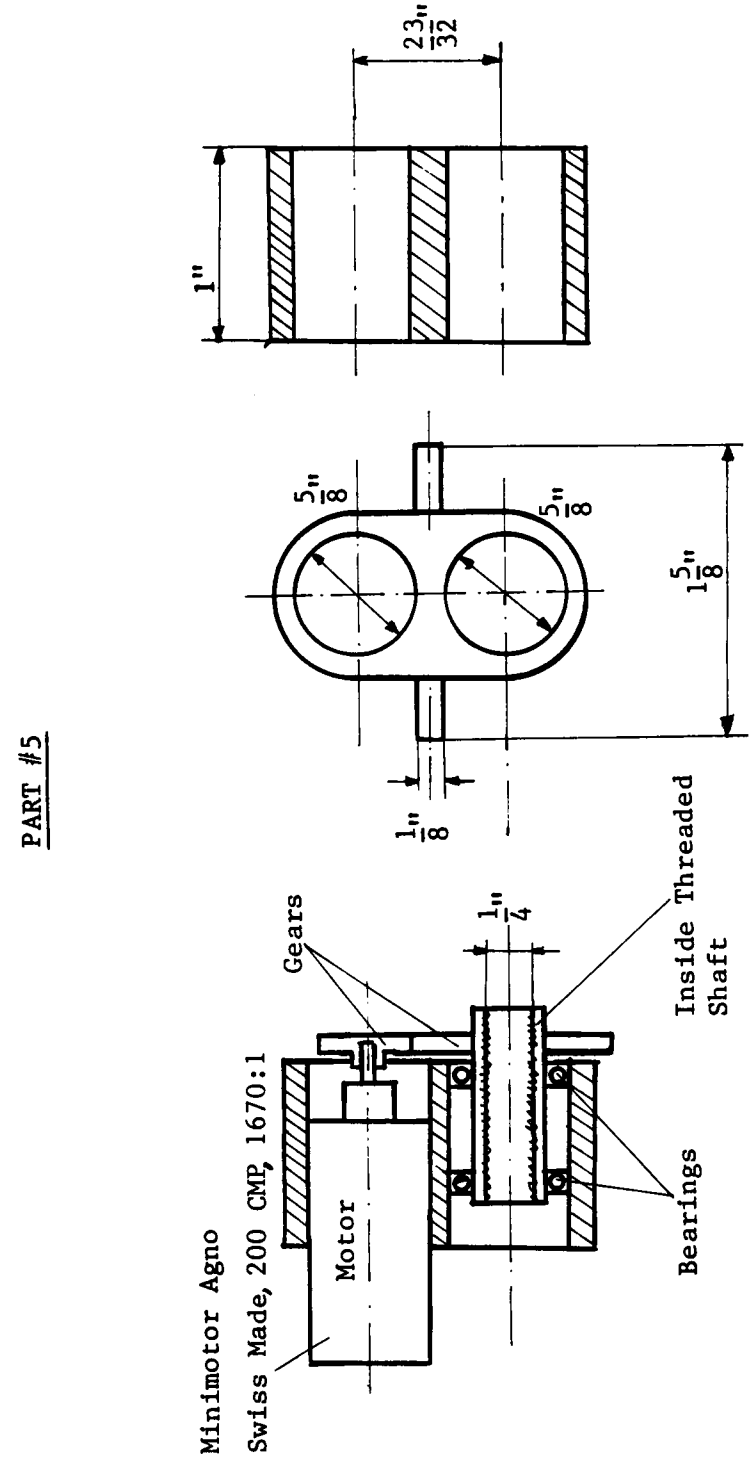
PART #5
23/32"
1"
5/8"
5/8"
1 5/8"
1/8"
1/4"
Gears
Inside Threaded Shaft
Bearings
Motor
Minimotor Agno
Swiss Made, 200 CMP, 1670:1

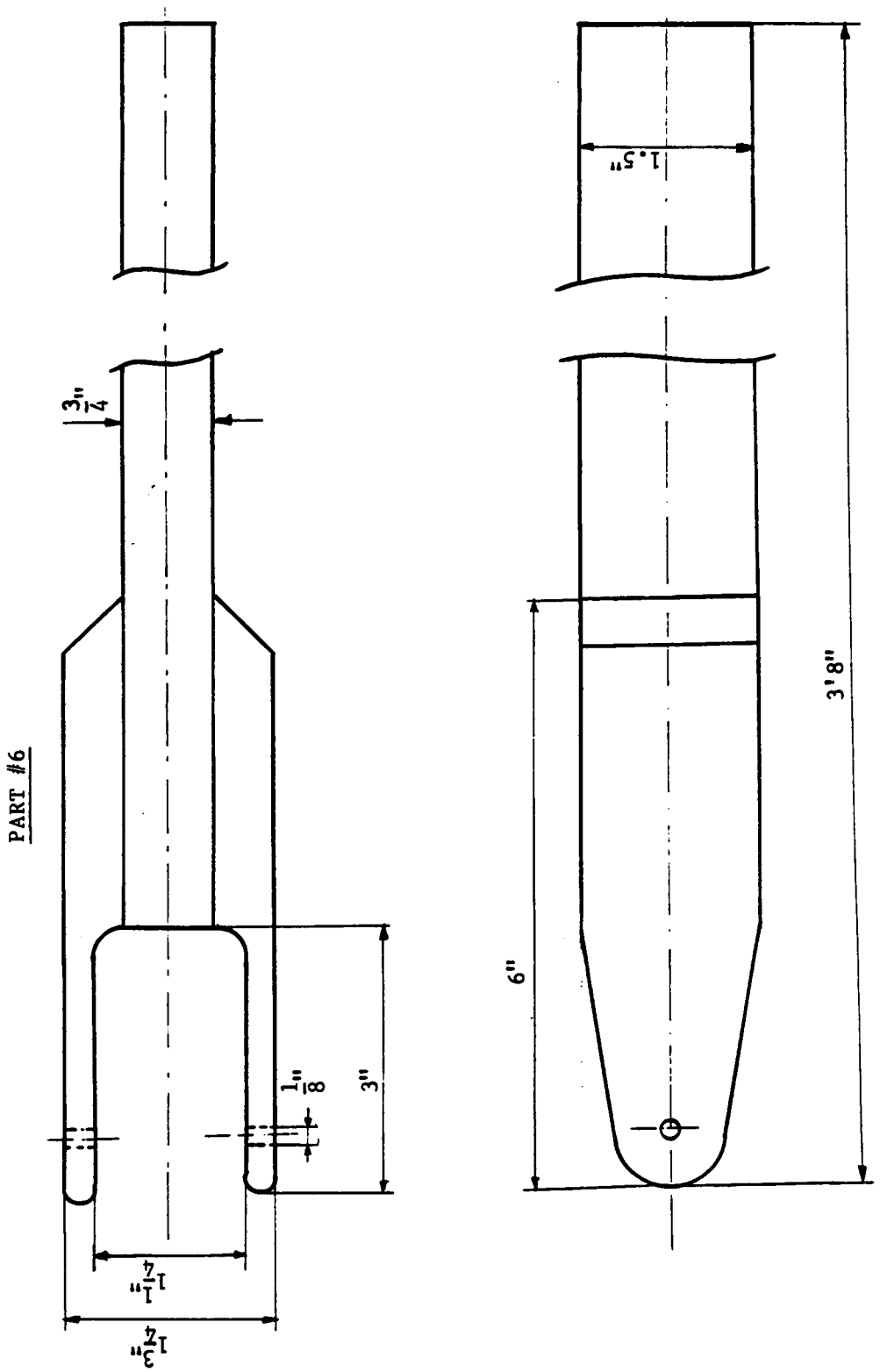

DETAILS OF THE PROBE ROTATOR MECHANISM

Appendix D

RESULTS FOR RECTANGULAR JETS WITH ROTATIONAL EXIT PROFILES

In this appendix, the pressure distribution and mean flowfield results for 90° and 60° rectangular jets will be presented. The rectangular jets used here had somewhat rotational velocity profile at their central part, when compared to the rectangular jets presented in the main text. Exit velocity profiles of these rectangular jets can be seen in the first four figures of this appendix and can be compared to the profiles in the main text. Comparison of the results presented in this appendix and the results presented in the main text didn't show a very significant difference, which is a good thing for the repeatability of the tests. Apparently, this level of swirl was too low to have any important effects. Pressure distribution results of the main text can be considered as having a better symmetry.

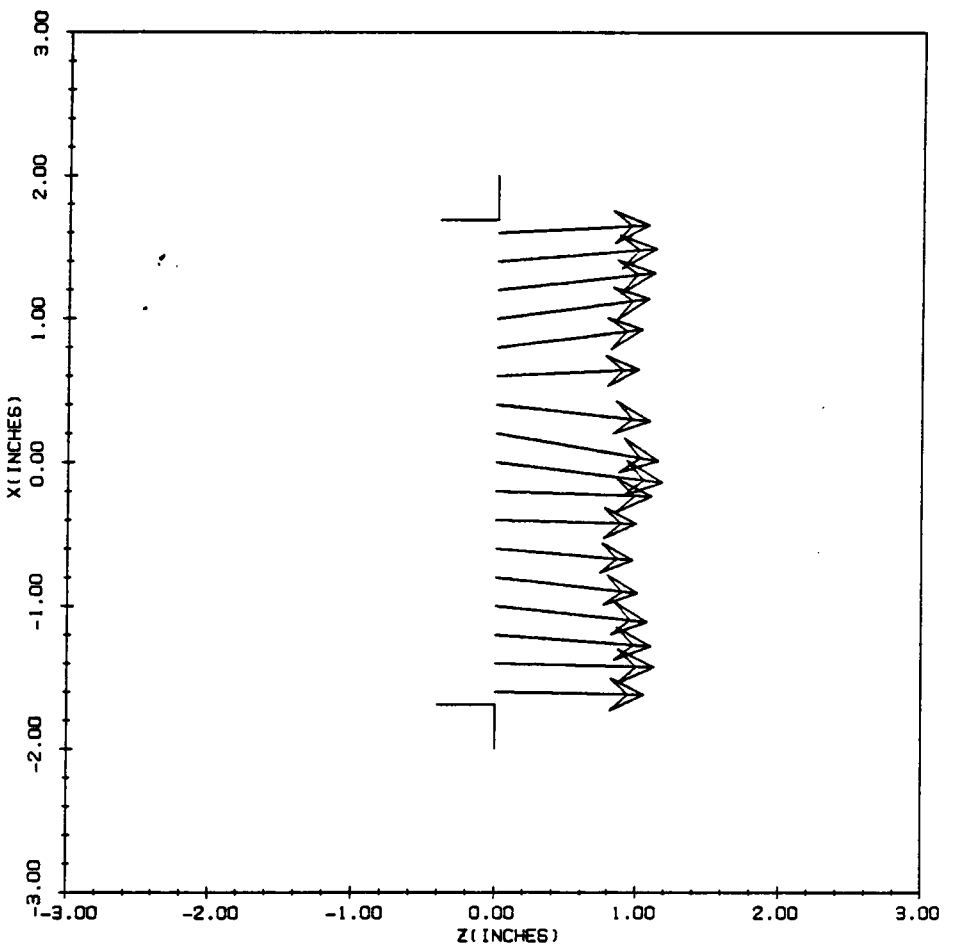

Figure 120. 90° rectangular jet exit profiles.

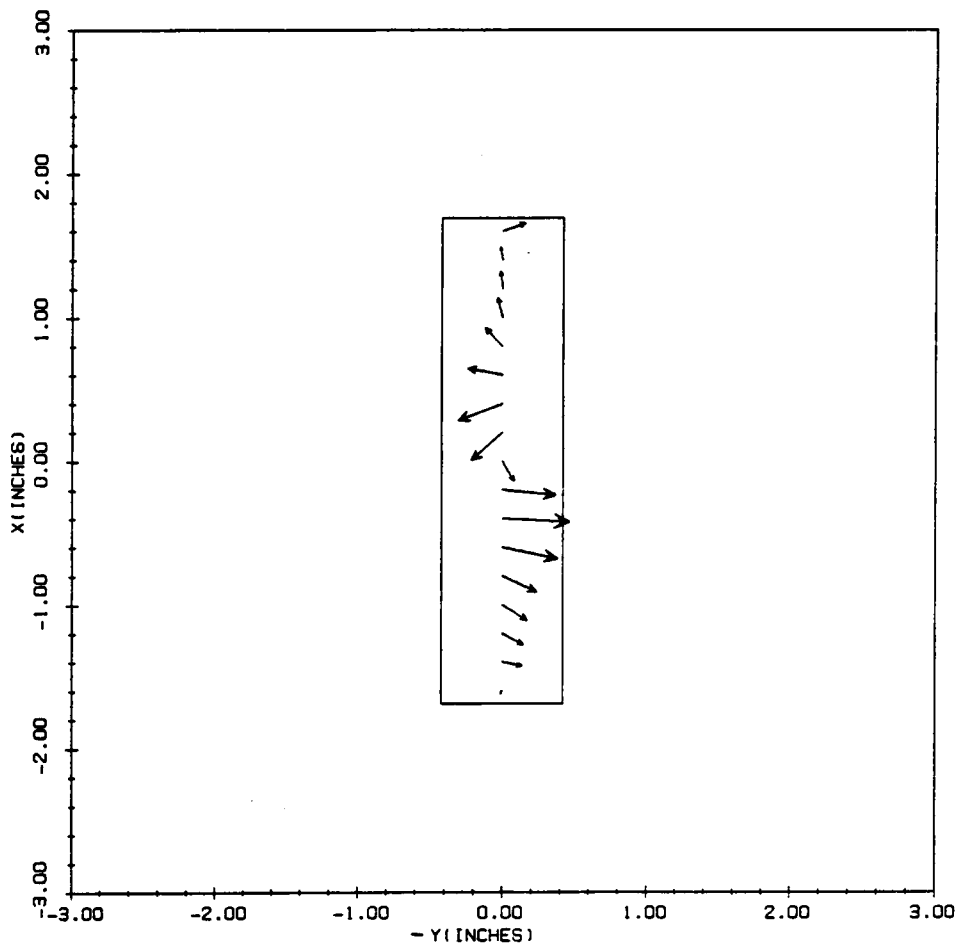

Figure 121. 90° rectangular jet exit profiles (continued).

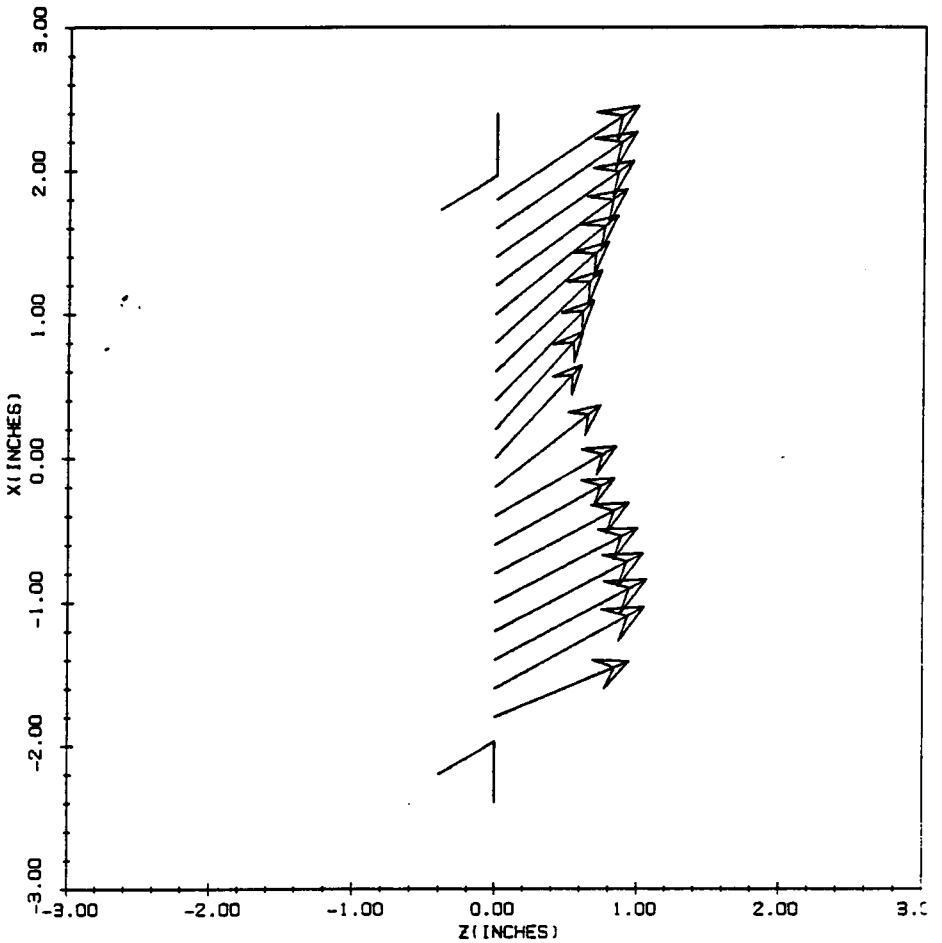

Figure 122. 60° rectangular jet exit profiles.

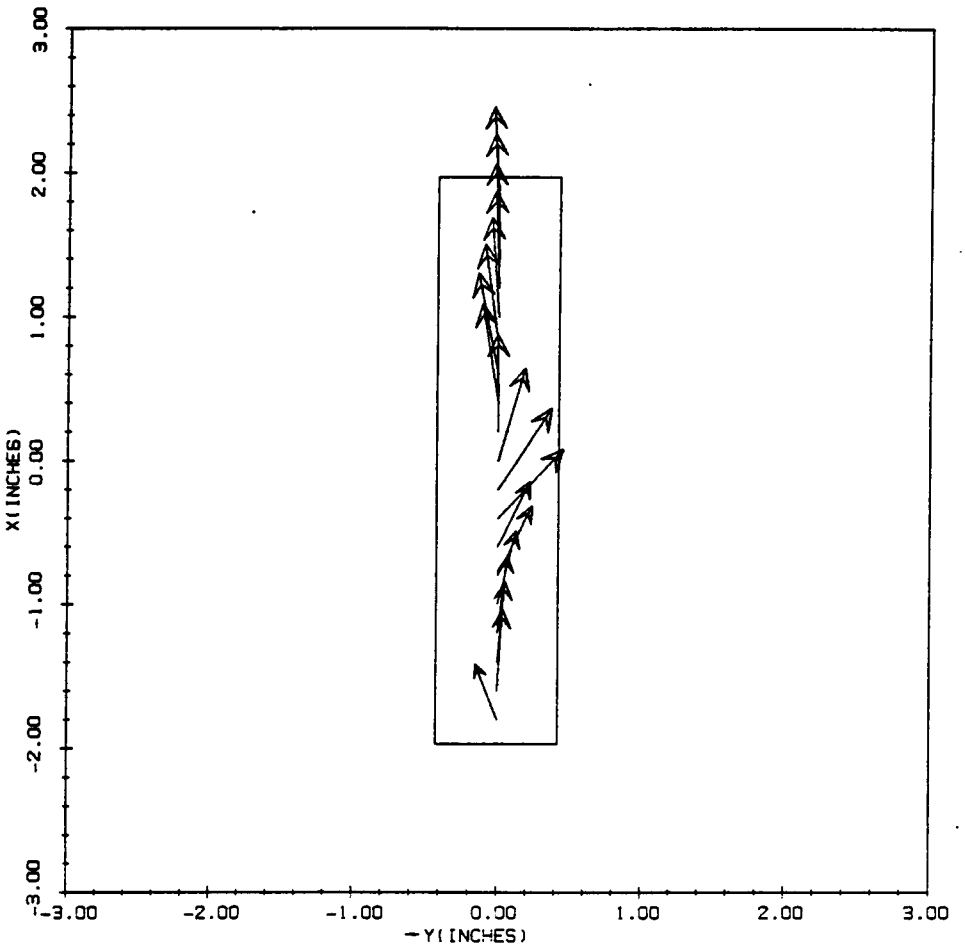

Figure 123. 90° rectangular jet exit profiles (continued).

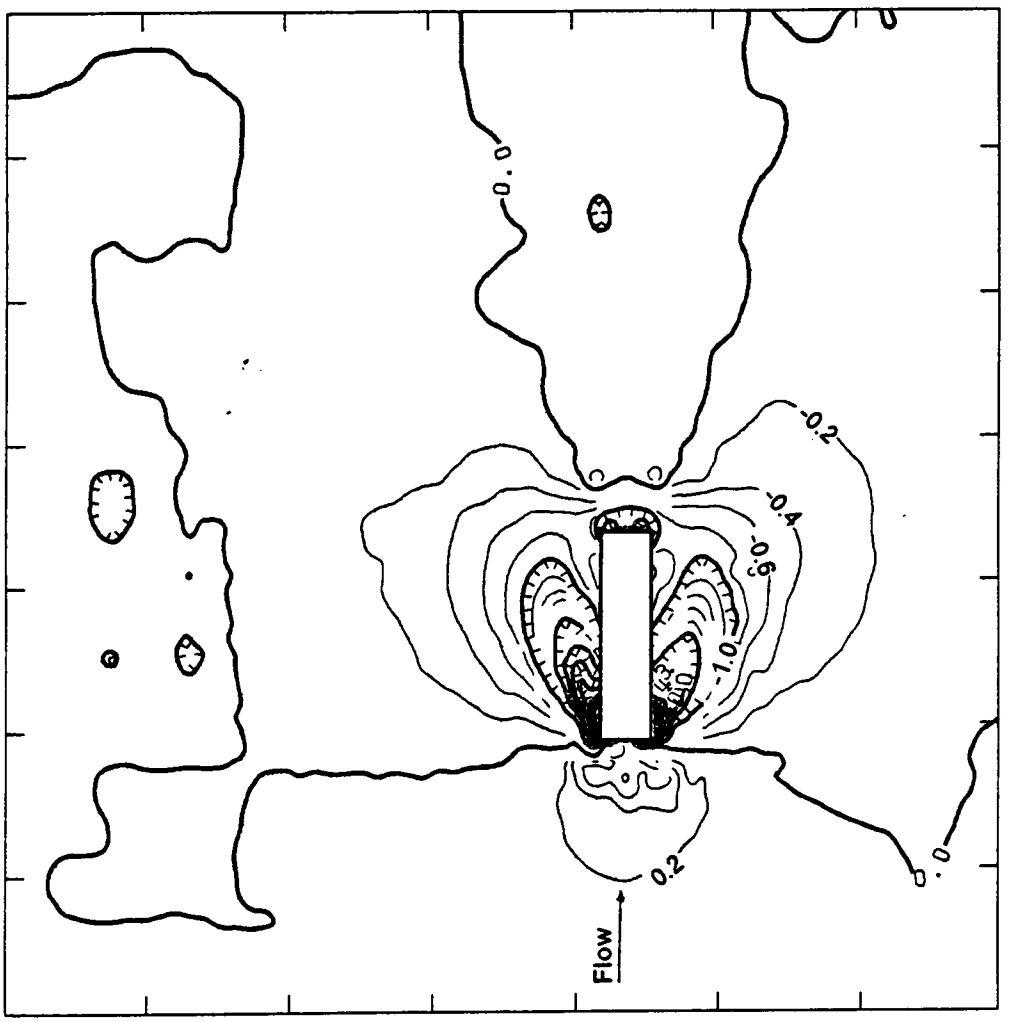

Figure 124. Surface pressures, 90° single rectangular jet, R = 2.2.

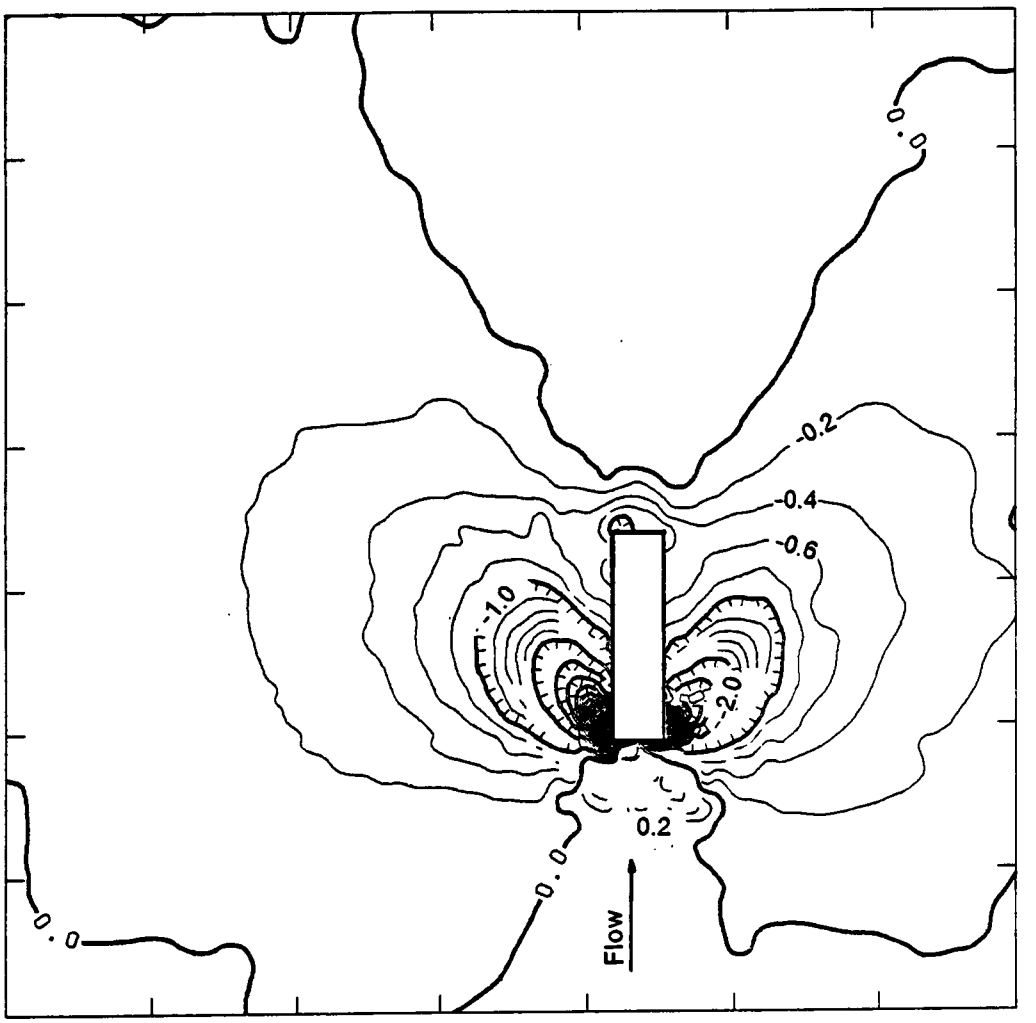

Figure 125. Surface pressures, 90° single rectangular jet, R = 4.0.

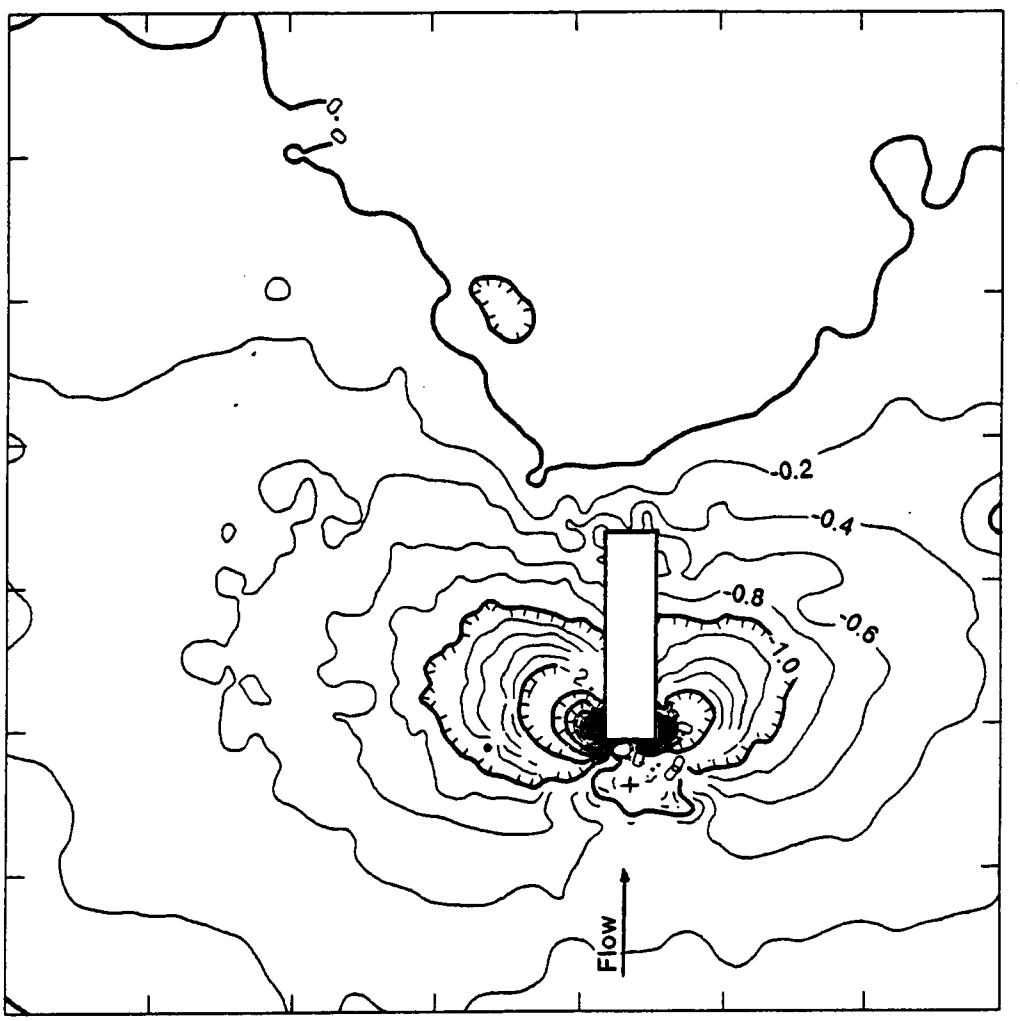

Figure 126. Surface pressures, 90° single rectangular jet, R = 8.0.

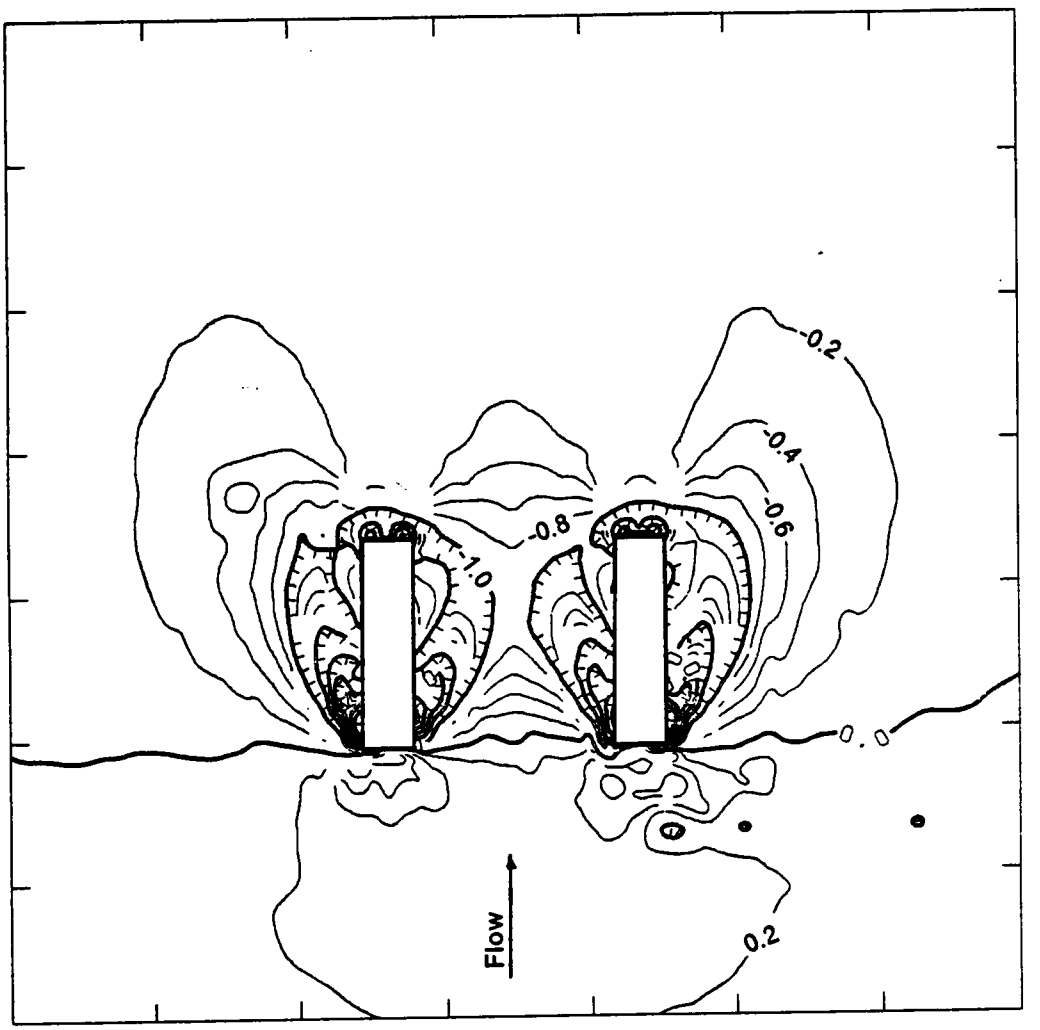

Figure 127. Surface pressures, 90° side-by-side rectangular, R = 2.2.

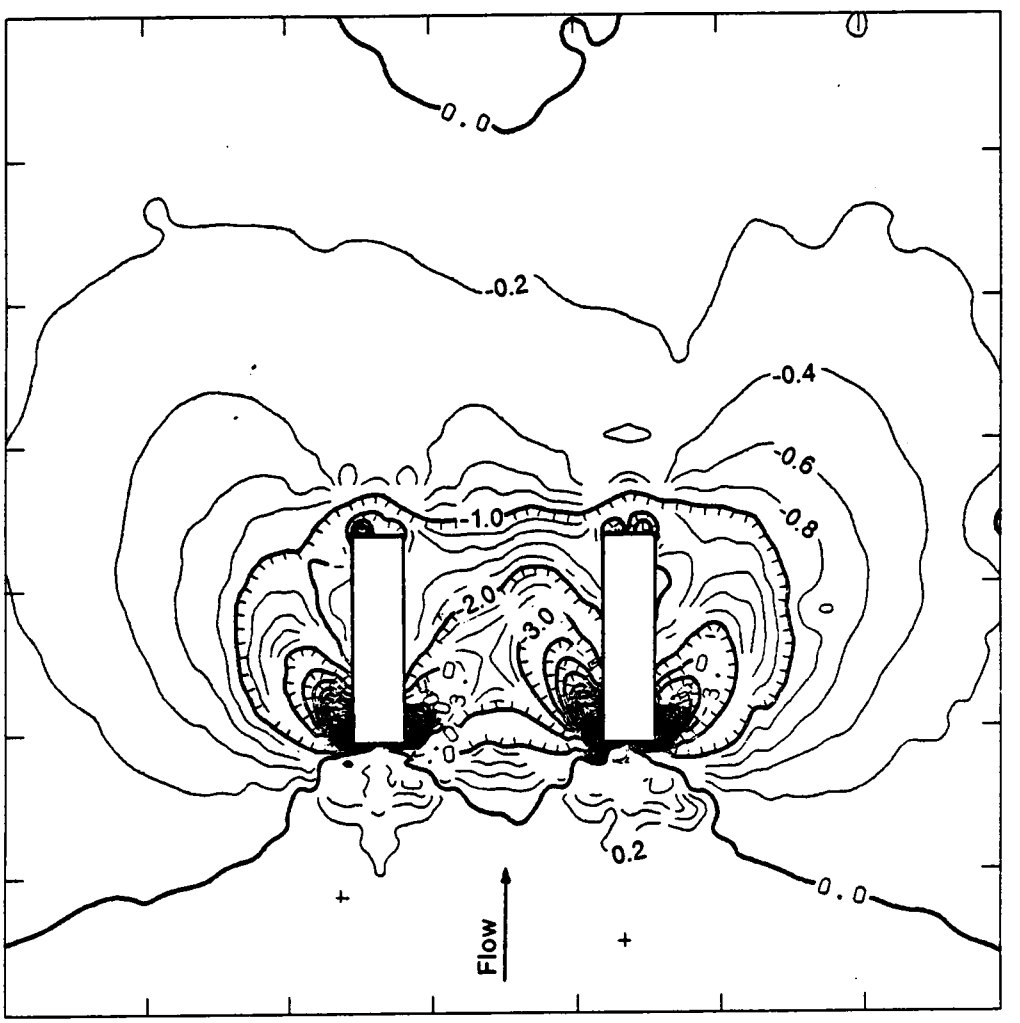

Figure 128. Surface pressures, 90° side-by-side rectangular, R = 4.0.

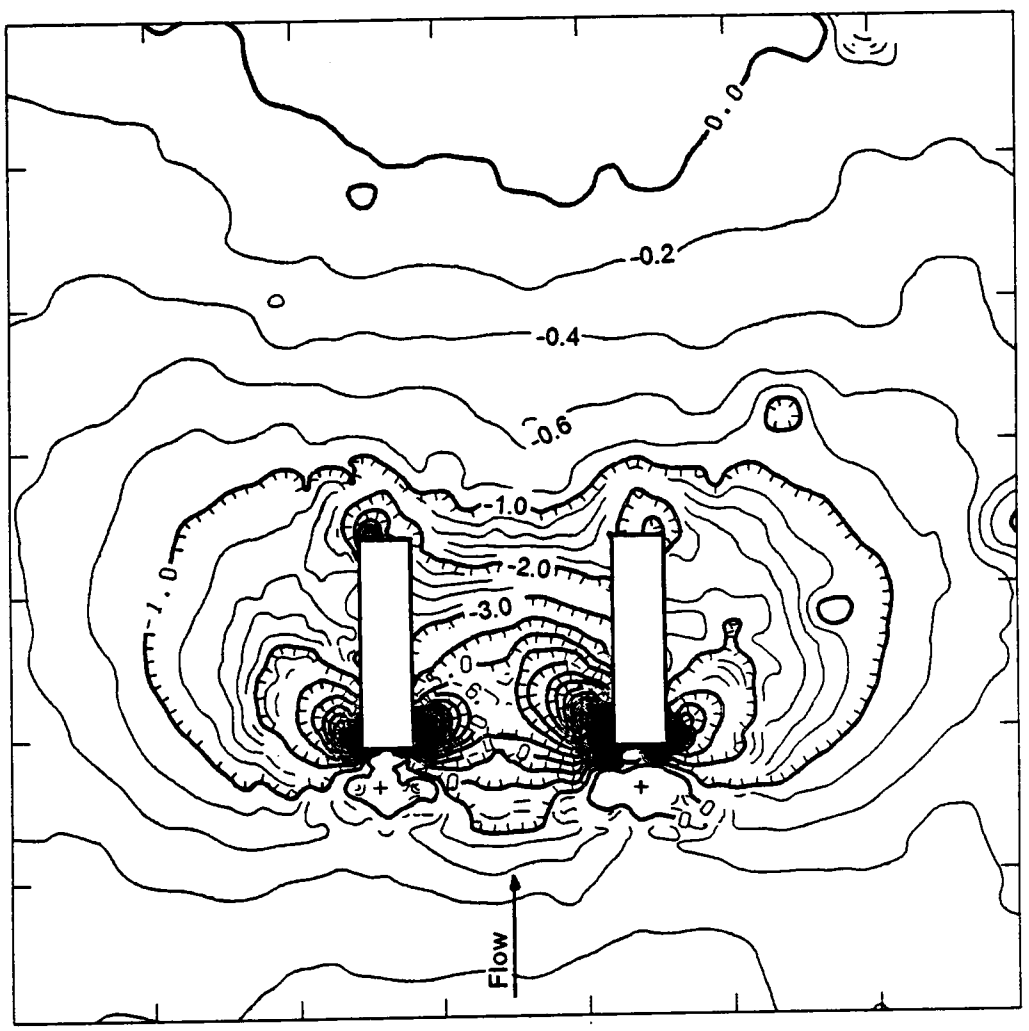

Figure 129. Surface pressures, 90° side-by-side rectangular, R = 8.0.

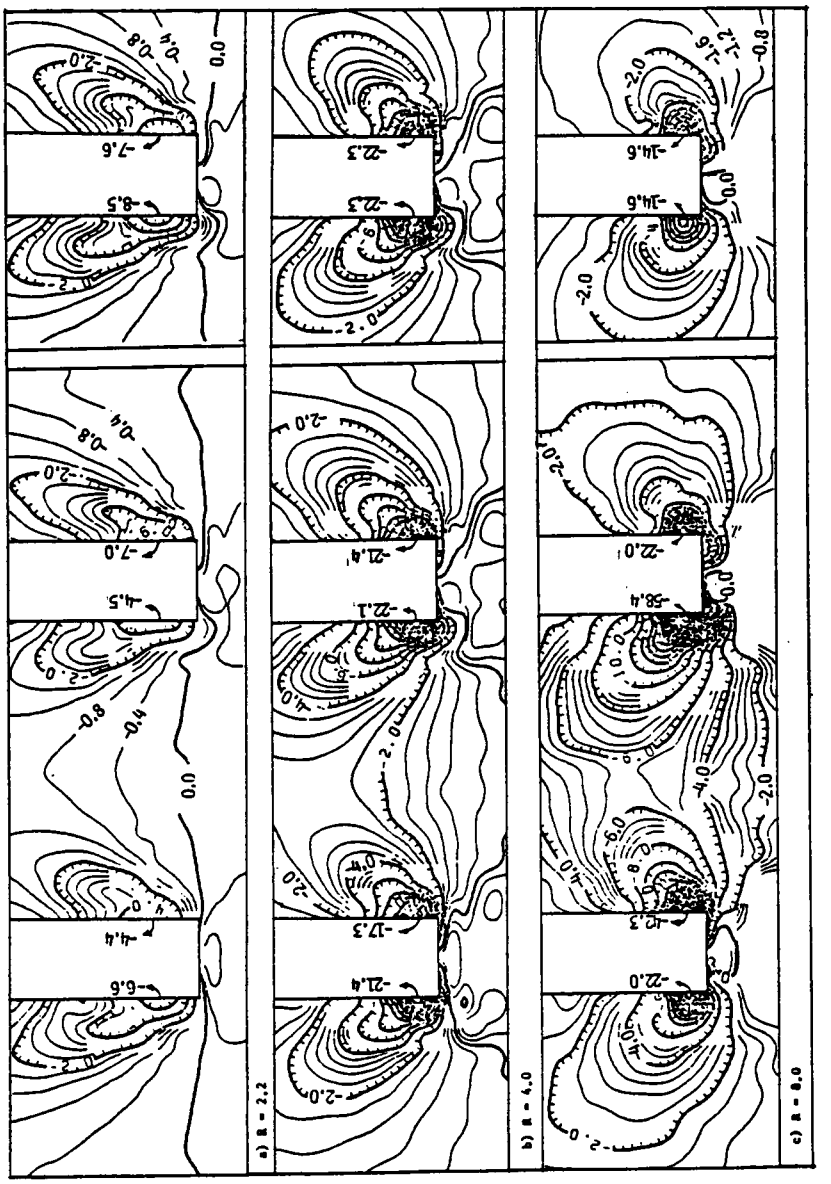

Figure 130. Surface pressures, 90° rectangular jets, enlarged front.

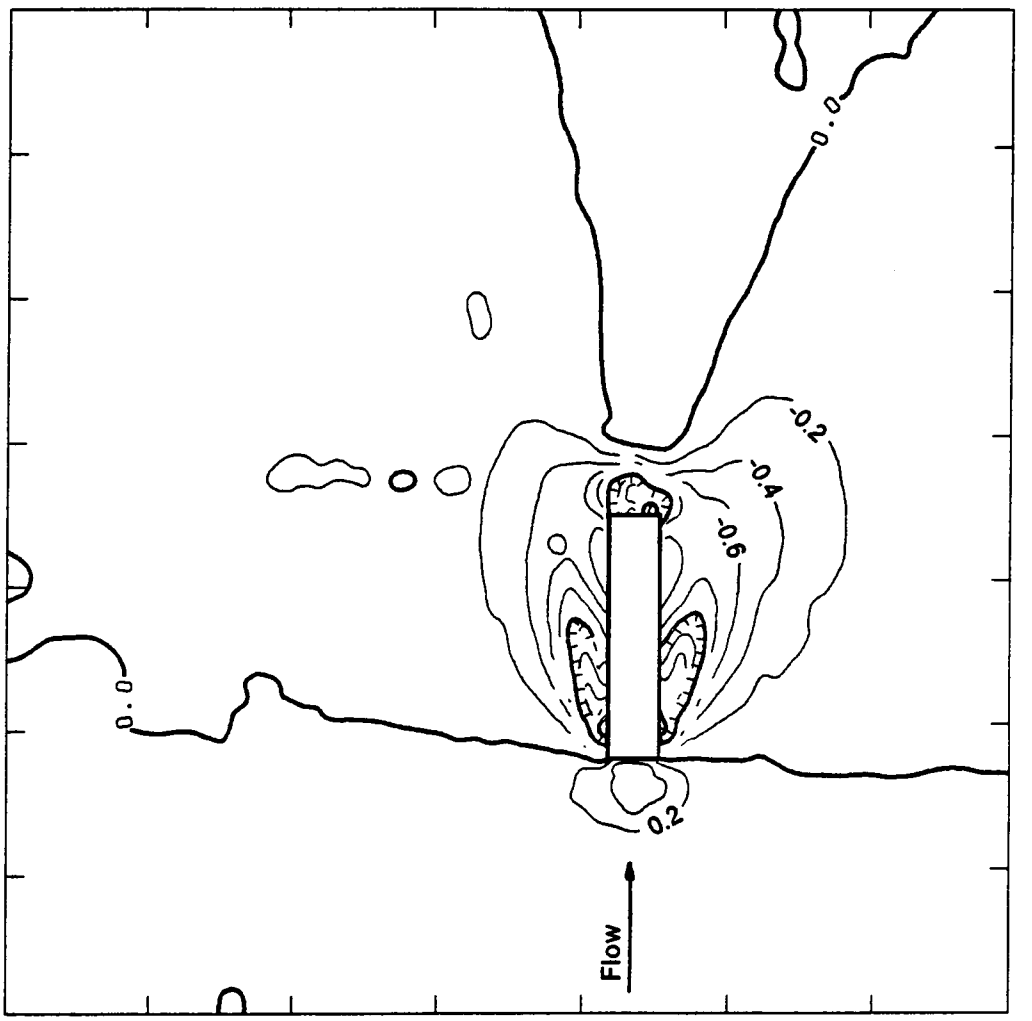

Figure 131. Surface pressures, 60° single rectangular jet, R = 2.2.

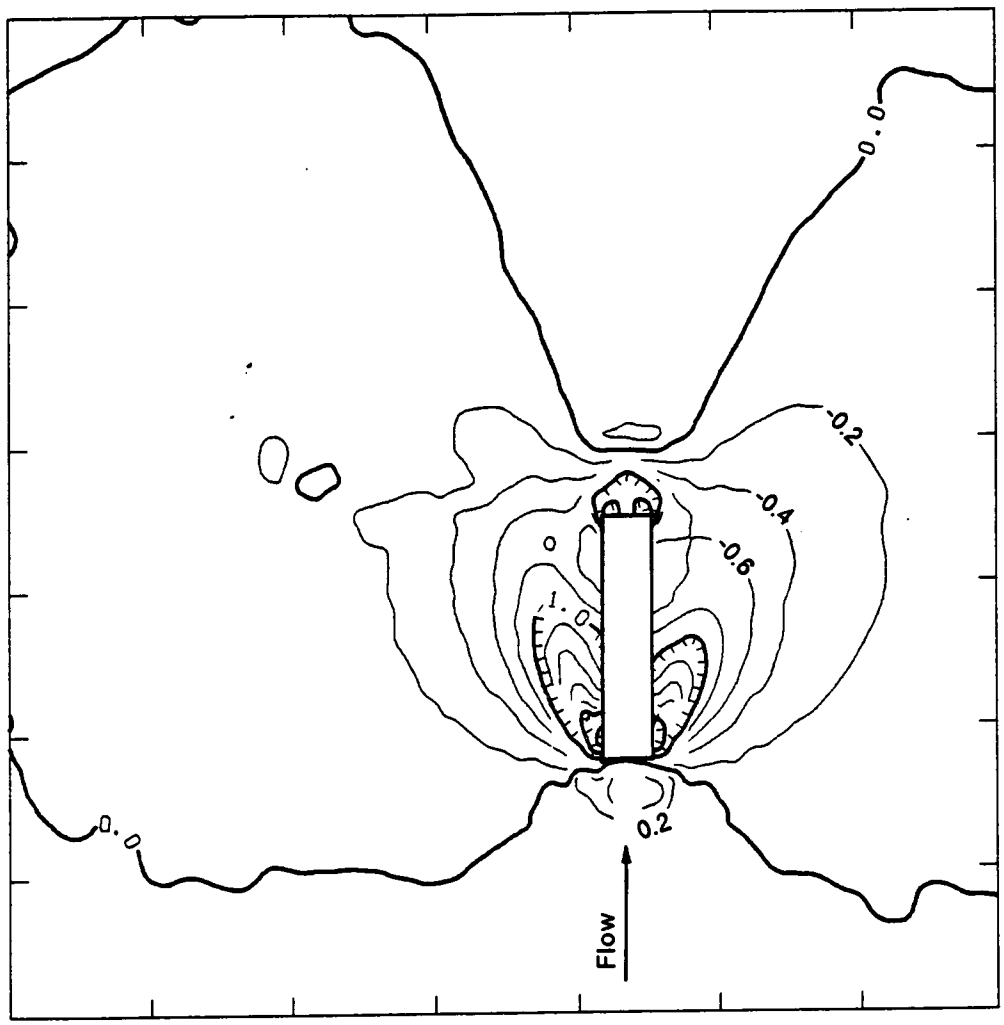

Figure 132. Surface pressures, 60° single rectangular jet, R = 4.0.

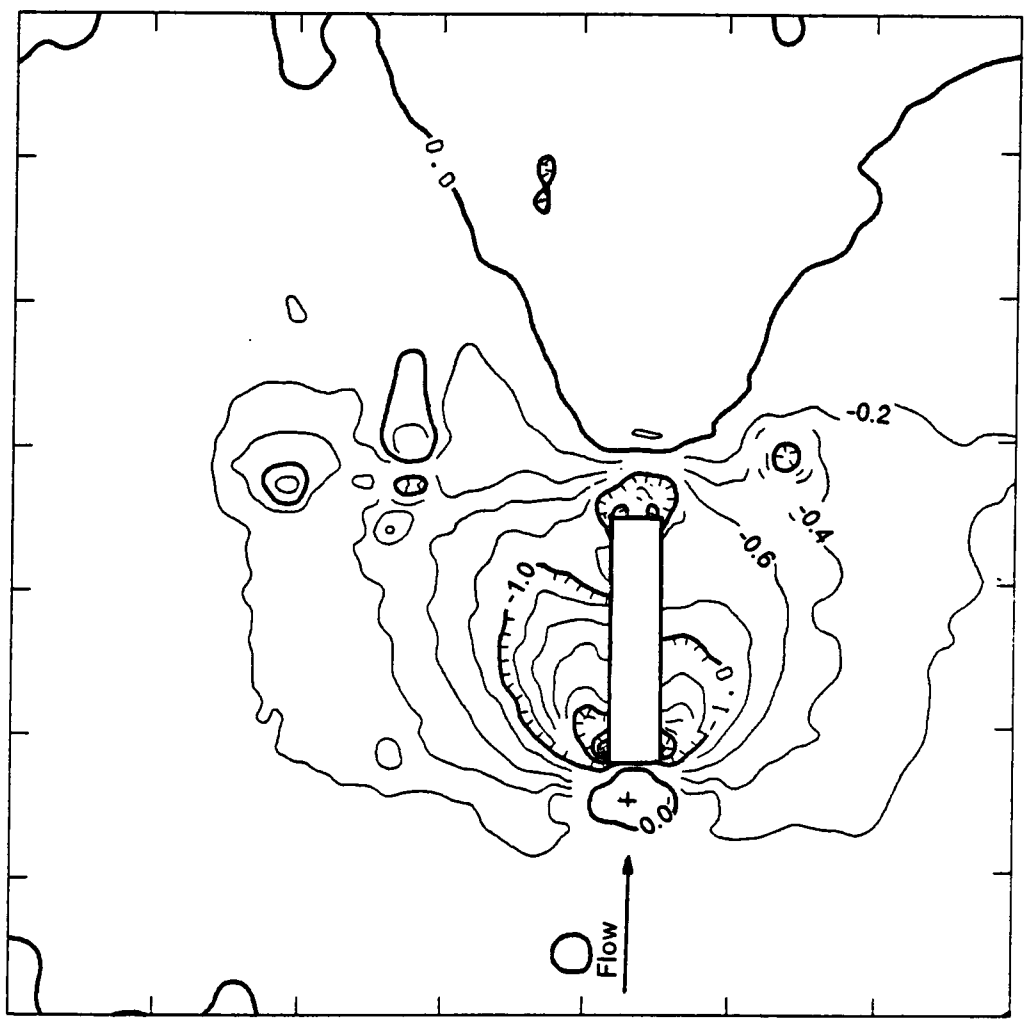

Figure 133. Surface pressures, 60° single rectangular jet, R = 8.0.

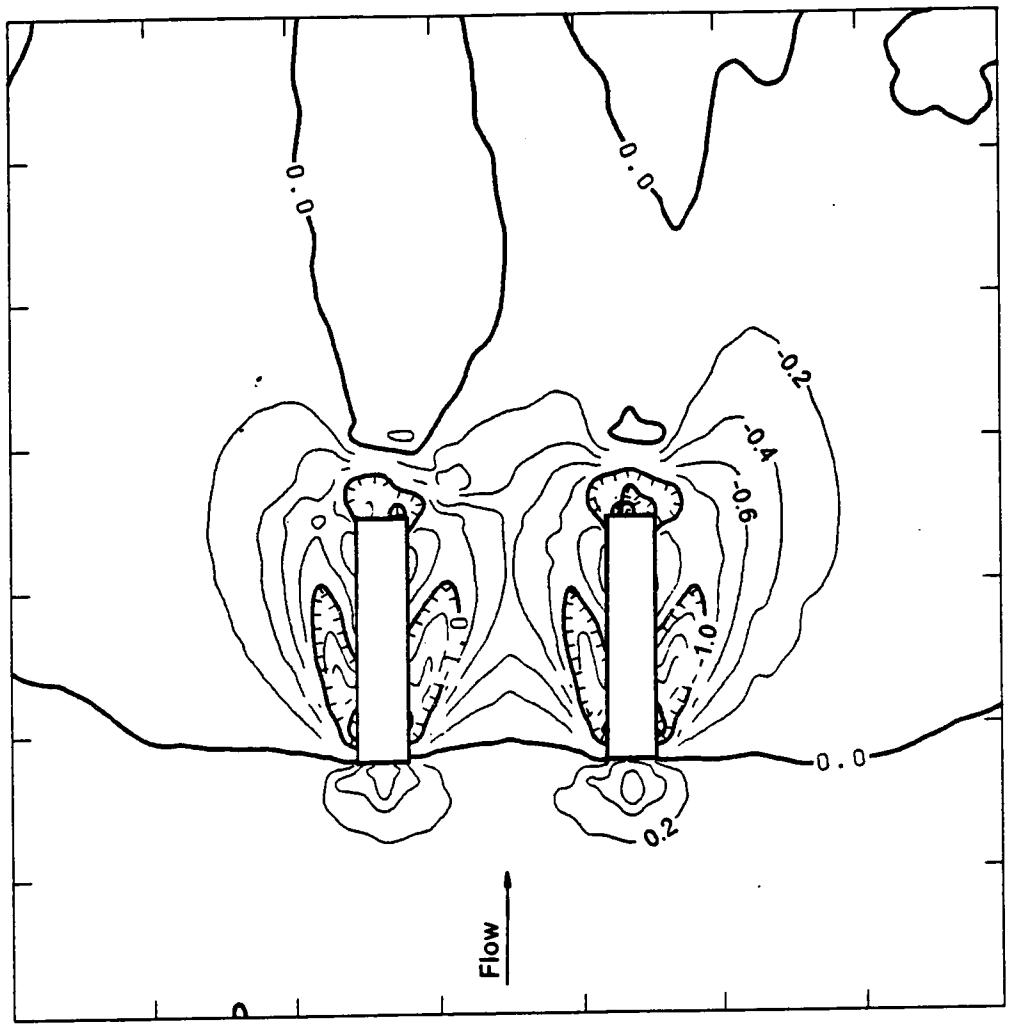

Figure 134. Surface pressures, 60° side-by-side rectangular, R = 2.2.

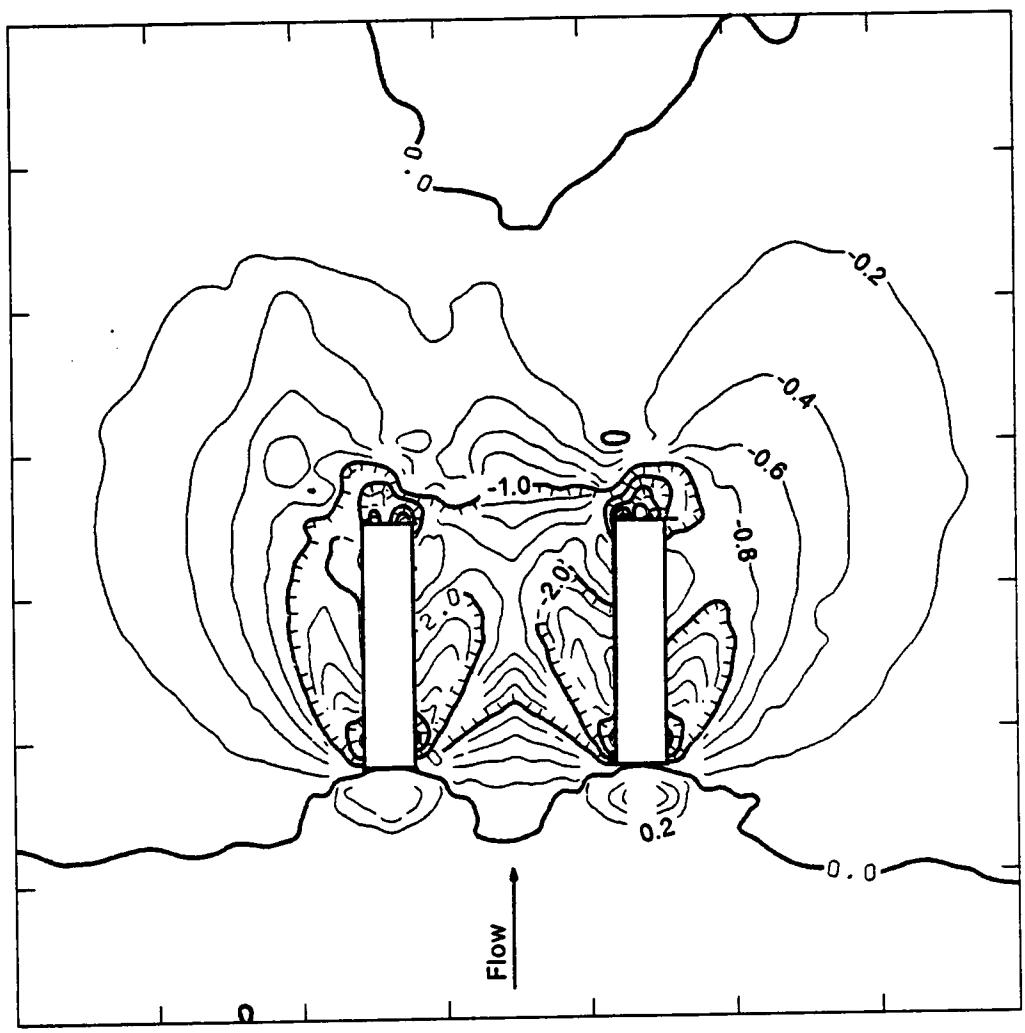

Figure 135. Surface pressures, 60° side-by-side rectangular, R = 4.0.

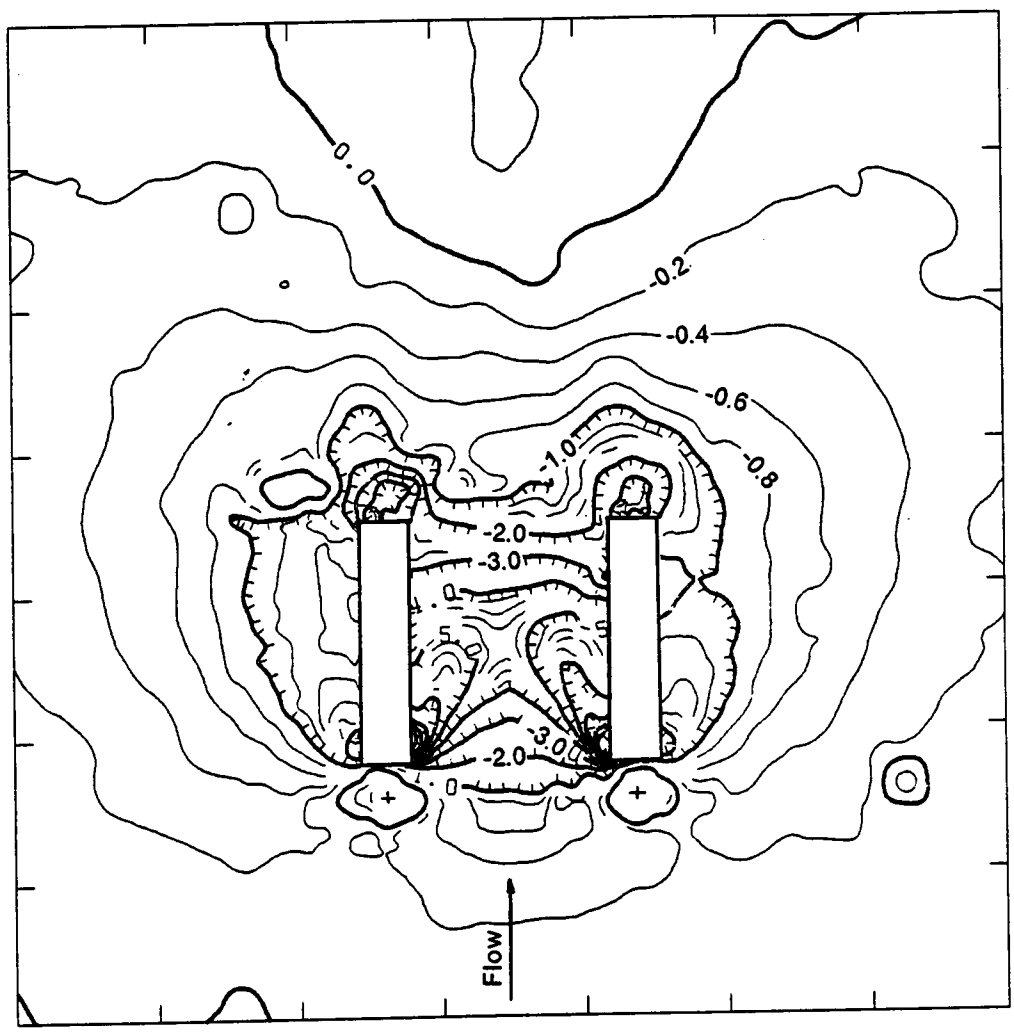

Figure 136. Surface pressures, 60° side-by-side rectangular, R = 8.0.

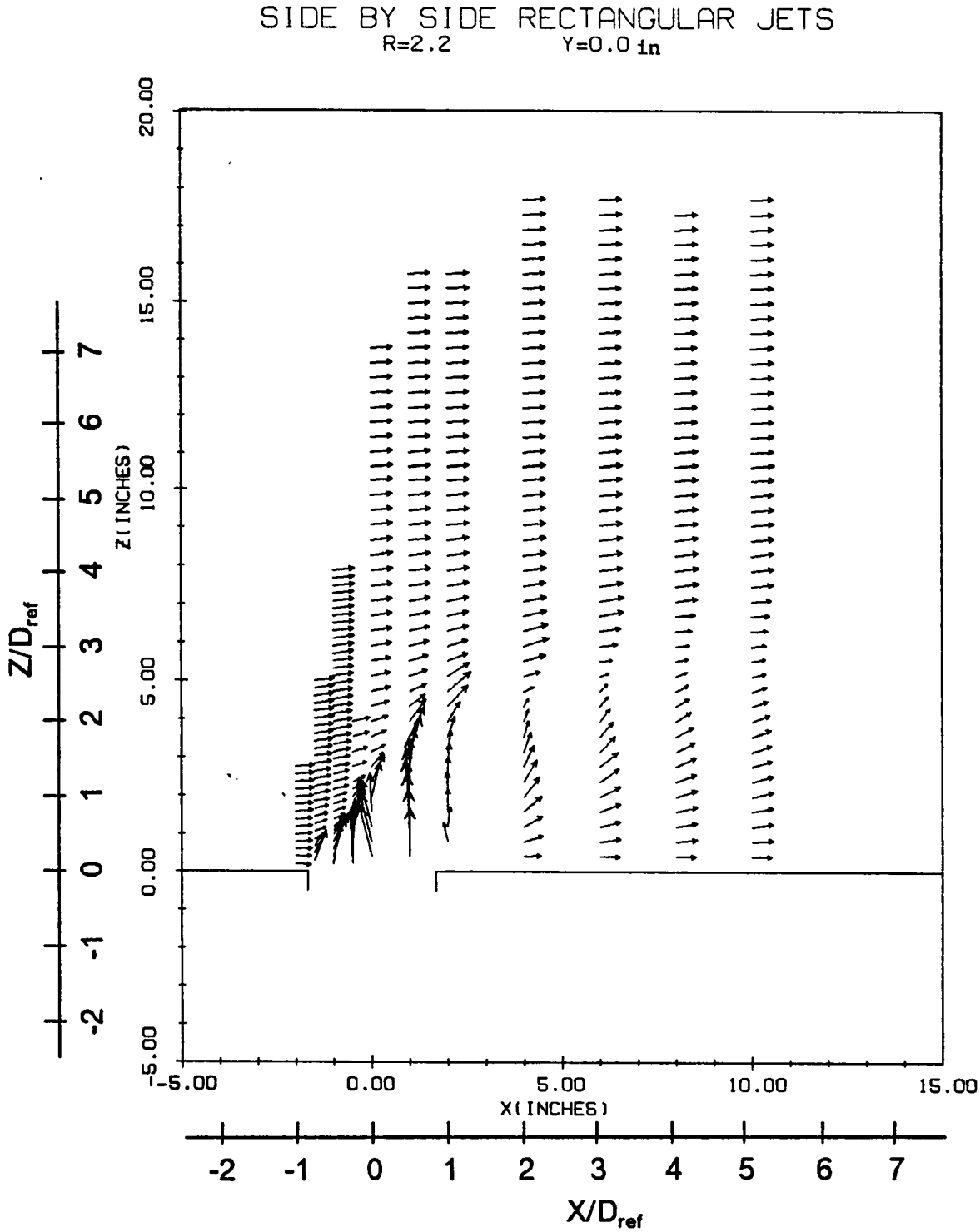

Figure 137. Mean flowfield, 90° side-by-side dual rectangular, R = 2.2.: $Y/D_{ref} = 0.0$.

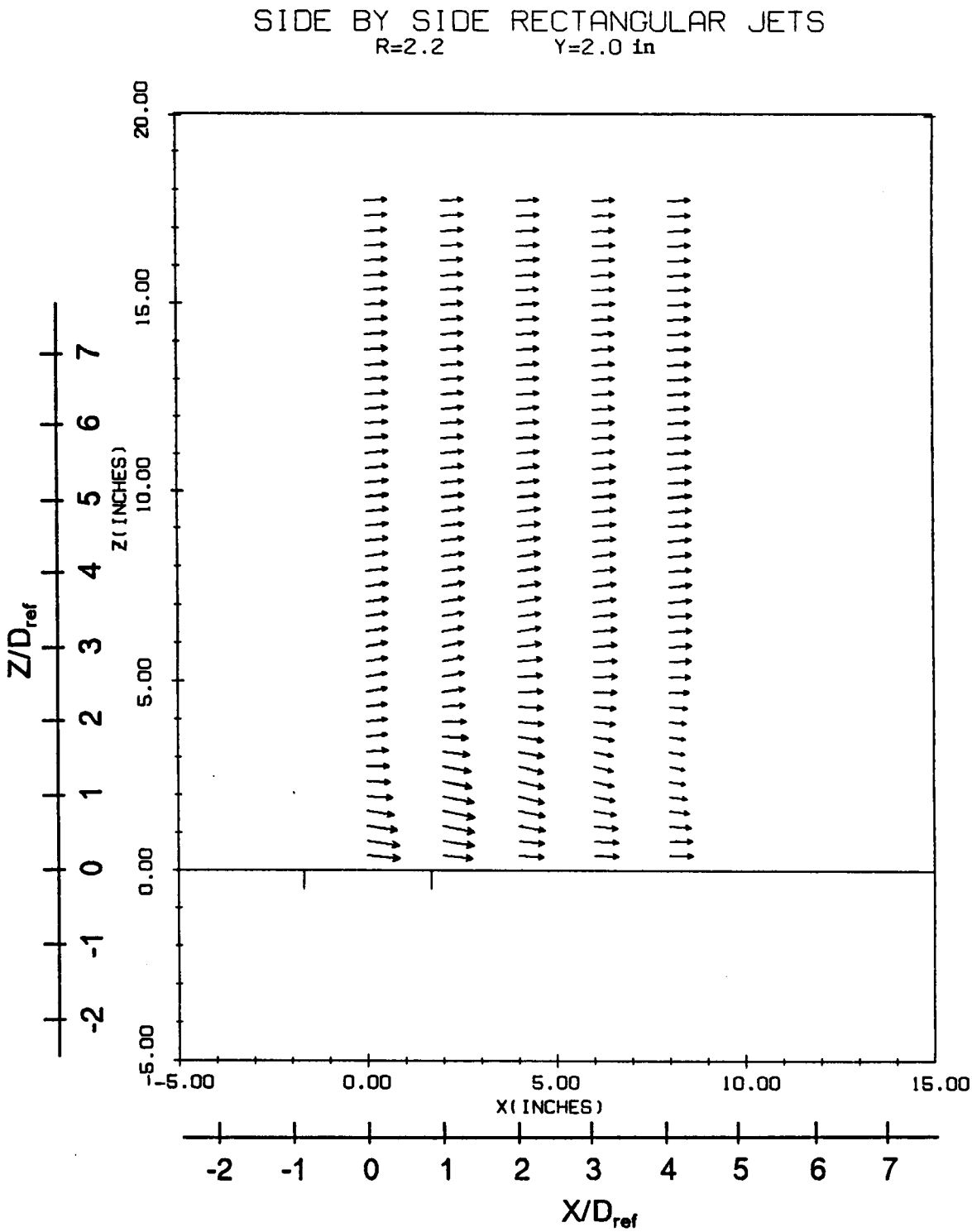

Figure 138. Mean flowfield, 90° side-by-side dual rectangular, R = 2.2.: $Y/D_{ref} = 1.026$

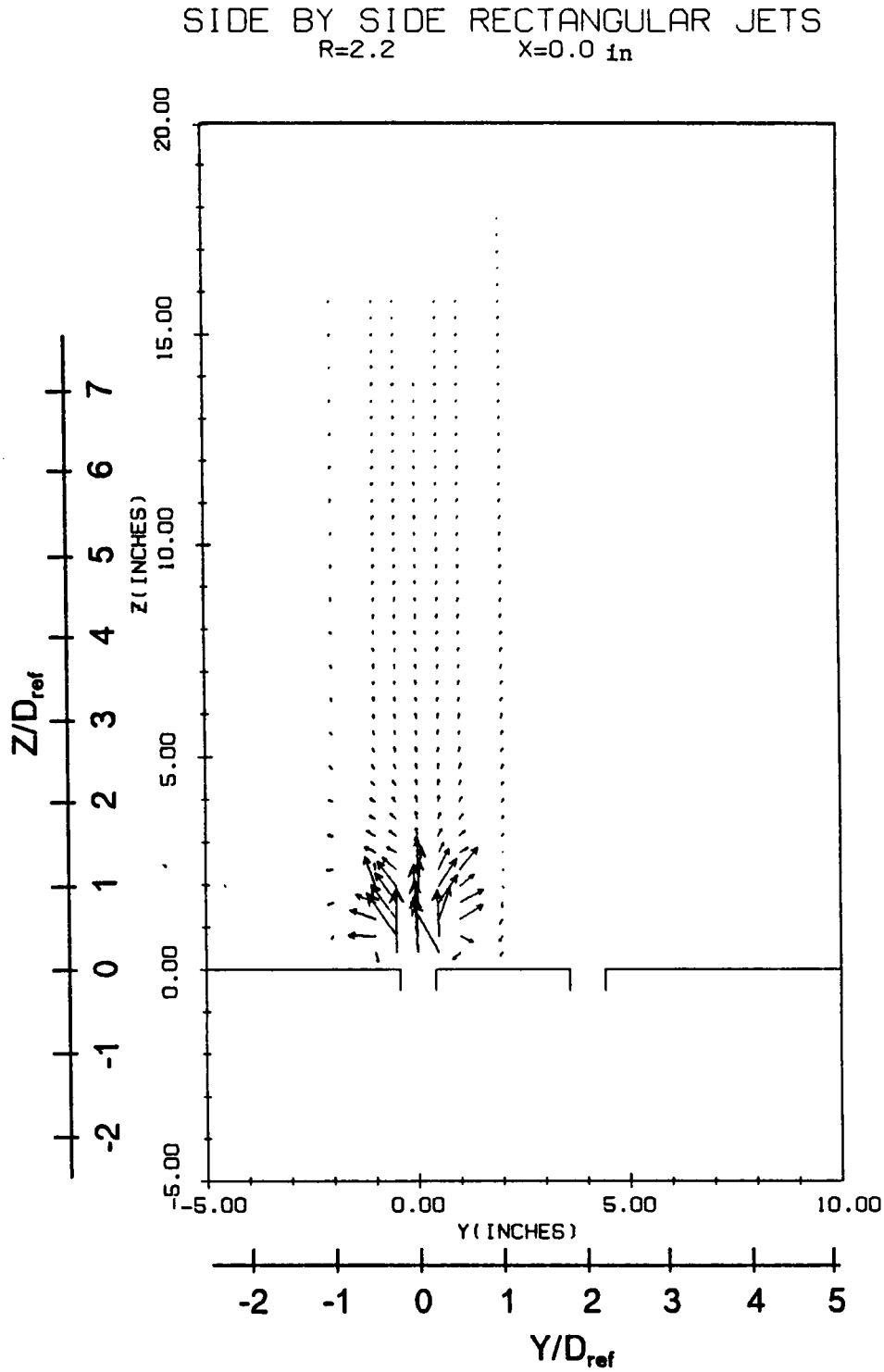

Figure 139. Mean flowfield, 90° side-by-side dual rectangular, R = 2.2.: $X/D_{ref} = 0.0$.

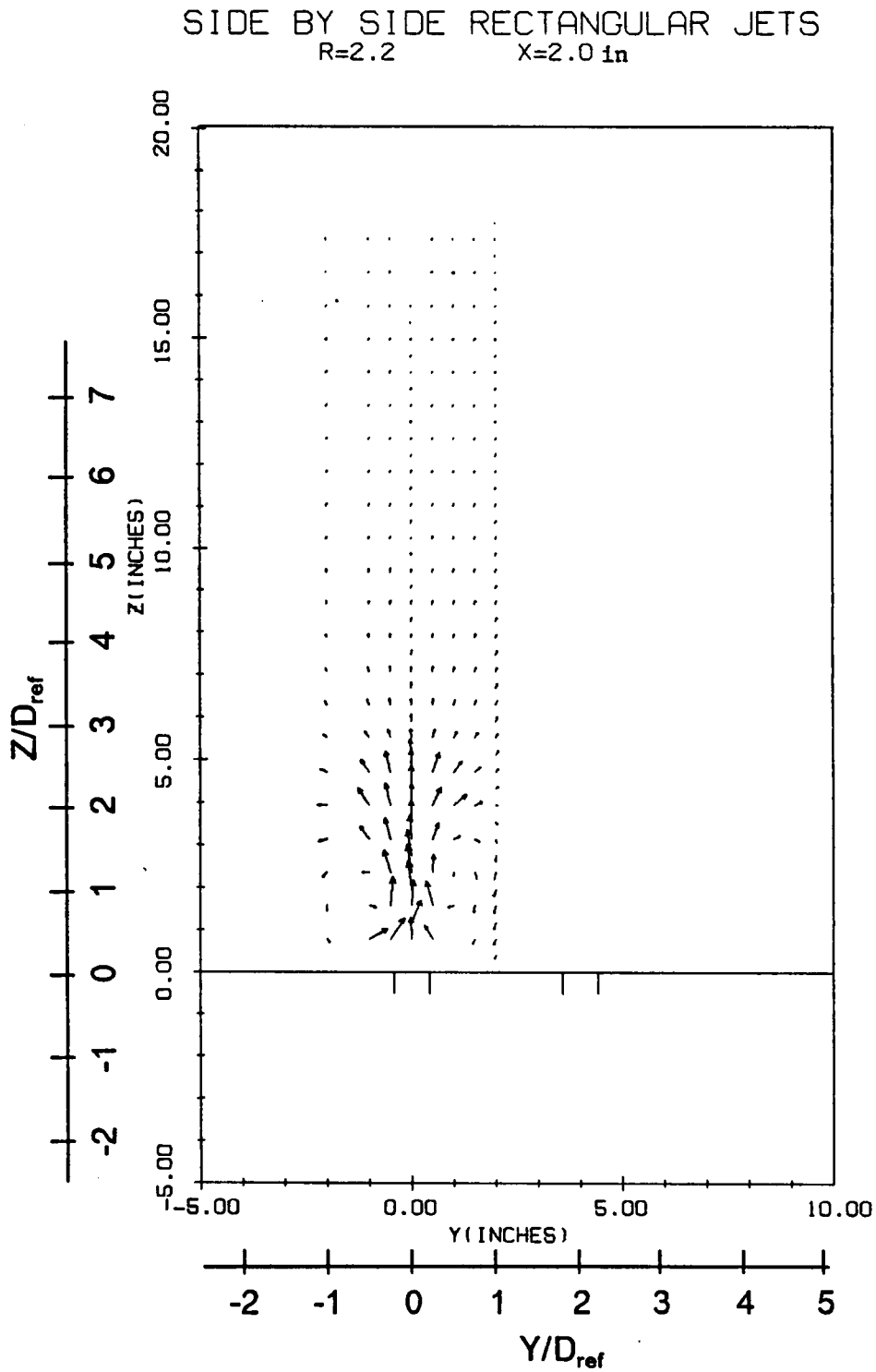

Figure 140. Mean flowfield, 90° side-by-side dual rectangular, R = 2.2.: $X/D_{ref} = 1.026$.

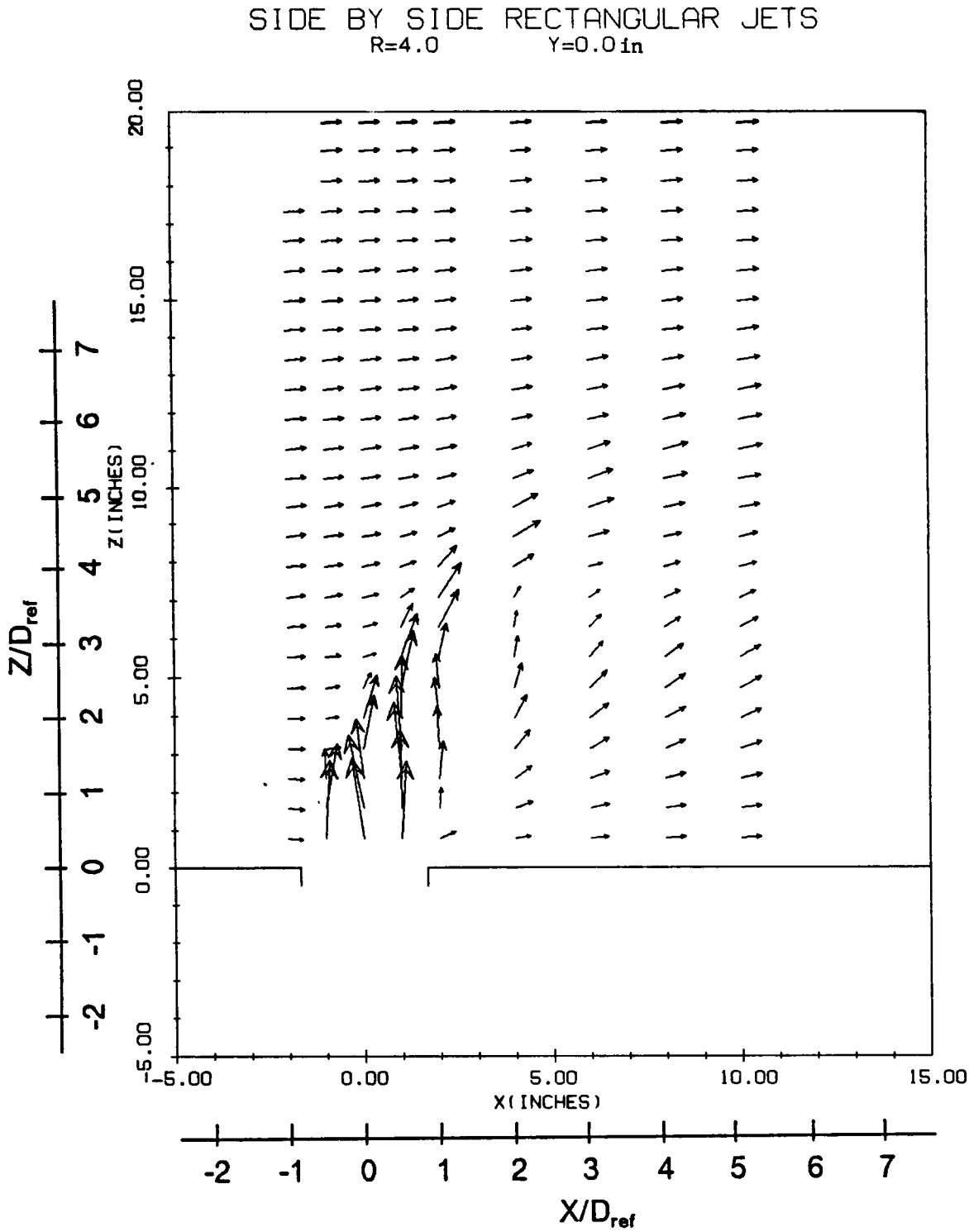

Figure 141. Mean flowfield, 90° side-by-side dual rectangular, R = 4.0.: Y/D_{ref} = 0.0.

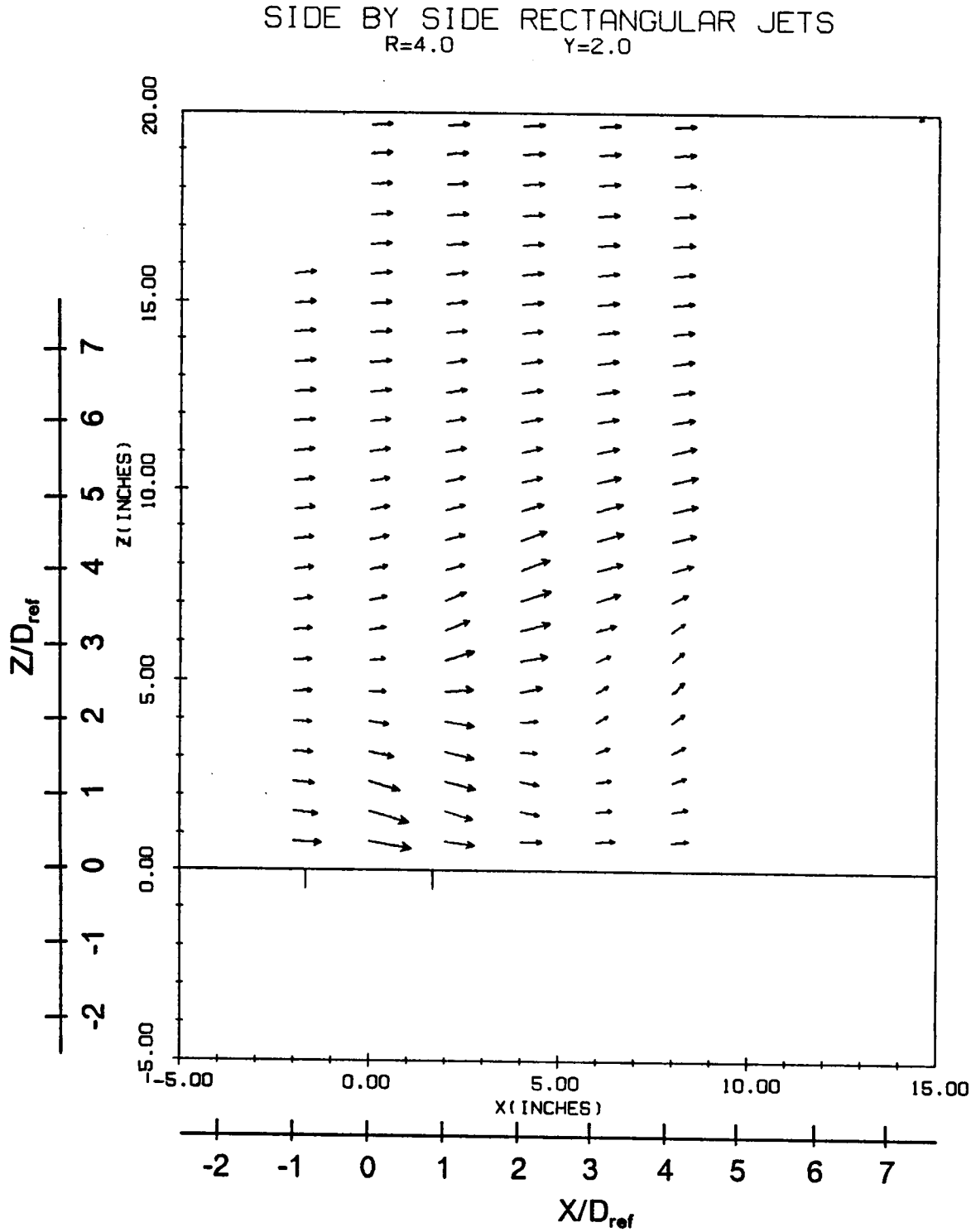

Figure 142. Mean flowfield, 90° side-by-side dual rectangular, R = 4.0.: $Y/D_{ref} = 1.026$.

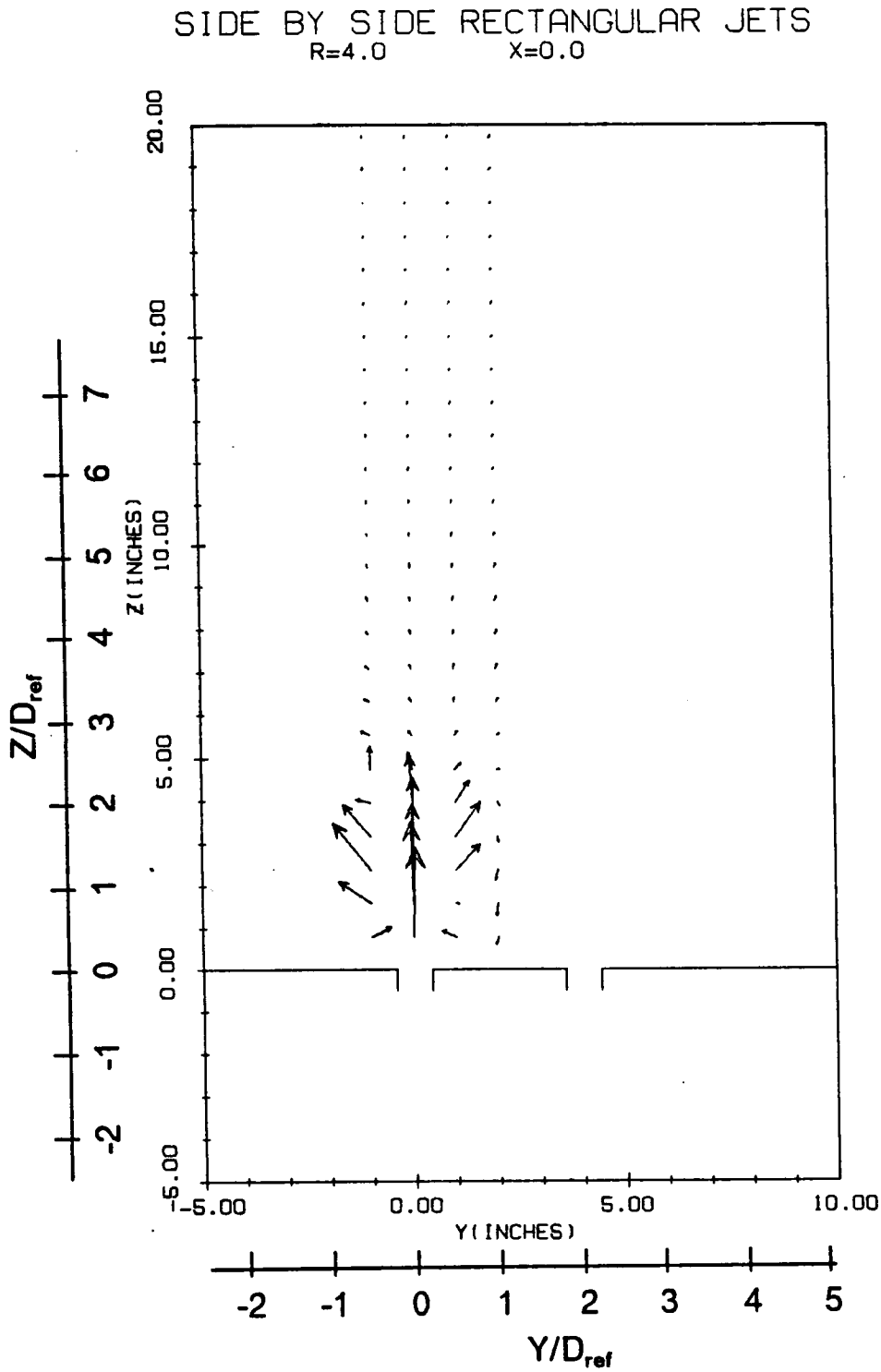

Figure 143. Mean flowfield, 90° side-by-side dual rectangular, R = 4.0.: X/D_{ref} = 0.0.

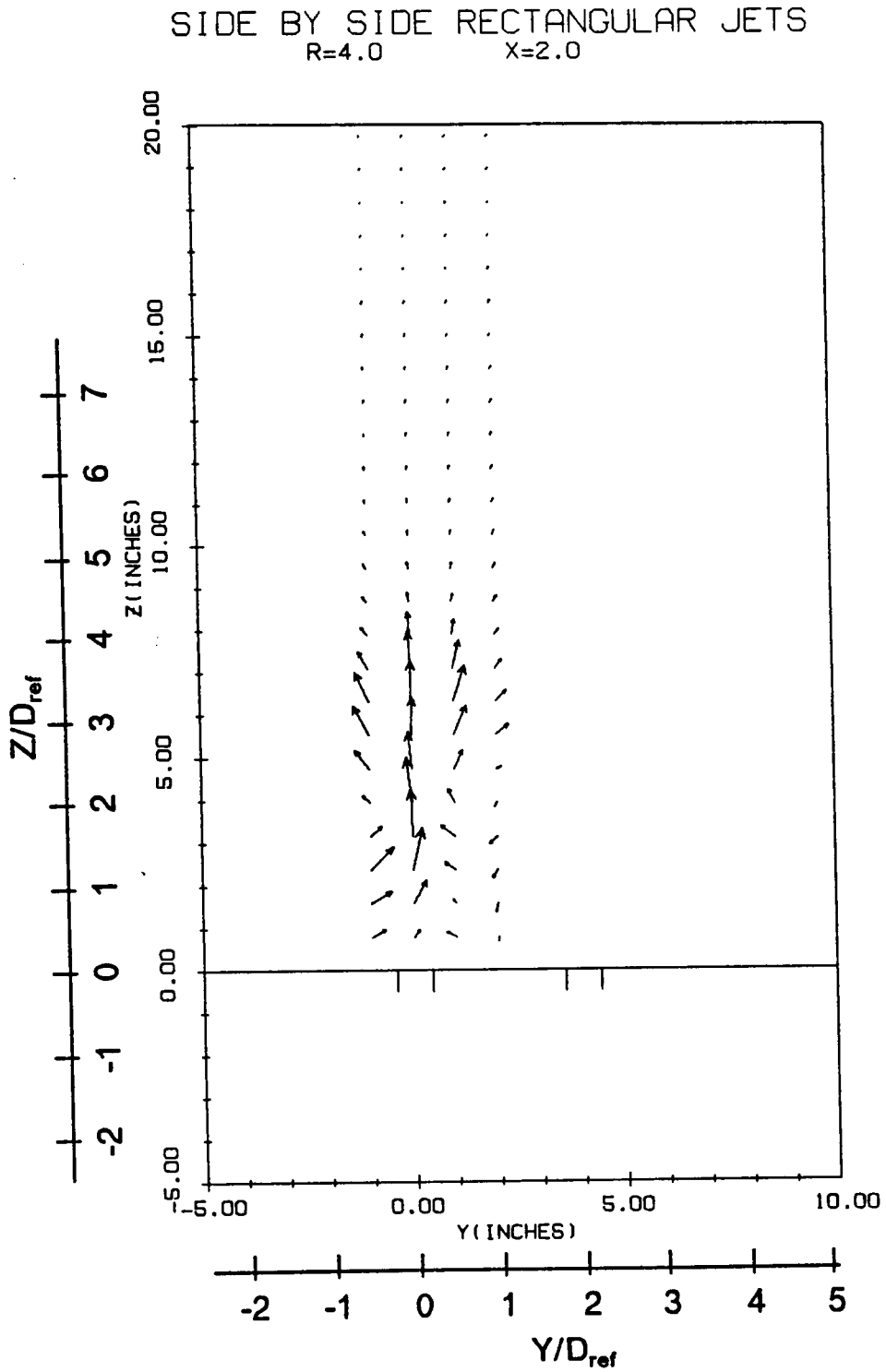

Figure 144. Mean flowfield, 90° side-by-side dual rectangular, R = 4.0.: $X/D_{ref} = 1.026$.

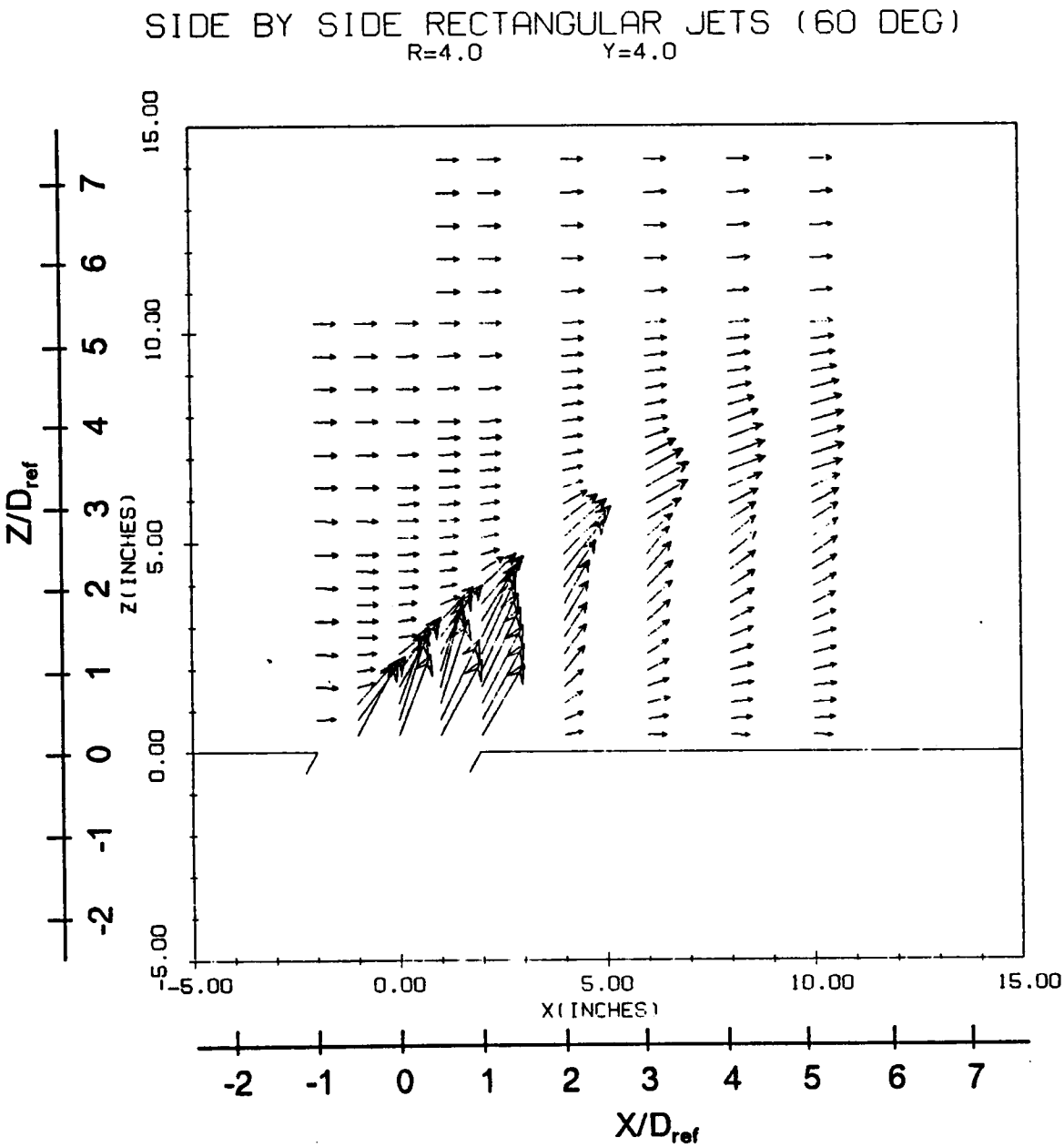

Figure 145. Mean flowfield, 60° side-by-side dual rectangular, R = 4.0.: Y/D_{ref} = 2.051.

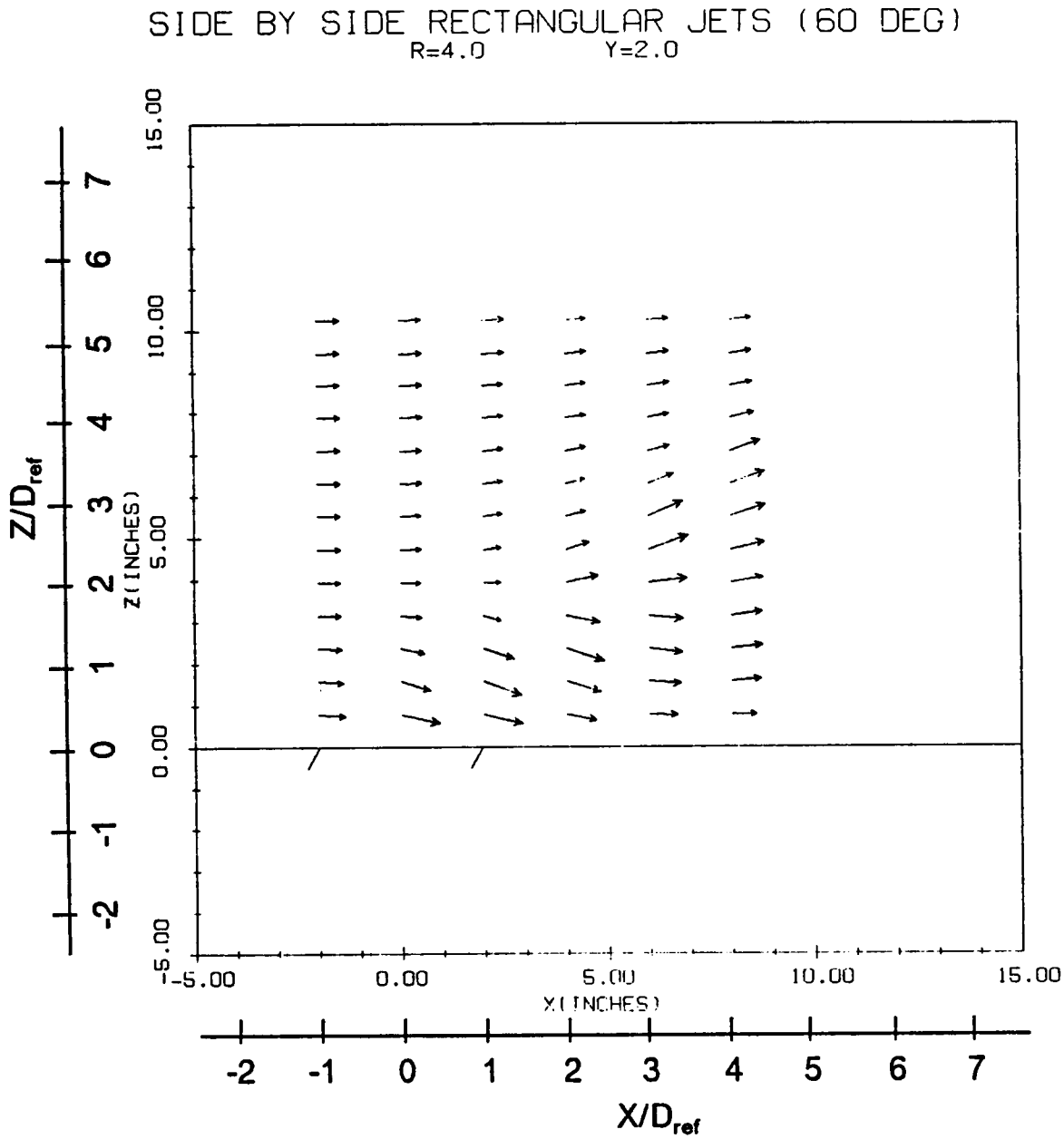

Figure 146. Mean flowfield, 60° side-by-side dual rectangular, R = 4.0.: $Y/D_{ref} = 1.026$.

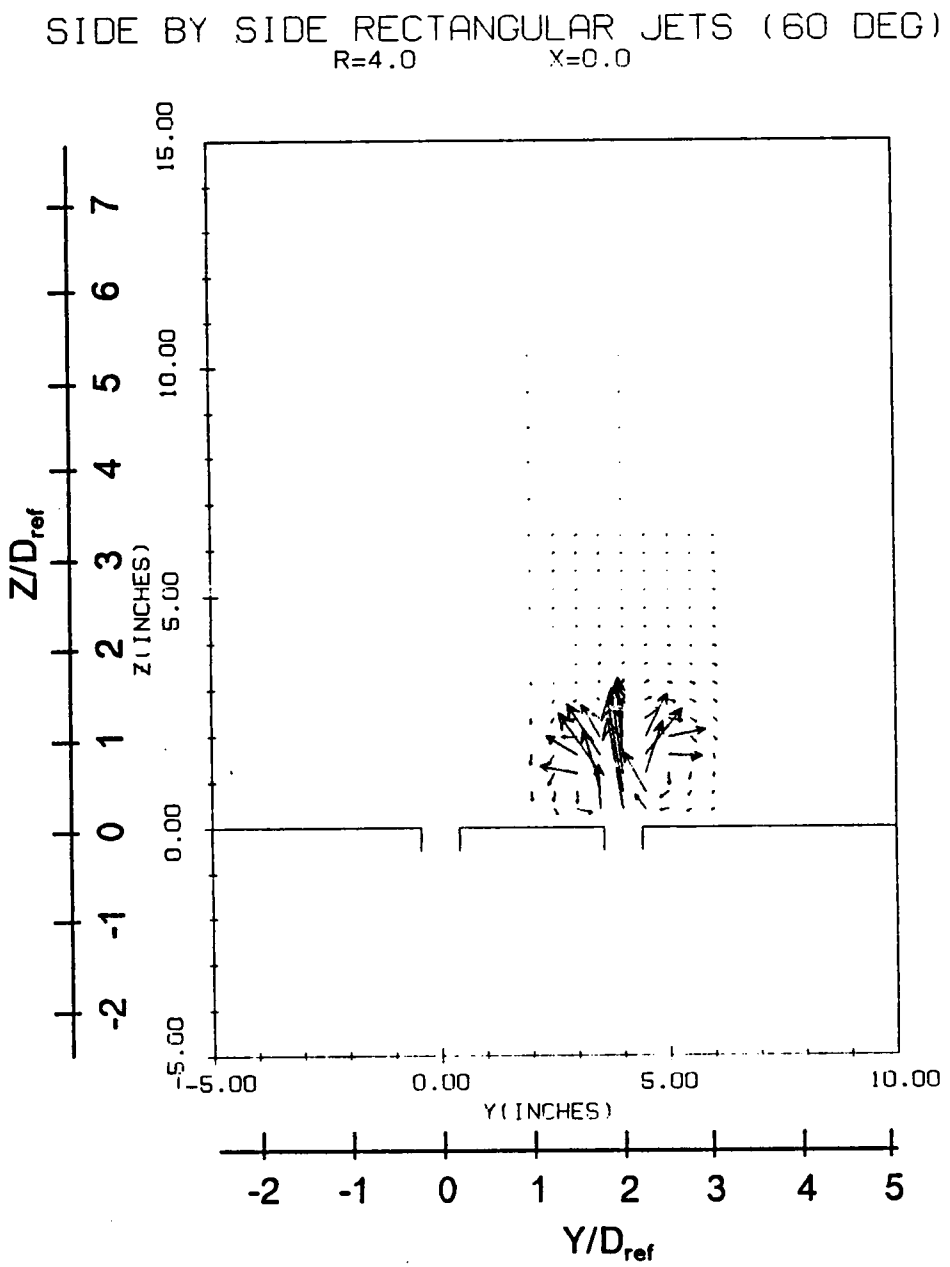

Figure 147. Mean flowfield, 60° side-by-side dual rectangular, R = 4.0.: $X/D_{ref} = 0.0$.

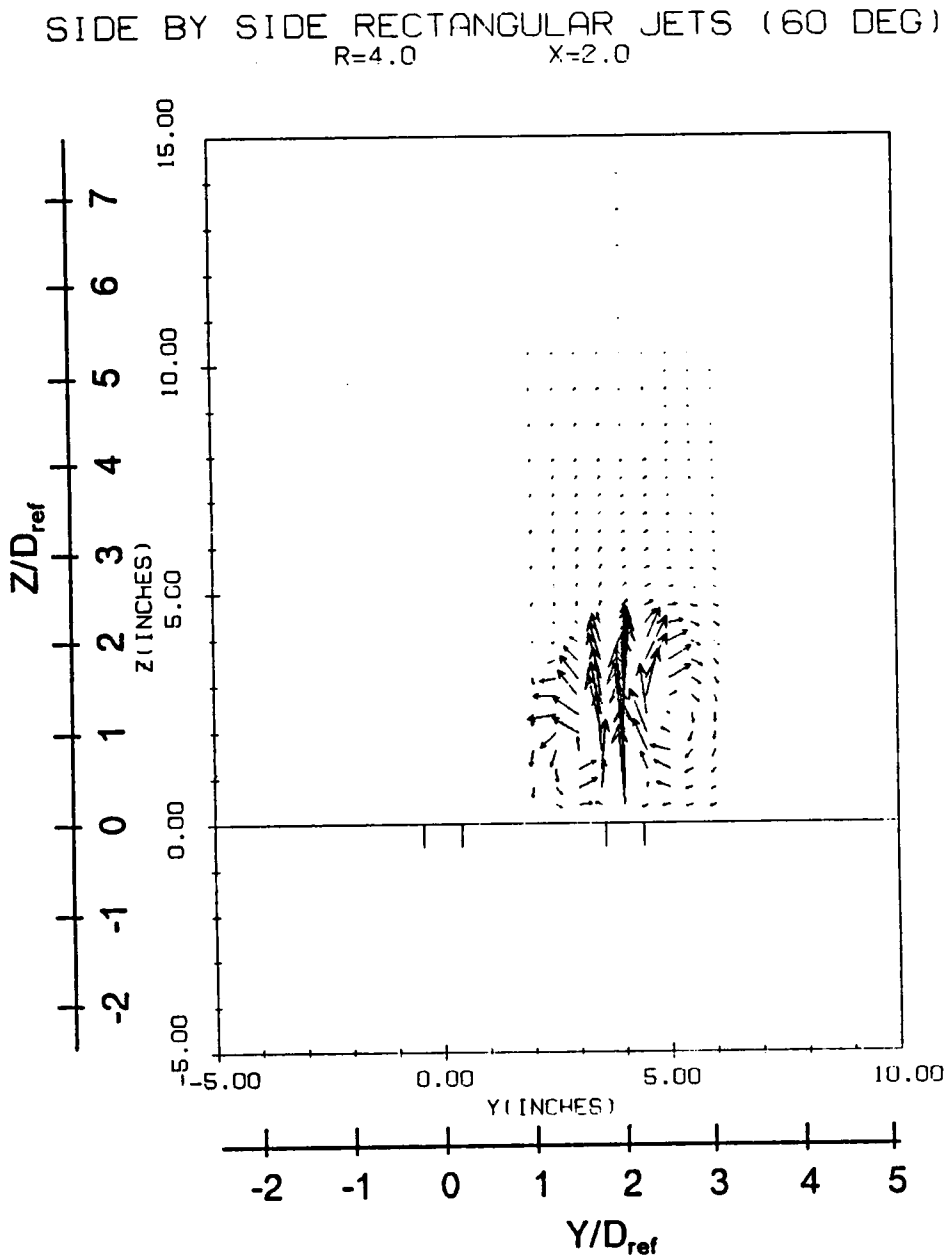

Figure 148. Mean flowfield, 60° side-by-side dual rectangular, R = 4.0.: $X/D_{ref} = 1.026$.

The vita has been removed from the scanned document